UNIVERSIDAD COMPLUTENSE DE MADRID

FACULTAD DE CIENCIAS BIOLÓGICAS

TESIS DOCTORAL

Modulación farmacológica y genética de la diferenciación celular como estrategia terapéutica en el cáncer de mama

Pharmacologic and genetic strategies for differentiation therapy in breast cancer

MEMORIA PARA OPTAR AL GRADO DE DOCTORA

PRESENTADA POR

Nuria García Martínez-Illescas

DIRIGIDA POR

María Salazar Roa

María Cristina Sánchez García

UNIVERSIDAD COMPLUTENSE DE MADRID

FACULTAD DE CIENCIAS BIOLÓGICAS

Programa de doctorado en Bioquímica, Biología Molecular y Biomedicina

TESIS DOCTORAL

MODULACIÓN FARMACOLÓGICA Y GENÉTICA DE LA DIFERENCIACIÓN CELULAR COMO ESTRATEGIA TERAPEÚTICA EN EL CÁNCER DE MAMA

PHARMACOLOGIC AND GENETIC STRATEGIES FOR DIFFERENTIATION THERAPY IN BREAST CANCER

MEMORIA PARA OPTAR AL GRADO DE DOCTORA

PRESENTADA POR

Nuria García Martínez-Illescas

DIRECTORAS

Dra. María Salazar Roa
Dra. María Cristina Sánchez García

Above everything be curious, learn all you can, and take a lifetime doing it.

Ruth Asawa

Agradecimientos

Esta tesis doctoral ha sido posible gracias a un Contrato Predoctoral de la Fundación Científica de la Asociación Española Contra el Cáncer (FC AECC, PRDMA19003GARC), así como a un contrato de estancia predoctoral Fulbright (PS00380044). Igualmente, ha contado con la financiación de los proyectos CNS2022-135364 y PID2022-136508OA-I00, concedidos por el Ministerio de Ciencia e Innovación.

Quiero expresar también mi agradecimiento al personal de los Centros de Apoyo a la Investigación que han colaborado en el desarrollo de esta tesis: el Animalario de la Facultad de CC. Biológicas, la Unidad de Citometría y Microscopía de Fluorescencia, y la Unidad de Genómica de la Facultad de CC. Biológicas.

Table of contents

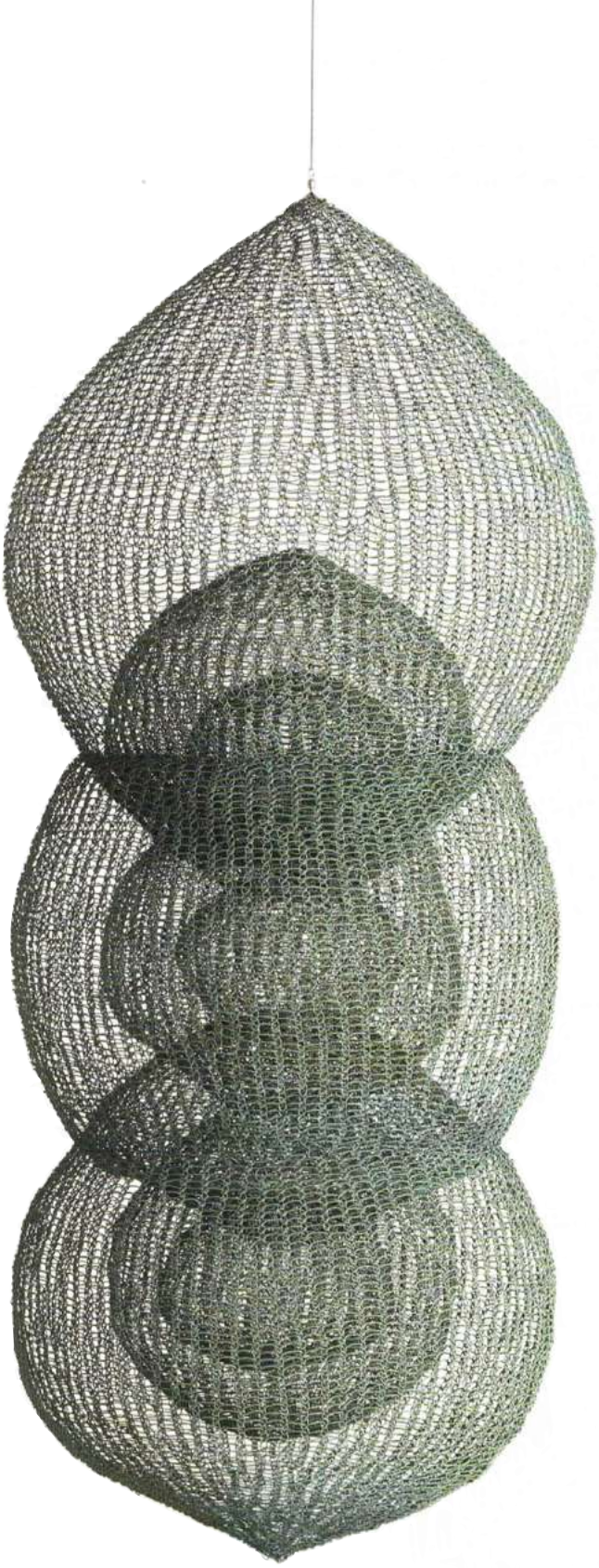

Abstract

Abstract

Breast cancer remains the most common malignancy among women worldwide and is the leading cause of female cancer-related mortality. Despite significant advances in prevention, early detection, and therapeutic interventions, intrinsic tumor heterogeneity and the persistence of cancer stem cells (CSCs) present major challenges for effective and durable clinical success. CSCs are characterized by their self-renewal capacity, multipotency, and dynamic ability to transition between stem-like and differentiated states. These properties not only drive tumor initiation, progression, and metastasis, but also contribute to therapeutic resistance and relapse. Standard therapies, while effective at reducing tumor mass, often fail to eradicate CSCs, allowing these residual stem-like cells to survive, repopulate tumors, and cause recurrence. This underscores the urgent need for innovative strategies that target CSC biology and tumor plasticity.

Cellular differentiation therapy represents a promising, potentially non-cytotoxic strategy that reprograms tumor cells into less aggressive states with diminished tumorigenic potential. In this Thesis, we present the first comprehensive demonstration that two distinct molecular modulators —the endocannabinoid system (ECS) ligands SR144528 (SR2) and Δ^9-tetrahydrocannabinol (THC), and microRNA-203 (miR-203)— act as differentiation-inducing agents in breast cancer cells.

The ECS, composed of cannabinoid receptors CB_1R and CB_2R, their endogenous ligands, and the endocannabinoid metabolic enzymes, regulates a wide range of physiological processes, incluiding neuromodulation, appetite control, and immune function. Of interest, dysregulation of the ECS has been related to poor prognosis in several cancer types. Notably, CB_2R overexpression correlates with poor patient prognosis and clinical outcome in breast cancer. Our findings reveal that cannabinoids, particularly the phytocannabinoid THC, a CB_1R/CB_2R mixed partial agonist, and the synthetic CB_2R inverse agonist SR2, profoundly reshape breast cancer cell plasticity. Remarkably, short-term, low-dose exposure to these compounds induces terminal differentiation of breast CSCs into a stable luminal-like phenotype. This reprogramming effect is durable and irreversible, locking cells into differentiated states, depleting stemness, suppressing invasiveness, and limiting metastatic capacity.

In parallel, we explored the role of miR-203, a microRNA that serves as a key developmental regulator of epithelial differentiation. During normal mammary gland development, miR-203 restricts stemness and promotes luminal lineage commitment. However, in breast tumors, miR-203 is frequently silenced through epigenetic mechanisms, thereby facilitating epithelial-to-

mesenchymal transition (EMT), invasion, and metastatic dissemination. Our results demonstrate that transient restoration of miR-203 expression in breast cancer cells is sufficient to induce epigenetic remodeling, reduce self-renewal capacity, and drive differentiation toward epithelial luminal fates. Functionally, miR-203 acts as a differentiation enhancer, amplifying intrinsic lineage-commitment programs and reducing both invasiveness and metastatic potential.

Although ECS modulation and miR-203 reactivation operate presumably through distinct molecular pathways, their functional outcomes converge on a shared cellular response: redirecting tumor evolution away from adaptive plasticity and toward stable differentiated states. These approaches (pharmacological and based on advanced molecular modulation) highlight the potential of differentiation-based strategies —not as cytotoxic alternatives but as targeted modulators of tumor adaptability. Together, these findings expand our understanding of cancer stemness regulation and provide a conceptual framework for targeting tumor plasticity at its root. By stabilizing tumor cell identity rather than focusing solely on cell elimination, differentiation therapy offers a sustainable, resistance-limiting approach with the potential to significantly improve patient outcomes.

Resumen

El cáncer de mama sigue siendo la neoplasia maligna más común entre las mujeres a nivel mundial y la principal causa de mortalidad femenina relacionada con el cáncer. A pesar de los avances en prevención, diagnóstico precoz y tratamiento, la heterogeneidad intrínseca del tumor y la persistencia de las células madre cancerosas (CSC, por sus siglas en inglés) representan aún obstáculos importantes para lograr resultados clínicos eficaces y duraderos. Las CSCs se caracterizan por su capacidad de autorrenovación, multipotencia y por su habilidad dinámica para transitar entre estados celulares indiferenciados y diferenciados. Estas propiedades no solo impulsan la iniciación, progresión y metástasis tumoral, sino que también contribuyen a la resistencia terapéutica y a las recidivas. Aunque las terapias convencionales suelen ser eficaces para reducir la masa tumoral, a menudo no logran erradicar las CSCs, permitiendo que estas células residuales sobrevivan, repueblen el tumor y den lugar a recurrencias. Esto pone de relieve la necesidad urgente de estrategias innovadoras que aborden tanto la plasticidad tumoral como la biología de las CSCs.

La terapia basada en la diferenciación celular surge como una estrategia prometedora que no busca eliminar directamente las células tumorales, sino reprogramarlas hacia estados menos agresivos, con menor potencial tumorigénico. En esta tesis, demostramos por primera vez que dos moduladores moleculares distintos— SR144528 (SR2) y Δ^9-tetrahidrocannabinol (THC), ligandos del sistema endocannabinoide (ECS, por sus siglas en inglés) y el microARN-203 (miR-203)— actúan como inductores de la diferenciación en cáncer de mama.

El ECS, compuesto por los receptores cannabinoides CB_1R y CB_2R, sus ligandos endógenos y las enzimas metabólicas de esos endocannabinoides, regula numerosos procesos fisiológicos, incluyendo la neuromodulación, el apetito y la función immune. Cabe destacar que se ha descrito una desregulación de este sistema en varios tipos de cáncer. En particular, la sobreexpresión de CB_2R se asocia con un mal pronóstico en cáncer de mama. Nuestros resultados muestran que los cannabinoides, especialmente el fitocannabinoide THC, agonista parcial de CB_1R y CB_2R, y el agonista inverso sintético de CB_2R, SR2, modifican notablemente la plasticidad celular en cáncer de mama. Una exposición breve y en dosis bajas a estos compuestos induce una diferenciación terminal irreversible de las CSCs hacia un fenotipo luminal estable, suprimiendo su capacidad de autorrenovación, invasión y potencial metastásico.

De manera paralela, estudiamos el papel del miR-203, un microARN clave en la regulación del desarrollo epitelial. Durante el desarrollo normal de la glándula mamaria, el miR-203 restringe la pluripotencia celular y promueve el compromiso con la línea luminal. Sin embargo, en tumores mamarios, este microARN suele estar silenciado mediante mecanismos epigenéticos, facilitando la transición epitelio-mesénquima (EMT, por sus siglas en inglés), la invasión y la diseminación metastásica. Nuestros resultados demuestran que la restauración transitoria de miR-203 en células de cáncer de mama es suficiente para inducir remodelaciones epigenéticas, reducir la capacidad de autorrenovación y promover la diferenciación hacia destinos epiteliales luminales. Funcionalmente, el miR-203 actúa como un potenciador de la diferenciación, reforzando los programas intrínsecos de compromiso celular y disminuyendo tanto la invasividad como el potencial metastásico.

Aunque la modulación del ECS y la re-expresión de miR-203 muy posiblemente actúen a través de rutas moleculares diferentes, convergen en un principio común: redirigir la evolución tumoral desde un estado de plasticidad adaptativa hacia estados diferenciados estables. Este trabajo pone de relieve el potencial terapéutico de las estrategias basadas en diferenciación, no como alternativas citotóxicas, sino como herramientas dirigidas a limitar la adaptabilidad tumoral. En conjunto, estos hallazgos amplían nuestra comprensión sobre la regulación de las CSCs y ofrecen un nuevo marco conceptual para abordar la plasticidad tumoral desde su raíz. Al estabilizar la identidad de las células tumorales en lugar de enfocarse únicamente en su eliminación, las terapias de diferenciación ofrecen un enfoque estable y con menor riesgo de resistencia, con el potencial de mejorar significativamente los resultados clínicos en pacientes.

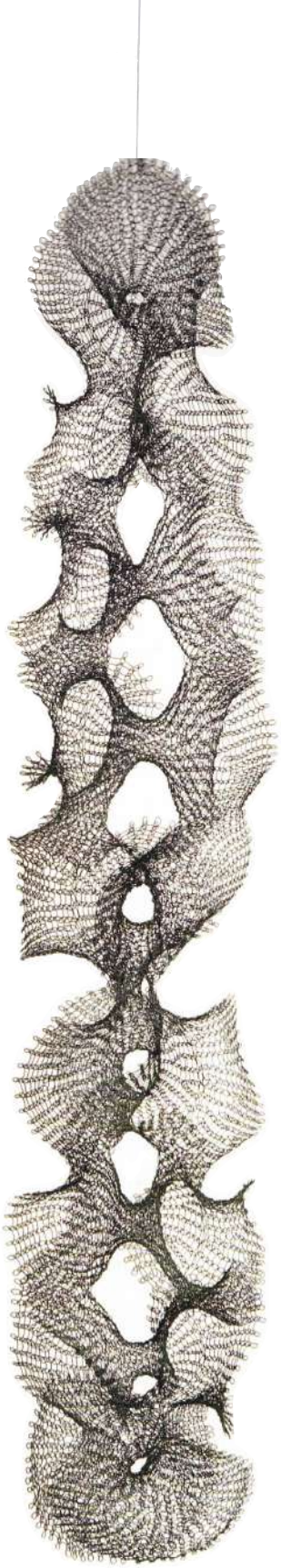

Abbreviations

2-AG: 2-Arachidonoylglycerol

AEA: N-arachidonoylethanolamine, Anandamide

APL: Acute promyelocytic leukaemia

BC: Breast cancer

BCSC(s): Breast cancer stem cell(s)

BIRADS: Breast Imaging Reporting and Data System

CAF(s): Cancer-associated fibroblast(s)

CB_1R: Cannabinoid receptor type 1

CB_2R: Cannabinoid receptor type 2

CB_2RKO: CB2 receptor knock-out

CB_2RWT: CB2 receptor wild-type

CBD: Cannabidiol

CK: Cytokeratin

CNS: Central nervous system

CSC(s): Cancer stem cell(s)

CTC(s): Circulating tumor cell(s)

DCIS: Ductal carcinoma *in situ*

Dox: Doxycycline

ECM: Extracellular matrix

ECS: Endocannabinoid system

EMT: Epithelial-to-mesenchymal transition

ER: Estrogen receptor

ESC(s): Embryonic stem cell(s)

GSEA: Gene set enrichment analysis

H&E: Hematoxylin and eosin

H3K27me3: Trimethylation of histone 3 at lysine 27

H3K4me3: Trimethylation of histone 3 at lysine 4

H3K9me3: Trimethylation of histone 3 at lysine 9

IDC: Invasive ductal carcinoma

ILC: Invasive lobular carcinoma

KEGG: Kyoto Encyclopedia of Genes and Genomes

LCIS: Lobular carcinoma *in situ*

mAEA: methanandamide

MaSC(s): Mammary gland stem cell(s)

MET: Mesenchymal-to-epithelial transition

Micro-CT: Micro-computed tomography

miRNA: MicroRNA

MMPs: Matrix metalloproteinases

MMTV: Mouse mammary tumor virus

P: Progesterone

PBMC(s): Peripheral blood mononuclear cell(s)

PCA: Principal component analysis

PML: Promyelocytic leukaemia protein

PR: Progesterone receptor

PRC: Polycomb repressive complex

PRL: Prolactin

PSC(s): Pluripotent stem cell(s)

PyMT: Polyoma virus middle T

RA: Retinoic acid

RARα: Retinoic acid receptor α

RNAseq: RNA sequencing

RT: Room temperature

SMA: Smooth muscle actin

SR1: SR141716A

SR2: SR144528

TAM(s): Tumor-associated macrophage(s)

TEB(s): Terminal end bud(s)

THC: Δ^9-Tetrahydrocannabinol

TMX: Tamoxifen

TNBC: Triple negative breast cancer

Introduction

Cancer

Cancer encompasses a diverse group of diseases that arise when the normal regulatory processes controlling cell growth, division, and death become disrupted, leading to a breakdown of cellular homeostasis. Tumorigenesis is driven by the accumulation of oncogenic mutations, which are influenced by a combination of genetic predisposition, epigenetic modifications, and environmental exposures. These changes collectively result in uncontrolled cell proliferation and disorganized tissue structure. Since such alterations can originate in any tissue through diverse molecular mechanisms, cancer is better understood as a collection of distinct diseases rather than a single entity [1]. Each cancer type can exhibit unique biological behavior, treatment response, and origins, reflecting specific interactions among environmental factors, genetic mutations, and lifestyle factors. Nonetheless, all cancers share common fundamental characteristics that disrupt normal organ function, presenting a major global health challenge expected to affect nearly 39 % of people worldwide during their lifetimes [2].

Traditionally, cancer was defined by its pathological hallmark: uncontrolled cell proliferation and the ability to invade surrounding tissues and metastasize (**Figure I1A-B**). Indeed, this understanding is captured in classical definitions, such as that from Oxford English Dictionary, which describes cancer as "a disease caused by an uncontrolled division of abnormal cells in a part of the body". Likewise, the U.S. National Insitute of Health (NIH) defines cancer as "a disease in which some of the body's cells grow uncontrollably and spread to other parts of the body". This unchecked growth and capacity to spread have historically guided diagnosis and treatment.

However, the discovery in the late 1970s of the first oncogenes and tumor suppressor genes revolutionized cancer biology by revealing the profound molecular diversity present even among tumors originating from the same tissue [3,4]. This insight marked a paradigm shift, moving from viewing cancer as merely upregulated cell division to understanding it as a complex, dynamic ecosystem (**Figure I1A, C**). Hanahan and Weinberg's influential framework further advanced this perspective by characterizing cancer as a disease shaped by interactions among genetic, epigenetic, and microenvironmental factors [5].

In their 2000 work, they identified six hallmarks of cancer, as biological capabilities acquired by tumorigenic cells which enable their growth and survival [5]. Thus, tumors were described by their ability to promote proliferative signaling, evade growth suppressors, resist cell death, enable replicative immortality, induce angiogenesis, and activate invasion and metastasis.

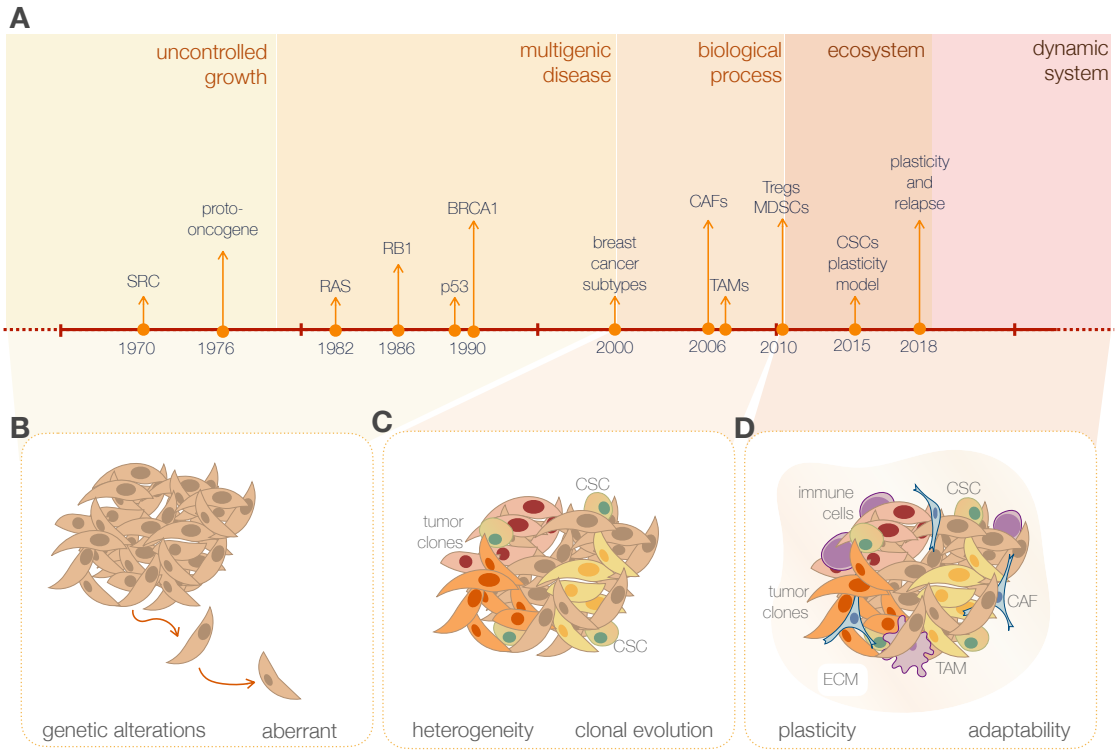

Figure I1. Timeline of the understanding cancer evolution from 1965 to the present. A, Timeline illustrating how successive discoveries reshaped the conceptualization of cancer. Firstly, cancer was defined as uncontrolled cell growth. The identification of proto-oncogenes such as SRC and Ras and tumor suppressors including RB1 and p53 established cancer as a multigenic disease, highlighting that coordinated genetic alterations drive transformation. Later, milestones including the cloning of BRCA1 and the recognition of distinct breast cancer subtypes illustrated the growing appreciation of cancer as a heterogeneous biological process, rather than a uniform genetic entity. From the 2000s onward, advances in tumor immunology and stromal biology highlighted the contribution of the tumor microenvironment—cancer-associated fibroblasts (CAFs), tumor-associated macrophages (TAMs), regulatory T cells (Tregs), and myeloid-derived suppressor cells (MDSCs) serving as key examples—broadening the definition of cancer into an ecosystem disease. Most recently, insights into cancer stem cells (CSCs), together with evidence of plasticity and adaptability, have underscored cancer as a dynamic and emergent system—multicellular, heterogeneous, and continually evolving system. **B-D,** Schematic representation of cancer as a gene alteration-driven and proliferative disease (**B**), as clonal and heterogeneous disease (**C**) and as multicellular, plastic, and heterogeneous emergent system (**D**).

Cancer cells maintain proliferative signals by deregulating growth pathways, producing growth factors, stimulating surrounding stromal cells, or altering growth factor receptors to be constitutively active. They evade growth suppressors by inactivating key tumor suppressor genes, such as *TP53* and *RB*, which normally act as molecular brakes on the cell cycle. Resistance to cell

death is achieved by disrupting apoptotic pathways through mechanisms like overexpressing anti-apoptotic proteins or losing pro-apoptotic signals. Cancer cells are able to bypass the natural limit on cell divisions by activating telomerase, which maintains telomere length and grants them replicative immortality. Tumors also stimulate angiogenesis by secreting factors like VEGF to ensure adequate blood supply, while invasiveness and metastasis result from loss of cell adhesion, extracellular matrix degradation, and enhanced motility, allowing cancer cells to spread to distant organs [5].

More recent insights emphasized the fact that tumors are complex tissues not only made of malignant cells but also a variate of normal stromal, immune, and vascular cells [6–8]. These non-malignant components are co-opted by cancer cells to support tumor growth and progression, creating a dynamic tissue-level ecosystem. This concept was reinforced by the updated hallmarks of cancer, which highlighted the crucial roles of the tumor microenvironment in enabling cancer's hallmark capabilities (**Figure I1A, D**) [9,10].

At a deeper level, cancer cells alter their metabolism to meet increased energy demands, evade immune destruction by subverting immune surveillance mechanisms, and foster a chronic inflammatory environment that promotes tumor progression [10]. In addition, they often exhibit increased mutation rates and chromosomal instability, which fuel genetic diversity and tumor evolution. Beyond genetic changes, nonmutational epigenetic reprogramming alters gene expression through chromatin remodeling, DNA methylation, or histone modification —without changing the underlying DNA sequence— thereby promoting malignancy. The accumulation of senescent cells in the tumor microenvironment contributes to cancer progression via pro-inflammatory and pro-tumorigenic secretions. Polymorphic microbiomes —the diverse microbial communities associated with tumors —can influence immune responses, inflammation, and drug metabolism, further shaping cancer development and therapeutic outcomes. Finally, unlocking cellular plasticity allows cancer cells to shift between differentiated and stem-like states, enhancing their ability to adapt. Together, these emerging hallmarks contribute to the plasticity of cancer cells, enabling them to respond to dynamic microenvironments, resist therapeutic pressures, and transition between phenotypic states that support tumor progression and metastasis [9].

Cancer plasticity

A defining feature of cancer complexity is its remarkable phenotypic plasticity [9]. During normal organ development, cells undergo terminal differentiation, a process in which they exit the cell cycle and acquire specialized functions that act as a barrier to uncontrolled proliferation. Cancer

cells, however, can evade this stable differentiated state by reverting to a more plastic, progenitor-like condition that facilitates adaptability, uncontrolled growth, and progression. This plasticity manifests in multiple ways: dedifferentiation (where mature cells revert to a less specialized state), blocked differentiation (where progenitor cells fail to complete differentiation), and transdifferentiation (where cells switch from one lineage to another). Such processes are often driven by epigenetic reprogramming triggered by microenvironmental cues (**Figure I2**) [11].

Dedifferentiation involves mature cells losing their specialized traits and regaining stem-like features, increasing their capacity for tumor growth, invasion, and metastasis (**Figure I2A**). This process is frequently driven by the upregulation of developmental transcription factors, such as HOXA5 and SMAD4 in colon carcinoma, or ATF2 in melanoma [12–14]. Blocked differentiation occurs when progenitor cells are unable to progress to a fully differentiated state (**Figure I2B**), as seen in acute promyelocytic leukemia, where a chromosomal translocation halts granulocyte maturation. It can also be induced by sustained expression of stem cell factors, such as SOX10 in melanoma, or metabolic alterations that impair differentiation, such as reduced α-ketoglutarate (αKG) in pancreatic cancer or oncometabolite accumulation from IDH mutations in liver cancer [15–17]. Blocked differentiation often correlates with dormant cells possessing stem-like properties capable of re-entering the cell cycle to promote metastasis or relapse [18]. Transdifferentiation describes the switch of one committed cell type into another and has been reporter in various cancers (**Figure I2C**). A classic example is Barrett's esophagus, where chronic inflammation induces the replacement of squamous epithelium by intestinal-like columnar cells [9]. Also, in pancreatic ductal adenocarcinoma, acinar cells can transition to a ductal phenotype through changes in transcription factors like PTF1a, MIST1, and SOX9 [19,20]. In prostate cancer, combined

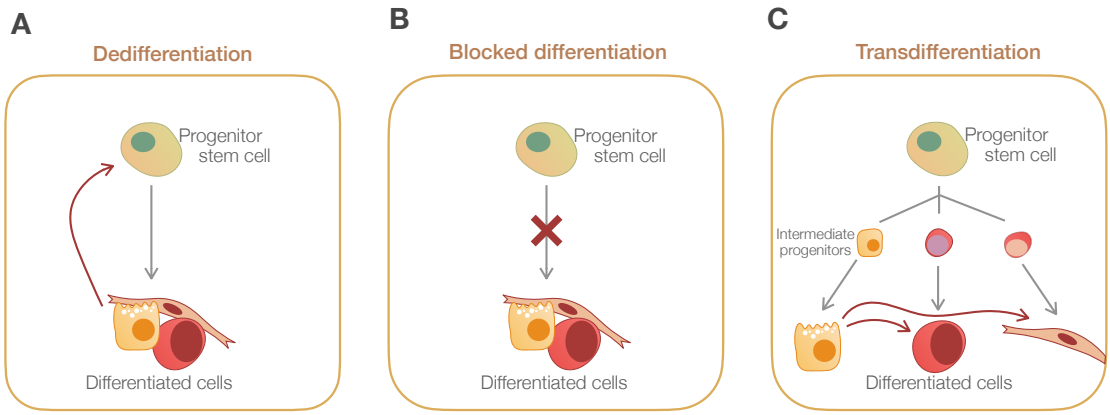

Figure I2. Plasticity is mainly driven by dedifferentation, blocked differentiation and transdifferentiation processes. A-C, Schematic representation of the dedifferentiation (**A**), blocked differentation (**B**), and transdifferentation (**C**).

loss of RB and p53 alongside SOX2 activation enables a switch from androgen receptor-positive adenocarcinoma to a neuroendocrine-like therapy-resistant state [21]. Epigenetically driven lineage switching has also been described as transdifferentiation driver, such as in basal cell carcinoma, where cells adopt a different basal stem cell identity, activating alternative signaling pathways and evading targeted therapies [22]. These lineage plasticity events, often governed by transcription factors and chromatin remodeling, allow cancer cells to evade lineage-specific treatments and promote tumor persistence.

Cancer stem cells

A key driver and consequence of the tumor plastic capacity is the presence of cancer stem cells (CSCs), a subpopulation capable of self-renewal and multilineage differentiation. Their inherent plasticity enables them to sustain tumor growth, generate intratumoral heterogeneity, and adapt to environmental or therapeutic pressures, fueling resistance and relapse [23].

The existence of CSCs was first demonstrated in 1997, when John Dick and Dominique Bonnet identified a population of acute myeloid leukemia cells with extensive proliferative potential, characterized by CD34+/CD38– surface markers [24]. These cells were uniquely capable of initiating leukemia in immunocompromised mice, providing the first direct evidence for a stem-like subpopulation driving tumor growth. Subsequent studies isolated CSCs from solid tumors, starting with breast cancer, where a CD44+/CD24–/low population was shown to form tumors upon transplantation [25]. Similar populations were identified in brain tumors, prostate, colorectal, and pancreatic cancers, underscoring the clinical relevance of CSCs [26–29].

Despite these advances, xenotransplantation assays revealed substantial heterogeneity within CSC populations. For instance, in acute myeloid leukemia, both CD34+/CD38– and CD34+/CD38+ cells demonstrated tumor-initiating potential [30]. Similarly, in breast cancer, an ALDH1+ population exhibited CSCs properties but did not completely overlap with the previously identified CD44+/CD24– subset [31]. These findings highlighted the dynamic, plastic nature of CSCs and tumors, where the frequency and phenotype of CSCs can shift over time in response to microenvironmental signals.

A major breakthrough in understanding CSCs came with lineage tracing technologies, which allow tracking of individual tumor cells and their progeny within their native microenvironment [32]. Unlike transplantation assays, lineage tracing preserves physiological interactions and revealed that CSCs exhibit dynamic clonal behaviors—some clones regress while others expand—further illustrating their contribution to tumor heterogeneity. For example, LGR5+ cells were identified

as CSCs in intestinal adenomas with self-renewal capacity, and similar dynamic behaviors were observed in breast CSCs [33,34].

Originally, CSCs were thought to exist within a rigid hierarchical structure resembling normal stem cell organization, where asymmetric division gives rise to one stem cell and one differentiated progenitor, that ultimately generate the proliferative differentiated tumoral population subclones (**Figure I3A**). However, lineage tracing studies showed that cancer cells can move bidirectionally within this hierarchy, undergoing differentiation, dedifferentiation, transdifferentiation, or blocked differentiation. This recognition of plasticity as a central feature of CSC biology reshaped our understanding of tumor organization [35]. CSCs can divide symmetrically or asymmetrically, switch between dormant and proliferative states, and adapt dynamically to niche signals, functioning as critical components of the tumor ecosystem (**Figure I3B**).

Their plasticity not only supports tumor maintenance but also facilitates metastatic colonization,

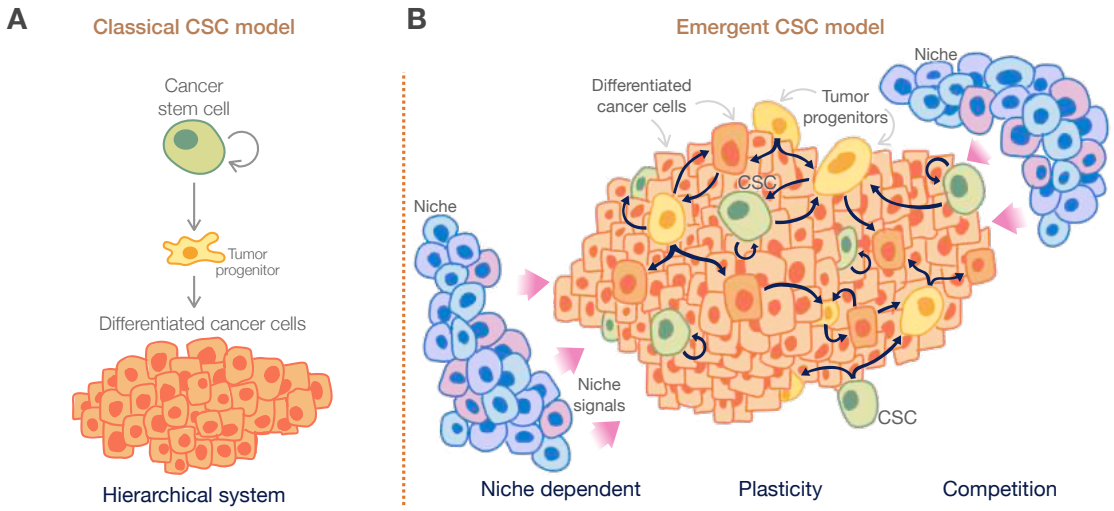

Figure I3. The CSC model evolved from a hierarchical system to an adaptive system. **A,** Representation of the classical CSC model, where CSCs self-renew and differentiate into progenitors, which in turn generate differentiated cancer cells, following a rigid organization. **B,** Representation of emergent CSC model, in which microenvironmental and tumor-derived cues drive plastic adaptation and interconversion between CSCs, progenitors, and differentiated cancer cells, forming a fluid and competitive system.

relapse, and dormancy. CSCs ability to transition between phenotypic states allows them to evade immune detection and survive hostile microenvironments, contributing to their long-term persistence. This adaptability underlies the resistance of many cancers to conventional therapies,

such as chemotherapy and radiotherapy, which primarily target rapidly dividing cells but often spare quiescent CSCs that can regenerate tumors after treatment [35]. Consequently, developing therapies that specifically target CSCs by disrupting their self-renewal, metabolic dependencies, or epigenetic regulators has become a critical priority.

Importantly, CSCs should be viewed as a dynamic state rather than a fixed identity, given their continuous phenotypic transformations. Targeting a single CSC subset risks therapeutic escape through phenotypic shifts, emphasizing the need to understand CSC plasticity within the broader context of the tumor microenvironment and cellular hierarchy. Moreover, pathways that regulate normal organ development and differentiation are frequently hijacked by cancer cells to facilitate the plastic transitions that define the CSC state, linking cancer pathogenesis to developmental biology.

Mammary gland

The mammary gland is a highly plastic tissue that undergoes extensive remodeling during puberty, pregnancy, lactation and involution [36].

This organ's development is largely postnatal and uniquely responsive to hormonal cues, allowing for cyclical and reversible transitions in structure and function across reproductive stages [37]. Its tightly coordinated morphogenesis and regeneration are controlled by signaling pathways that are often dysregulated in cancer, highlighting the relevance for understanding how normal developmental programs are co-opted during tumorigenesis.

Mammary gland morphological structure

The mammary gland is organized as a tree branching tubular network embedded within a connective stromal and adipose tissue. The ducts radiate from bunch of grapes-like alveolar structures called lobules, which are the functional units of milk production, and terminate at the nipple, where milk is ejected (**Figure I4A**). Both ducts and lobules consist of a bilayered epithelium supported by a collagen-rich extracellular matrix (ECM) forming the basement membrane. This membrane is surrounded by stromal fibroblasts and immune cells embedded in the adipocyte-rich fat pad (**Figure I4B**) [36].

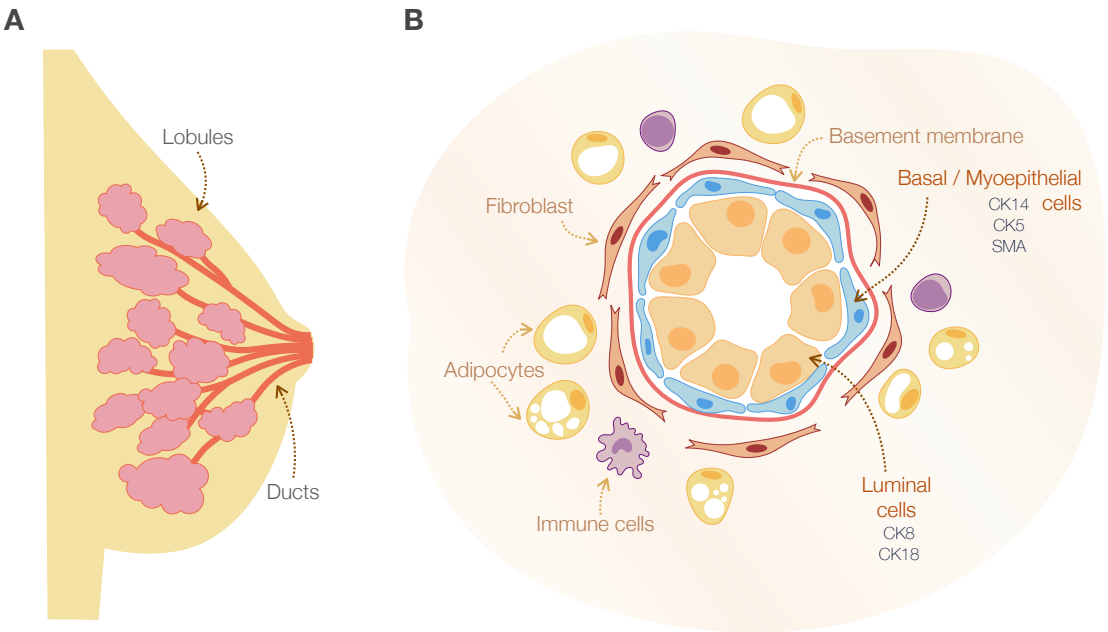

Figure I4. Mammary gland architecture and cellular organization. A, Schematic representation of the structure of the mammary gland. **B,** Cellular distribution within mammary gland ducts and lobules.

The epithelial bilayer is arranged concentrically and comprises luminal and basal cells [37]. Luminal epithelial cells are polarized cells that face the duct or alveolar lumen and express Cytokeratins 8 and 18 (CK8 and CK18, respectively), along with adhesion molecules such as E-cadherin and EpCAM, that highlight their strong epithelial feature. Luminal cells include alveolar cells (milk-producing in lobules) and ductal cells (lining at ducts), with the latter housing hormone-sensitive populations expressing estrogen and progesterone receptors (ER and PR, respectively) that signal alveolar cells to initiate milk production. Basal myoepithelial cells, that surround luminal cells, contact the basement membrane, and possess contractile properties essential for milk ejection and tissue remodeling. They express high molecular weight cytokeratins (such as 5 and 14, CK5 and CK14, respectively) and smooth muscle actin (SMA), coordinating tissue architecture and maintaining epithelial integrity (**Figure I4B**).

While the epithelial bilayer is central to mammary gland function, its activity is tightly regulated by interactions with the surrounding microenvironment. Among the key stromal regulators are fibroblasts, residing in the adipose-rich fat pad. Fibroblasts produce ECM components like type I collagen, facilitating ductal branching by remodeling the matrix via proteolytic enzymes such as matrix metalloproteinases (MMPs) [38,39]. They also release growth factors to regulate epithelial cell proliferation and differentiation processes [40,41]. In addition to fibroblasts, the mammary gland microenvironment contains adipocytes, that serve as lipid reservoirs needed for milk synthesis and support angiogenesis to vascularize the fat pad. Meanwhile, immune cells, particularly macrophages and neutrophils, assist in development and remodeling, mainly during involution, by promoting epithelial apoptosis and adipocyte repopulation, and inhibiting epithelial expansion during quiescence [42]. Together, these cell populations coordinate mammary gland homeostasis and adaptation through life stages.

Mammary gland development

Mammary gland development is hormonally regulated and occurs in three major stages: (1) embryonic development, (2) puberty, and (3) pregnancy, lactation and involution cycles (**Figure I5A**).

Embryonic development

Development begins at mid-gestation with epithelial-mesenchymal interactions. The mammary lines form from ectoderm thickening, giving rise to mammary placodes—early epithelial structures committed to the mammary lineage. This is regulated by transcription factors like TBX3, LEF1, and GLI3 via Wnt/β-catenin signaling [43]. In mice, mammary lines and placodes appear around embryonic day (E) 10.5–11.5. By E13.5, placodes invaginate into the mesenchyme to

form mammary buds, which elongate by E15.5 into the fat pad precursors, establishing a rudimentary ductal tree by E18.5. At this point, the gland enters into a relatively quiescent state until puberty [44].

Puberty

Puberty triggers branching morphogenesis under estrogen and growth hormone influence. The leading structures in this process are the terminal end buds (TEBs), highly proliferative, multilayered epithelial structures located at the tips of growing ducts [42].

TEBs comprise the cap cells (outer layer), that are migratory cells responsible for ductal invasion, and the body cells (inner region), which constitute proliferative cells contributing to duct elongation (**Figure I5B**). TEB morphogenesis is a dual process which involves epithelial-to-mesenchymal transition (EMT) of cap cells to induce the expansion, and apoptosis in body cells to shape ductal lumens. This process is tightly regulated by key signaling pathways including those of WNT and TGF-β, with regulators like OVOL2 controlling EMT-related genes.

Interestingly, during this developmental stage, key transcriptional regulators necessary for future lactational function are activated. GATA3 is present in the body cells where it is vital for the luminal cell lineage specification. In partnership with FOXA1, GATA3 boosts the accessibility of estrogen receptor chromatin, which is essential for branching and establishing estrogen-

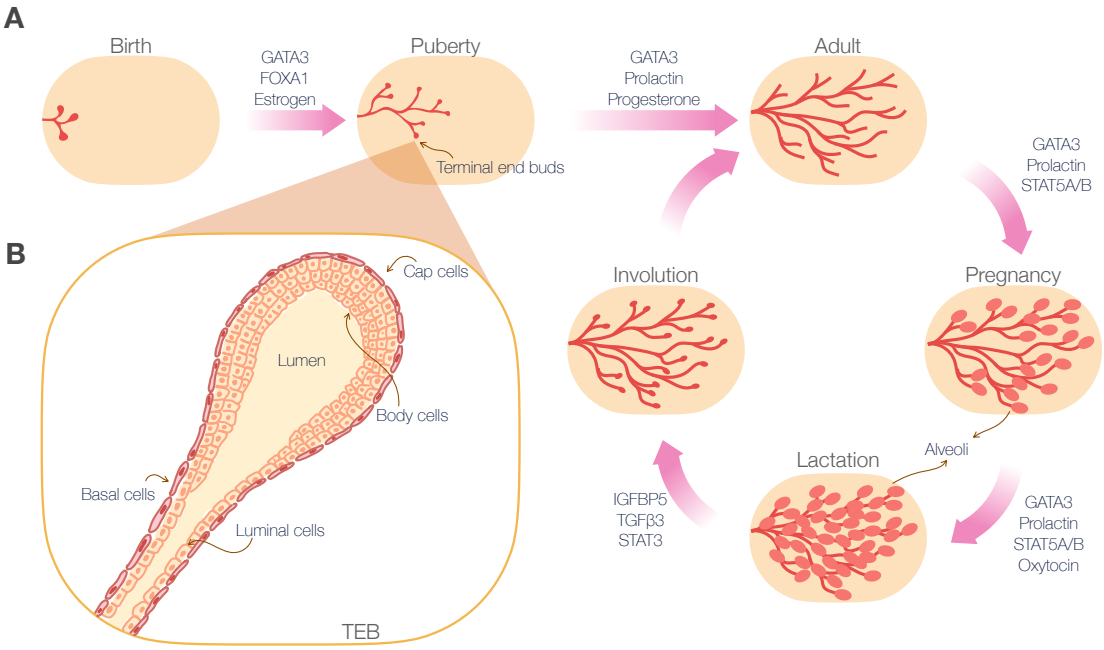

Figure I5. Mammary gland development process. A, Stages of mammary gland development, from embryonic formation to adult tissue maturation. **B,** Morphological structure of the terminal end bud (TEB) at puberty.

responsive cell lineages crucial for proper mammary gland development and subsequent lactational activity [44].

Pregnancy-lactation-involution

During the adulthood at pregnancy, the mammary gland undergoes proliferation and apoptosis cycles, regulated by ovarian hormones. Mainly, progesterone (P) promotes side branching and alveolar expansion, in tight coordination with prolactin (PRL) [41].

At pregnancy, P, PRL, and estrogen (E) drive further secondary and tertiary branching and alveologenesis [45]. P activates Wnt/β-catenin signaling to promote alveolar formation. Then, luminal epithelial cells differentiate into secretory alveolar cells under PRL signaling. Meanwhile, sustained high P levels during pregnancy downregulate PRL receptors, temporarily inhibiting milk production until birth. During this process, GATA3 expression in luminal cells becomes critical for alveolar lineage commitment.

At parturition, the drop in progesterone lifts repression, allowing PRL to activate PRL receptors and STAT5, inducing milk protein expression and secretory differentiation [45]. Post-lactation involution involves epithelial cell apoptosis and thus reconstitution of adult mammary gland structure to a normal state. At this process, macrophage- and eosinophil-mediated phagocytosis, and ECM remodeling by fibroblast-secreted MMPs, have an important role in restoring the gland to this pre-pregnancy state [42].

Mammary gland stem cells and progenitors

The development of the mammary gland throughout its various stages is intrinsically linked to the behavior and differentiation of mammary stem cells (MaSCs) and progenitor populations. These cells are the reservoirs that continuously fuel the remodeling and expansion of the gland.

MaSCs were first functionally characterized in 1959, by transplantation assays showing that mammary epithelium fragments can regenerate ducts [46]. These cells reside mainly in the basal epithelial layer, particularly in active growth zones like the TEBs [47,48]. They have been identified by several surface molecules such as CD49f, CD29, LGR5, and AXIN2 [49–53]. However, no single marker uniquely defines them due to their high heterogeneity.

Early embryonic and pubertal stem epithelial cells co-express luminal and basal genes, reflecting high multipotency, which is subsequently reduced upon adulthood. Indeed, functional studies revealed that adult stem cells often act as unipotent progenitors maintaining either luminal or basal lineages. Still, certain populations can exhibit bipotency in specific conditions, such as

hormone-responsive AXIN2+ cells during pregnancy, highlighting their plasticity and microenvironmental responsiveness [54].

Over time, MaSCs commit to lineage-restricted states as luminal and basal progenitors [41]. That happens especially during pregnancy, when luminal progenitors bifurcate into estrogen receptor-positive (ER+) or -negative (ER–) precursors. In this context, ER– progenitors (expressing CD61, c-KIT, ELF5) expand to support alveologenesis, while ER+ progenitors (expressing SCA1, FOXA1) contribute to ductal and hormone-sensing lineages (**Figure I6**).

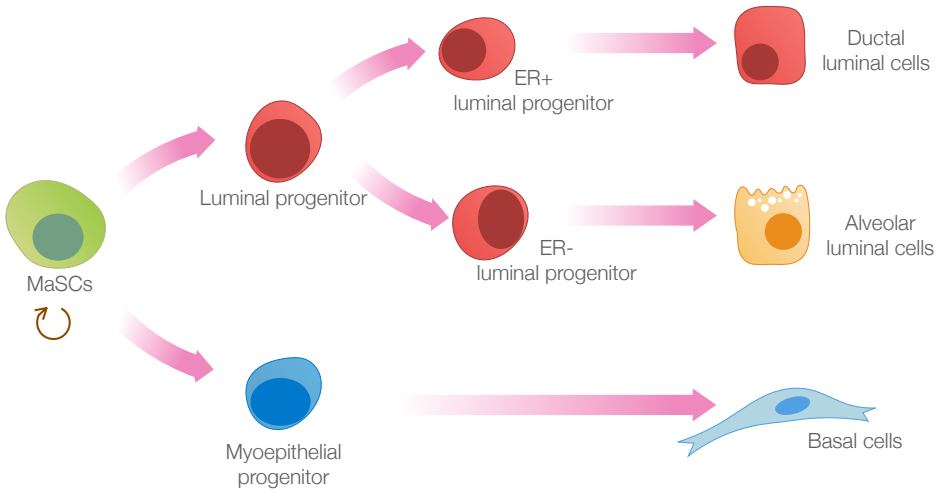

Figure I6. Hierarchical differentiation from MaSCs to mature luminal and basal cells. MaSCs are capable of self-renew and generate bi-potent progenitors, which subsequently differentiate into myoepithelial (basal) and luminal lineages.

Adding further complexity, a subset of MaSCs remains quiescent as a long-term regenerative reservoir, activated by hormonal signals, injury, or stress, acting as a supportive highly stem population [37]. This plasticity is essential for normal gland function but can also be hijacked in cancer to promote tumor growth and metastasis.

Breast cancer

As described above, the mammary gland is a highly dynamic organ, undergoing cyclic remodeling from puberty throughout adulthood. However, this normal developmental process can become dysregulated, potentially leading to cancer.

Breast cancer remains the most frequently diagnosed cancer among women worldwide, with approximately 2.3 million new cases and 670 000 deaths reported in 2022 alone [55]. Representing about one-quarter of all new female cancer cases and over 15 % of cancer-related deaths, breast cancer is a major cause of morbidity and mortality across nearly every country.

One of the challenges in understanding and treating breast cancer lies in its marked heterogeneity. This variability exists not only between distinct molecular and histological subtypes but also within individual tumors, where cancer cells display diverse phenotypes and behaviors.

Classification of breast cancer

Histologically, breast cancer is classified based on the affected mammary gland component and the extent of tumor invasion. Tumors may arise from the ducts or lobules and can be classified as *in situ* when confined to the epithelial layer, or invasive when they infiltrate the surrounding stroma (**Figure I7A**). The most common type is invasive ductal carcinoma (IDC), accounting for 50 to 80 % of all cases, followed by ductal carcinoma *in situ* (DCIS), which represents about 20 % of new diagnoses. Invasive lobular carcinoma (ILC) constitutes 5-15 % of breast cancers and is generally associated with a poorer prognosis than ductal forms [56]. Less common histological types, such as medullary, apocrine, and mucinous carcinomas, occur infrequently but contribute to the overall diversity of breast cancer pathology.

Grading tumors provides additional prognostic insight for breast cancer classification. The Nottingham histologic score assesses differentiation based on tubule formation, mitotic activity, and nuclear pleomorphism, categorizing tumors into three grades. Well-differentiated grade I tumors tend to grow slowly and resemble normal cells, whereas grade III tumors are poorly differentiated and often aggressive, and grade II tumors display intermediate features with a moderate degree of dedifferentiation [57].

Beyond histology, breast cancer can be classified by the number of tumor foci present [58]. Unifocal cancers involve a single tumor, while multifocal and multicentric breast cancers include multiple

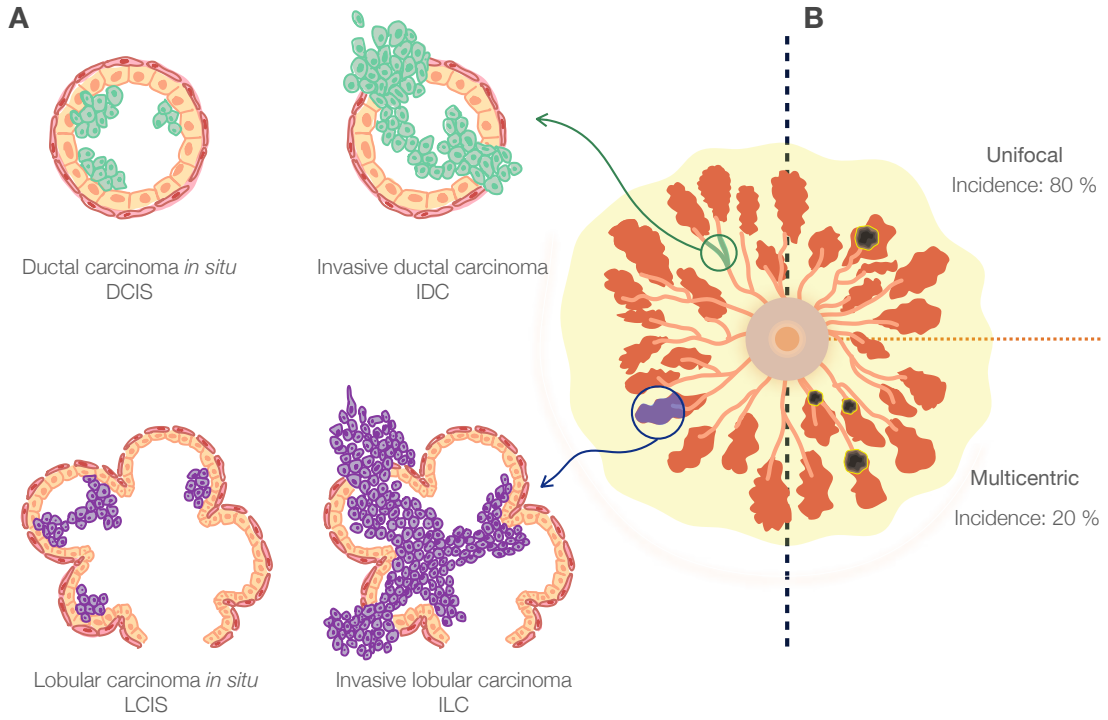

Figure I7. Histological classification of mammary gland tumors. **A,** Representation of tumor types based on histological location within ducts or lobules, and on their growth as *in situ* or invasive. **B,** Classification of tumors according to foci: unifocal tumors contain a single focus, whereas multicentric/multifocal tumors present multiple foci.

tumors within the same breast (**Figure I7B**). Multifocal tumors—multiple foci present in the same quadrant of the mammary gland—and multicentric tumors —foci present in different quadrants of the gland— are often used interchangeably in the literature due to their subtle distinction, and together represent about 20 % of cases. Historically, multicentric disease was treated with mastectomy, but evidence now supports breast-conserving surgery for both unifocal and multifocal tumors, as long as clear surgical margins are achieved [59–62].

Staging of breast cancer utilizes the TNM system, established by the American Joint Committee on Cancer (AJCC), which evaluates tumor size (T), lymph node involvement (N), and distant metastases (M). The combined TNM stage goes from 0 to IV summarizing local and distant disease extent [63]. This staging framework helps guide prognosis and treatment decisions.

Despite its utility, morphological and pathological classification alone cannot fully predict breast cancer behavior. Molecular classification, based on gene expression profiles, has revolutionized our understanding of the disease [64,65]. Established by Perou and Sorlie in 2001, molecular subtypes categorize breast tumors into four main groups based on the expression of estrogen receptor (ER), progesterone receptor (PR), human epidermal growth factor receptor 2 (HER2), and KI67

proliferation marker: luminal A, luminal B, HER2-positive (HER2+), and triple negative (**Figure I8**). These biomarkers underpin routine clinical classification and guide therapy choices. However, advances in technology have led to multigene assays —such as PAM50, MammaPrint, and Oncotype DX— which analyze the expression of multiple genes and provide more accurate assessments of recurrence risk while predicting the potential benefit of targeted treatments [63].

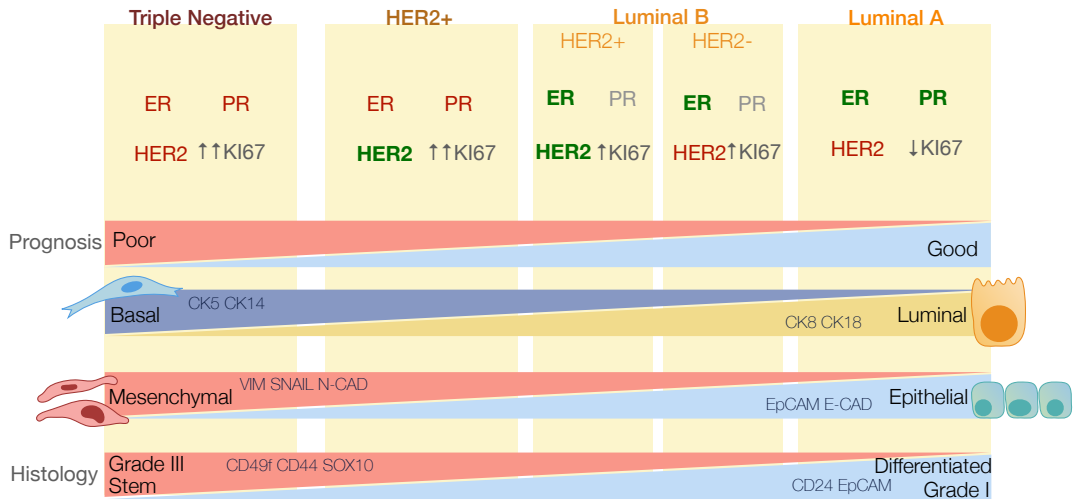

Figure I8. Molecular classification of breast cancer. Subtypes are defined based on ER, PR, HER2 and KI67 status (markers shown in green when are expressed and in red when are not expressed). The molecular classification is further correlated with prognosis, ranging from poor to good, and with biological features: basal–luminal identity, mesenchymal–epithelial state, and stem–differentiated characteristics.

Luminal A tumors, the most common subtype, typically express ER and high levels of PR, with low HER2 and Ki67, resembling mature luminal epithelial cells. They generally carry a favorable prognosis associated to histological grade I and respond well to endocrine therapies such as selective estrogen receptor modulators as tamoxifen and aromatase inhibitors such as anastrozole.

Luminal B are more aggressive and heterogeneous than luminal A tumors, although they also express high levels of hormone receptors, and account for 20-30 % of breast cancers. Subdivided based on HER2 status, they tend to show lower PR expression and higher proliferation rates than luminal A subtype. Treatment often combines endocrine therapy with chemotherapy, with HER2-targeted agents added when appropriate.

HER2+ tumors represent 15-20 % of new diagnoses. They lack hormone receptor expression but exhibit HER2 overexpression, driving aggressive oncogenic signaling. Historically associated with poor outcomes, the introduction of HER2-targeted therapies like the humanized anti-HER2 monoclonal antibody trastuzumab has significantly improved patient survival.

Triple negative breast cancer (TNBC) represents around 10 % of cases and are defined by the absence of ER, PR and HER2 expression, along with high proliferative activity. They are typically high-grade tumors with a poor prognosis and high metastatic potential. TNBC displays notable heterogeneity, including subtypes such as claudin-low —the most undifferentiated and aggressive form— and mesenchymal-like tumors, complicating treatment due to the lack of effective targeted therapies. Chemotherapy remains the mainstay, with emerging options such as PARP inhibitors for select patients.

Heterogeneity of breast cancer

This molecular diversity at tumor subtypes mirrors the complexity of the normal mammary epithelial hierarchy [41]. The most undifferentiated claudin-low tumors resemble the dormant MaSCs subset. Meanwhile, the luminal lineage correlates with the rest of the subtypes. The luminal progenitor subset shares a similar molecular profile with basal-like tumors, which resemble ER- luminal progenitors. And the remaining luminal maturation reflects the HER2+, luminal B and luminal A subtypes, with luminal A showing the closest resemblance to mature luminal cells (**Figure I9**).

These similarities between subtypes and distinct mammary cell lineages suggest that breast cancer arises from aberrant transformation of specific progenitor or stem cell populations. However, studies with mouse models revealed that this relationship is not straightforward, emphasizing the intrinsic plasticity of mammary epithelial cells and their ability to adapt to differentiation states [66,67].

It may be due to this intrinsic plasticity that no single driver mutation dominates across all breast cancers, but several recurrent oncogenic genes are implicated in particular contexts such as MYC, GATA3, FOXA1, MLL3 or even epigenetic modulation. Amplification of MYC is linked to ER-negative tumors and poor prognosis, and epigenetically reprograms cells toward stem-like, tumor initiating phenotypes. GATA3 mutations are associated with ER-positive tumors and promote luminal differentiation, often correlating with disease progression [36]. FOXA1 regulates steroid receptor activity and epigenetic modifications, with mutations linked to better outcomes [68]. MLL3 and other histone methyltransferases frequently harbor loss-of-function mutations contributing to tumor epigenetics, stemness, and aggressive phenotypes [69,70]. DNA methylation patterns also reflect molecular subtype distinctions and offer prognostic value [71].

Adding to tumor heterogeneity, breast cancers also contain diverse non-cancerous cell types that interact with tumor cells and evolve alongside them, further increasing tumor complexity. The

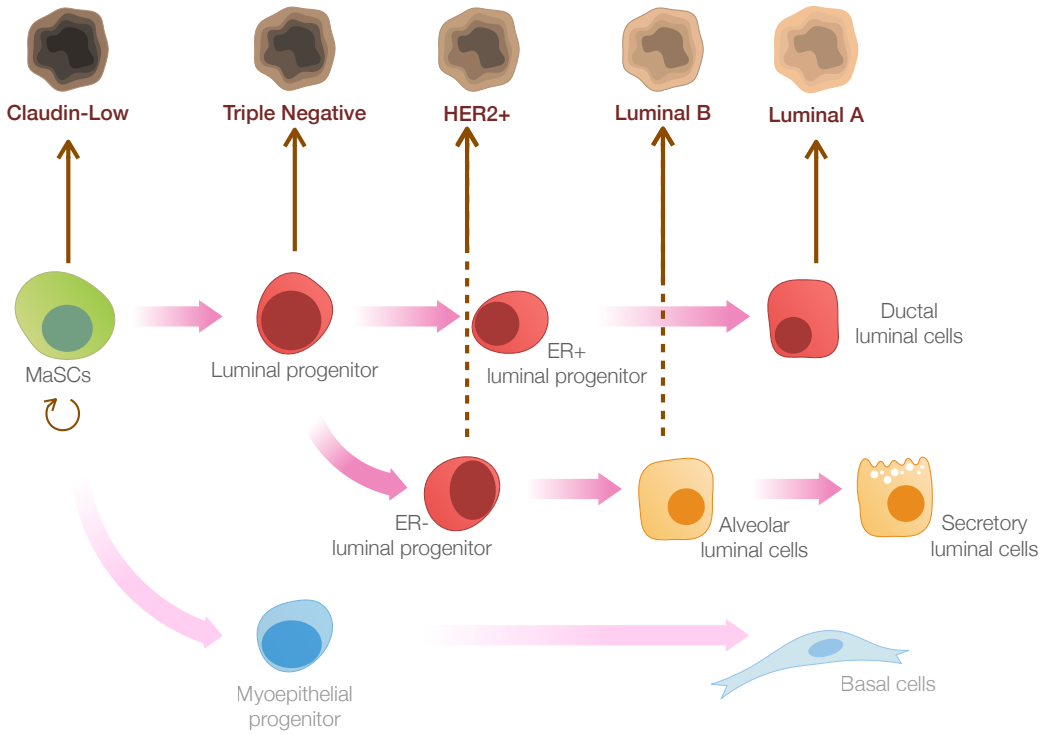

Figure I9. Schematic correlation between breast cancer subtypes and mammary gland epithelial hierarchy. Upper part represents the different molecular subtypes of breast cancer. Below, the scheme illustrates the corresponding normal mammary epithelial cell types and their relative state of differentiation, highlighting how tumor subtypes relate to the healthy mammary epithelial hierarchy.

tumor microenvironment, composed of immune cells, fibroblasts, and other stromal components, plays a critical role in tumor progression and plasticity. For example, cancer-associated fibroblasts (CAFs) modulate growth and invasion by remodeling the extracellular matrix and secreting cytokines —functions that mirror the role of normal fibroblasts in mammary gland development during puberty and reproductive cycles [72]. Tumor-associated macrophages (TAMs) contribute to enhanced stemness and metastasis through factors like TGF-β, while myeloid-derived suppressor cells promote stemness via IL-6 and nitric oxide signaling pathways [73,74].

Breast cancer stem cells

Within this complex milieu, breast cancer stem cells (BCSCs) represent a subpopulation with self-renewal and differentiation capabilities, driving tumor initiation, progression, metastasis and resistance to therapy [75].

Initially identified by markers such as CD44+/CD24– and ALDH1+, BCSCs exhibit metabolic flexibility, switching between glycolysis and oxidative phosphorylation to adapt to microenvironmental conditions. They also undergo EMT and revert via mesenchymal-to-epithelial transition (MET), enabling invasion, dissemination, and colonization at distant sites [76]. In addition, BCSCs express stemness-associated transcription factors such as SOX2, NANOG, and OCT4 —which are absent in normal MaSCs but are essential for maintaining pluripotency and preventing differentiation of CSCs [75].

These key properties of BCSCs are modulated by complex signaling pathways (**Figure I10**) [77]. Among them, the Wnt/β-catenin pathway is particularly prominent, driving self-renewal and drug resistance. NF-κB signaling overactivation in BCSCs promotes chemoresistance and facilitates EMT, enhancing the acquisition of mesenchymal traits. Similarly, the Hippo/YAP pathway becomes oncogenically activated promoting cellular invasion in cancer context. TGF-β signaling

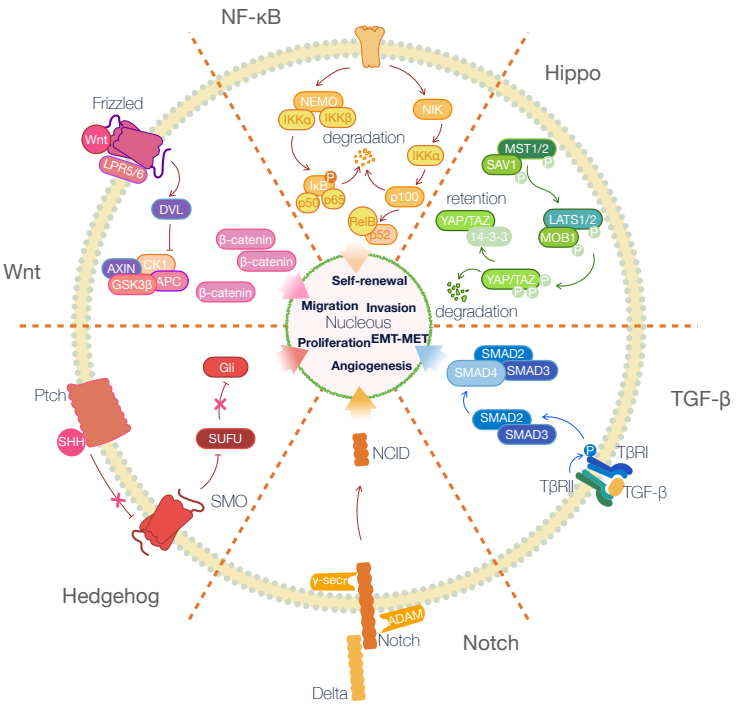

Figure I10. Main signaling pathways altered at BCSCs. The Wnt, NF-KB, Hippo, TGF-β, Notch and Hedgehog pathway elements are overexpressed in breast cancer stem cells, and regulate key features, inducing self-renewal and stemness potential.

contributes to apoptosis resistance and metastasis. The Notch pathway, essential for normal mammary stem cell regulation, is linked in breast cancer to poor prognosis and angiogenesis. Hedgehog signaling reactivates in cancer to block differentiation and reinforce stemness. Notably, the interplay and dynamic regulation of these pathways allow BCSCs to adapt, expand, and sustain tumor growth despite therapeutic pressures. Thus, several components of these pathways are targets for therapeutic elimination of CSCs in breast cancer [23,77].

Importantly, BCSCs themselves are heterogeneous, with varying pathway activation depending on tumor subtype and stage. This plasticity underlies their resilience, and the challenges faced in developing effective targeted therapies. Understanding and disrupting the intricate signaling networks of BCSCs holds promise for improving breast cancer treatment and preventing relapse.

This biological complexity and heterogeneity of breast cancer, together with the dynamic nature of BCSCs, require robust experimental systems capable of recapitulating tumor behavior and differential potential. Transgenic mouse models, such as MMTV-PyMT, C3(1)-SV40, MMTV-Neu or MMTV-WNT1, have been crucial in breast cancer research [78]. These models reproduce key molecular subtypes and pathological features of the disease, enabling the modeling of heterogeneity in tumor initiation, progression, and metastasis *in vivo*. Patient-derived xenografts (PDXs) further enhance this translational relevance by preserving the molecular and cellular diversity of primary tumors, including the plasticity of stem-like populations. However, classical PDX models are limited by immunodeficiency, which constrains the study of tumor-microenvironment interactions [79]. Humanized PDX models, in which mice are engrafted with human immune cells, partially overcome this limitation, allowing the recapitulation of tumor-immune dynamics, thereby enhancing the representation of tumor-stroma heterogeneity [80].

In parallel, *in vitro* analysis have advanced beyond traditional 2D cultures that fail to reproduce heterogeneity and cell-to-cell interactions, towards primary 3D organoid cultures which maintained tumor architecture and variability, more closely mimicking tumor biology and plasticit. To further emulate the tumor dynamics and integrate the environmental factors, microfluidic organ-on-chip systems incorporate multiple cell lineages within perfused 3D matrix, recreating dynamic cell-cell communication and tumor-stroma crosstalk (**Figure I11**) [80]. Altogether, these approaches enable the study of tumor heterogeneity and BCSCs dynamics, accelerating the development of targeted therapies.

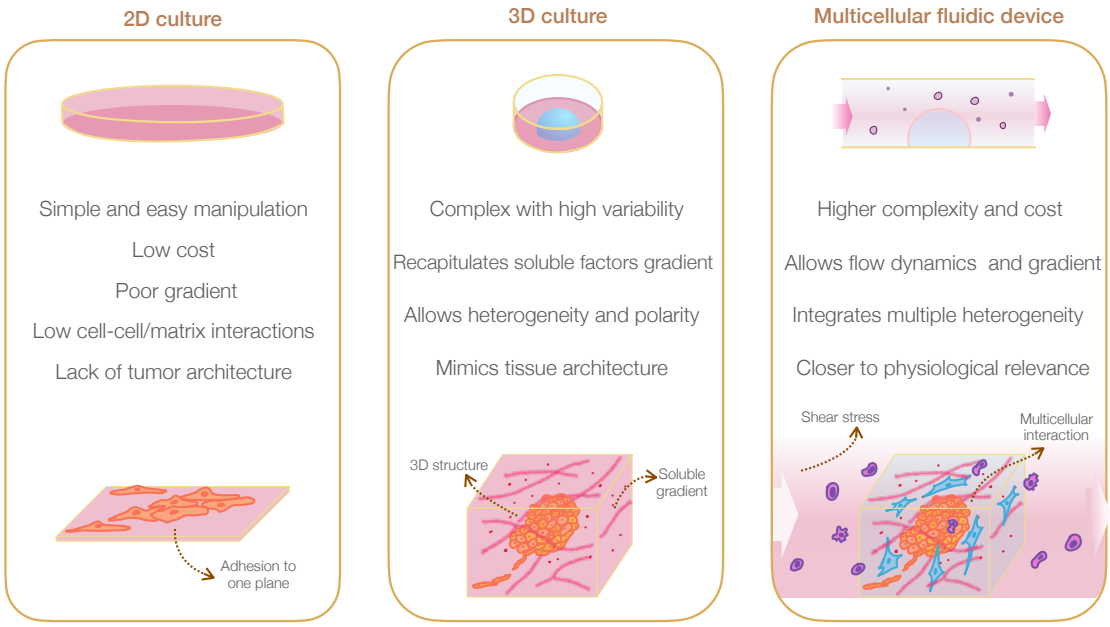

Figure I11. Schematic representation of primary cell culture methods used to model tumor biology. In 2D culture, cells grow as a monolayer, lacking physiological architecture. In 3D culture, cells are embedded within an extracellular matrix (ECM), matrigel, enabling organoid formation that better mimics tissue organization and soluble factor gradients. The multicellular microfluidic device integrates multiple cell types under dynamic flow conditions, recreating the physiological features of invasion and tumor heterogeneity with higher fidelity than the previous static systems.

Differentiation therapies in cancer

As described above, CSCs, including BCSCs, are highly heterogeneous tumor cell subpopulations defined by their ability to self-renew and their remarkable plasticity. Many therapeutic strategies have attempted to eradicate these cells completely, but their dynamic nature often allows them to evade treatment and develop resistance, thereby sustaining tumor growth and recurrence. In recent years, differentiation therapies have emerged as a promising approach aimed at reversing the aggressive stem-like phenotype. By promoting differentiation, these therapies suppress invasive properties and enhance tumor cell sensitivity to chemotherapy and other conventional treatments.

Emergence of differentiation therapies

The concept of differentiation therapy targeting CSCs first gained traction in the 1980s with the use of retinoic acid (RA) to treat acute promyeolocytic leukemia (APL), a subtype of myeloid leukemia [81]. APL is driven by a specific chromosomal translocation, t(15;17), which generates a fusion protein between promyelocytic leukemia protein (PML) and RA receptor α (RARα), known as PML-RARα. Under normal conditions, RARα binds RA and regulates differentiation in embryonic stem cells and myeloid lineages, while PML is involved in nuclear body formation, controlling post-transcriptional modifications and activating p53 to regulate apoptosis and senescence [82].

In APL, the PML-RARα fusion protein reduces the DNA-binding specificity of RARα, leading to epigenetic repression of differentiation genes and disrupting PML nuclear bodies, which impairs p53 signaling. At treatment, RA binds to the RARα portion of fusion protein, displaces co-repressors, reverses epigenetic silencing, and induces terminal differentiation of leukemic cells. Moreover, RA promotes degradation of the fusion protein, restoring PML nuclear body formation and reactivating p53 pathways [83]. This remarkable success established RA as a prototype for differentiation therapy.

Following this, RA and its derivatives were evaluated in other acute myeloid leukemias and later extended to solid tumors (**Figure I12**). The first differentiation-induction approaches in solid tumors were in neuroblastoma, where 13-cis RA effectively induced morphological changes resembling normal neural differentiation and maturation [84]. This treatment downregulated MYCN, a gene highly amplified in neuroblastoma, leading to growth arrest and increased

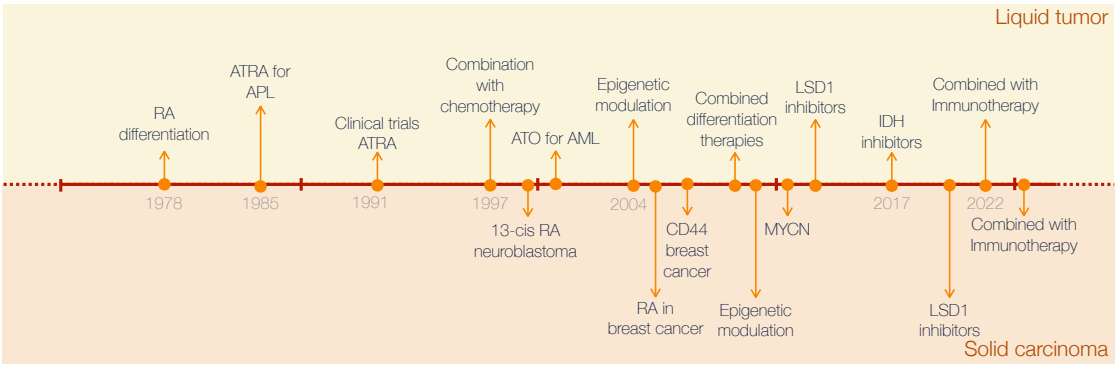

Figure I12. Timeline of the evolution of differentiation therapies. The upper panel outlines the historical trajectory of differentiation therapies in hematological malignancies, where pioneering work with retinoic acid (RA) and its derivative all-trans retinoic acid (ATRA) revolutionized the treatment of acute promyelocytic leukemia (APL). Their success, later consolidated through clinical trials, combinations with chemotherapy, and the addition of arsenic trioxide (ATO) in acute myeloid leukemia (AML), established a paradigm for targeted differentiation strategies. Building on this foundation, more recent approaches include isocitrate dehydrogenase (IDH) and lysine-specific demethylase 1 (LSD1) inhibitors, which are often evaluated alongside epigenetic modulation or immunotherapy to overcome resistance and broaden efficacy. The lower panel illustrates how these principles have been progressively translated into solid tumors. Early efforts with 13-cis RA in neuroblastoma and exploratory trials of RA in breast cancer opened the field, while subsequent studies identified CD44 as a marker and therapeutic target in breast cancer. More recent developments include strategies directed against MYCN in neuroblastoma and the adaptation of LSD1 inhibitors in solid tumor contexts, again frequently tested in combination with immunotherapy.

progression-free survival. Subsequently, RA derivatives have been explored in breast cancer, cervical carcinoma, lung cancer, hepatocellular carcinoma, and gliomas [83].

Despite RA's pivotal role in differentiation, its effectiveness is most pronounced in APL due to the direct targeting of the PML-RARα fusion protein and the relatively hierarchical nature of hematopoietic lineages. Solid tumors, by contrast, exhibit far greater complexity, including a higher mutational burden, strong tumor microenvironment interactions, and extensive cellular plasticity, all of which complicate differentiation-based therapeutic strategies.

Building on RA's role in regulating MYCN in neuroblastoma and considering that MYC family proteins are critical regulators of differentiation during development, modulating MYCN represents a potential differentiation strategy. MYCN is frequently overactivated in over 70 % of human cancers, including colorectal, hepatocellular, and prostate cancers. Thus, several MYCN inhibitors have been investigated as potential differentiation-inducing agents [85]. However,

targeting MYCN is challenging due to its essential functions in both normal and tumor cells, raising concerns about toxicity and off-target effects.

More recent differentiation approaches have focused on targeting epigenetic alterations, since some plastic characteristics that distinguish CSCs from the bulk tumor population are driven by epigenomic regulation. Histone deacetylase (HDAC) inhibitors, for example, have been used to induce differentiation in neuroblastoma in combination with 13-cis RA, and have also been explored in breast cancer, liver cancer, and acute myeloid leukemia [86–89]. Another target is EZH2, the catalytic subunit of Polycomb repressive complex 2 (PRC2), responsible for methylating H3K27. Inhibition of EZH2 with agents like berberine has successfully promoted differentiation in neuroblastoma models [90].

Despite notable advances in differentiation therapies over the past decade, these treatments often only delay disease progression, as resistance frequently arises through transcriptional reprogramming. A key challenge remains achieving terminal differentiation—a state in which cancer stem cells irreversibly adopt a mature phenotype, thereby preventing dedifferentiation and recurrence.

Differentiation-inducing drugs inevitably shift the balance between CSCs and the bulk tumor population, reshaping the tumor ecosystem that sustains growth and survival. However, these induced changes can sometimes lead to unintended consequences, including the emergence of new CSC populations. Thus, differentiation strategies should not only induce differentiation but also inhibit dedifferentiation processes. Crucially, future therapies must target the plastic capacity of tumor cells to regain stem-like properties, with the ultimate goal of halting tumor growth, invasion, metastasis, and relapse permanently.

Endocannabinoid system

To effectively target tumor stemness in breast cancer, it is essential to understand the molecular mechanisms regulating mammary gland development and homeostasis. Given the high plasticity of tumors, therapies targeting cancer-altered mechanisms that also function in normal developmental processes present a complex but promising approach to counter tumor adaptability and progression.

Notably, the endocannabinoid system (ECS) has been shown to play a key role in the development of multiple cell lineages, and its modulation influences tumor cell proliferation, metastasis, angiogenesis, and survival across various cancer types.

The ECS is a complex signaling network essential for maintaining physiological homeostasis. It was discovered in the 1990s during investigations into how cannabinoids from *Cannabis sativa* exert their effects [91]. This plant produces over 120 phytocannabinoids, of which Δ^9-tetrahydrocannabinol (THC) and cannabidiol (CBD) are the most abundant and therapeutically relevant. THC is the primary psychoactive compound, first characterized in 1964, while CBD, characterized in 1963, does not produce intoxicating effects [92,93].

Research into how these phytocannabinoids act led to the discovery of two cannabinoid receptors: type 1 cannabinoid receptor (CB_1R) and type 2 cannabinoid receptor (CB_2R) [91,94]. Soon after, endogenous ligands—endocannabinoids—were identified, along with enzymes responsible for their synthesis and degradation [95,96].

The ECS regulates numerous physiological processes, including appetite, pain perception, mood, energy balance, and immune function. Dysregulation—through altered receptor expression, endocannabinoid levels, or enzyme dysfunction—has been detected in conditions ranging from chronic pain and neurodegenerative diseases to cardiovascular disorders and various cancers, making it a compelling therapeutic target [97].

Components of the ECS

Cannabinoid receptors —CB_1R and CB_2R— are G protein-coupled receptors (GPCRs) with notable functional versatility in cellular signaling. They bind diverse type of ligands granting their adaptability across tissue types. They form both homo- or heterodimers with other receptors, which shapes their pharmacological properties and downstream effects. Additionally, cannabinoid receptors can localize either at the membrane and within intracellular

compartments, allowing them to play a role in various cellular processes [98]. This versatility enables activation of multiple signaling cascades to maintain homeostasis across cell types.

Upon activation, cannabinoids receptors most classically couple to $G\alpha_{i/o}$ proteins, inhibiting adenylate cyclase activity, which lowers cAMP levels and consequently reducing protein kinase A (PKA) signaling [99]. However, this is only part of their signaling repertoire; they can also engage alternative G protein subtypes and interact with a range of intracellular adapter proteins, broadening the scope of possible cellular responses. The downstream consequences of cannabinoid receptor modulation include regulation of mayor signaling pathways such as mitogen-activated protein kinases (MAPK) and the phosphoinositide 3-kinase-AKT/protein kinase B (PI3K-AKT/PKB) axis [99]. These cascades control critical cellular functions, like survival, proliferation, differentiation, and apoptosis. Through this spectrum of mechanisms, they maintain physiological balance and adapt cellular responses to changing environmental cues, underscoring their central role in the modulation of diverse biological processes.

CB_1R is highly expressed in the brain but is also found in peripheral organs including the adrenal glands, lungs, heart, prostate, and reproductive system, among others [100]. In contrast, CB_2R is predominantly expressed in immune cells and hematopoietic tissues, though it is also present in specific brain regions, intestine, liver, pancreas, and reproductive organs, to name a few [101]. Thus, CB_1R research often focuses on neural functions, while CB_2R studies emphasize immune regulation.

Cannabinoid receptors are regulated by short-lived lipid molecules called endocannabinoids (eCBs). The two main eCBs are 2-arachidonoylglycerol (2-AG) and N-arachidonoylethanolamine (anandamide, AEA) (**Figure I13**), although other arachidonic acid derivates such as N-arachidonyl dopamine, can also activate these receptors [102]. 2-AG is a full agonist at both CB_1R and CB_2R, whereas AEA acts as a partial agonist with lower intrinsic activity [103].

These lipids are synthesized from membrane phospholipids via enzymatic pathways: AEA production involves N-acyltransferase and N-arachidonoylphosphatidylethanolamine phospholipase D (NAPE-PLD) sequential action. This AEA is degraded by fatty acid amide hydrolase (FAAH). 2-AG is produced by phospholipase C (PLC)-mediated diacylglycerol (DAG) formation followed by diacylglycerol lipase (DAGLα/β) hydrolysis, and is primarily degraded by monoacylglycerol lipase (MAGL) [97].

Cannabinoids include not only endocannabinoids but also phytocannabinoids and synthetic cannabinoids. Phytocannabinoids are plant metabolites with different affinities for the

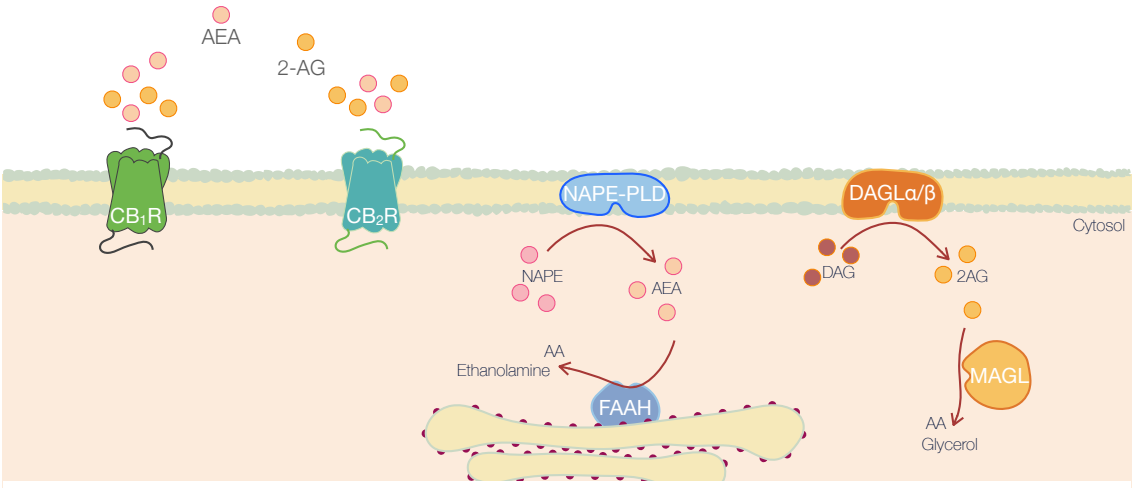

Figure I13. Main components of the endocannabinoid system. The ECS consists of two cannabinoid receptors (CB_1R and CB_2R), the endocannabinoid ligands: AEA and 2-AG, and the enzymes responsible for their synthesis (NAPE-PLD and DAGL) and degradation (FAAH and MAGL). In this pathway, arachidonic acid (AA) is a metabolic product derived from AEA and 2-AG degradation.

cannabinoid receptors that, when binding to them, can act as agonists, antagonists, or inverse agonists [104]. As previously mentioned, THC, the main plant psychoactive compound, acts as a partial agonist of both CB_1R and CB_2R, whereas CBD binds receptors with very low affinity [105]. Both have shown promise in modulating ECS activity in various diseases. In fact, a few cannabinoid-based drugs have been approved by the U.S. Food and Drug Administration (FDA) and the European Medicines Agency (EMA): the two phytocannabinoid-based formulations Epidiolex (CBD for pediatric seizures) and Sativex (a 1:1 THC:CBD ratio plant-derived extract for neuropathic pain and spasticity associated with multiple sclerosis), as well as the two synthetic THC analogs dronabinol and nabilone, which are used to combat chemotherapy-induced nausea and stimulate appetite [104].

Beyond these approved formulas, patients have traditionally made use of whole-plant cannabis preparations—including flowers, oils, extracts, and tinctures—for millennia to manage diverse conditions. These formulations contain not only phytocannabinoids but also other plant-derived constituents, such as terpenes, which may act in concert. In this context, the so-called “entourage effect” has been proposed, suggesting that multiple chemical components of *Cannabis sativa* could interact synergistically to produce enhanced therapeutic outcomes [106]. Although this remains a theoretical concept with limited supporting evidence, preclinical studies have begun to explore it; for example, in cell and animal models of the different subtypes of breast cancer, a cannabis

extract showed greater antitumor activity than pure THC, supporting the idea that whole-plant preparations may provide therapeutic advantages beyond single compounds [107].

On the other hand, synthetic cannabinoids have been developed to modulate ECS activity for research. Examples include selective agonists such as HU-210 for CB_1R, HU-308 or JWH-133 for CB_2R, as well as inverse agonists such as SR141716A (Rimonabant) for CB_1R or SR144528 for CB_2R [108,109].

In addition to their canonical signaling through CB_1R and CB_2R, cannabinoids can engage other non-canonical receptors such as GPR55, GPR18, GPR119, GPR92, nuclear receptors PPARα and PPARγ, and members of the TRPV family such as TRPV1 and TRPV2 [98].

The ECS and development

The ECS is highly expressed in the central nervous system (CNS) and in the immune system, thus it is well studied in neurotransmission and immunoregulation.

Indeed, the ECS is markedly upregulated during inflammatory processes in various immune cell types, including macrophages, T cells, and B cells. Primarily through CB_2R activation, the ECS mediates immunosuppression and regulates immune cell proliferation and apoptosis in response to inflammatory stimuli [101]. The ECS also directs migration and differentiation of hematopoietic progenitors primarily via CB_2R, cooperating with chemokine signaling [110,111].

In the CNS, the ECS acts as a neuromodulator by regulating neurotransmitter release. It contributes to differentiation and maturation of neural stem cells and progenitors through CB_1R [112,113] and CB_2R [114,115] activation, with their expression inversely correlated during differentiation [116].

Beyond the CNS, the ECS plays roles in early embryogenesis: AEA maintains embryonic stem cell survival during blastocyst formation, with CB_1R regulating trophoblast proliferation/differentiation and CB_2R maintaining pluripotency of inner cell mass cells[117]. The ECS also regulates differentiation of mesenchymal-derived cells: CB_2R promotes fibroblast maturation, CB_1R modulates adipocyte differentiation, and both receptors coordinate osteoblast maturation. In the epidermis, CB_1R and CB_2R have opposing roles in keratinocyte terminal differentiation [117].

Regarding the mammary gland, the ECS function remains poorly understood. It has been recently shown that adult mammary gland stem cells show elevated CB_1R expression, while luminal progenitors and mature luminal cells express higher CB_2R, suggesting receptor-specific roles. Also, anandamide appears to regulate luminal lineage differentiation primarily via CB_1R [118].

The ECS and cancer

ECS dysregulation occurs in various diseases, including cancer, involving altered receptor expression and endocannabinoid levels. Although the ECS contributes to tissue homeostasis, it remains unclear whether such disruption is a consequence of malignancy or a factor that facilitates or impairs tumorigenesis.

Elevated cannabinoid receptor expression has been reported in colon, liver and prostate cancers, and gliomas among others, where it correlates with invasion, proliferation, adhesion, and motility [119]. However, the role of the ECS in cancer progression remains poorly understood.

In breast cancer, ECS alterations predominantly involve CB_2R overexpression compared to normal tissue. CB_2R levels correlate with high histological grade and poor prognosis, particularly in HER2+ and TNBC subtypes. Although, CB_1R is detectable in breast cancer, its expression is low and does not show a strong association with specific subtypes or prognosis [120]. Interestingly, in HER2+ tumors, CB_2R forms heteromers with the HER2 oncoprotein, enhancing its pro-oncogenic signaling. In fact, it has been described that disrupting this interaction yields antitumor effects in preclinical models [121–123].

These insights have spurred research into endo-, phyto-, and synthetic cannabinoids as ECS modulators with potential antitumor actions in this type of cancer (**Figure I14**). The first evidence of cannabinoid antiproliferative effects in breast cancer was reported in 1998, when AEA was shown to inhibit breast cancer cell proliferation via CB_1R in breast cancer cell lines [124]. Subsequent studies further confirmed this effect with additional cannabinoids, including THC and CBD (via CB_2R), methanandamide, (metAEA, a synthetic AEA analog), and synthetic agonists such as WIN 55,212-2 (via CB_1R and CB_2R) and JWH-133 (via CB_2R) which were able to suppress cancer cell proliferation [120,122,125,126].

In addition to their antiproliferative action, cannabinoids also have been shown to impair the invasive capacity of breast cancer cell lines, primarily through CB_2R activation [120,125,127–132]. Moreover, studies using mouse models demonstrated that cannabinoids, including THC, reduced tumor growth, angiogenesis, and metastasis potential *in vivo* [122,123,125,127,129,132,133].

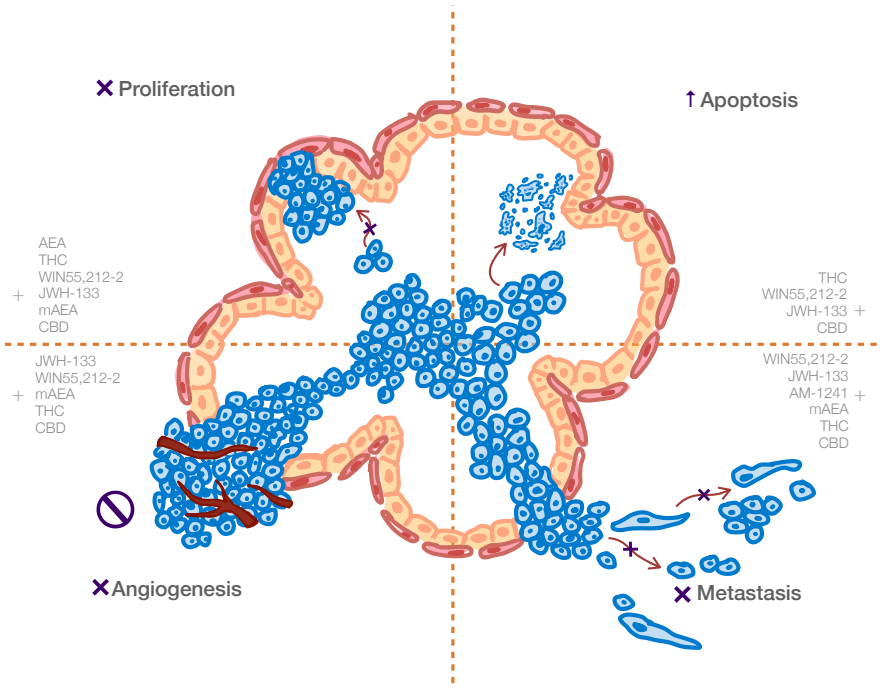

Figure I14. Cannabinoid effects on breast cancer. Cannabinoids modulate breast cancer progression through activation of the ECS by plant-derived, endogenous, or synthetic ligands, leading to inhibition of proliferation, induction of apoptosis, suppression of angiogenesis, and prevention of metastasis.

Despite promising effects on tumor growth and progression, the impact of cannabinoids on cancer cell plasticity—and the long-term consequences of the ECS modulation—remain largely unexplored in breast cancer. So far, only a few studies in gliomas have begun to investigate cannabinoid-induced differentiation, reporting a reduction in tumor-initiating capacity following ECS activation [134,135]. Although these findings are preliminary and limited to specific contexts, they underscore an underexplored therapeutic opportunity: harnessing the ECS to promote cancer cell differentiation. In breast cancer and other malignancies characterized by high plasticity, further elucidation of ECS-driven differentiation programs may offer a promising, less toxic strategy to curb stemness, adaptability, and disease progression.

MicroRNAs

microRNAs (miRNAs) act as endogenous post-transcriptional regulators that orchestrate gene expression programs involved in mammary gland development, cellular identity, and tissue remodeling [136]. Their dysregulation in cancer disrupts these finely tuned networks, contributing to aberrant plasticity, therapy resistance, and tumor progression.

miRNAs are small non-coding RNA molecules, typically 19 to 24 nucleotides in length, that regulate gene expression by binding complementary sequences in the 3' untranslated regions (3' UTRs) of target messenger RNAs (mRNAs), leading to translational repression or mRNA degradation (**Figure I15**) [137]. miRNAs were first discovered in 1993 in the model organism *Caenorhabditis elegans*, when the microRNA lin-4 was shown to control differentiation during embryogenesis [138]. The first human miRNA was later discovered in 2000 [139]. Since then, thousands of miRNAs have been annotated in databases such as miRBase, which currently catalogs nearly 50 000 sequences.

Beyond their fundamental roles in development and differentiation, miRNAs are essential for maintaining tissue homeostasis. Notably, their functional relevance often becomes pronounced under stress or injury; for instance, deletion of miR-143/145 shows minimal effects in homeostatic conditions but markedly impairs epithelial regeneration following damage [140].

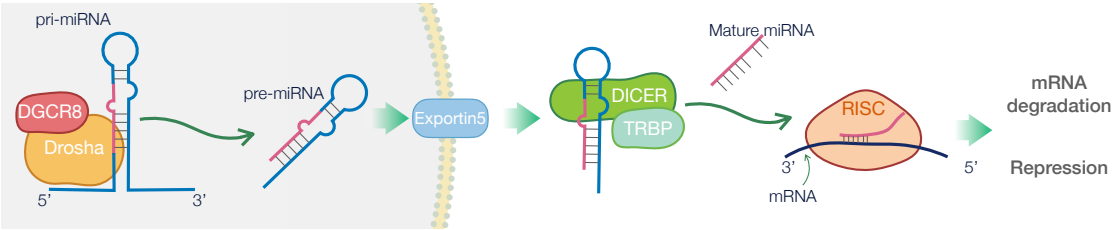

Figure I15. Mechanism of microRNA formation. microRNA biogenesis begins in the nucleus, where the microprocessor complex—comprising Drosha and its cofactor DGCR8 (DiGeorge syndrome critical region gene 8)—cleaves primary miRNA (pri-miRNA) into precursor miRNA (pre-miRNA). The pre-miRNA is then exported to the cytoplasm via Exportin-5. In the cytoplasm, the Dicer complex, together with the cofactor TRBP (TAR RNA-binding protein), further processes pre-miRNA into a mature miRNA duplex. One strand of the mature miRNA is loaded onto the RNA-induced silencing complex (RISC), which guides the miRNA to target mRNAs, leading to either degradation or translational repression.

microRNAs in mammary gland development and breast cancer

miRNAs are critical regulators of embryonic stem cell differentiation and influence stem cell renewal in a context-dependent manner, varying with cell type, environment, and developmental stage. Their importance is underscored by the fact that disruption of miRNA processing enzymes such as Dicer results in embryonic lethality [136]. Beyond embryogenesis, miRNAs continue to orchestrate organ-specific development, including that of the mammary gland. They modulate essential processes such as ductal morphogenesis, alveolar differentiation, and involution, ensuring timely tissue remodeling necessary for mammary gland function [141].

Because mammary gland development and breast cancer progression share biological processes—such as EMT, proliferation, apoptosis, angiogenesis, and stem cell regulation—miRNAs involved in normal development often become dysregulated in cancer. For instance, miR-34a restricts progenitor cell expansion in TEBs during puberty and, when expressed in breast cancer, suppresses EMT, stemness, and chemoresistance. Conversely, miR-21 promotes proliferation during pregnancy-associated ductal expansion and, when overexpressed in breast cancer, enhances invasion and therapy resistance [142].

In cancer, miRNAs exhibit dual functions: they can act as oncogenes promoting invasion, metastasis, and plasticity or as tumor suppressors limiting tumor growth and progression. Their regulation of stem cell maintenance and differentiation makes miRNAs promising therapeutic targets or agents for reprogramming cancer stem cell plasticity. By modulating developmental-like programs within tumors, miRNAs can disrupt tumor initiation, progression, and resistance to therapy, ultimately reshaping tumor homeostasis [143,144].

microRNA-203

miR-203 was first described in 2008 as a suppressor of stemness and promoter of differentiation in the epidermis [145]. In the same year, it was identified as one of eight miRNAs inversely correlated with metastatic potential in human breast cancer cell lines [146].

Building on its role in stemness regulation, our group demonstrated that transient upregulation of miR-203 in pluripotent stem cells (PSCs) enhances their differentiation potential across multiple lineages [147]. Brief exposure of mouse and human PSCs to miR-203 induces a temporary activation of a 2-cell-like transcriptional program through direct repression of the DNA methyltransferases Dnmt3a and Dnmt3b. This repression leads to reversible global DNA methylation changes that reset the epigenetic landscape and expand the developmental plasticity of PSCs.

Consistent with its role in PSCs, miR-203 functions as a key regulator of stem cell fate in the mammary gland, where it is induced during lactogenic and luminal differentiation [148]. It directly represses ΔNp63α, a master regulator of mammary stem cell self-renewal, thereby promoting commitment to luminal lineages. miR-203 also influences MET, reducing the stem-like population.

Beyond normal development, miR-203 plays significant roles in cancer biology. It modulates oncogenic pathways including BCR-ABL1 signaling in hematopoietic tumors, EMT and stemness in nasopharyngeal, cervical, and colorectal carcinomas, and proliferation and migration in prostate and renal cancers [149–155].

Since its initial identification, miR-203 has been extensively studied in breast cancer, where its expression is often silenced—mainly through epigenetic mechanisms [156,157]. Loss of miR-203 facilitates EMT, enhances CSC plasticity, and promotes metastasis (Figure I16). Functionally, restoring miR-203 inhibits tumor growth and migration in breast cancer cell lines and reduces expression of stemness markers [158,159]. Altogether, these findings position miR-203 not only as a key regulator of epithelial differentiation but also as a promising candidate for differentiation-based therapies in breast cancer. By reactivating silenced developmental programs, therapeutic restoration of miR-203 may help limit cancer cell plasticity, reduce stemness, and suppress metastatic potential.

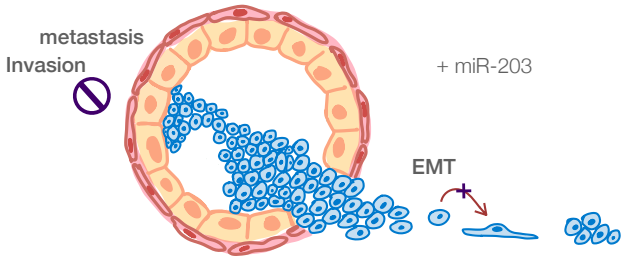

Figure I16. Role of miR-203 in breast cancer. Overexpression of miR-203 blocks epithelial-to-mesenchimal transition (EMT) in tumor cells, thereby suppressing metastasis and invasion.

Aims

Breast cancer represents the first leading cause of cancer-related death in women worldwide. A major factor contributing to its lethality is the recurrence and metastasis observed in approximately 25 % of patients, often years after initial remission [2]. These events are mainly driven by a clinically undetectable, highly plastic subpopulation of tumor cells known as cancer stem cells. CSCs possess the ability to evade conventional therapies. They can enter a dormant, quiescent state for extended periods, and later reactivate to regenerate the tumor or initiate distant metastases. Given their central role in disease persistence and progression, there is a critical need for therapeutic strategies that specifically target CSCs. Indeed, it is critical not only to eliminate them, but also to better understand the mechanisms enabling cancer cells to transition in and out of the stem-like state. In recent years, differentiation therapies—an approach with historical precedent in hematological cancer— have gained renewed interest. These therapies aim to "disarm" CSCs by forcing them out of their stem-like state into differentiated, therapy-sensitive phenotypes.

This doctoral Thesis hypothesizes that differentiation therapy can disrupt the tumor-promoting functions of stem-like cells by inducing a stable shift in cell identity, thereby interfering with the organizational and evolutionary dynamics of breast cancer. This strategy conceptualizes cancer as an adaptive, emergent system analogous to embryonic development and social structures in nature like an anthill —where distinct cell types, such as large, queen-like cancer stem cells and worker-like differentiated cells play specific roles in tumor survival and expansion—. Just as organisms adapt to environmental cues during development, cancer cells dynamically respond to therapeutic pressures and microenvironmental changes, underscoring the need for strategies that stably alter their identity and function.

With this in mind, the specific objectives of the Thesis were:

1. **To evaluate the differentiation potential of cannabinoid receptor 2 (CB_2R) modulation in breast cancer cells,** given that CB_2R is the most deregulated component of the ECS in this disease.
    - To determine whether modulation of CB_2R promotes breast tumor cell differentiation, using breast cancer-derived organoids as a model.
    - To characterize the phenotypical and functional consequences of CB_2R-modulation in breast cancer.
    - To assess the stability and irreversibility of CB_2R-driven modulation.

- To determine whether CB_2R-induced effects sensitizes breast cancer cells to subsequent endocrine therapy.

2. **To investigate the differentiation potential of microRNA-203 (miR-203) in breast cancer cells**, based on its capacity to enforce lineage commitment.
   - To investigate the effect of miR-203 activation on lineage commitment and stemness in breast cancer organoids.
   - To define the molecular programs induced by miR-203 exposure that underpin its effects.
   - To assess the impact of miR-203 treatment regimens on tumor initiation, growth, and metastasis progression.

Methods

Animals

All animal procedures were conducted in accordance with protocols approved by the Animal Experimentation Committee of the Complutense University of Madrid (CEIyBA) and the Regional Government of Madrid, following European regulations on animal research. Animals were housed in the animal facility of the Complutense University under a 12-hour light-dark cycle, with *ad libitum* access to food and water.

PyMT [FVB/N-Tg(MMTV-PyMT)$^{634Mul/J}$] mice were kindly provided by Miguel Quintela (Spanish National Cancer Research Center, CNIO, Spain). In the PyMT model, transgenic mice express the Polyoma Virus middle T (PyMT) antigen under the control of the mouse mammary tumor virus (MMTV) promoter (**Figure M1A**). The PyMT breast cancer model in FVB strain has a strong resemblance to TNBC at late stage: tumors in this model exhibit high proliferative rates and show a progressive loss of the hormone receptors (ER and PR). While ERBB2 expression is initially low, it increases as the disease advances [160]. Histologically, these tumors arise from luminal cells, and closely mimic IDC in humans [161]. Hemizygous MMTV-PyMT females develop rapidly growing, highly penetrant mammary tumors that metastasize to the lungs, making this model a particularly valuable tool for studying breast cancer initiation, progression, and invasion.

The miR-203 knock-in model [Col1A1(miR-203/mir-203); Rosa26/rtTA)] was generated by cloning a 482 bp genomic fragment of the mmu-mir-203 sequence downstream of a TetO promoter into the pBS31 vector for site-specific recombination, inserted in the Col1A1 locus of embryonic stem cells. The resulting mice were then crossed with the Rosa26-M2rtTA line [Rosa26(rtTA)] to enable doxycycline-inducible expression, as previously described [147] (**Figure M1C**). To generate the PyMT:miR-203$^{KI/KI}$ strain, PyMT mice were backcrossed with the miR-203-inducible model. For *in vivo* induction of miR-203 expression, doxycycline (Dox) was administered in diet using Doxycycline delayed-release pellets (Jackson laboratories). As a control, Dox treatment was also applied to PyMT: miR-203$^{+/+}$ mice.

The MMTV-neu:$CB_2R^{KO/KO}$ strain was previously generated and described in our laboratory [121]. MMTV-neu [FVB/N-Tg(MMTV-neu)$^{202Mul/J}$] mice were obtained by screening the MMTV-neu:$CB_2R^{WT/KO}$ colony and selecting only $CB_2R^{WT/WT}$ individuals (**Figure M1B**). The MMTV-neu model is widely used to model the human HER2+ breast cancer type. In this model, the rat *ERBB2/neu* oncogene, the homolog of human *HER2*, is expressed under the control of the MMTV promoter [162]. MMTV-neu females develop mammary tumors with longer latency compared to

PyMT mice, and they are particularly valuable for studying tumor progression in response to HER2-targeted treatments.

To generate the PyMT:$CB_2R^{KO/KO}$ strain, PyMT mice were crossed with MMTV-neu:$CB_2R^{KO/KO}$ mice (**Figure M1D**). The $CB_2R^{KO/KO}$ allele was introduced into the PyMT model through four generations of backcrossing, and the *neu* transgene was also removed in the process.

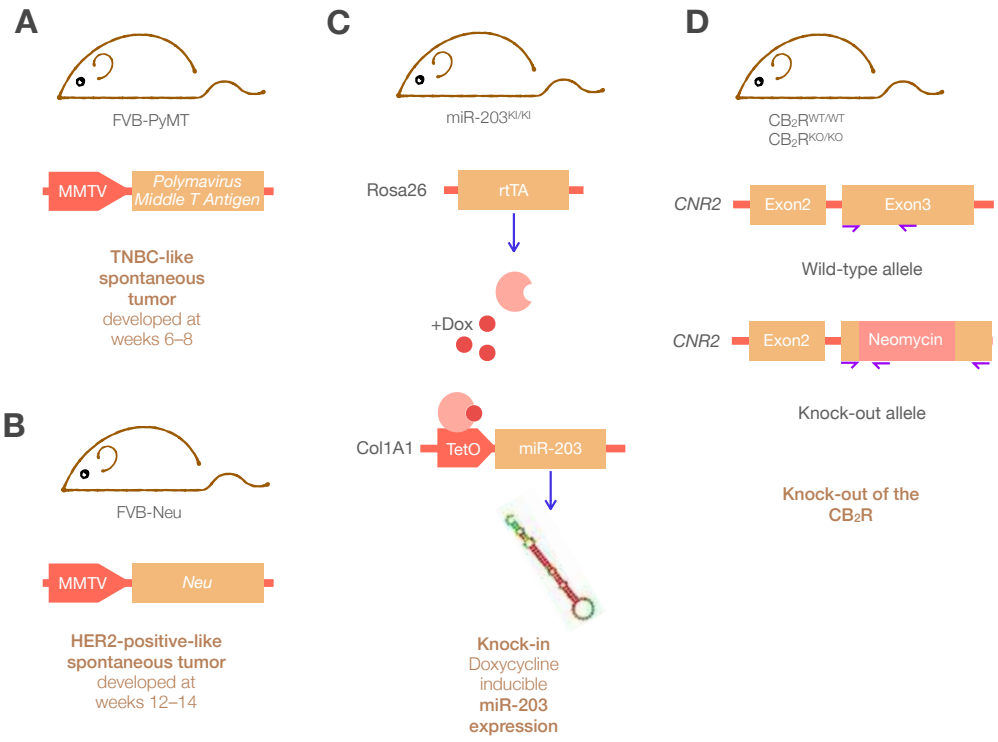

Figure M1. Scheme of the mouse models used for the experimental procedures. A, PyMT mouse model, a transgenic model that contains the Mouse Mammary Tumor Virus (MMTV) promoter, which directs the expression of the PyMT oncogene specifically in the mammary gland, generating TNBC-like breast tumors in female mice. **B**, MMTV-Neu mouse model, characterized by the over-expression of the rat ortholog of the *ERBB2* gene, *Neu*, in the mammary gland, resulting in a HER2-positive-like breast cancer model. **C**, miR-$203^{KI/KI}$ mouse model using the Tet-ON inducible system. The rtTA gene is expressed at the Rosa26 locus, while the TetO promoter controls the inducible expression of miR-203 inserted at the Col1A1 locus, allowing regulated expression of miR-203 upon doxycycline administration. **D**, $CB_2R^{KO/KO}$ mouse model, which carries a neomycin resistance cassette inserted in exon 3 of the *CNR2* gene, resulting in a loss-of-function allele for the CB_2R protein. Purple arrows indicate the primers used to detect either the wild-type or knock-out alleles. The miR-$203^{KI/KI}$ and $CB_2R^{KO/KO}$ models were crossed with the PyMT model to generate the transgenic lines PyMT:miR-$203^{KI/KI}$ and PyMT:$CB_2R^{KO/KO}$ respectively.

One unique PCR scheme was optimized for the detection of *PyMT* and *Neu* transgenes, and CB_2R wild-type and knock-out detection using the following settings: 95 °C for 15 min; 30 cycles at 94 °C for 30 s, 63 °C for 45 s; 72 °C for 1 min; 72 °C for 10 min; and then soaking at 4 °C. The following primers were used for *PyMT* transgene, CB_2R knock-out (CB_2RKO) and *Neu* transgene identification: For *PyMT* detection, which yields a product of 250 bp, the primers used were forward TGC CGG GAA CGT TTT ATT AG and reverse GGA ACA AGT ACC CCA GCT CA. For CB_2R, the wild-type allele produces a 550 bp fragment using forward CTA CAA AGC TCT AGT CAC CCG and reverse GGC TCC TAG GTG GTT TTC ACA TCA GCC TCT primers, while the knock-out allele, which amplifies a 300 bp fragment corresponding to the region where the neomycin cassette interrupts CB_2R transcription, was detected using same forward as wild-type allele and reverse CTA AAG CGC ATG CTC CAG AC. For *Neu* transgene detection, which results in an 80 bp product, the primers used were forward GCT CAG AGA CCT GCT TTG GA and reverse AGG AGG ACG AGT CCT TGT AGT G.

Micro-computed tomography

For micro-computed tomography (micro-CT), PyMT:miR-$203^{KI/KI}$ mice were anesthetized with a continuous flow of 1 to 2.5 % isoflurane/oxygen mixture (2 L/min). Acquisitions were performed using a micro-CT scanner Argus-Vista (SEDECAL) including the whole body in 2-bed position. Tomographic images were reconstructed using a 3D-FBP (filtered back projection) algorithm that produced 55 slices measuring 55º ⌀ 55 pixels each. The isotropic resolution of this instrument was 45 µm. The micro-CT image acquisition consisted of 400 projections collected in one full rotation of the gantry in approximately 10 min per bed position. The X-ray tube settings were 80 kV and 450 µA. For image analysis and quantification, 3D Slicer software was used. Tumor volumes were measured once per week by micro-CT, to determine accurately the tridimensional tumor mass. Micro-CT measurements were performed in all cases with no information about the genotype or treatment of every mouse tested.

Reagents

For inducing transient miR-203 over-expression, mir-203 knock-in organoid cultures were treated with doxycycline at 1 µg/mL (Sigma, D9891) for 5 days. For differentiation to mammary epithelial lineage, cultures were switched to MEGM® Mammary Epithelial Cell Growth Medium BulletKit® (Lonza CC-3150), and maintained for 5 days.

Cannabinoid-based treatments included phytocannabinoids such as THC and CBD (THC Pharm), a cannabis extract with high THC content, a balanced cannabis extract with a 1:1 THC:CBD ratio

(Extract 1:1, both from Grupo Curativa) (**Table M1**), synthetic cannabinoids as selective inverse agonist of CB_1R SR141716A (SR1, Tocris Bioscience, 0923), selective inverse agonist of CB_2R SR144528 (SR2, Tocris Bioscience 1464), and methanandamide (mAEA, Cayman Chemical, 90050). Tamoxifen (Sigma T5648) was used as a reference endocrine-modulating compound commonly used in the treatment of luminal breast cancer.

Compounds	THC extract (mg/mL)	THC:CBD extract (mg/mL)
THC	138.092	67.712
THCV	1.932	0.92
CBD	5.52	78.016
CBG	22.172	11.96
CBGA	ND	1.196
CBC	5.52	5.336
CBN	5.06	3.404
Terpenes	65.541	62.226

Table M1. Composition of cannabis extracts. The table includes the quantified cannabinoids and terpenes expressed in mg/mL. Abbreviations for cannabinoids are as follows: Δ^9-tetrahydrocannabinol (THC), tetrahydrocannabivarin (THCV), cannabidiol (CBD), cannabigerol (CBG), cannabigerolic acid (CBGA), cannabichromene (CBC), cannabinol (CBN). Terpene comprise caryophyllene, nerolidol 2, α-pinene, δ-limonene, linalool, β-myrcene, guaiol, camphene, β-ocimene, nerolidol 1, (–)-isopulegol, 3-carene, γ-terpinene, terpinolene, (–)-β-pinene, geraniol, α-terpinene, humulene, oxo-caryophyllene, and eucalyptol. ND indicates not detected.

Stock solutions of all reagents were prepared for a final 1:1 000 dilution. The solvents used for each compound were as follows: mAEA was dissolved in ethanol, while THC, CBD, Extract, Extract 1:1, SR1, SR2 and tamoxifen were dissolved in DMSO. Vehicle-treated groups were included in all experiments by supplementing the culture medium with equivalent volumes of the corresponding solvent (DMSO or ethanol).

Primary tumor cell extraction and culture

PyMT mice were euthanized at 6-8 weeks of age when palpable tumors appeared. Tumors were excised and kept on ice in tumor cell medium (DMEM, Corning 10-017-CV) supplemented with 1X Glutamax (Invitrogen, 12634-034), 10 % FBS (Gibco, A5256701), and antibiotics. Under aseptic conditions, tumors were minced into small fragments using a sterile scalpel. For enzymatic digestion, 5 mL of freshly prepared digestion solution [tumor cell medium supplemented with 0.125 mg/mL collagenase (Sigma, C9407) and 0.125 mg/mL dispase II (Gibco, 17105041)] was prewarmed at 37 °C and then added to the minced tumor. The tissue suspension was incubated at 37 °C with agitation at 150 rpm for 2 h.

Following digestion, the suspension was filtered through a 100 µm pore filter to remove undigested tissue fragments. The suspension was centrifuged at 400 x g, resuspended in tumor cell medium and plated. Cells were incubated at 37 °C for 20 min to allow adherence of tumor cells. After incubation, non-adherent cells were removed by washing three times with phosphate-buffered saline (PBS) to eliminate contaminating fibroblasts and other stromal cells. Fresh tumor medium was then added to the attached cells in the plate.

Primary tumor cells were identified as positive for pan-cytokeratin by immunofluorescence (Abcam, AB7753). Cells were maintained at 37 °C in a humidified atmosphere and 5 % CO_2 and weekly tested for mycoplasma contamination. They were passed when reached confluence, every 4 days.

Generation and culture of breast cancer organoids

PyMT, PyMT:$CB_2R^{KO/KO}$ and MMTV-neu mice were euthanized at 6-8 weeks of age, and tumors were extracted. Organoids were generated and maintained as previously described [163]. In the organoid system, tumor-derived cells are cultured within 3D extracellular matrix (ECM) hydrogels [Cultrex growth factor-reduced BME type 2 (Trevigen, 3533-010-02)], which provide a physiologically relevant structure that preserve the organ organization [164]. Organoid cultures closely resemble the tumor of origin by maintaining gene expression patterns, intratumor heterogeneity, and structural architecture, while also retaining the capacity for self-renewal, self-organization and plasticity. Briefly, tumors were minced and digested in a pre-warmed digestion solution [DMEM, 1X Glutamax, 1 % FBS, and antibiotics (wash medium), supplemented with 0.125 mg/mL collagenase and 0.125 mg/mL dispase II] at 37 °C with constant shaking at 150 rpm for 2 h.

The resulting suspension was subjected to sequential centrifugation at 500 x g to remove residual fat from the mammary gland using cold wash medium. Cells were then resuspended in basal

medium [Advanced DMEM/F-12 (Invitrogen 12634-034), 1X Glutamax, 10 mM HEPES (Invitrogen 15630-056), and antibiotics] and centrifuged again at 500 x g. Pellets were carefully resuspended in 10 mg/mL cold BME, and 40 µL drops were plated in a pre-warmed 24-well plate. After BME solidification, 650-1 000 µL of pre-warmed BC organoid expansion medium was added per well.

The BC organoid expansion medium was prepared by supplementing the basal medium with 10% homemade R-Spondin-1 conditioned medium, 1X B27 supplement (Gibco 17504-44), 1X N2 Supplement (Gibco 17-502-001), 10 mM nicotinamide (Sigma N0636), 1.25 mM N-acetylcysteine (Sigma A9165), 10 nM gastrin I (Sigma G9145), 100 ng/mL FGF10 (Peprotech 100-26), 50 ng/mL noggin (Peprotech 120-10C), 50 ng/mL EGF (Peprotech AF-100-15), 5 nM neuregulin 1 (Peprotech 100-03), 5 µM Y27632 (Abmole), 500 nM A83-01 (Tocris 2939), 500 nM SB202190 (Sigma S7067) and Primocin (Invitrogen Ant-pm-1).

Organoids were cultured with expansion medium refreshed every two days and passaged weekly as follows: organoids were resuspended in basal medium; next, residual BME was removed and organoids were dissociated by at least two cycles of centrifugation at 500 × g and resuspension in basal medium; then, organoids were reseeded at a 1:2 to 1:3 ratio in fresh BME and incubated with freshly prepared BC organoid expansion medium. Primary organoids derived from PyMT were identified as negative for ER (Biolegend 916201) and PR (Cell Signaling 8757T) by immunofluorescence.

Generation and culture of patient-derived organoids

Breast cancer diagnosed patient tumor samples were obtained from two sources: (1) a single cylinder from the initial core-needle tumor biopsy at Hospital 12 de Octubre (Madrid, Spain) from patients diagnosed with BIRADS 4C-5-6, in which lesions classified as 4C or higher indicate a high suspicion of malingnancy or confirmed cancer (6), prior to any treatment, and (2) lumpectomy resections following neoadjuvant chemotherapy at Hospital La Paz (Madrid, Spain). BIRADS (Breast Imaging Reporting and Data System) is a standardized classification system used to report breast imaging finidings and estimate the likelihood of malignancy on a scale from 0 to 6 [165].

To guarantee the protection of patients enrolled in this study, we have strictly followed the hospitals guidance, the local regulations, the “Declaration of Helsinki” and the Guidelines of good clinical practice from the “International Conference on Harmonization” ICH E6 (R2), effective from June 14, 2017. The technical protocols for patient-derived sample collection and processing, and any additional material delivered to the patient (such as Patient Information Sheets or the

Informed Consent Document) were carefully evaluated and approved by the corresponding Clinical Research Ethics Committee, in accordance with national legislation.

Patient-derived excisions were minced and digested in previously described pre-warmed digestion solution at 37 °C with constant shaking for 2 h. Suspension was subjected to sequential centrifugation at 500 x g. Cells were carefully resuspended in BME, and 20 µL drop was plated in a pre-warmed 24-well plate. After BME solidification, Patient BC organoid expansion medium (basal medium supplemented with 20 % homemade R-spondin-1 conditioned medium, 1X B27 supplement, 1X N2 Supplement, 10 mM nicotinamide, 1.25 mM n-acetylcysteine, 10 nM gastrin I, 100 ng/mL FGF10, 100 ng/mL noggin, 50 ng/mL EGF, 5 nM neuregulin 1, 5 µM Y27632, 500 nM A83-01, 500 nM SB202190 and Primocin) was added. Organoids were passed every 10 days and the expansion medium was refreshed every two days.

Transient induction of miR-203 in patient-derived organoid culture

After 7 days of culture establishment and organoid amplification, patient-derived 3D cultures were transiently transfected with miR-203 mimics, followed by miR-203 withdrawal for three additional weeks. Hsa-miR-203 mimics were purchased from Sigma-Aldrich (MISSION microRNA mimics), and transient transfection was performed using Lipofectamine 3000 (Invitrogen, L3000001), following manufacturer's instructions.

Briefly, organoids were collected and centrifuged at 500 x g. Pellets were then incubated in pre-warmed trypLE Select enzyme (Gibco 12563011) at 37 °C for 15 min to achieve dissociation into single cells. Following enzymatic digestion, basal medium was added to stop enzymatic reaction, and samples were centrifuged at 500 x g. Ten thousands single cells from organoid cultures were resuspended in 900 µL of basal medium (without antibiotics) and seeded into non-adherent 24-well plates. For transfection, 3 µL of Lipofectamine 3000 were diluted in basal medium (without antibiotics) and incubated at room temperature (RT) for 5 min. Then, 250 nM of miR-203 mimic was mixed with 2 µL of P3000 reagent and added to the Lipofectamine solution to reach a final volume of 100 µL. The mixture was added to the cell suspension and incubated at 37 °C for 4 h.

After incubation, cells were collected and centrifuged at 500 x g. The resulting pellet was resuspended in 40 µL of ice-cold BME per well and plated in a pre-warmed 24-well plate at a final concentration of 1x 10^4 cells per well. BME drops were allowed to solidify at 37 °C for 1-2 min before the addition of 600–1 000 µL of BC organoid expansion medium per well. The medium was refreshed every two days, and organoid re-formation was monitored over time. For control conditions, cells were transfected with Lipofectamine 3000 in the absence of miR-203 mimic.

Cancer-associated fibroblast extraction and culture

Mammary gland-derived tumors were harvested from PyMT mice at 6-8 weeks of age to isolate CAFs [166,167]. Briefly, tumors were minced into small fragments with a sterile scalpel and incubated with pre-warmed digestion solution (wash medium supplemented with 0.125 mg/mL collagenase, 0.125 mg/mL dispase II and 0.1 mg/mL DNase I) at 37 °C with constant shaking at 150 rpm for 2 h.

After digestion, the cell suspension was filtered through a 100 µm cell strainer and centrifuged at 500 x g. Cells were then incubated at selection medium [DMEM supplemented with 10 % FBS, 1X Insulin-Transferrin-Selenium (ITS -G, Gibco 41400045) and antibiotics] for 30 min to allow selective adherence of fibroblast. After incubation, non-adherent tumor cells were removed by washing three times with PBS. Fresh CAF medium (DMEM, 10 % FBS, 1X Glutamax and antibiotics) was then added. CAFs were maintained in culture and identified by immunostaining: CAFs were Vimentin-positive (Vimentin antibody, BD bioscience 5505013) and Cytokeratin-negative (pan-Cytokeratin antibody, Abcam AB7753).

Peripheral blood mononuclear cell isolation

Peripheral blood was collected from 6-8 weeks adult PyMT tumor-bearing mice for the isolation of peripheral blood mononuclear cells (PBMCs). Briefly, whole blood was obtained via cardiac puncture and transfered to 1M EDTA (PanReac 141952) pre-coated tubes to prevent coagulation. Collected blood samples were diluted in HBSS (Gibco 14025092) at a 1:2 ratio. To isolate PBMCs, density gradient centrifugation was performed using Ficoll-Paque™ PLUS (VWR 17-1440-02), applying 1 mL of Ficoll per 3 mL of blood. The diluted blood was carefully layered over Ficoll and centrifuged at 1600 rpm for 27 min at RT, with no brake and low acceleration. The PBMC layer was carefully collected and transferred to a clean tube. Cells were washed three times with PBS supplemented with 1 % FBS and antibiotics. Finally, cells were counted using a Neubauer counting chamber and cryopreserved in 10% DMSO in FBS until further use in co-culture experiments.

Breast cancer organoid-CAF co-culture

PyMT-derived organoids were dissociated and co-seeded with primary CAFs in a 1:250 organoid-to-CAF ratio. CAFs were harvested from confluent primary cultures by incubation with 0.25 % Trypsin, 0.1 % EDTA (Corning 25-053-CI) for 4 min at 37 °C. Detached cells were collected in previously described CAF medium, centrifuged at 500 x g and preserved on ice.

Simultaneously, organoids were collected after first passage, when the culture is established. Organoids were mechanically disrupted by pipetting up and down in basal medium, then

subjected to two sequential washes by centrifugation at 500 × g to remove residual BME. Then, CAFs were added to organoid suspension. The mixture was centrifuged at 500 x g and the resulting pellet was carefully resuspended with cold BME. A 20 µL drop per well was plated in pre-warmed 8-well chamber slides (Ibidi 80841). After BME polymerization at 37 °C, 200-300 µL of pre-warmed BC organoid expansion medium were added per well.

As experimental controls, organoids were cultured under the same conditions either alone (without fibroblasts) or co-seeded with NIH/3T3 fibroblasts (ATCC CRL-1658™), following the same procedure and ratio. Co-cultures and their corresponding controls were evaluated after 4 and 10 days of culture and further analyzed by immunofluorescence staining.

Organoid-CAF-PBMC co-culture under shear stress in a bioreactor system

Previously extracted PyMT-derived breast cancer organoids were dissociated after the first passage, when cultures were well established, and co-seeded with CAFs and PBMCs in a multicellular microfluidic device. Organoids and CAFs were co-cultured at a 1:250 ratio and seeded into µ-Slide III 3D Perfusion chambers (Ibidi 80371) as described above. Following seeding, co-cultures were incubated in breast cancer organoid expansion medium (previously described) for 2 h at 37 °C, 5 % CO_2, and controlled humidity to allow cell attachment.

After incubation, µ-Slide chambers were connected to a controllable flow-loop bioreactor system [168]. The flow loop consisted of a peristaltic pump (ISMATEC MCP 78002-00) with an 8-roller, 12-channel pump head (ISMATEC Type IBM733A 78002-36), and 1.52 mm diameter ISMATEC PharMed BPT tubing (95723-36) integrated into the loop. µ-Slides were connected using Ibidi elbow Luer connectors (Ibidi 10802) and serial connectors for µ-Slides (ibidi 10830) to 3.18 mm sterile Silastic tubing (Dow Corning 515-012) (**Figure M2**).

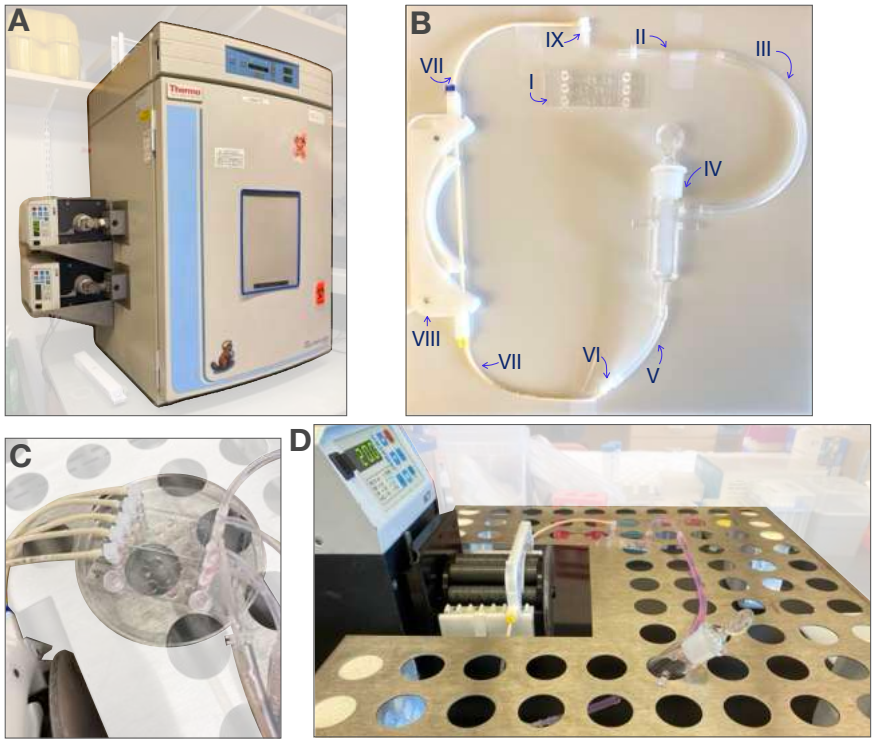

Figure M2. Bioreactor system for flow-controlled induction. **A,** Bioreactor incubator equipped with a peristaltic pump system installed on the side. The flow rate is regulated via a control panel located laterally, while temperature and CO_2 levels are controlled from the upper panel. **B,** Schematic of the continuous flow system: (I) Ibidi plate containing the samples, connected to (II) an Ibidi Luer tube that allows fluid to exit the plate and flow into (III) a 15-cm long, 3.18 mm silastic tubing, which discharges into (IV) a glass reservoir. From there, fluid is recirculated through (V) a 5-cm long sterile silastic tubing connected via (VI) a tube size adapter to (VII) 1.52 mm BPT tubing. This tubing is placed in a rotor holder (VIII), which induces flow via a pump mechanism, and finally connects to an elbow fitting (IX) that closes the loop back to the Ibidi plate. **C,** Example of plate connection within the flow system using organoids co-cultured with CAFs under circulating PBMC conditions. **D,** External setup showing the plate connected to the flow system. The entire assembly is set up and activated inside a biosafety cabinet using the external peristaltic pump positioned on the left. Once the flow is initiated and the circuit is closed, the setup is transferred to the bioreactor-incubator system (as shown in **A**), where the peristaltic speed is adjusted via the left side panel to achieve controlled flow movement.

Organoid-CAF co-cultures were subjected to a continuous physiological capillary (2.6 dynes/cm^2) shear stress flow system by using 20 rpm as pump speed (**Figure M3**). PBMCs were introduced into the circulating breast cancer expansion medium, allowing dynamic interaction with the organoid-CAF co-culture under the constant flow conditions.

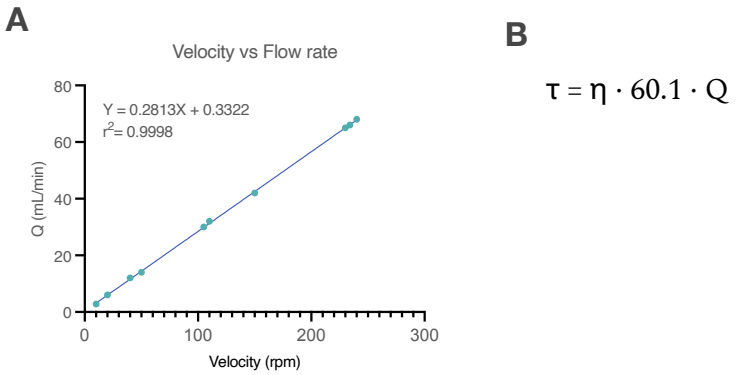

Figure M3. Calibration of flow rate and shear stress in the perfusion system. A, Relationship between pump speed (rpm) and flow rate (Q, mL/min) using Pharmed BPT tubing with an inner diameter of 1.52 mm. A linear regression was applied to the data points, resulting in the linear equation shown on the graph. **B,** Equation provided by Ibidi to calculate the shear stress (τ, dyn/cm^2) generated in the µ-Slide III 3D Perfusion chamber, where η is the dynamic viscosity of the medium (0.0072 dyn·s/cm^2) and Q is the flow rate in mL/min. To achieve a physiological shear stress of 2.6 dyn/cm^2, a flow rate of 6 mL/min is required. According to the linear equation from panel (**A**), this corresponds to a pump speed of 20 rpm.

PBMCs, CAFs, and organoids used in each co-culture replicate were derived from the same individual PyMT mouse to preserve syngenic cellular interactions and ensure experimental consistency.

Experimental conditions included: (1) organoids alone under static conditions, (2) organoids exposed to flow (shear stress only), (3) organoids co-seeded with CAFs under flow, (4) organoid-CAF co-cultures exposed to both flow and PBMCs, and (5) organoid-CAF-PBMC co-cultures treated with either THC or SR2. All conditions were evaluated after 4 and 10 days of culture.

Mammary gland orthotopic injection *in vivo*

PyMT-derived organoids were treated with 10 nM THC for 4 days. After 10 days of culture following cannabinoid withdrawal, organoids were resuspended with basal medium and centrifuged at 500 x g. Pellets were disaggregated into single cells using an incubation for 20 min with trypLE Select enzyme at 37 °C under agitation. Thousand organoid-derived cells in 100 µL (50 µL cell suspension and 50 µL BME) were orthotopically injected into the left inguinal mammary fat pad of the 10-week-old PyMT wild-type littermate females, corresponding to the sister counterparts of organoid-derived mice.

Mice were monitored three times a week for tumor growth, measuring length and width with an external caliper. Tumor volume was calculated as $(4\pi/3) \times (\text{width}/2)^2 \times (\text{length}/2)^2$. When tumors

reached a 1 000 mm^3 volume, mice were euthanized, and tumors were collected for further evaluation. Tumors were fixed with 10 % formalin and prepared for immunohistochemistry analysis.

Evaluation of lung seeding/invasion *in vivo*

PyMT-derived organoids were differentiated using the phytocannabinoid THC (10 nM) for 4 days, then used after 10 days of culture. Organoids were dissociated into a single-cell suspensions using TrypLE incubation for 20 min. A total of 5 x 10^5 organoid-derived cells per mouse were injected into the lateral tail vein of 10-week-old PyMT wild-type sister mice to induce lung invasion. Mice were euthanized four weeks after injection. Lungs were fixed and prepared for immunohistochemistry and immunofluorescence analysis.

Secondary organoid formation assay

Organoids were collected for single-cell disaggregation to assess their self-renewal and secondary organoid-forming potential. Samples were centrifuged at 500 x g and pellets were incubated with pre-warmed TrypLE for 20 min at 37 °C. Gentle mechanical dissociation was performed every 5 min. Disaggregation suspensions were then centrifuged at 500 x g. Single cells were resuspended with BME at 1 x 10^4 cells per 40 µL, seeded in a 24-well plate and incubated to allow BME solidification at 37 °C for 1-2 min. Then, 650-1 000 µL of breast cancer organoid expansion medium were added to each well. Cells were maintained at 37 °C in a humidified incubator with 5% CO_2. The medium was replaced every two days. Organoid formation was evaluated after 10 days in culture by visually counting well-defined, compact 3D structures relative to the total number of cells seeded.

Flow cytometry sorting and organoid culture of PyMT CB_2RWT and CB_2RKO tumors

Mammary gland tumors from PyMT CB_2RWT and CB_2RKO mice were excised and processed for flow cytometry analysis. Tumors were minced and enzymatically digested using digestion solution (wash medium supplemented with 0.125 mg/mL collagenase and 0.125 mg/mL dispase II) for 1 h at 37 °C on a shaker at 180 rpm.

For single-cell disaggregation, the resulting suspension was centrifuged at 600 x g and filtered through a 100 µm cell strainer using 10 mL of blocking buffer (wash buffer supplemented with 5 mM EDTA). Cells were then centrifuged again at 600 x g, and erythrocytes were lysed for 15 min at RT. Red blood cell lysis buffer was prepared using 10 % tris saline buffer [composed of 5 mM Tris-HCl (PanReac A10865000), 136 mM sodium chloride (Sigma S9625), and 2.7 mM potassium chloride (Sigma 49360500)] supplemented with 7.47 g/L ammonium chloride (Sigma A9434).

Following a second filtration through a 100 µm cell strainer, samples were centrifuged once more at 600 x g and resuspend in FACS buffer (PBS supplemented with 2 % FBS, 0.01 % sodium azide and antibiotics) at a concentration of 1 x 10^6 cells per 100 µL. Fc receptors were blocked by incubating with anti-CD16/32 antibody (BioLegend 101320) at 1:100 dilution for 20 min on ice.

After blocking, cells were washed and resuspended in the antibody staining solution containing EpCAM-FITC (BioLegend 118207) at 1:200 dilution and CD49f- Alexa Fluor™ 647 (BioLegend 313610). Cells were incubated with the antibody mix for 20 min on ice in dark conditions. After staining, samples were centrifuged at 1000 x g at 4°C and resuspended in FACS buffer at a concentration of 1x10^6 cells in 100 µL and stained with 7-AAD (BioLegend, 420404) as a viability marker at 1:50 dilution. Cells were sorted on a FACSAria cell sorter (BD Biosciences) into four distinct populations based on differential expression of CD49f and EpCAM. For data analysis, FlowJo™ software was used. Each sorted population was collected independently and used to initiate organoid cultures.

Sorted cells were seeded at a density of 1x 10^4 cells per well in 40 µL of BME in a 24-well plate prewarmed to 37 °C. After matrix polymerization, 650-1000 µL of breast cancer organoid expansion medium were added to each well. Cultures were maintained at 37 °C in a humidified incubator with 5 % CO_2. Unsorted cells were used as a control for organoid formation. Medium was refreshed every 48 h. After 10 days in culture, organoid formation was evaluated to assess the growth potential of each sorted population.

Cell cycle analysis

After the corresponding differentiation protocol, organoid cultures were harvested and centrifuged at 500 x g. Organoids were dissociated into single cells by incubation with TrypLE Select at 37 °C for 20 min, with gentle pipetting every 5 min. Cells were then fixed in ice-cold 70 % ethanol for 30 min on ice, allowing both cellular fixation and membrane permeabilization to enable intracellular DNA labelling. Following fixation, cells were centrifuged at 1000 x g.

Fixed cells were incubated with 100 µg/mL RNase A (Sigma R5503) to degrade RNA and permit selective DNA staining. Subsequently, 400 µL of 50 µg/mL propidium iodide (Sigma P-4170) were added per 1 x 10^6 cells. Samples were incubated on ice for 10 min and analyzed using a FACScalibur flow cytometer (BD Biosciences). Data analysis was evaluated using FlowJo™ software.

Apoptosis assay by flow cytometry

Organoid cultures were extracted and transferred to a tube for disaggregation into single-cell suspensions. Pre-warmed TrypLE Select was used for enzymatic dissociation, with an incubation for 20 min at 37 °C. Following digestion, cells were centrifuged at 500 x g.

Apoptosis analysis was performed using the Dead Cell Apoptosis Kit with Annexin V for Flow Cytometry (Invitrogen V13445), according to the manufacturer's instructions. Briefly, cells were stained with 1:100 dilution of annexin V-Alexa Fluor™ 488 and 0.2 µg/mL of propidium iodide (PI) solution in the annexin-binding buffer provided in the kit. Samples were incubated at RT for 15 min in the dark and subsequently analyzed using FACScalibur flow cytometer.

Viability assay

Organoids and primary tumor cells derived from PyMT mice were assessed for viability based on intracellular ATP content using the CellTiter-Glo® 3D Cell Viability Assay (Promega G9682), following manufacturer's instructions. Briefly, cells were lysed with CellTiter-Glo 3D reagent and incubated for one hour at RT in the dark. After incubation, luminescence was measured using an IVIS Spectrum system (Perkin Elmer). Background signal from medium was subtracted, and relative luminescence units (RLU) were normalized to control conditions.

Cell migration analysis from patient-derived samples

To investigate cell migration traits in detail, we employed the HoloMonitor® M4, an automated live-cell imaging cytometer that performs time-lapse analysis. This system allows for the imaging and quantification of unstained, living cells directly within their culture vessels inside the incubator, enabling real-time monitoring of various morphological and migratory parameters. Based on digital holographic microscopy, the HoloMonitor measures phase shifts in light as it passes through cells, which the software then uses to reconstruct high-resolution topographic images.

For our experiments, we used Ibidi® plastic 24-well plates fitted with HoloLid™ lids—specifically designed to reduce image artifacts caused by surface vibrations and condensation. We quantified the following parameters: cell area (μm^2), the surface area occupied by each cell; irregularity, the degree to which a cell's outline deviates from a perfect circle; migration (µm), the shortest linear distance between a cell's initial and final positions; motility (µm), the total path length traveled by a cell; and motility speed (µm/h), the motility distance divided by the observation time.

Statistical analyses were performed using R software (version 4.5.0). For each parameter, we calculated the mean ± standard error of the mean (SEM). A linear model (lm) was fitted to assess the impact of experimental conditions on each variable. Model residuals were examined to verify assumptions of normality and homoscedasticity.

Cytokine profiling from co-culture conditioned media

Cytokine secretion profiles from co-culture condition were analyzed using the Proteome Profiler Mouse Cytokine Array Kit, Panel A (R&D Systems ARY006), following the manufacturer's protocol. Briefly, 1 mL of conditioned media was collected from cell cultures and centrifuged at 500 x g to remove cellular debris. Supernatants were transferred to fresh tubes and stored at -20 °C until simultaneous processing.

Array membranes were first blocked, while samples were incubated with the Detection Antibody Cocktail. Membranes were then incubated overnight at 4 °C with the antibody-sample mixture. The following day, membranes were washed, incubated with Streptavidin-HRP for 30 min, and developed using a chemiluminescent reagent. Signals were detected using the ChemiDoc XRS+ imagen system (BioRad). Cytokine spot intensities were quantified using Fiji (ImageJ) and normalized to the internal positive controls.

Immunofluorescence

For immunofluoresce (IF) analysis, organoids were seeded into 8-well chamber slides with removable wells (Nunc™ Lab-Tek™ II Chamber Slide™ System 154534). Cells were rinsed briefly with PBS before fixation. Organoids were fixed using 10 % formalin (PanReac 143091.1214) for 1 hour at RT. Permeabilization was performed using 3 % Triton X-100 (Sigma T9284) in PBS for 20 min, followed by three washes with 0.1 % Triton X-100 in PBS. Samples were blocked using blocking solution [PBS + 0.1 % Triton X-100 + 2 % bovine serum albumin (BSA) (Sigma A6003)] for 2.5 h at RT. Primary antibodies were added at required ratio in the blocking solution as specified in **Table M2**. Samples were incubated overnight at 4 °C.

Primary antibody	Host	Clonality	Supplier	Reference	dilution
Cytokeratin 14	Rabbit	Monoclonal EPR17350	Abcam	ab181595	1:100
Cytokeratin 8/18	Rat	Monoclonal TROMA-I	DSHB	ab_531826	1:100
Ki67	Mouse	Monoclonal B56	BD Bioscience	550609	1:400
E-CAD	Rabbit	Monoclonal 24E10	Cell Signaling	3195S	1:500
SNAIL	Mouse	Monoclonal L70G2	Cell Signaling	3895	1:250
CD49f	Rat	Monoclonal GoH3	Biolegend	313610	1:100
EpCAM	Rat	Monoclonal G8.8	Biolegend	118207	1:200
SOX10	Rabbit	Monoclonal EPR4007	Abcam	Ab155279	1:250
ER	Rat	Monoclonal W23263D	Biolegend	648843	1:50
PR	Rabbit	Monoclonal D8Q2J	Cell Signaling	8757T	1:1 000
CD24	Rat	Monoclonal M1/69	Biolegend	101816	1:800
CD24	Mouse	Monoclonal ML5	BD Pharmigen	561644	1:20
CD44	Rat	Monoclonal IM7	Biolegend	103023	1:20
H3K9me3	Rabbit	Polyclonal	Abcam	Ab8898	1:400
H3K4me3	Rabbit	Monoclonal EPR20551-225	Abcam	Ab123224	1:100
H3K27me3	Mouse	Monoclonal 6002	Abcam	Ab6002	1:200
Vimentin	Mouse	Monoclonal RV202	BD Pharmigen	550513	1:250

Table M2. Primary antibodies used for immunofluorescence staining. The table includes the target antigen, host species, clonality, supplier, catalog number (labelled as "Reference") and dilution used for staining.

Following incubation, samples were washed with PBS and secondary antibodies were added using 1:500 dilution in the blocking solution (**Table M3**). Incubation was performed at RT for 1.5 h in dark conditions. After secondary incubation, samples were washed twice with PBS. For F-actin staining, phalloidin-rhodamine (Invitrogen R415) was diluted 1:200 in PBS, and added to each well for a 30-min incubation. For nuclear staining, DAPI was diluted 1:1000 in PBS, and added to each well for a 10-min incubation. After staining, cells were mounted using Mowiol 4-88 (Calbiochem 475904) as mounting media.

Secondary antibody	Host	Clonality	Supplier	Reference
anti-Rabbit IgG- Alexa Fluor™ 488	Goat	Polyclonal	Invitrogen	A-11008
anti-Mouse IgG - Alexa Fluor™ 594	Goat	Polyclonal	Invitrogen	A-11005
anti-Rat IgG - Alexa Fluor™ 647	Goat	Polyclonal	Invitrogen	A-21247
anti-Rabbit IgG - Alexa Fluor™ 594	Goat	Polyclonal	Invitrogen	A-110112
anti-Rat IgG - Alexa Fluor™ 488	Goat	Polyclonal	Invitrogen	A-11006

Table M3. Secondary antibodies used for immunofluorescence staining. The table includes the target secondary antigen, host species, clonality, supplier and catalog number (listed as "Reference"). All antibodies were used at a dilution of 1:500 for staining.

Samples were examined under the TCS SP8 laser scanning confocal microscope (Leica). Image acquisition was achieved in a sequential scanning mode by optimizing lasers and spectral detectors for each specific fluorescent dye. Z-stacks were obtained by 2.5 µm z-steps, a 20X oil immersion objective and a 1024 x 1024 scanning resolution. Image analysis and processing were performed using Fiji (ImageJ). 3D projections were generated using the brightest point projection method.

Immunohistochemistry

Mammary glands and lung tissue samples were fixed in 10 % formalin, paraffin-embedded, cut a 4 µm slices, mounted in superfrost plus slides and dried overnight. Sections were stained with hematoxylin and eosin (H&E) or subjected to immunohistochemistry.

Antigen retrieval was first performed, endogenous peroxidase was blocked using peroxide hydrogen at 3 % (Sigma H1009), and slides were incubated with primary antibodies (**Table M4**). Secondary antibodies were conjugated with horseradish peroxidase (OmniRabbit, Ventana, Roche 05269679001), and the immunohistochemical reaction was developed using 3,30-diaminobenzidine tetrahydrochloride (DAB) as a chromogen (Chromomap DAB, Ventana, Roche 05266645001), and nuclei were counterstained with Carazzi's hematoxylin (Sigma H3393). Finally, the slides were dehydrated, cleared and mounted with a permanent mounting medium for microscopic evaluation.

Primary antibody	Host	Clonality	Supplier	Reference
Cytokeratin 14	Rabbit	Polyclonal AF64	Covance	PRB-155P
Cytokeratin 8/18	Rabbit	Monoclonal	Dako	IR094
Ki67	Rabbit	Monoclonal D3B5	Cell Signaling	12202
SOX9	Rabbit	Polyclonal	Millipore	AB5535
SOX10	Goat	Polyclonal N-20	SantaCruz	c-17342
Estrogen receptor α	Mouse	Monoclonal CRET94D/H9	CNIO Patology Unit	AM
Cleaved Caspase 3	Rabbit	Monoclonal ASP175	Cell Signaling	9661
Cytokeratin 5	Rabbit	Polyclonal AF138	Covance	PRB-160P
CD44	Rabbit	Polyclonal	Abcam	Ab157107
H3K27me3	Rabbit	Monoclonal C36B11	Cell Signalling	9733
Prolactin	Rabbit	Polyclonal	Dako	A0569
Progesterone receptor	Rabbit	Monoclonal SP2	Thermo Scientific	RM-9102-R7
NeuN	Mouse	Monoclonal A60	Millipore	MAB377
E-cadherin	Mouse	Monoclonal 36	BD Bioscience	610182
Aldh1/2	Mouse	Monoclonal H-8	SantaCruz	Sc-166362
Smooth muscle actin	Mouse	Monoclonal 1A4	Dako	IR611

Table M4. Primary antibodies used for immunohistochemistry staining. The table includes the target antigen, host species, clonality, supplier and catalog number (listed as "Reference").

RNA extraction and RT-qPCR

RNA was extracted using NucleoZOL™ following the manufacturer's instructions. Briefly, samples were lysed in NucleoZOL™ and mixed with nuclease-free water to induce phase separation. Samples were incubated for 15 min at RT and centrifuged at 12 000 x g at 4 °C to separate RNA from cellular debris. RNA was precipitated by isopropanol addition and incubated overnight at -20 °C to improve yield from organoid samples. The RNA was pelleted by centrifugation at 12 000 x g at 4 °C, washed twice with 70 % ethanol, air-dried at RT, and resuspend in nuclease-free water. Samples were stored at -20 °C until simultaneous processing.

RNA concentration was determined using a NanoDrop One spectrophotometer (Thermo Scientific, ND-ONE-W). Reverse transcription was performed from 1 µg of RNA using the

Transcriptor First Strand cDNA Synthesis Kit (Roche 04379012001) using random hexamer primers from the kit. Then, real-time quantitative PCR was performed using the PowerUp™ SYBR™ Green Master Mix (Applied biosystems, A25742) according to the manufacturer's instructions, using 50 ng of cDNA and a final concentration of 1 µM for each primer per well in 384 well-plates. Data were acquired with a QuantStudio™ 12K Flex system (Applied Biosystems). The primers used are listed in **Table M5**.

Gene	Forward Sequence	Reverse Sequence
Krt5	TCC TGT TGA ACG CCG CTG AC	CGG AAG GAC ACA CTG GAC TGG
Krt14	CAG CCC CTA CTT CAA GAC CA	GTC GAT CTG CAG GAG GAC AT
Krt8	GGA CAT CGA GAT CAC CAC CT	TGA AGC CAG GGC TAG TGA GT
Krt18	CAA GTC TGC CGA AAT CAG GGA C	TCC AAG TTG ATG TTC TGG TTT T
Cdh1	AGG AAA TGC ACC CCT CCA AT	AAT CGG CCA GCA TTT TCT G
Cdh2	GCC ATC ATC GCT ATC CTT CT	CCG TTT CAT CCA TAC CAC AAA
Vim	CCA ACC TTT TCT TCC CTG AAC	TTG AGT GGG TGT CAA CCA GA
Sox10	ATC AGC CAC GAG GTA ATG TCC AAC	ACT GCC CAG CCC GTA GCC
EpCAM	GAT TCT GCA CGT GAG ACC TG	GAT ACC AAG TCA AAC CGA GAA CTT

Table M5. List of primer used for real-time quantitative PCR. The table above lists the gene names along with their corresponding forward and reverse primer sequences. All sequences are presented in the 5' to 3' direction.

RNAsequencing analysis

RNA was extracted as described before using NucleoZOL™ following manufacturer's instructions. RNAseq sample processing and data analysis were performed by Novogene using their standard protocols. Briefly, high-quality RNA sample triplicates were assessed for integrity using the Agilent Bioanalyzer 2100. mRNA was isolated using poly-T-oligo-attached magnetic beads and fragmented prior to cDNA synthesis. Both non-stranded and strand-specific libraries were prepared following Illumina standard protocols. Library quality and concentration were evaluated using Qubit fluorometric quantification, according to Novogene's standard workflow. Sequencing was performed on the Illumina NovaSeq 6000 platform using sequencing-by-synthesis technology to generate high-throughput paired-end reads.

All bioinformatic processing was performed by Novogene. Raw FASTQ files underwent quality control, adaptor trimming, and filtering of low-quality reads using Novogene's internal pipelines. Clean reads were aligned to the mouse reference genome (GRCm38) using HISAT2, and differential gene expression analysis was conducted using DESeq2 with thresholds of adjusted $p \leq 0.05$ and $|\log2FC| \geq 1$. Functional enrichment analysis was performed using the clusterProfiler R package across GO, KEGG, Reactome, DO, and DisGeNET databases.

RNAseq data has been deposited in the SRA repository under BioProject accession number PRJNA1276513.

Statistical Analysis

All experiments were performed with at least three independent biological replicates. Data are presented as mean ± SEM, and p values ≤ 0.05 were considered statistically significant. Unpaired, independent groups of two were analyzed by two-tailed Student's t-test. Correlative associations between two variables were calculated by Pearson's r. For multi-group comparison, data were analyzed by 1-way ANOVA with post-Tukey's multiple comparison test, or by 2-way ANOVA when required. Statistical analyses were conducted using GraphPad Prism software (GraphPad Software, version 10.1.2, licensed).

Results

CB_2R modulation induces differentiation of breast cancer stem cells

Low-dose, transient THC exposure durably reprograms mammary tumor organoids, disrupting cancer cell plasticity *in vitro* and *in vivo*.

Cannabinoids have been widely studied for their antitumor properties —suppressing proliferation, invasion, metastasis and promoting autophagy and cell death in preclinical models of cancer [169]. In most *in vitro* studies, concentrations ranging from 1–10 μM are used to induce tumor cell death. However, the role of cannabinoids in regulating tumor cell differentiation remains poorly understood. Since differentiation therapies align with adaptive treatment strategies aimed at reducing tumor evolution and therapeutic resistance [170], we first examined whether THC could stably modulate tumor cell plasticity under long-term conditions.

To assess the effects of THC on tumor-derived cell populations, we exposed 2D primary tumor cultures from MMTV-PyMT mouse model to an increasing concentration range of THC (10 nM to 5 μM). After 10 days, ATP levels were measured as an indirect readout of cell viability. We then applied the same treatment to 3D tumor organoids derived from the same specimens, which more faithfully preserve intratumoral heterogeneity.

As expected, high THC concentrations induced cytotoxicity in 2D cultures, while lower concentrations (10-100 nM) had no significant effect (**Figure R1A**). In contrast, organoid cultures showed a partial sensitivity to high-doses of THC —approximately half the effect observed in 2D cultures. Interestingly, organoids treated with 10 nM THC exhibited a significant reduction in ATP levels (**Figure R1B**). Notably, unlike 2D cultures, this decrease in ATP did not correlate with impaired organoid viability as observed by imaging, suggesting that the reduction in ATP may instead be associated with decreased metabolic activity. Moreover, two weeks post-treatment initiation, organoids previously exposed to high THC concentrations developed invasive-like morphologies, accompanied by high expression of the CSC marker Sox10 (**Figure R1C**).

We next evaluated the effects of nanomolar THC using a continuous exposure for 14 days —when visual changes are observed in the culture (**Figure R1D**). Organoids treated with low THC concentrations (10-50 nM) displayed a morphological shift from bunch of grapes-like clusters to cystic structures, while higher concentrations produced no observable effect. Staining for CK14 and CK8/18 —basal and luminal markers, respectively— reveals decreased CK14 and increased CK8/18 treated organoids. CD24, the luminal differentiation marker, localized toward the interior of these treated organoids, while CD49f, a progenitor basal marker, was reduced compared with other conditions, consistent with the observed morphological remodeling (**Figure R1D**).

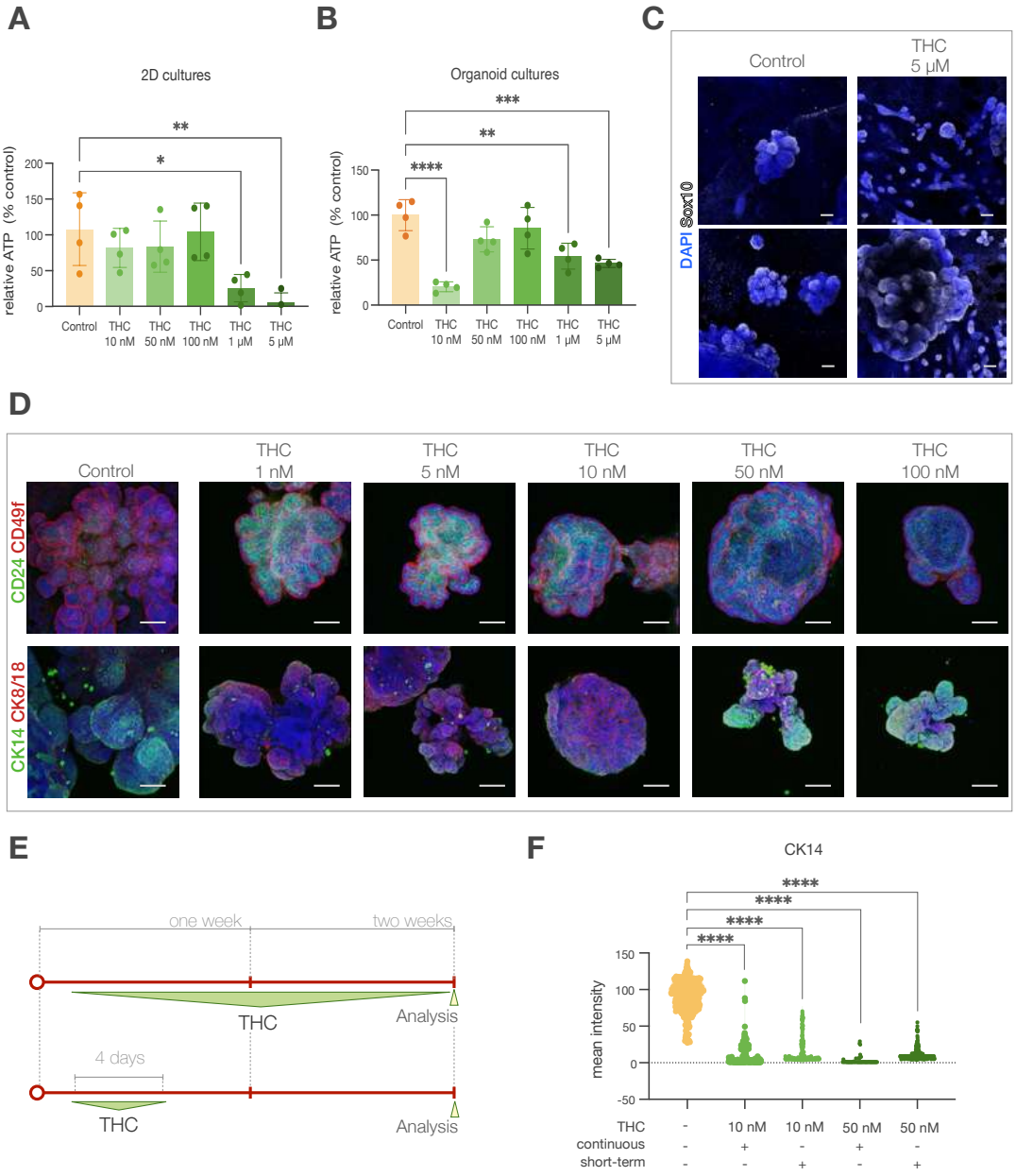

Figure R1. Short-term exposure to nanomolar THC induces long-term changes in MMTV-PyMT mammary tumor 3D organoids, but not in 2D cultures. A, Viability of 2D cancer cell cultures derived from FVB-MMTV-PyMT mammary tumors, exposed to vehicle (DMSO) or varying THC concentrations for 4 days, with analysis 10 days post-treatment. n=4 independent experiments; *p<0.05; **p<0.01 vs. control (One-way ANOVA). **B,** Viability of 3D organoid cultures derived from FVB-MMTV-PyMT mammary tumors, treated similarly with vehicle or THC for 4 days, with analysis 10 days later. n=3 independent experiments; **p<0.01; ***p< 0.001; ****p<0.0001 vs. control (One-way ANOVA). **C,** Representative confocal images of vehicle and THC-treated organoids (5 µM) assessed 14 days post-treatment. Organoids were stained for Sox10 (white) and DAPI for nuclei (blue). n=3 independent experiments. Scale bar: 100 µm. **D,** Representative confocal images of organoids treated with varying THC concentrations for 14 days, stained for CD24 (green) and CD49f (red) in the upper panels, or CK14 (green) and CK8/18 (red) in the lower panels. Note the changes in organoid shape and marker expression following 10 nM THC exposure. DAPI (blue) was used for nuclei staining. All images show 3D stacks of

the examples depicted. n=3 independent experiments. Scale bar: 100 µm. **E,** Schematic of the experimental design. PyMT-derived tumor organoids were treated with vehicle (DMSO) or 10 nM THC for continuous exposure for 14 days or 4 days, followed by extended drug withdrawal culture. **F,** Violin plot from CK14 quantification of fluorescence intensity. ****p<0.0001 vs. control (One-way ANOVA).

We then selected the two low-dose conditions (10 and 50 nM) that exhibited changes relative to controls and evaluated two treatment regimens: (1) continuous exposure for 14 days, and (2) short-term (4-day) treatment followed by a 10-day withdrawal period (**Figure R1E**). Both approaches yielded similar outcomes, suggesting that even brief THC exposure was sufficient to induce durable changes without triggering evidence of reversible adaptation (**Figure R1F**).

Based on these findings, we established a protocol involving a 4-day pulse of 10 nM THC —the lowest concentration able to generate the effect—, followed by extended drug withdrawal (**Figure R2A**). Strikingly, this brief low-dose exposure consistently induced a morphological transition in organoids—from a granular, bunch of grapes-like structure, through an intermediate phase, ultimately forming cystic, spherical organoids (**Figures R2B, R3A**), resembling those derived from healthy mammary luminal progenitors [171]. This transition began within the first week post-

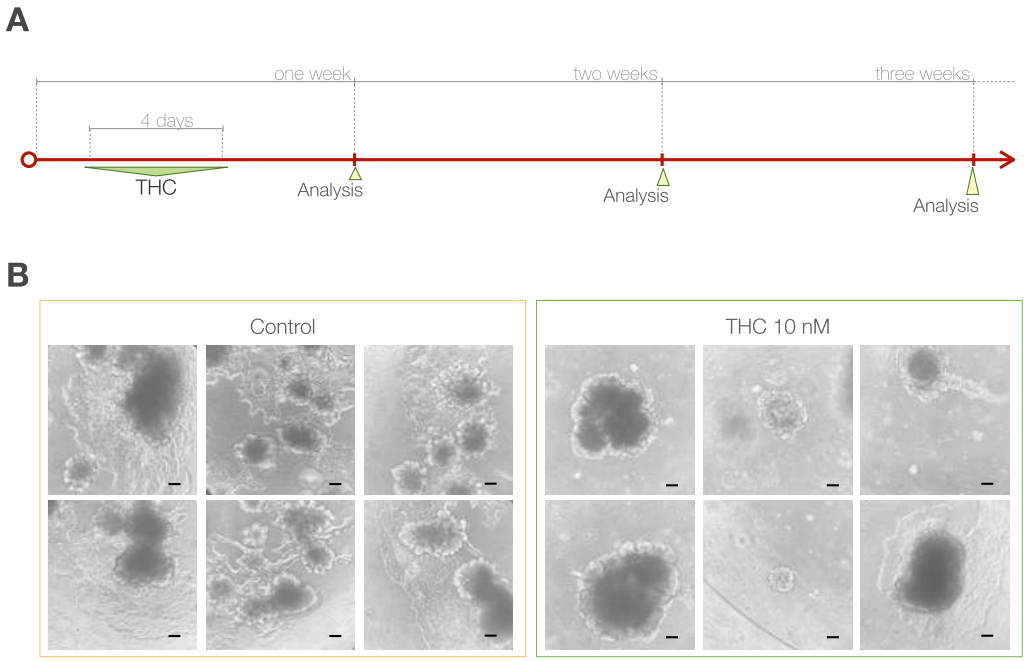

Figure R2. Experimental design and long-term morphological effects of transient THC exposure on tumor organoids. A, Schematic of the experimental design. PyMT-derived tumor organoids were treated with vehicle (DMSO) or 10 nM THC for 4 days, followed by extended drug withdrawal culture. Analyses were performed at 1, 2, and 3 weeks post-treatment. **B,** Representative bright-field images of control and THC-treated organoids at 2 weeks. n=6 independent experiments. Scale bar, 100 µm.

treatment and intensified over time (**Figure R3B**), accompanied by a reduction in organoid size, indicating decreased proliferation (**Figure R3C**).

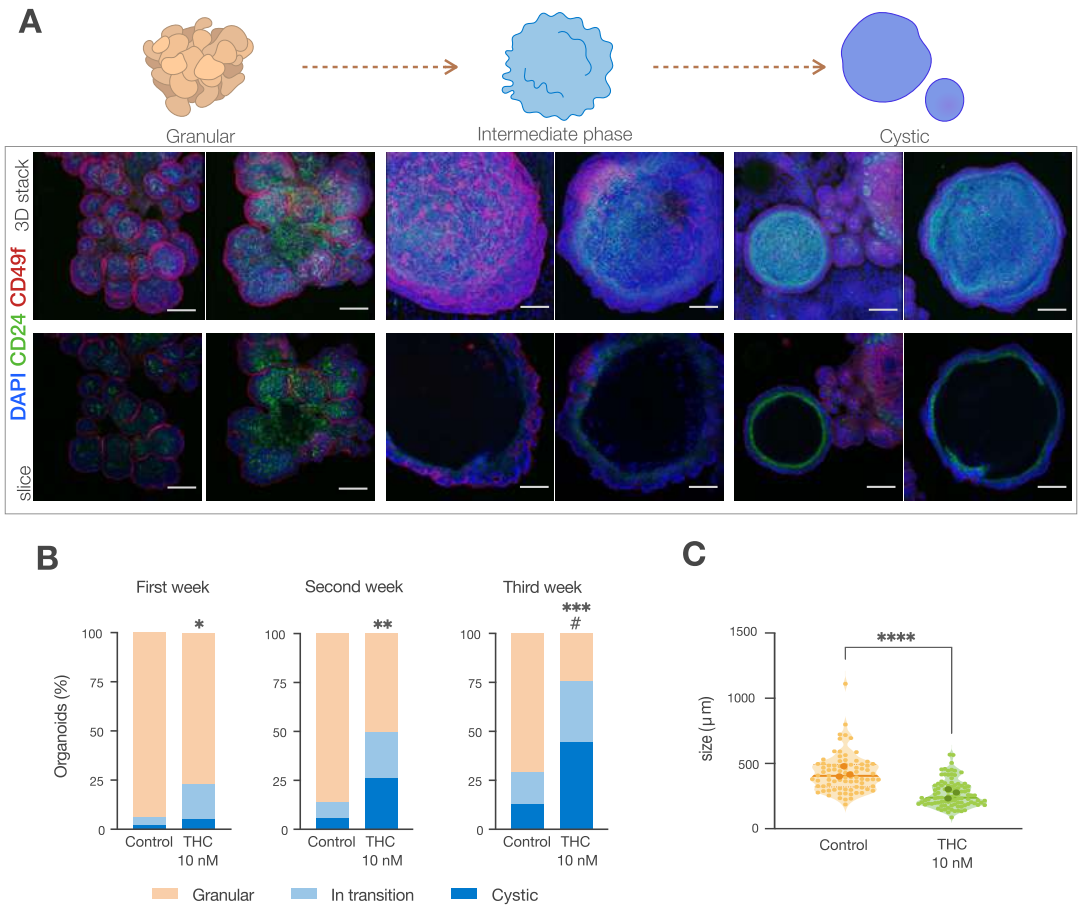

Figure R3. THC induces time-dependent morphological differentiation in mammary tumor organoids. A, Confocal images of organoids stained for CD24 (green) and CD49f (red) -cell surface markers of mammary gland precursors- at 1, 2, and 3 weeks, showing temporal changes in morphology and marker expression after THC exposure. DAPI (blue) stains nuclei. Upper panels show 3D stacks; lower panels show representative single slices. n=3 independent experiments. Scale bar, 100 µm. **B,** Quantification of organoids classified as granular (basal-like), in transition (intermediate), or cystic (luminal-like/rounded) over time. n=3 independent experiments; *p<0.05, **p<0.01, ***p<0.001 vs control (granular); #p=0.014 vs. control (cystic) (Two-way ANOVA). **C,** Quantification of organoid size (µm) at endpoint. n=3 independent experiments; 80–100 organoids per condition; ****p<0.0001 vs. control (unpaired Student's t-test).

The morphological changes were paralleled by a phenotypic shift from a basal-like to a luminal-like identity. This was confirmed by reduced expression of basal markers such as CK14 (*Krt14*) and CK5 (*Krt5*), alongside increased expression of luminal marker CK18 (*Krt18*), despite CK8 (*Krt8*) remaining unchanged across conditions (**Figure R4A-B**). In addition, a significant increase in the hormone receptors ER and PR—particularly in PR levels—was observed (**Figure R4C**).

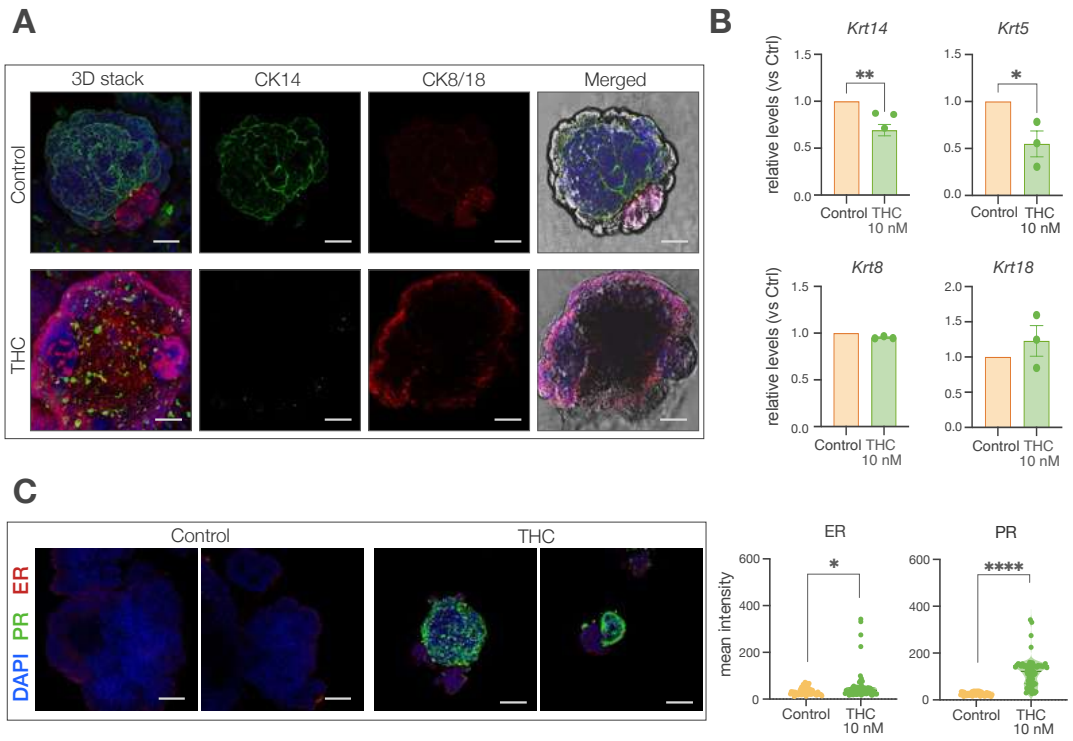

Figure R4. THC treatment induces basal-to-luminal phenotypic shift in organoids. A, Confocal images of organoids at 2 weeks stained for CK14 (green; basal marker) and CK8/18 (red; luminal markers). Left: 3D stacks; middle: single slices of individual markers; right: merged with bright-field. DAPI (blue) stains nuclei. n=4 independent experiments. Scale bar, 100 µm. **B,** qPCR analysis of cytokeratin genes (*Krt14/5* and *Krt8/18*, denoting basal-like and luminal-like phenotypes, respectively) at endpoint, normalized to *Gapdh*. n=3 independent experiments; *p<0.05, **p<0.01 vs. control (unpaired Student's t-test). **C,** Confocal images of organoids at 2 weeks stained for PR (green) and ER (red).DAPI (blue) stains nuclei. n=3. Violin plots show quantification of fluorescence intensity. *p<0.05; ****p<0.0001 vs. control (unpaired Student's t-test). Scale bar, 100 µm.

It has been previously described that organoids derived from invasive and de-differentiated tumors, such as those originating from TNBC, exhibit an invasive behavior that closely mimics *in vivo* collective migration [172,173]. In our experiments, we observed that untreated organoids similarly displayed invasion-like structures involving a coordinated group of cells, with a leading edge composed of mesenchymal-like cells promoting migration —expressing mesenchymal and basal markers Snail and CK14, respectively—, followed by a cohort of epithelial cells —labelled by E-cadherin and CK8/18— that provide structural support (**Figure R5A**).

In this context, pre-treatment with THC inhibited the collective migration process, progressively reducing the number of organoids displaying this behavior over time (**Figure R5B**). Not only was the ability to initiate new collective migration structures impaired, but also the proliferative and adhesive capacity of these structures, as reflected in the reduced area occupied by the collective

migration (**Figure R5C**). This inhibitory effect on migration was associated with a MET, as evidenced by morphological changes and marker expression patterns (**Figure R5D**).

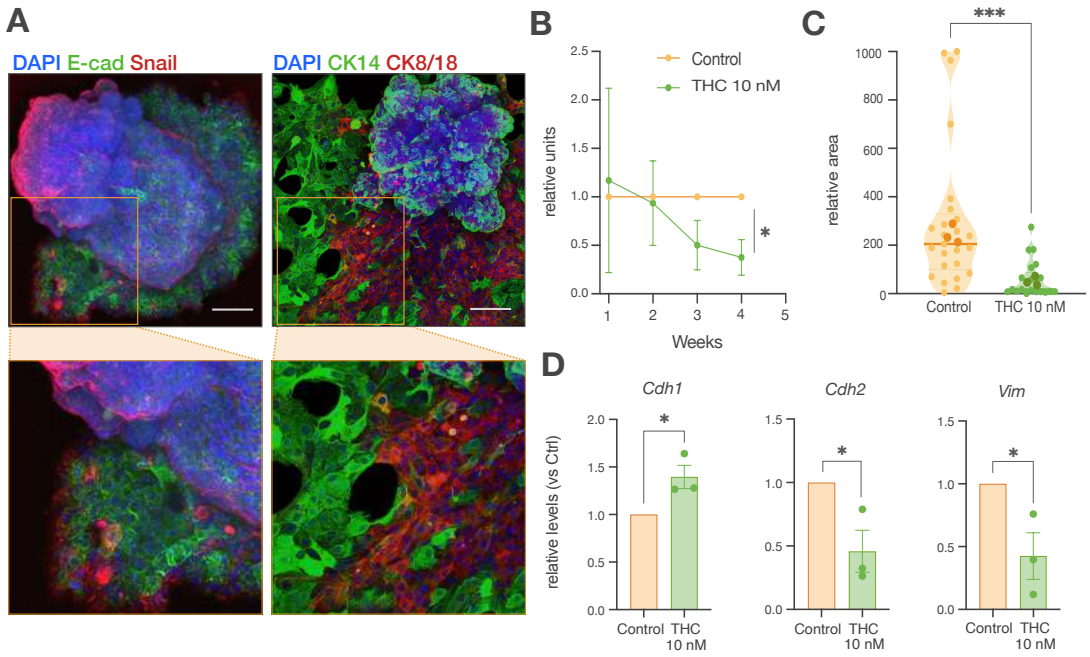

Figure R5. Brief exposure to nanomolar THC prevents collective migration in mammary tumor organoids. A, Representative confocal images of PyMT-derived untreated organoids showing collective migration in control cultures. Organoids are stained for E-Cad (green) and Snail (red) (left) –as EMT markers– or CK14 (green) and CK8/18 (red) (right). Note the cellular projections extending from the organoid edges and attaching to the substrate. The inset highlights preserved E-Cad staining in migrating areas, indicating cohesive cell movement. DAPI (blue) stains nuclei. n=3 independent experiments. Scale bar, 100 µm. **B,** Time-course comparison of organoids displaying collective migration in control vs. THC-treated conditions. n=3 independent experiments; *p<0.05 vs. control (unpaired Student's t-test). **C,** Quantification of the two-dimensional area of collective migratory projections in control vs. THC-treated cultures at 2 weeks. n=3 independent experiments; 25–30 organoids per condition; ***p<0.001 vs. control (unpaired Student's t-test). **D,** qPCR analysis of EMT-related genes at day 14: E-cadherin (*Cdh1*), N-cadherin (*Cdh2*) and Vimentin (*Vim*). mRNA levels were normalized to *Gapdh*. n=3 independent experiments; *p<0.05 vs. control (unpaired Student's t-test).

Alongside the observed shifts at both basal-to-luminal and mesenchymal-to-epithelial axes, the low dose THC pulse also reduced stem-like features. This was evidenced by decreased expression of stem cell markers such as Sox10 and CD49f, accompanied by increased in the epithelial marker EpCAM (**Figure R6A-B**).

To further assess stem cell properties as a hallmark of de-differentiation, organoids were dissociated into single cells and re-seeded under organoid-forming conditions after 10 days of

THC withdrawal—at this point morphological changes were evident, thus luminal-like spherical organoids had already emerged— (**Figure R6C**). Consistently, self-renewal capacity was reduced, as demonstrated by a diminished ability to form secondary organoids from single-cell seeding—a property typically restricted to cells with stem-like potential (**Figure R6D**). These findings indicate a reduction in the stem-like cell population within the culture, suggesting a shift from a de-differentiated, mesenchymal and basal-like state toward a more luminal-like/differentiated and epithelial identity.

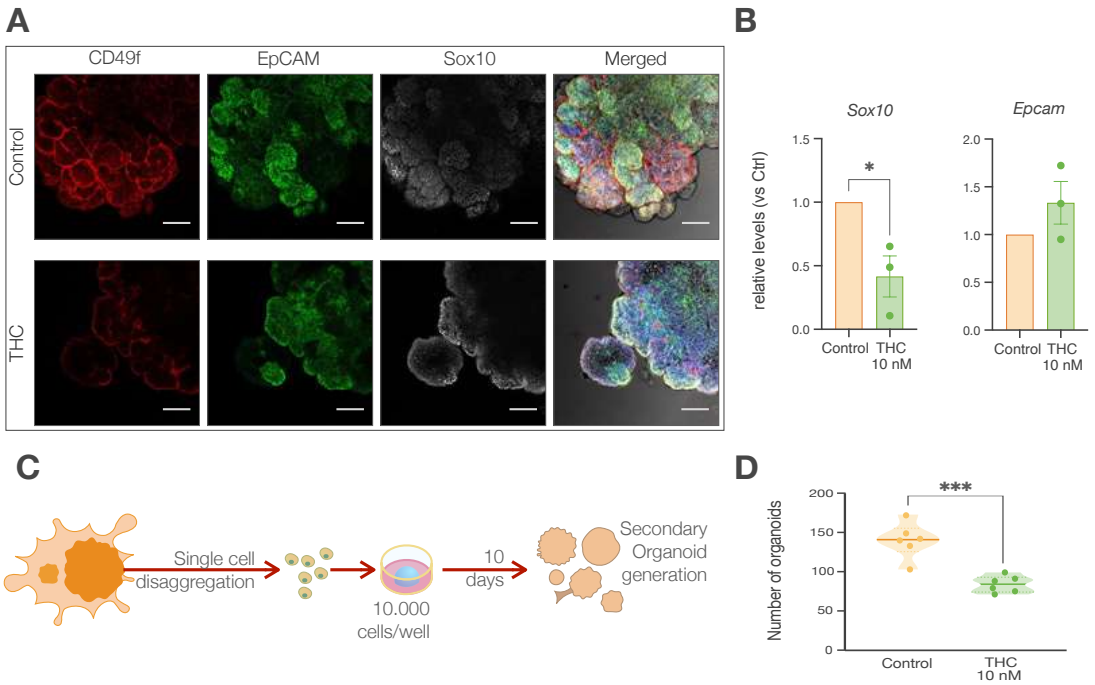

Figure R6. Brief exposure to nanomolar THC reduces stem-like features and self-renewal capacity in breast cancer organoids. A, Confocal images of organoids stained for CD49f (red), EpCAM (green), and Sox10 (white) after treatment with vehicle or 10 nM THC and analyzed at 2 weeks when phenotype is established. DAPI (blue) stains nuclei. Merged images with bright-field are shown on the right. n=4 independent experiments. Scale bar, 100 µm. **B,** qPCR analysis of stemness and differentiation markers (*Sox10* and *EpCAM*, respectively) at day 14. Data normalized to *Gapdh*. n=3 independent experiments; *p<0.05 vs. control (unpaired Student's t-test). **C,** Schematic of the self-renewal analysis. PyMT-derived tumor organoids were disaggregated into single cells, then 10 000 cells were seeded per well. New secondary organoids were detected from 10 days after seeding. **D,** Quantification of secondary organoid formation from single-cell dissociation at 21 days, indicating self-renewal capacity. n=6 independent experiments; ***p<0.001 vs. control (unpaired Student's t-test).

To confirm that THC-driven differentiation is not model-specific, we performed similar experiments in organoids derived from MMTV-Neu tumors (HER2-positive-like). The MMTV-Neu mouse model develops mammary neoplasms through targeted overexpression of the rat *HER2*

ortholog *Neu*, resulting in tumors with slower progression and reduced invasiveness compared to those from the MMTV-PyMT (TNBC-like) model [78]. As expected and consistent with this reduced porliferative capacity, organoids derived from MMTV-Neu tumors showed a lack of collective migration behavior (**Figure R7A**).

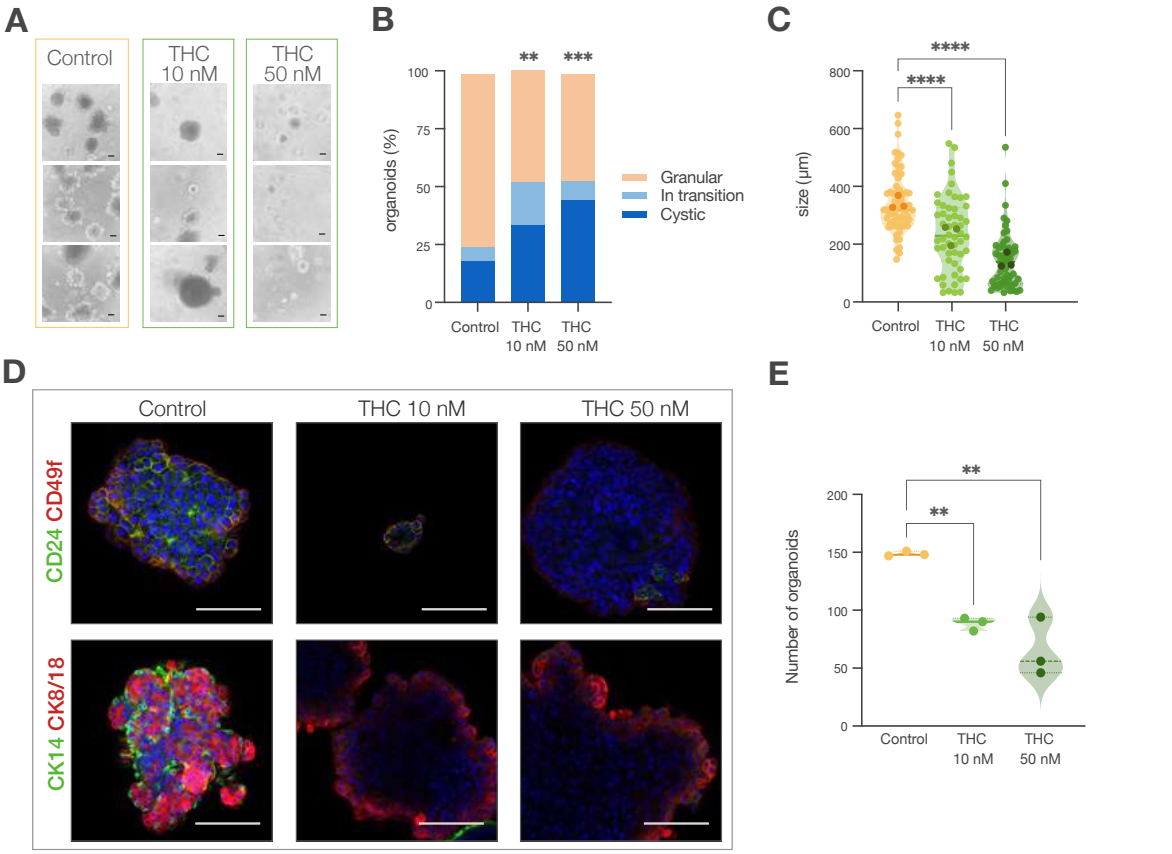

Figure R7. Brief exposure to nanomolar THC induces comparable effects in organoids derived from MMTV-PyMT and MMTV-neu transgenic mammary tumors. A, Representative bright-field images of MMTV-neu-derived tumor organoids treated with vehicle (control), 10 nM THC, or 50 nM THC, following the schedule indicated in Figure R2A. Organoids were analyzed at 2 weeks post-treatment. n=3 independent experiments. Scale bar: 100 µm. **B,** Quantification of organoid morphology at 14 days after treatment, categorizing them as granular (basal-like), in transition, or cystic (luminal-like/rounded). Data show a significant increase in cystic organoids following THC treatment. n=3 independent experiments; **p<0.01; ***p<0.001 vs. control (Two-way ANOVA), comparing granular organoids vs. control. **C,** Quantification of organoid size (µm) for each treatment group, measured at 14 days post-treatment. n=3 independent experiments, with 80–100 organoids counted per condition; ****p<0.0001 vs. control (Two-way ANOVA). **D,** Confocal images of organoids treated with THC (10 nM or 50 nM) and stained for CD24 (green) and CD49f (red), or CK14 (green) and CK8/18 (red). Nuclei are stained with DAPI (blue). Images represent 3D stacks of organoids analyzed 14 days post-treatment. n=3 independent experiments. Scale bar: 100 µm. **E,** Total number of secondary organoids generated from single-cell dissociation, indicating the self-renewal capacity of the cultures, evaluated 21 days after treatment. n=3 independent experiments; **p<0.01 vs. control (Two-way ANOVA).

HER2-positive-derived organoids were treated with either 10 nM or 50 nM THC in a 4-day pulse, and differentiation outcomes were assessed 14 days post-treatment (**Figure R7A**). Treated organoids showed a significant increase in the proportion of cystic, luminal-like structures, indicating a clear morphological transition in response to THC (**Figure R7B**). In addition, treated cultures exhibited reduced proliferation, as evidenced by a decrease in overall organoid size (**Figure R7C**). Expression of basal and stem-like markers —including CK14 as basal, and CD24 and CD49f for stem-like behavior— was decreased, while luminal markers such as CK8 were maintain following treatment (**Figure R7D**). Consistently, self-renewal capacity was again significantly reduced with only half the number of secondary organoids formed from single-cell seeding compared to untreated controls (**Figure R7E**).

Once the differentiation effects were demonstrated in both mouse models, we further validated these phenotypes in patient-derived breast cancer organoids. A post-chemotherapy mammary tumor sample was obtained from a patient with triple negative invasive ductal carcinoma, treated at Hospital Universitario La Paz (Madrid, Spain). Following organoid amplification, organoids were treated with THC using the 4-day pulse, followed by a withdrawal period prior to analysis (**Figure R8A**).

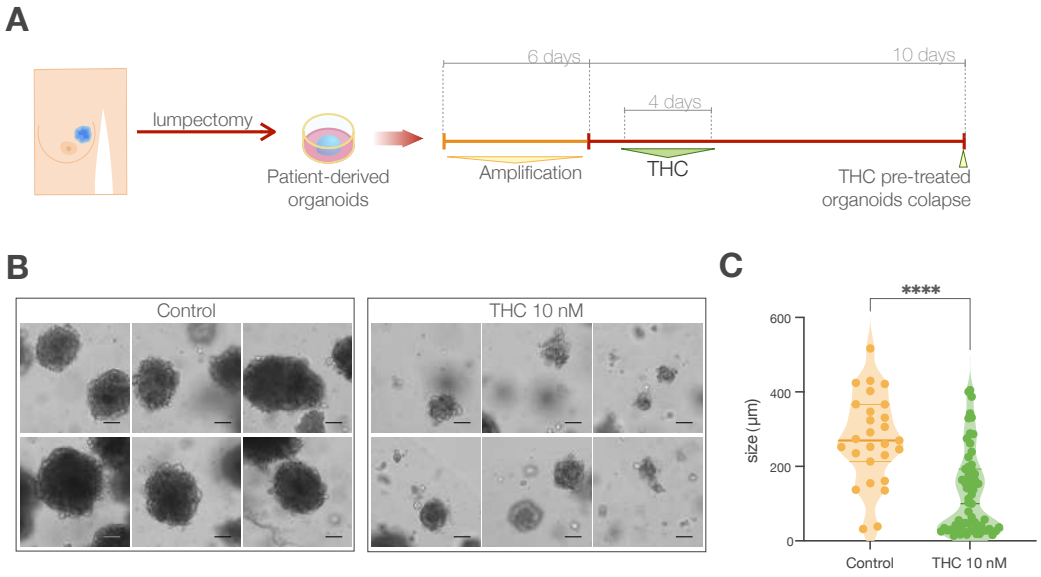

Figure R8. THC promotes differentiation in patient-derived breast cancer organoids. A, Experimental design. Surgery samples were used to establish patient-derived organoid cultures. After amplification, organoids were treated with vehicle or THC (10 nM) for 4 days and maintained for one week without treatment. THC-treated organoid cultures collapsed by ~day 10. **B,** Representative bright-field images of organoids treated with vehicle or THC (10 nM), analyzed one week after treatment. n=3 independent experiments. Scale bar, 100 µm. **C,** Quantification of organoid size (µm) in both conditions. n=3; 80–100 organoids per condition; ****$p<0.0001$ vs. control (unpaired Student's t-test).

Interestingly, THC-pretreated organoids collapsed by day 10 of culture, whereas control organoids continued to grow. In the same direction, organoid size was markedly reduced following treatment (**Figure R8B-C**). In addition, collective cell migration was diminished in THC-treated conditions, which was accompanied by an increase in CK8 expression (**Figure R9**), indicating a luminal shift.

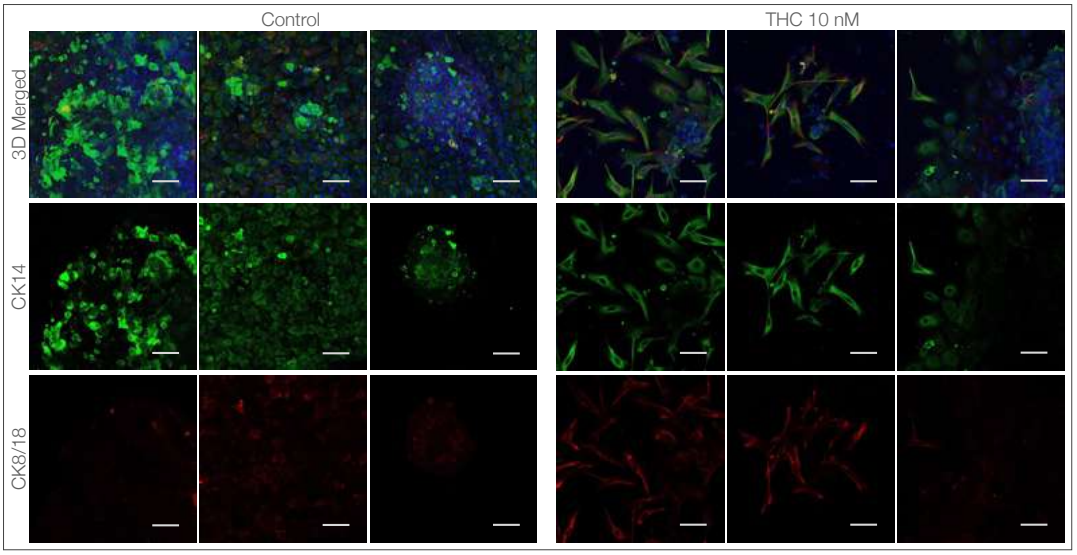

Figure R9. THC induces an early epithelial marker remodeling in patient-derived breast cancer organoids. Confocal images of organoids stained for CK14 (green) and CK8/18 (red), analyzed one week post-treatment. DAPI stains nuclei (blue). Shown are 3D stacks of representative examples. n=3; scale bar, 100 µm.

Altogether, these results indicate that THC induces differentiation changes in breast cancer organoids either in mouse-derived or patient-derived cell cultures. To evaluate the long-term functional consequences of THC treatment, the *in vivo* behavior of THC-differentiated cells was assessed. As described in the Introduction section, some tumor cells retain the capacity to revert to a stem-like phenotype after undergoing differentiation, whether driven by tumor-intrinsic mechanisms or external cues. Thus, this functional analysis aimed to determine whether THC-induced differentiation leads to an irreversible loss of stem cell potential.

Organoids were derived from the PyMT mouse mammary tumors and exposed to a 4-day 10 nM pulse of THC (**Figure R10A**). Following the 10-day withdrawal period —at which time differentiation was confirmed (**Figure R10B**)— the organoids were dissociated into single cells and orthotopically injected into the left posterior mammary fat pad of wild-type female PyMT mice.

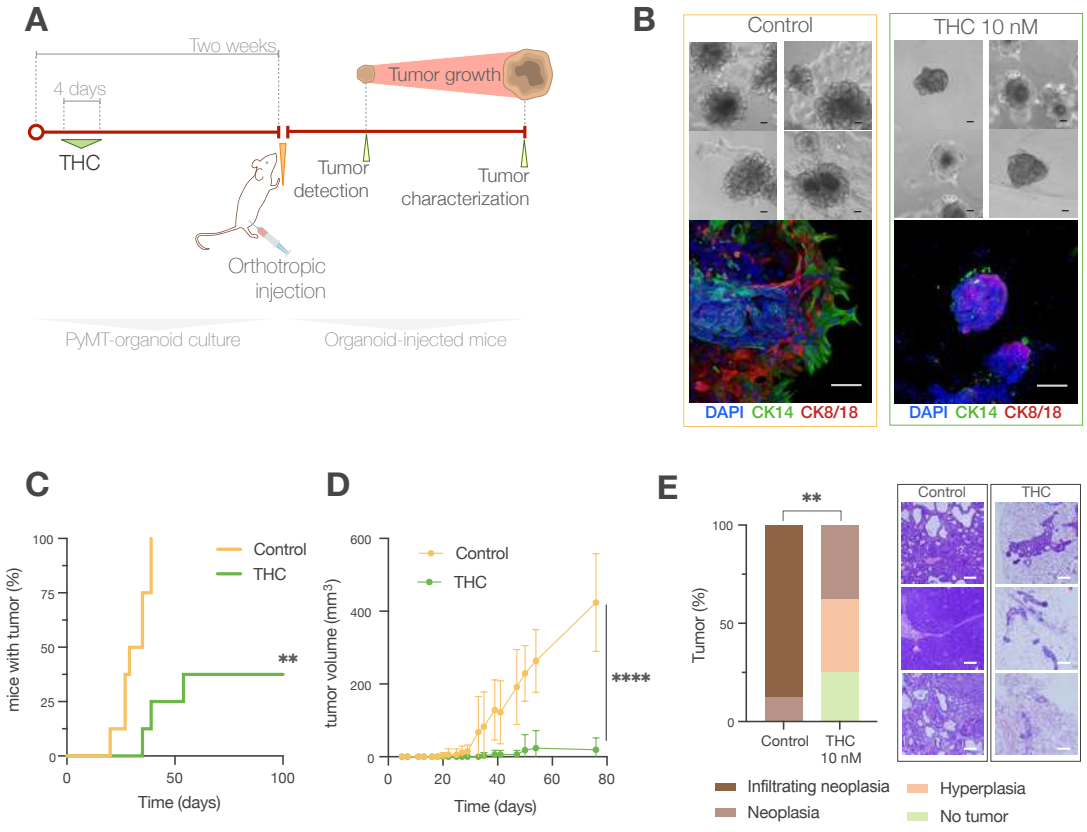

Figure R10. THC pre-treatment delays tumor initiation and limits malignancy in orthotopic organoid transplantation. A, Schematic of the experimental design. MMTV-PyMT-derived organoids were treated with vehicle or THC (10 nM) for 4 days, cultured drug-free for 10 days, and orthotopically injected into PyMT wild-type littermates. Mice (n=8 vehicle, n=8 THC) were monitored for 100 days to assess tumor onset and growth. **B,** Bright-field and immunofluorescence images of organoids treated as indicated and analyzed before injection. Organoids marked by basal (CK14; green) and luminal (CK8/18; red) markers. DAPI (blue) stains nuclei. Scale bar, 100 µm. **C,** Kaplan-Meier plot showing tumor onset (% of mice with tumors) over time. **p<0.01 vs. control (Two-way ANOVA). **D,** Quantification of tumor volume (mm^3) in both groups. ****p<0.0001 vs. control (Two-way ANOVA). **E,** Histopathological classification of tumors at endpoint (100 days): expanded infiltrating neoplasia, local neoplasia, hyperplasia, or no tumor detection. **p<0.01 vs. control (Two-way ANOVA). Right: H&E-stained images of representative infiltrating neoplasia (control) and localized hyperplasia (THC). Scale bar, 500 µm.

While 100 % of control organoid-injected mice developed tumors, only 37.5 % of mice receiving THC-pretreated organoids did so, indicating a significant reduction in tumor-initiating capacity (**Figure R10C**). Tumor onset was markedly delayed by THC pretreatment (**Figure R10C-D**). Moreover, the few tumors that did form in the THC group exhibited significantly slower growth over the 11-week observation period, in contrast to controls, which reached the experimental endpoint due to tumor burden (**Figure R10D**).

Histological analysis, performed by an independent pathologist in a blinded evaluation, revealed that tumors derived from control organoids were predominantly infiltrating neoplasias, observed in nearly 90 % of mice, with clear evidence of invasion beyond the mammary tissue. In contrast, tumors derived from THC-treated organoids were restricted to localized neoplasias or hyperplasias, with limited invasion (**Figure R10E**).

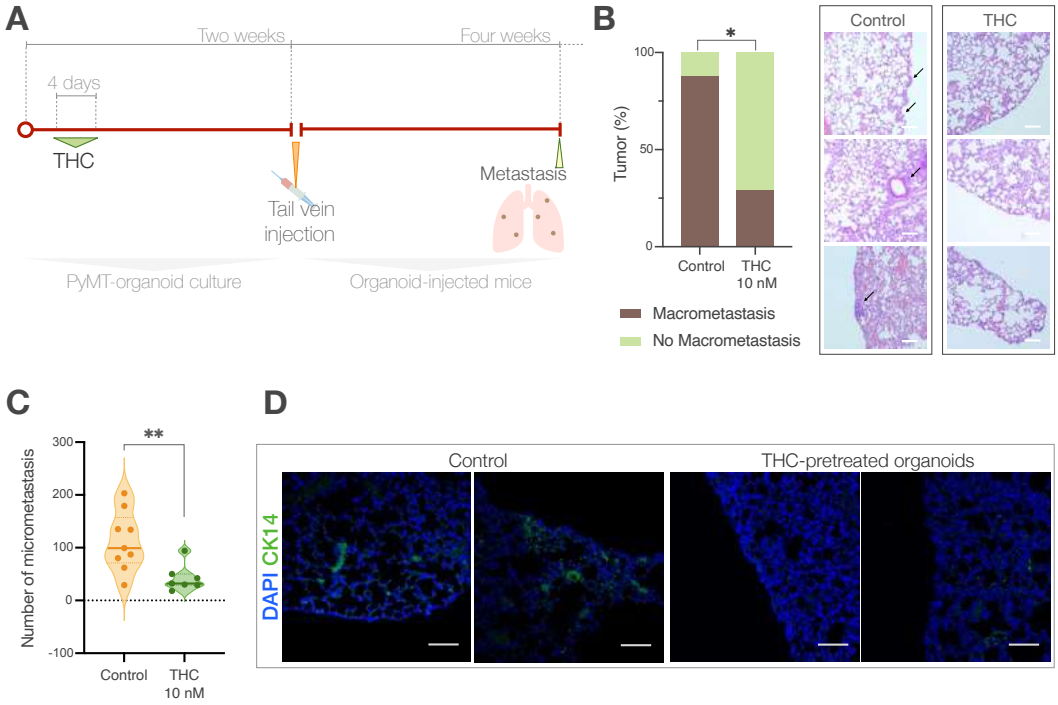

Figure R11. THC pre-treatment reduces metastatic potential of breast cancer organoids *in vivo*. A, Schematic of metastasis assay. Organoids were treated with vehicle or THC (10 nM) for 4 days, cultured for 2 additional weeks, and injected via tail vein into PyMT wild-type mice. Lung metastases were assessed one-month post-injection (n=9 vehicle, n=7 THC). **B,** Distribution of macro-metastases in lung tissue per condition. *p<0.05 vs. control (Two-way ANOVA). Right: H&E-stained images of representative lung metastases. Scale bar, 500 µm. **C,** Quantification of micro-metastases per animal. Each dot represents one mouse. **p<0.01 vs. control (Two-way ANOVA). **D,** Immunofluorescence of lung sections stained for CK14, indicating micro-metastases. DAPI (blue) stains nuclei. Scale bar, 500 µm.

Given that collective migration is associated with metastatic dissemination, we assessed metastatic capacity after THC treatment. THC-pretreated organoids were injected via tail vein into wild-type PyMT mice to assess their capacity to form lung invasion (**Figure R11A**). Remarkably, THC-pretreated organoids gave rise to significantly fewer lung macro-metastases, as determined by H&E staining in an independent, blinded pathological evaluation (**Figure R11B**). While nearly 90 % of mice injected with control organoids developed lung metastases, only 29 % of those injected with THC-pretreated organoids exhibit detectable metastases. Further analysis using CK14 immunostaining, that labels specifically breast-derived tumor cells, confirmed fewer and smaller metastatic foci in the lungs of mice injected with THC-pretreated organoids (**Figure R11C-D**).

Together, these findings reveal that brief, low-dose THC exposure durably reprograms tumor cell fate, reducing plasticity, stemness, and metastatic potential both *in vitro* and *in vivo*. THC effectively reprograms the three key axis of breast cancer biology: the treatment induces (1) a shift from a basal-like phenotype to a luminal-like cell state, (2) a transition from a mesenchymal to an epithelial phenotype, and (3) a progression from a de-differentiated to a more differentiated cellular profile. These axis-specific changes were consistently observed in both aggressive TNBC-like and HER2-positive-like mouse models, as well as in TNBC patient-derived organoids, and were associated with a marked reduction in cell proliferation, invasion and tumor-initiating potential —effects that were also challenged in *in vivo* context.

CB_2R mediates cannabinoid-induced differentiation in breast cancer organoids.

To further explore the effect of other cannabinoids in tumor cell differentiation, we compared the action of pure phytocannabinoids, *Cannabis sativa* extracts, and methanandamide (mAEA) —a stable non-hydrolysable form of the endocannabinoid AEA and dual CB_1R/CB_2R agonist— on PyMT-derived mammary tumor organoids.

We evaluated cannabidiol (CBD), known for its low affinity for cannabinoid receptors and lack of psychoactive effects compared to THC, yet it has been implicated in tumor modulation. Alongside pure CBD, we tested two plant-derived extracts: one enriched in THC and another containing a 1:1 ratio of THC and CBD. These full-spectrum extracts include a complex variety of cannabinoids and terpenes, that, in some contexts, may produce synergistic effects [174,175].

In parallel, mAEA was used to model increased endogenous cannabinoid tone through physiological activation of both CB_1R and CB_2R. This allowed us to distinguish between effects mediated by direct endogenous ligands *versus* those driven by plant-derived compounds.

As shown in **Figure R12A-B**, treatment with phytocannabinoids —either pure CBD or full-spectrum extracts— induced a significant morphological transition in the organoids, evidenced by the formation of cystic structures observed 10 days after drug withdrawal. In contrast, mAEA did not elicit such changes, suggesting that observed remodeling is somehow specific to phytocannabinoid exposure.

Additionally, CBD and extract treatments reduced overall organoid size, implying decreased proliferative activity similar to that previously observed with THC, whereas mAEA induced a significant increase in organoid growth (**Figure R12C**), consistent with a proliferative response to physiological endocannabinoid signaling. Moreover, phytocannabinoid treatments significantly suppressed collective migration, as shown by a reduction in the migratory area (**Figure R12D**), an effect not observed with mAEA.

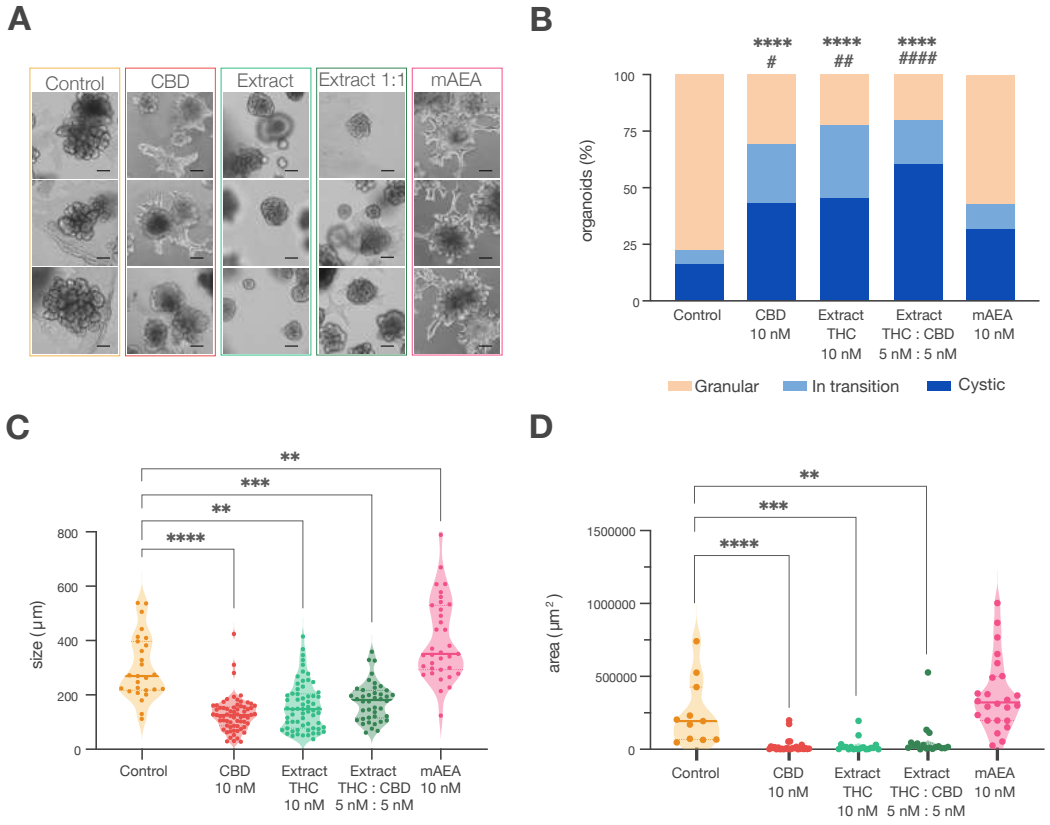

Figure R12. Cannabis extracts derived from *Cannabis sativa* produce effects similar to those of pure phytocannabinoids on tumor cell differentiation, in contrast to endogenous cannabinoid AEA. A, Representative bright-field images of organoid cultures treated with vehicle, CBD (10 nM), THC-rich extract from *Cannabis sativa* (10 nM, "Extract"), a THC:CBD 1:1 extract (5 nM each, "Extract 1:1"), or methanandamide (10 nM mAEA, a stable AEA analogue). Organoids were treated for 4 days, followed by 2 weeks of drug withdrawal, and analyzed at the end of the period. n=3 independent experiments. Scale bar: 100 µm. **B,** Quantification of organoid morphology at 14 days post-treatment, categorizing them as granular (basal-like), in transition, or cystic (luminal-like/rounded). n=3 independent experiments; ****p<0.0001 (Two-way ANOVA), comparing granular organoids vs control; #p<0.05; ##p<0.01; ####p<0.0001 (Two-way ANOVA), comparing cystic organoids vs. control. **C,** Quantification of organoid size (µm) for each treatment condition, measured 14 days post-treatment. n=3 independent experiments, with 80–100 organoids counted per condition; **p<0.01; ***p<0.001; ****p<0.0001 vs. control (One-way ANOVA). **D,** Quantification of the two-dimensional area (µm^2) of collective migratory projections in organoids treated with the five conditions, evaluated at 14 days. n=3 independent experiments, with 25–30 organoids counted per condition; **p<0.01; ***p<0.001; ****p<0. vs. control (unpaired Student's t-test).

Further supporting a differentiation response, phytocannabinoid-treated organoids underwent a phenotypic switch from a basal-like to a luminal-like state, which was not observed under mAEA treatment. This was evidenced by a marked reduction of CK14 marker in the phytocannabinoid-

treated conditions, an effect absent in the mAEA-pretreated organoids (**Figure R13**). Collectively, these findings suggest that plant-derived cannabinoids modulate tumor cell plasticity through a mechanism that is distinct from canonical CB_1R/CB_2R activation by endogenous ligands.

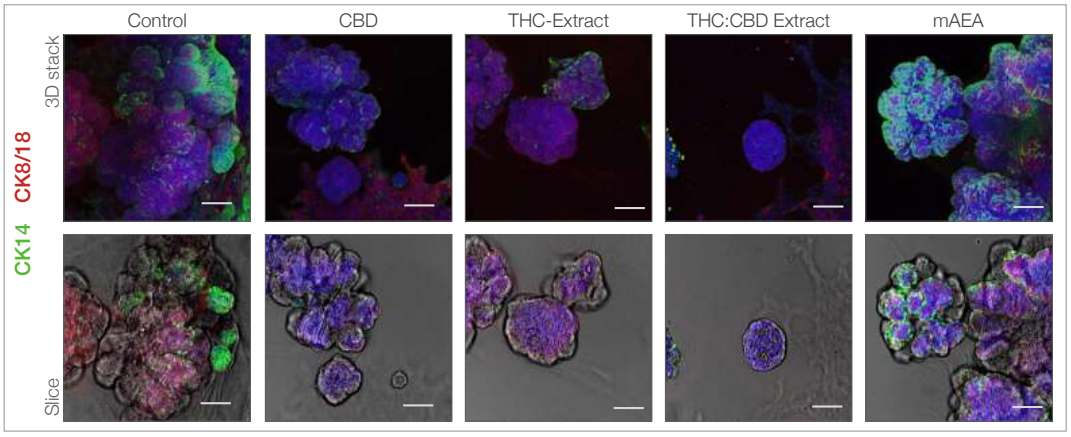

Figure R13. Phytocannabinoid modulation of tumor cell differentiation is associated with a basal-to-luminal molecular switch. Representative confocal images of organoids treated as indicated and stained for CK14 (green) and CK8/18 (red) at 14 days post-treatment. Nuclei are stained with DAPI (blue). Upper panels show 3D stacks, and lower panels show representative slices. n=4 independent experiments. Scale bar: 100 µm.

To further explore the contribution of cannabinoid receptor signaling to the differentiation response, we tested the effect of selective synthetic inverse agonists: SR1 (targeting CB_1R) and SR2 (targeting CB_2R). Short-term treatment with SR2, but not SR1, recapitulated key phenotypic changes observed under THC exposure (**Figure R14A**). SR2 induced a similar morphological transition, including cystic structure formation (**Figure R14B**), and significantly reduced organoid size (**Figure R14C**), indicating decreased proliferation.

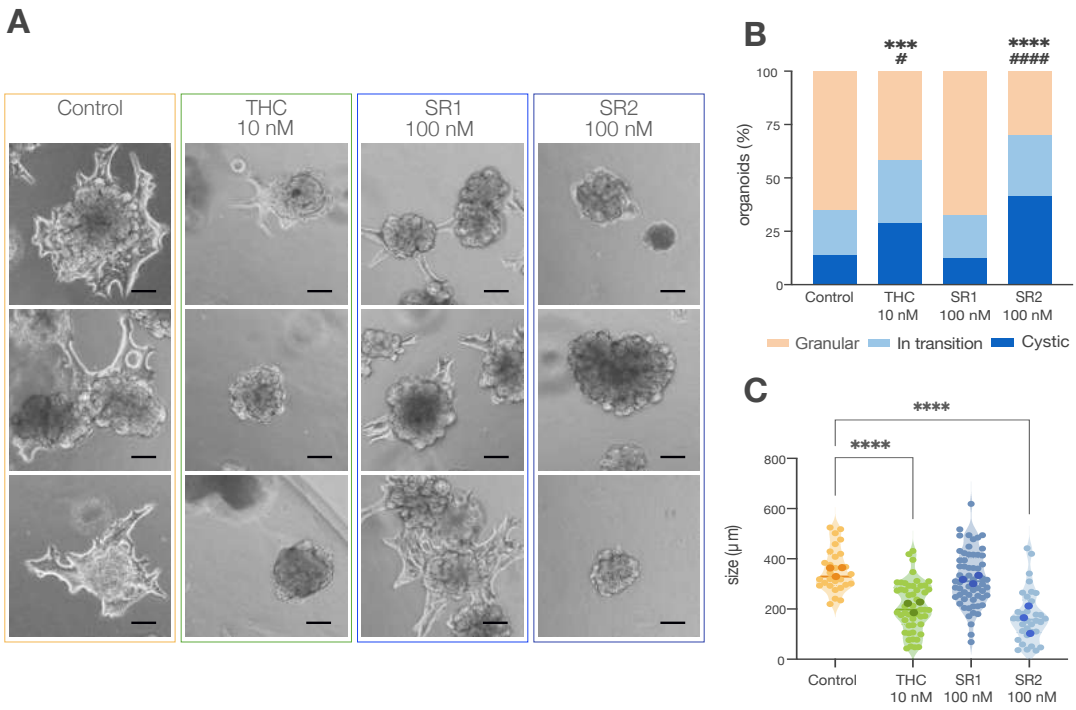

Figure R14. SR2 recapitulates THC-induced long-term morphological and phenotypical changes. A, Representative bright-field images of organoids treated for 4 days with vehicle, THC (10 nM), SR1 (100 nM), or SR2 (100 nM), and analyzed after two weeks of drug withdrawal. n=4 independent experiments. Scale bar, 100 µm. **B,** Quantification of organoid morphology (granular, in transition, cystic) in each condition at 14 days. ***p<0.001; ****p<0.0001 (Two-way ANOVA, granular vs. control); #p<0.05; ####p<0.0001 (cystic vs. control). **C,** Organoid size (µm) measured at 14 days. n=80–100 organoids/condition across 4 experiments; ****p<0.0001 vs. control (One-way ANOVA).

In addition, SR2 treatment triggered a sustained basal-to-luminal-like phenotypic switch and suppressed collective migration, recapitulating the THC-mediated effects on tumor plasticity (**Figure R15A-B**). SR2 also impaired the self-renewal capacity of organoids in secondary formation assays (**Figure R15C**), suggesting a reduction in stem-like potential.

Collectively, these results support a functional role for CB_2R in modulating tumor cell plasticity during differentiation. The ability of SR2 to mimic THC remodeling —despite acting as an inverse agonist rather than a partial receptor agonist—suggests a non-canonical, receptor tone-dependent mechanism through which CB_2R regulates mammary tumor cell fate.

Given that THC appear to functionally behave similarly as SR2 —CB_2R inverse agonist— we hypothesized that its effects might result from inhibition of CB_2R. However, the differentiation effects observed under THC treatment could also be mediated through CB_1R, as THC has been described as a partial agonist of both receptors. In this hypothetical framework, CB_1R

involvement could reflect either direct activation by THC or compensatory activation triggered by SR2, potentially explaining both differentiation-mediated processes.

To test this, we co-treated organoid with THC and either SR1 (to block CB_1) or SR2 (to block CB_2), aiming to determine whether blocking one receptor during THC exposure could prevent the differentiation phenotype.

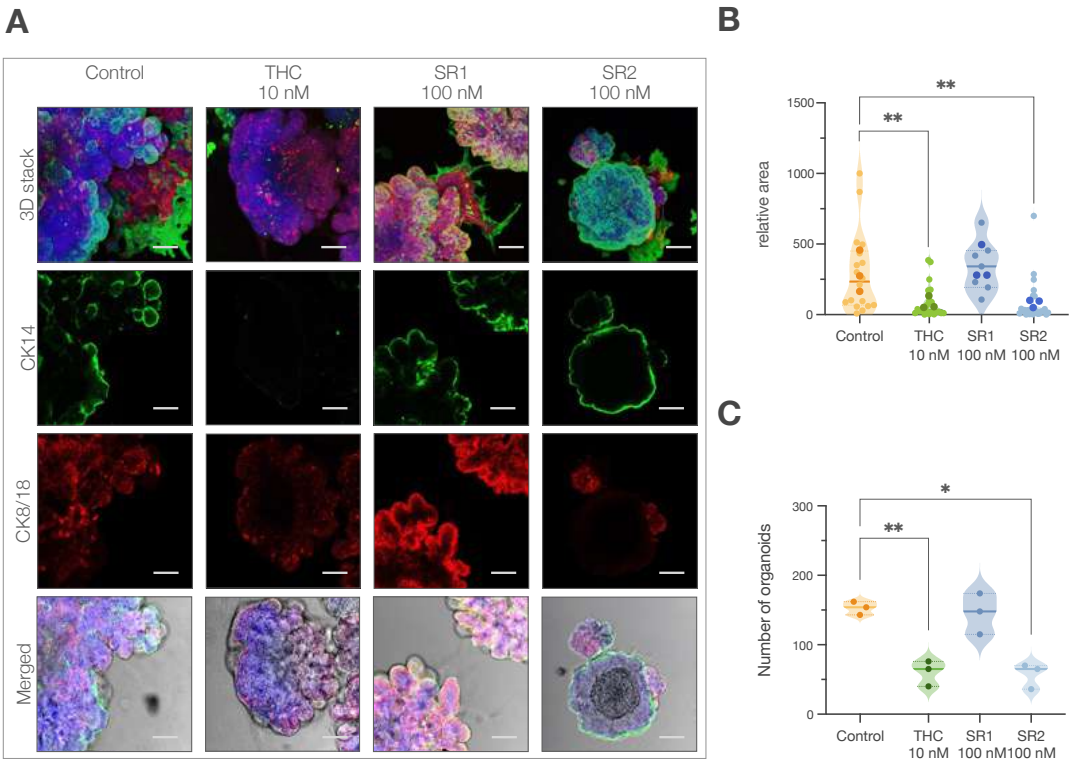

Figure R15. SR2, but not SR1, mimics THC in promoting a basal-to-luminal switch, blocking collective migration, and reducing self-renewal in mammary tumor organoids. A, Confocal images of organoids stained for CK14 (green) and CK8/18 (red), showing marker changes 2 weeks after treatment. DAPI (blue) stains nuclei; bottom panels show merged IF and bright-field images. n=4. Scale bar, 100 µm. **B,** Quantification of collective migratory projection area in all conditions at 2 weeks. n=25–30 organoids/condition; **p<0.01 vs. control (unpaired Student's t-test). **C,** Number of secondary organoids formed from single-cell dissociation (indicating self-renewal) at 21 days. n=3 independent experiments; *p<0.05; **p<0.01 vs. control (One-way ANOVA).

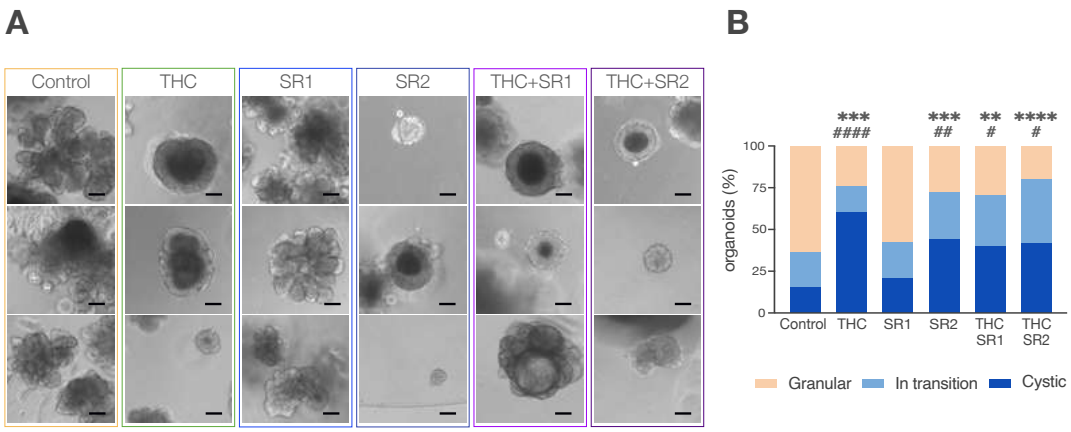

Figure R16. CB_2R or CB_1R blockade does not prevent THC-induced morphological differentiation in tumor organoids. A, Representative bright-field images of organoid cultures treated with vehicle (DMSO), THC (10 nM), CB_1R inverse agonist SR1 (100 nM), CB_2R inverse agonist SR2 (100 nM), or combinations of THC with SR1 or SR2. Treatments were applied for 4 days, followed by 2 weeks of drug withdrawal. n=3 independent experiments. Scale bar: 100 µm. **B,** Quantification of organoid morphology at 14 days post-treatment, categorizing them as granular (basal-like), in transition, or cystic (luminal-like/rounded). No significant differences were observed between THC alone and the combinations with SR1 or SR2. n=3 independent experiments; **p<0.01; ***p<0.001; ****p<0.0001 vs. control (Two-way ANOVA), comparing granular organoids vs. control; #p<0.05; ##p<0.01; ####p<0.0001 (Two-way ANOVA), comparing cystic organoids vs. control.

Again, both THC and SR2 alone induced the same morphological changes. Notably, co-treatment with SR1 or SR2 did not inhibit THC response: the same phenotypic transition occurred in THC, SR2, THC+SR1, and THC+SR2 conditions, while SR1 alone had no effect (**Figure R16**). Furthermore, reduced proliferation and migration were consistently observed in all THC- or SR2-containing conditions, but were absent with SR1 alone (**Figure R17A-B**). These results suggest that THC and SR2 may converge on a common pathway to drive differentiation, that may not be related, in short term, to CB_1R direct modulation.

To further investigate receptor dynamics, we examined the expression levels of CB_1R (*Cnr1*) and CB_2R (*Cnr2*) across all treatment conditions at three time points: during drug exposure, and four- and ten-days post-withdrawal (**Figure R17C**). In differentiation-responsive conditions, CB_2R expression showed a modest increase during drug exposure, followed by a decline and stabilization, particularly in the combined treatments. In contrast, CB_1R expression seemed to decrease early upon treatment and remained mildly suppressed throughout the course of differentiation. Interestingly, in the SR1 condition, both CB_1R and CB_2R appeared to be initially downregulated during exposure. However, upon withdrawal, CB_1R levels seemed to return to

baseline, while CB_2R expression appeared to increase approximately twofold, suggesting a delayed compensatory response.

The differentiation phenotype induced by THC and SR2 correlates with a transient CB_2R increase, a response that is not prevented by CB_1R blockade. This transient effect appears sufficient to trigger a long-term differentiation process. In contrast, CB_1R expression patterns remained relatively consistent across conditions, indicating a limited role in driving the observed phenotype. This reinforces the idea that CB_2R plays a central role in modulating tumor cell plasticity, independently of classical receptor agonism or compensatory CB_1R activity.

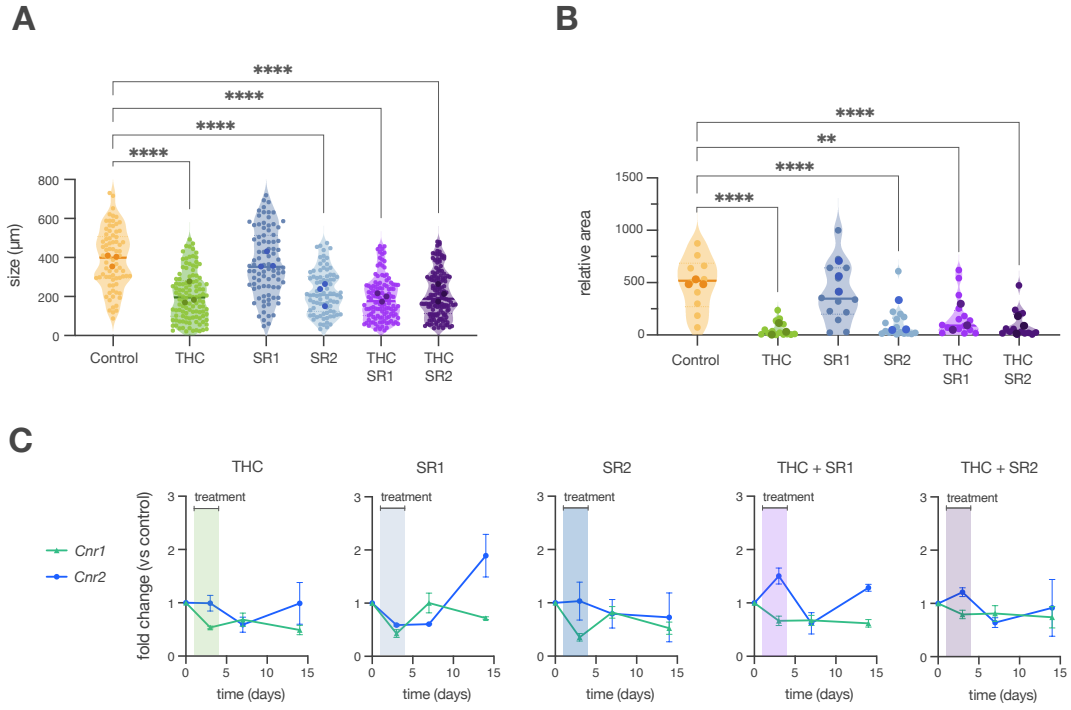

Figure R17. THC-induced reduction in organoid size and migration is not altered by CB_1R or CB_2R blockade. A, Quantification of organoid size (µm) in all conditions at 14 days post-treatment. No significant changes were observed between THC and the combinations with SR1 or SR2. n=3 independent experiments, with 80–100 organoids counted per condition; ****p<0.0001 vs. control (One-way ANOVA). **B,** Quantification of the two-dimensional area of collective migratory projections in organoids treated with the five conditions, analyzed at 14 days. No significant difference was found between THC and the combinations with SR1 or SR2. n=3 independent experiments, with 10–20 organoids counted per condition; **p<0.01; ****p<0.0001 vs. control (unpaired Student's t-test). **C,** mRNA expression levels of CB_1R (*Cnr1*, green) and CB_2R (*Cnr2*, blue) measured by qPCR at various time points: before, during, or after treatment. mRNA levels were normalized to *Gapdh* housekeeping gene. n=3 independent experiments; no significant changes detected (unpaired Student's t-test).

To directly assess the role of CB_2R on tumor differentiation, we generated CB_2R knock-out mice on the PyMT background (PyMT $CB_2R^{KO/KO}$). Compared to wild-type controls, CB_2R-deficient mice showed significantly delayed tumor onset, with tumors appearing over 17 days later (**Figure R18A**), consistent with previous reports [121].

Histological analysis revealed no relevant differences in basal (CK14) or luminal (CK8/18) marker expression. However, CB_2R-deficient tumors exhibited reduced expression of the proliferation marker Ki67, and lower levels of stemness-associated transcription factors Sox9 and Sox10 (**Figure R18B**), suggesting impaired proliferative and stem-like capacity.

Based on the delay of tumor onset and the reduced expression of stem-like markers in CB_2R knock-out tumors, we next evaluated the distribution of mammary cell lineage using EpCAM and CD49f surface markers. These markers are commonly used to define distinct cell subpopulations within the mammary epithelium. We identified four cell populations: luminal progenitors ($EpCAM^+/CD49f^+$), mature luminal cells ($EpCAM^+/CD49f^-$), stem-like cells ($EpCAM^-/CD49f^+$), and differentiated basal cells ($EpCAM^-/CD49f^-$). Due to ambiguity in distinguishing mature luminal cells, this group was excluded from analysis (**Figure R18C**).

Unexpectedly, flow cytometry revealed no significant differences in the distribution of these populations between CB_2KO and wild-type tumors (**Figure R18C**), suggesting that the observed phenotypes in tumor onset and stem-like marker expression are not due to alterations in subpopulation composition, but may instead reflect changes in the functional plasticity of the cells. To test this, we assessed the ability of each sorted subpopulation to form organoids.

Interestingly, cells from the double-negative ($EpCAM^-/CD49f^-$) population could adhere to the culture plate despite being embedded within the matrix and plated onto non-treated surfaces, showing their basal-like capacity and strong mesenchymal features. However, these cells failed to expand, or form mature organoid structures. In contrast, only the EpCAM+/CD49f+ luminal progenitor cells demonstrated the capacity to consistently generate organoids in both CB_2KO and wild-type backgrounds (data not shown). Notably, the number of organoids generated was significantly reduced in CB_2KO tumors (**Figure R18D**), suggesting that CB_2R plays an important, though not entirely indispensable, role in tumor initiation and maintenance of stem-like plasticity within the mammary tumor.

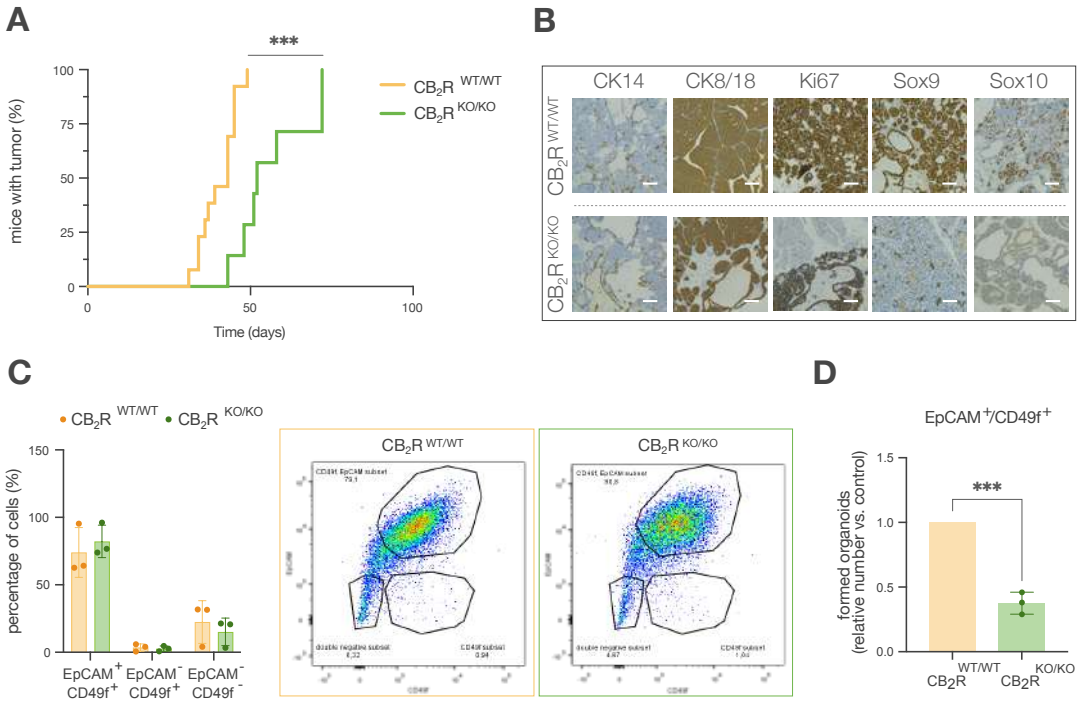

Figure R18. Knock-out of CB_2R delays tumor onset and impairs stem-like potential in luminal progenitor cells. A, Kaplan-Meier plot showing tumor onset in MMTV-PyMT $CB_2R^{WT/WT}$ and $CB_2R^{KO/KO}$ mice over 100 days, measured as the percentage of mice with tumors. $CB_2R^{WT/WT}$ n=15, $CB_2R^{KO/KO}$ n=12 animals; ***p<0.001 vs. control (Two-way ANOVA). **B,** Representative images of tumor molecular characterization. Protein expression levels of CK14 (basal marker), CK8/18 (luminal marker), Ki67 (proliferation marker), Sox9 and Sox10 (stemness markers) were evaluated by immunohistochemistry. Scale bar: 500 µm. **C,** Flow cytometry analysis of EpCAM/CD49f subpopulations in $CB_2R^{WT/WT}$ and $CB_2R^{KO/KO}$ tumors: EpCAM+/CD49f+ (luminal progenitors), EpCAM-/CD49f+ (stem-like mammary cells), EpCAM-/CD49f- (differentiated basal cells). Left panel shows the percentage of cells in each subpopulation. Right panel shows representative flow cytometry plots for each subpopulation. n=3 independent experiments. **D,** Relative comparison of the number of organoids generated from the EpCAM+/CD49f+ subpopulation (luminal progenitors) of tumor cells. Only organoids derived from luminal progenitors are shown, as other EpCAM/CD49f subpopulations did not generate stable organoid cultures. n=3 independent experiments; ***p<0.001 vs. control (unpaired Student's t-test).

To further examine the role of CB_2R in THC mediated action, we generated and characterized organoids derived from CB_2-depleted tumors. Interestingly, organoids lacking CB_2R displayed distinct morphological features consistent with a luminal-like phenotype and showed a marked reduction in *CK14* expression, consistent with diminished basal features (**Figure R19A-C**).

Beyond these morphological alterations, CB_2R-deficient organoids displayed additional impairments associated with cell differentiation. We observed a significant decrease in their proliferative capacity (**Figure R19D**), reduced collective migration behavior (**Figure R19E**), and a

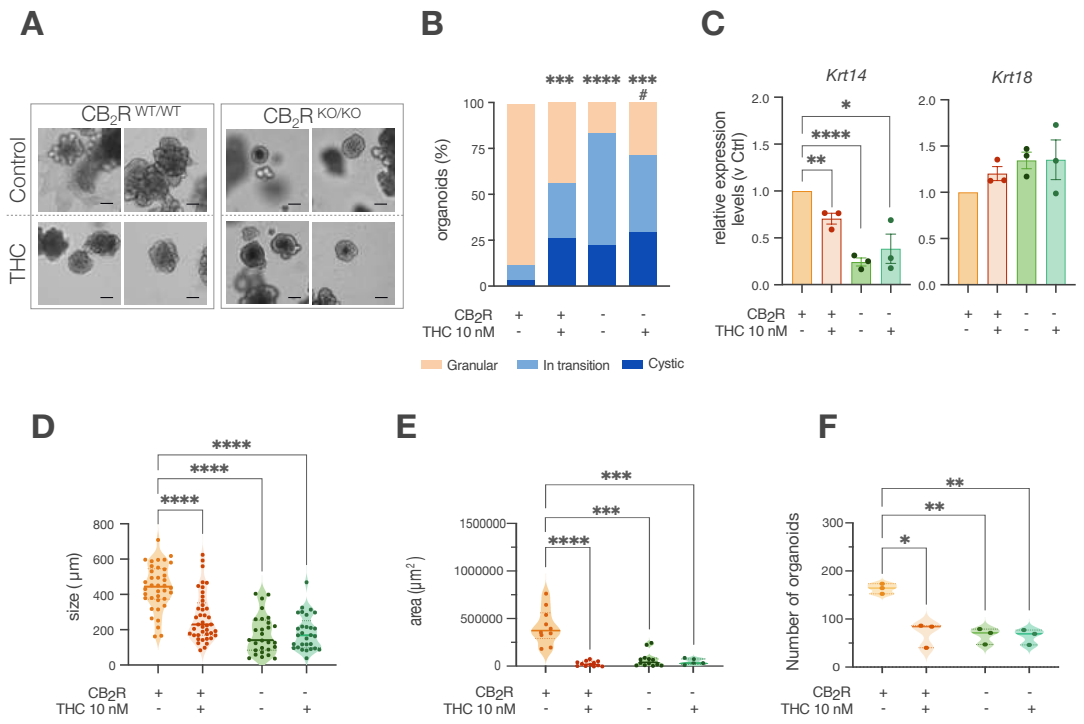

Figure R19. Loss of CB_2R mimics THC-induced differentiation and impairs self-renewal in breast tumor organoids. A, Representative bright-field images of organoid cultures derived from $CB_2R^{WT/WT}$ and $CB_2R^{KO/KO}$ tumors treated with vehicle or THC (10 nM). Treatments were applied for 4 days, followed by 2 weeks of drug withdrawal. n=3 independent experiments. Scale bar: 100 µm. **B,** Quantification of organoid morphology at 14 days post-treatment, categorizing them as granular (basal-like), in transition, or cystic (luminal-like/rounded). n=3 independent experiments; ***p<0.001; ****p<0.0001 vs. control (Two-way ANOVA), comparing granular organoids vs. control; #p<0.05 (Two-way ANOVA), comparing cystic organoids vs. control. **C,** mRNA expression levels of basal (*Krt14*) and luminal (*Krt18*) markers, measured by qPCR. mRNA levels were normalized to *Gapdh*. n=3 independent experiments; *p<0.05; **p<0.01; ****p<0.0001 vs. control (unpaired Student's t-test). **D,** Quantification of organoid size (µm) at 14 days post-treatment. n=3 independent experiments, with 80–100 organoids counted per condition; ****p<0.0001 vs. control (One-way ANOVA). **E,** Quantification of the two-dimensional area (μm^2) of collective-migratory projections in organoids analyzed at 14 days. n=3 independent experiments, with 10–20 organoids counted per condition; ***p<0.001; ****p<0.0001 vs. control (unpaired Student's t-test). **F,** Total number of secondary organoids generated from single-cell disaggregation (reflecting self-renewal capacity) in the four conditions tested, evaluated at 21 days post-treatment. n=3 independent experiments; *p<0.05; **p<0.01 vs. control (One-way ANOVA).

compromised long-term self-renewal potential, as evidenced by diminished secondary organoid formation from single cells (**Figure R19F**). Notably, these changes closely mirrored those observed in wild-type organoids treated with THC. Importantly, THC treatment on CB_2KO organoids failed to further enhance the differentiation phenotype already induced by CB_2R deletion: it did not increase the percentage of cystic organoids, nor further reduced proliferative features or self-renewal capacity, suggesting that CB_2R loss phenocopies the effects of THC. This highlights a critical role of CB_2R in maintaining stem-like characteristics, proliferative dynamics and regenerative capacity within the tumor plasticity.

Collectively, these findings identify CB_2R signaling as a key modulator of tumor differentiation, capable of driving durable reprogramming in breast cancer organoids. CB_2R appears to play a critical role in regulating cellular plasticity, facilitating the transition toward a stem-like state necessary for tumor initiation. Notably, the specific modulation of CB_2R by THC and SR2 can alter this plastic potential, promoting differentiation and thereby reducing tumorigenic capacity. These results underscore the potential of CB_2R as a target for manipulating tumor cell fate and limiting cancer progression.

THC and SR2 trigger an early, transient epigenetic reprogramming in breast cancer organoids, driving sustained cellular differentiation.

Cellular differentiation is tightly linked to epigenetic remodeling; however, the relationship between CB_2R signaling and epigenetic regulation in cancer remains poorly defined [169]. To investigate this connection, we conducted transcriptomic profiling of mammary tumor organoids treated with either THC or SR2, focusing on genes implicated in epigenetic control and stemness.

To capture transcriptional changes associated with the differentiation, RNAseq was conducted at two distinct time points: during early drug exposure (day 3) and after drug withdrawal (day 14), the latter coinciding with a presumed completion of differentiation (**Figure R20A**).

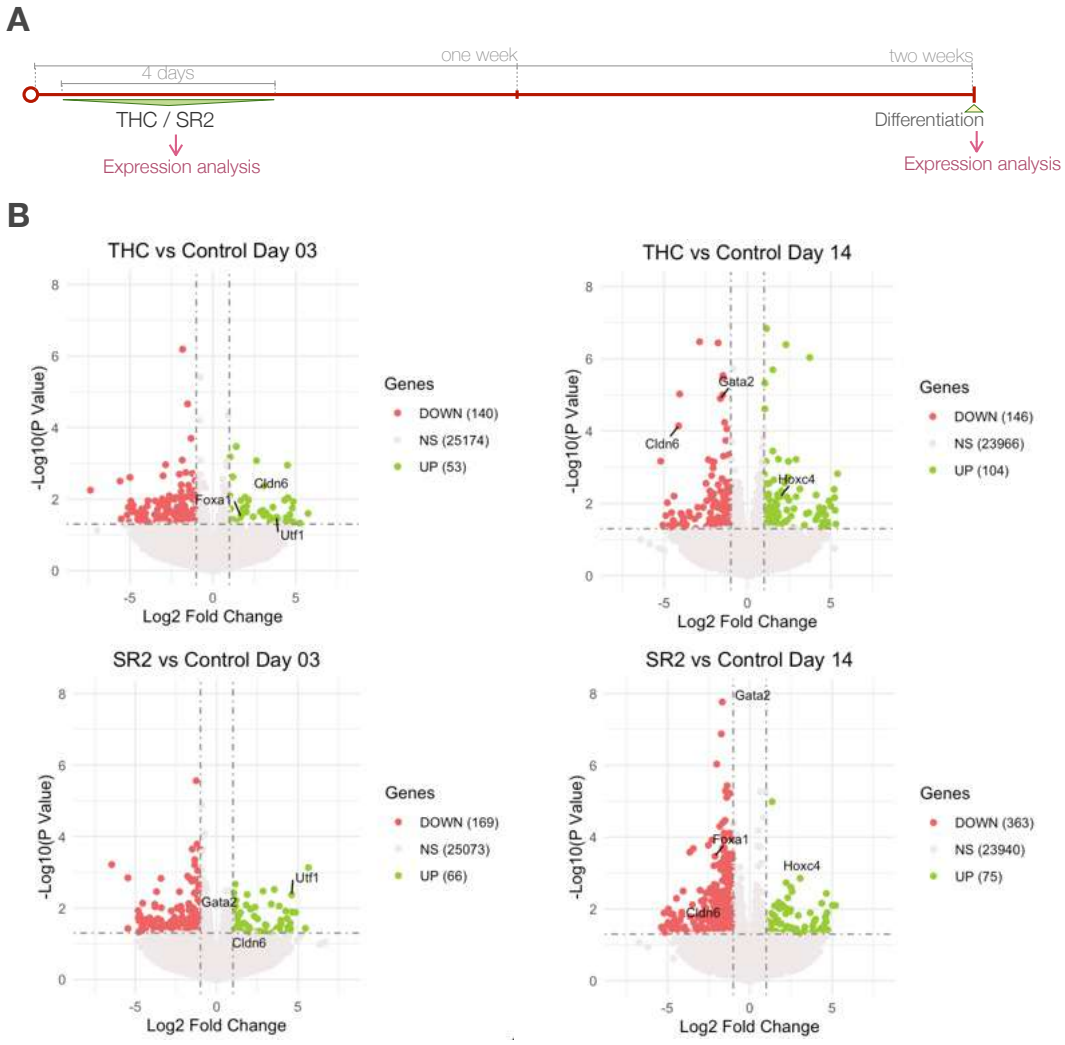

Figure R20. Transcriptional dynamics in organoids following CB_2R modulation. A, Schematic timeline of the experimental workflow. **B,** Volcano plots showing differentially expressed genes in organoids treated with THC (10 nM) or SR2 (100 nM) vs. vehicle at day 3 and day 14 post-treatment. Genes with $\log_2$ fold change between –1 and 1 are considered unchanged. n=3 independent experiments.

Initial analysis of volcano plots displaying differentially expressed genes at day 3 revealed an upregulation of pluripotency-associated markers, including *Utf1* — undifferentiated embryonic cell transcription factor 1, a master regulator in embryonic stem cells— and *Cldn6*, a tight junction protein selectively expressed during early embryogenesis [176,177], in response to both THC and SR2 treatment (**Figure R20B**). Notably, *Foxa1*, a transcription factor essential for epithelial lineage specification, was specifically induced by THC, whereas *Gata2*, a key regulator of mammary progenitor cell fate, was selectively upregulated by SR2 [178,179]. These stemness-related genes were subsequently downregulated by day 14. At this later stage, a consistent upregulation of *Hoxc4* — a member of *Hoxc* family associated with mammary lineage commitment [180] — was observed (**Figure R20B**).

Building on these preliminary transcriptional dynamics, gene set enrichment analysis (GSEA) revealed significant enrichment in pathways associated with pluripotency and stem cell regulation upon SR2 treatment (**Figure R21A**). In parallel, differential expression analysis

A

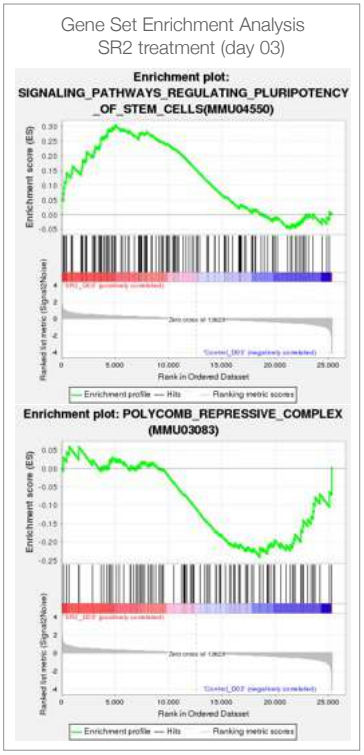

B

Control enrichment sets vs SR2

Day 03	NES	Size
N-acetyltransferase activity	-2.00	78
N-acyltransferase activity	-1.89	94
Acetyltransferase activity	-1.81	99
Peptide n-acetyltransferase activity	-1.80	64
Histone exchange	-1.66	16
Histone acetyltransferase activity	-1.54	56
Histone H3K9 modif cation	-1.53	43
Cromatin silencing	-1.53	60
Histone binding	-1.49	174
Histone H3K9 methylation	-1.49	119
Methylation dependent protein binding	-1.43	62

Figure R21. Enrichment of epigenetic and pluripotency pathways in SR2-treated organoids at early time point. A, Gene Set Enrichment Analysis (GSEA) of pathways related to pluripotency (top) and Polycomb Repressive Complex 2 (PRC2; bottom) in SR2-treated vs. control organoids at day 3 of treatment. **B,** Gene Ontology (GO) enrichment analysis at day 3 of treatment, showing epigenetic regulation pathways significantly altered in SR2-treated organoids compared to control. Normalized Enrichment Score (NES) and gene set size are indicated.

demonstrated broad SR2 modulation of genes encoding epigenetic regulators, including those involved in histone modification, chromatin remodeling, and DNA methylation (**Figure R21B**).

These transcriptomic changes were accompanied by increased of Polycomb Repressive Complex (PRC) signature, suggesting that CB_2R signaling may influence tumor plasticity through modulation of Polycomb-mediated chromatin states (**Figure R21A**).

At day 3, transcriptomic profiles of organoids treated with THC or SR2 were enriched for embryonic and pluripotency-associated gene signatures. This transcriptional landscape closely resembled early reprogramming stages observed in embryonic stem cells (ESCs), accompanied by active epigenetic remodeling. The transient increase in cellular plasticity was followed by a clear transition toward a differentiation-associated profile by day 14, underscoring a temporally structured reprogramming process (**Figure R22**). KEGG pathway analysis identified activation of hormone signaling pathways in response to both THC and SR2 —including estrogen, prolactin and oxytocin regulators— which are known to drive epithelial differentiation in the mammary gland. Additionally, enrichment of pathways involved in cell adhesion further supported the acquisition of epithelial characteristics during later maturation.

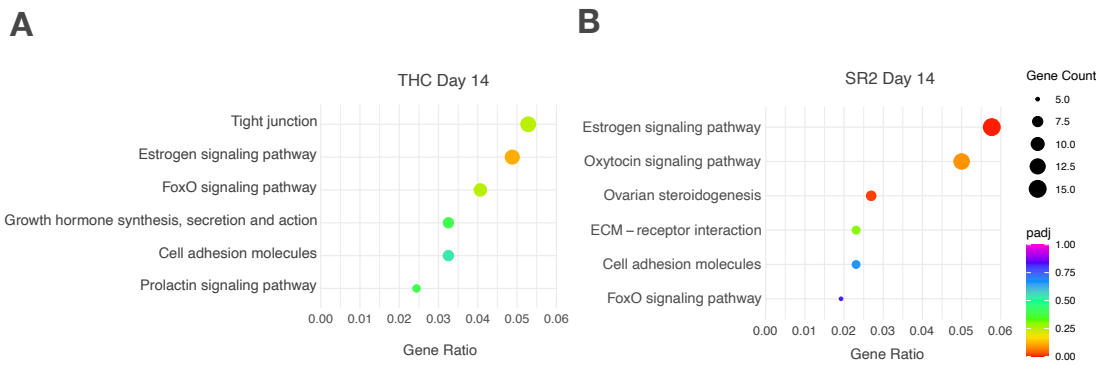

Figure R22. Enrichment of differentiation-associated pathways at later stages of CB_2R modulation. Dot plots showing KEGG pathway enrichment analysis of differentially expressed genes following THC (**A**) or SR2 (**B**) treatment and evaluated at day 14.

GSEA also revealed modulation of epigenetic regulators (**Figure R21B**), suggesting that CB_2R signaling may facilitate transcriptional priming and epigenetic poising of differentiation programs. Notably, among the top transiently expressed genes, *Utf1* emerged as key player. Known for its role in regulating PRC activity and maintaining pluripotency [181,182], *Utf1* was upregulated early in response to THC or SR2 exposure and and returned to baseline levels at later stages (**Figure R20**), mirroring the shift from a transcriptionally plastic to a more differentiated cellular state.

To further explore this transition, we examined the expression dynamics of validated *Utf1* and PRC2 target genes [182]. PRC2, a central chromatin-modifying complex involved in maintaining pluripotency in ESCs, plays a pivotal role in preserving pluripotency and regulating differentiation commitment. Its activity has been associated with both tumor-suppressive and tumor-promoting contexts, depending on cellular environment [183]. Through deposition of the repressive H3K27me3 mark, PRC2 maintains gene silencing while preserving readiness for transcriptional activation [184,185]. In contrast, *Utf1* counterbalances PRC2 activity by preventing excessive repression, enabling a responsive transcriptional landscape during differentiation [186].

At day 3, we observed upregulation of both *Utf1* and PRC2 target genes under THC and SR2 treatment conditions (**Figure R23A**), indicating coordinated activation of these regulatory networks. At later stages of differentiation, by day 14, these targets no longer differed from controls (**Figure R23B**), suggesting a diminished influence of *Utf1* and PRC2 on the differentiated transcriptome. Interestingly, under SR2 treatment at day 14, a pronounced downregulation of PRC2 targets was detected relative to controls. This finding mirrors the earlier enrichment of the same targets at day 3, suggesting a potential compensatory or rebound mechanism in the differentiation process.

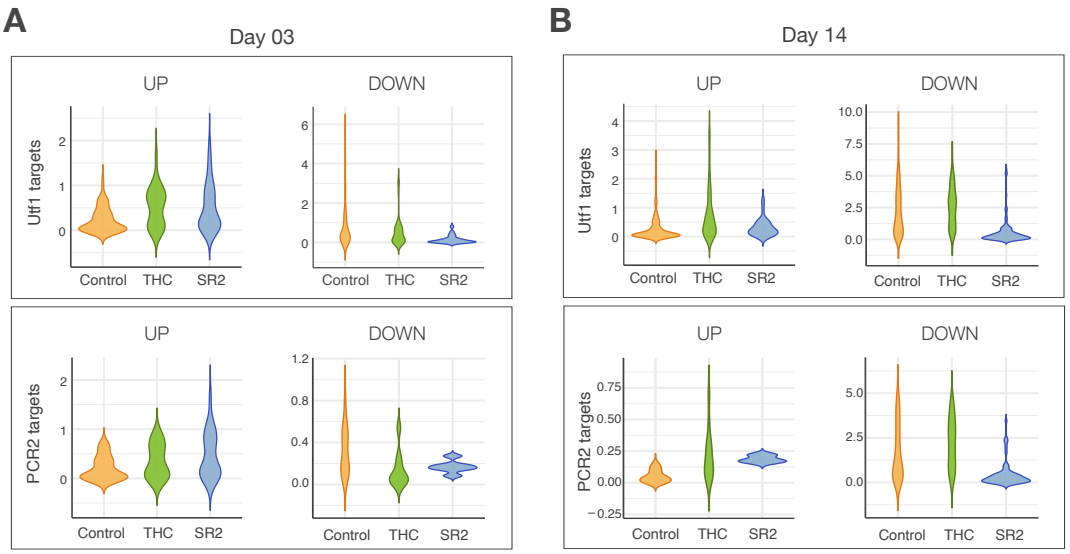

Figure R23. Early activation and later attenuation of *Utf1* and PRC2 target gene expression following CB_2R modulation. A-B, Violin plots showing expression scores of previously identified *Utf1* (top) and PRC2 (bottom) targets[182] at day 3 (**A**), and at day 14 post-treatment (**B**).

To investigate deeper into the epigenetic landscape, we assessed histone modifications associated with transcriptional activation and repression, specifically the trimethylation of histone 3 at lysine 9 (H3K9me3), lysine 4 (H3K4me3), and lysine 27 (H3K27me3) under both treatment and differentiation conditions. As previously mentioned, these histone modifications play critical roles in modulating chromatin architecture and gene accessibility, thereby influencing lineage specification [187].

H3K9me3, a well-established marker of transcriptional repression associated with lineage commitment and the maintenance of tissue-specific differentiation [188,189], showed a slight but statistically significant increase in nuclear intensity at day 3 following THC or SR2 treatment, indicative of early chromatin compaction and transcriptional repression (**Figure R24A**). This elevated H3K9me3 signal persisted through day 14 (**Figure R24B**), suggesting a lasting repressive environment that may contribute to stable differentiation.

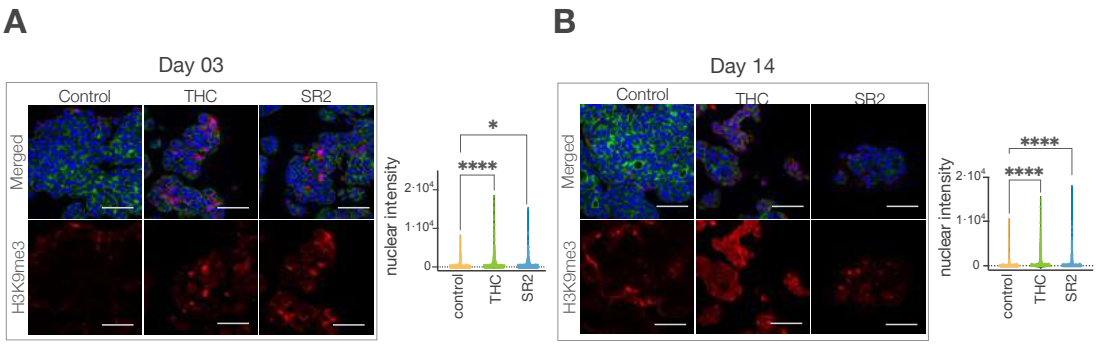

Figure R24. Temporal dynamics of H3K9me3 expression during CB_2R-induced differentiation. Organoids stained for H3K9me3 (red) and phalloidin (cytoskeleton marker; green) with DAPI (blue) staining nuclei at day 3 (**A**) and day 14 (**B**). Violin plots show quantification of total nuclear fluorescence intensity per nucleus (800-1500 nuclei were evaluated per condition). n=3 independent experiments. *p<0.05; ****p<0.0001 vs. control (One-way ANOVA). Scale bar, 100 µm.

We also examined the previously mentioned bivalent histone marks, notably H3K4me3 (active) and H3K27me3 (repressive), regulated by PRC2 and *Utf1*. At day 3, treated organoids displayed increased H3K4me3 levels and reduced H3K27me3, resulting in a lower H3K27me3/H3K4me3 ratio (**Figure R25A and C**). This shift suggests a permissive chromatin environment conductive to transcription and lineage commitment. By day 14, this trend reversed: H3K4me3 levels declined, while H3K27me3 levels significantly increased, leading to a higher H3K27me3/H3K4me3 ratio (**Figure R25B and D**). These changes may suggest that chromatin repression is being re-established as cells progress through differentiation.

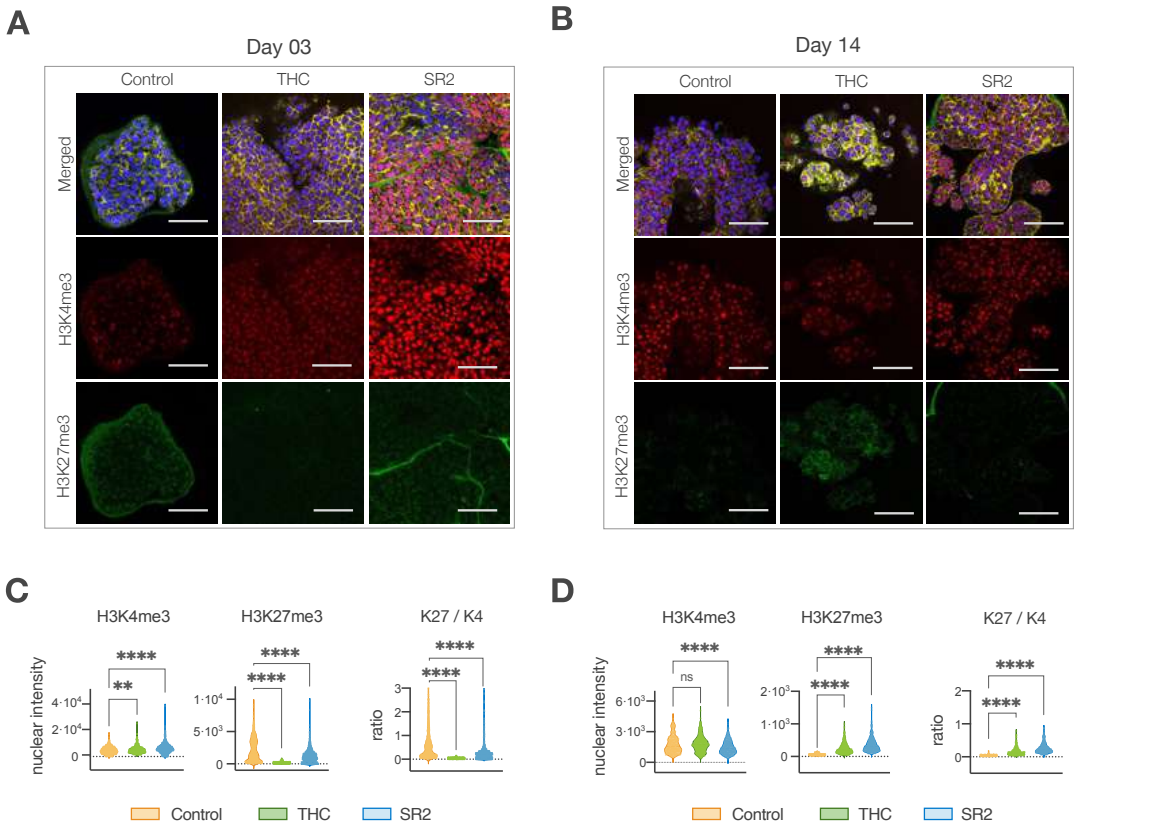

Figure R25. Dynamic regulation of chromatin bivalency marks H3K4me3 and H3K27me3 during CB_2R-mediated differentiation. Organoids stained for H3K4me3 (red), H3K27me3 (green) and phalloidin (yellow) at day 3 (**A**) and day 14 (**B**), with DAPI (blue) staining nuclei. **C-D,** Violin plots show quantification for day 03 (C) and day 14 (D) of total nuclear fluorescence intensity per nucleus (800-1500 nuclei were evaluated per condition) for every staining, and the H3K27me3/H3K4me3 ratio in same nuclei, indicating chromatin bivalency. n=3 independent experiments. ***p<0.001; ****p<0.0001 vs. control (One-way ANOVA). Scale bar, 100 µm.

Collectively, these findings demonstrate that short-term CB_2R modulation via THC or SR2 induces a transient epigenetic reprogramming, characterized by early upregulation of pluripotency genes, coordinated expression of *Utf1* and PRC2 targets, histone methylation shifts, and enrichment in stemness pathways at day 3. This epigenetic shift is subsequently followed by a transition to a transcriptional and epigenetic landscape dominated by differentiation signals at day 14. These results suggest that CB_2R signaling modulates cellular plasticity by transiently enhancing pluripotency-associated features, thereby priming mammary tumor organoids for robust and sustained differentiation.

CB_2R-driven differentiation locks tumor cells into a stable, irreversible phenotype.

A critical limitation of current differentiation therapies is their potential reversibility, particularly under microenvironmental conditions that promote stemness and tumor aggressiveness [82]. To assess the stability of CB_2R-induced differentiation in such contexts, we developed a dynamic co-culture system that mimics a pro-tumorigenic niche. This system incorporates cancer-associated fibroblast (CAFs), peripheral blood mononuclear cells (PBMCs), and continuous shear stress, delivered via a flow-controlled bioreactor.

The tumor microenvironment is not solely defined by the intrinsic heterogeneity of tumor cells but is also profoundly shaped by stromal and immune components that contribute to tumor initiation, maintenance and progression. Key players include CAFs, pro-tumorigenic immune cells, and the extracellular matrix (ECM), which provides biochemical cues that enhance tumor growth and survival. Mechanical stimuli, such as shear stress —typically absent in static *in vitro* systems— further enhance the dynamic nature of the tumor microenvironment. Within this context, CAFs exert pro-tumorigenic influences through the secretion of growth factors, induction of chronic inflammation, modulation of metabolic reprogramming, and ECM remodeling [72]. These activities directly impact angiogenesis, tumor proliferation and invasion.

To better replicate these interactions, we established a CAF-organoid co-culture model that emulates key aspects of the tumor niche. The fibroblast-to-organoid ratio was adjusted to reflect physiological proportion observed in PyMT tumors, where CAFs represent 1-2.5 % of total tumor cells [190]. Based on this, CAFs were embedded together with the organoids at a 1:250 ratio (250 CAFs per organoid, with each organoid consisting of approximately 1×10^4 cells). Outcomes were assessed on days 4 and 10 (**Figure R26A**).

To distinguish the specific effects of CAFs from those of general fibroblasts, we included a control condition using NIH 3T3 mouse fibroblasts (**Figure R26B**). Notably, CAFs did not enhance tumor cell proliferation to the extent seen with normal fibroblast (**Figure R26C**). Instead, their primary influence was on invasive behavior: CAFs promoted mesenchymal traits in the organoids, as evidenced by a higher frequency of collective migration, a feature absent when normal fibroblasts were co-cultured with organoids (**Figure R26D**). Consistent with this, a significantly larger migration area was observed in CAF-organoid cultures (**Figure R26E**). These findings indicate that CAFs selectively enhance invasiveness without promoting proliferation, specifically reinforcing invasion front dynamics.

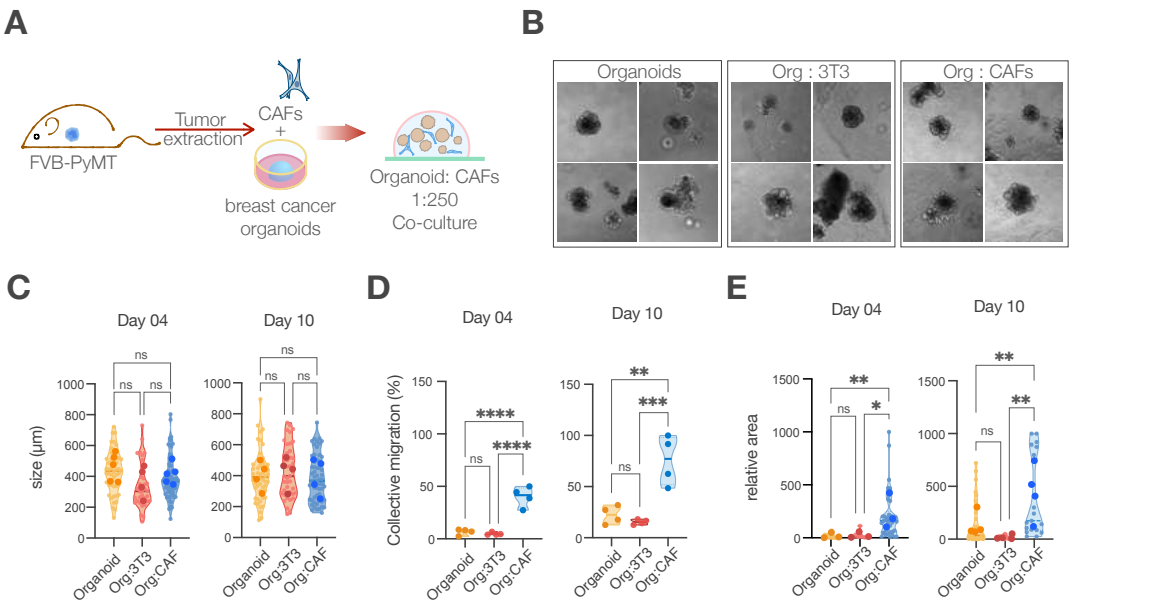

Figure R26. CAFs promote organoid growth and collective migration in a 3D co-culture system. A, Schematic of the initial co-culture setup. MMTV-PyMT–derived organoids were embedded in BME and co-cultured with either primary cancer-associated fibroblasts (CAFs) or NIH3T3 fibroblasts at a 1:250 ratio. **B,** Representative bright-field images of organoids cultured alone (left), with 3T3 fibroblasts (middle), or with CAFs (right) at day 10. **C,** Quantification of organoid size (µm) at day 4 and day 10 across the conditions shown in (**B**). n=4 independent experiments; ns, not significant (One-way ANOVA). **D,** Percentage of organoids displaying collective migration at day 4 and day 10. n=4 independent experiments; **p<0.01; ***p<0.001; ****p<0.0001 vs. control (One-way ANOVA). **E,** Quantification of collective migratory projection area across conditions at day 4 and day 10. n=3 independent experiments; *p<0.05; **p<0.01 vs. control (One-way ANOVA).

We next investigated whether the observed pro-invasive effect was mediated by soluble factors released by CAFs or required direct cell-cell interactions. To test this, organoids we cultured with CAF-conditioned media. Despite the known influence of CAFs on organoid invasion, treatment with conditioned media did not reproduce the collective migration patterns observed in direct co-culture (**Figure R27**). These results suggest CAF-mediated invasion likely depends on direct cellular interactions between CAFs and tumor cells or ECM remodeling, rather than secreted factors alone.

To further enhance the aggressiveness of the model, we introduced additional pro-invasive stimuli: shear stress and PBMCs extracted from the same tumor-bearing mice, thereby integrating additional cellular players known to interact with tumor cells and drive plasticity and aggressiveness. Shear stress —the mechanical force exerted by fluid flow on cells lining on blood vessels —has been implicated in promoting stemness in vascular endothelial cells [168] and modulating the behavior of circulating tumor cells (CTCs). It has been demonstrated that this

force facilitates epithelial-to-mesenchymal transitions (EMT), enhances cell-cell and cell-matrix adhesion, and improves tumor cell survival during vascular transit [191–193].

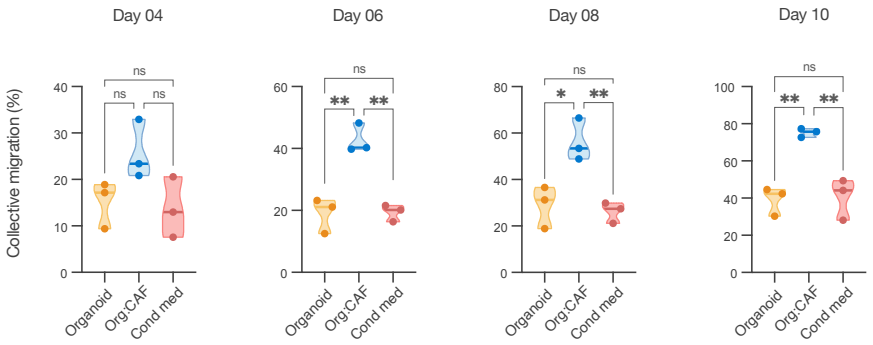

Figure R27. CAFs enhance organoid collective migration via direct co-culture but not by conditioned media. Percentage of organoids displaying collective migration at day 4, day 6, day 8, and day 10. n=3 independent experiments; *p<0.05; **p<0.01 (One-way ANOVA).

In this context, PBMCs derived from metastatic breast cancer patients have been reported to cooperate with CTCs, facilitating EMT, invasion, and metastatic colonization. Such interactions underscore the role of PBMCs in establishing and supporting the metastatic niche [194,195]. Therefore, incorporating shear stress and PBMCs into the co-culture system, allowed us to recreate a physiologically relevant tumor microenvironment in which to assess the stability of CB_2R-induced differentiation.

In this enhanced model, organoids were co-cultured with CAFs and PBMCs under shear stress in a bioreactor, replicating peripheral vascular conditions (**Figure R28A**). To dissect the contributions of individual components, we sequentially introduced (1) shear stress, (2) CAFs, and (3) PBMCs, evaluating their single and combined effects on tumor organoids (**Figure R28B**).

Notably, shear stress alone significantly increased organoid proliferation from the onset of exposure —a trend sustained throughout the culture period (**Figure R28C**). While the addition of CAFs and PBMCs maintained the increase in organoid size, these effects were not statistically significant compared to shear stress alone, suggesting that shear stress is the primary proliferative driver.

The most prominent changes, however, were observed in collective migration. Organoids exposed to shear stress exhibited early and robust formation of invasive structures, which expanded considerably, as reflected by the significantly increased area by day 10 (**Figure R28D-E**). The inclusion of CAFs amplified collective migration formation, and the subsequent addition of

PBMCs further enhanced this effect. Thus, the sequential incorporation of each element resulted in a significant increase in collective migration, indicating that the bioreactor model fosters a highly invasive and plastic tumor phenotype.

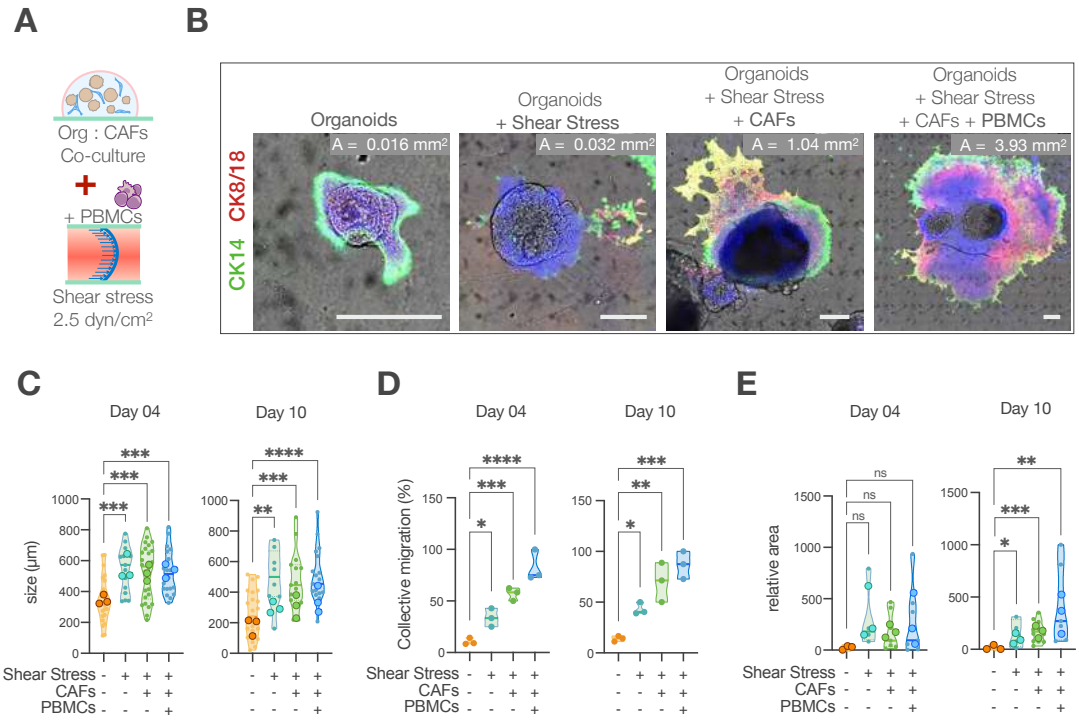

Figure R28. Integration of immune cells and shear stress amplifies collective migration and organoid growth in an advanced 3D immune-stroma-tumor co-culture. **A,** Schematic of the advanced 3D co-culture model. Organoids were embedded in BME, co-cultured with syngeneic CAFs (1:250), and exposed to circulating peripheral blood mononuclear cells (PBMCs) under continuous shear stress (2.6 dyn/cm^2) via pumped flow. **B,** Confocal images of organoids stained for CK8/18 (red) and CK14 (green), with DAPI (blue) marking nuclei, under the conditions shown in (A) at day 10. Representative slices of collective migration are included. Quantified area (A) corresponds to the region of collective migration. n=3 independent experiments. Scale bar, 250 µm. **C,** Organoid size (µm) measured at day 4 and day 10 in the conditions shown in (A). n=3 independent experiments; **p<0.01; ***p<0.001; ****p<0.0001 (One-way ANOVA). **D,** Percentage of organoids with collective migration at day 4 and day 10. n=3 independent experiments; *p<0.05; **p<0.01; ***p<0.001; ****p<0.0001 (One-way ANOVA). **E,** Quantification of collective migratory projection area (µm^2) at day 4 and day 10. n=3 independent experiments; *p<0.05; **p<0.01; ***p<0.001 (Unpaired Student's t-test).

With this model established, we evaluated whether CB_2R modulation by THC or SR2 could overcome these complex and aggressive microenvironmental conditions. The co-culture bioreactor system was exposed to a four-day pulse of THC or SR2 treatment, followed by withdrawal, and outcomes were analyzed at day 10 (**Figure R29A**).

Remarkably, even under these challenging conditions, both THC and SR2 treatments successfully reprogrammed tumor organoids toward a luminal-like, cystic phenotype consistent with earlier organoid-alone experiments (**Figure R29B**). Organoid proliferation was significantly reduced, as early as day 4 and this effect persisted after withdrawal (**Figure R29C**).

Furthermore, the proportion of organoids exhibiting collective migration structures fell to approximately 20 % in treated groups, compared to 68-90 % in untreated controls. Notably, treated organoids did not develop new invasive features over time, as the proportion of organoids with collective migration structures remained stable from day 4 to day 10, whereas controls continued

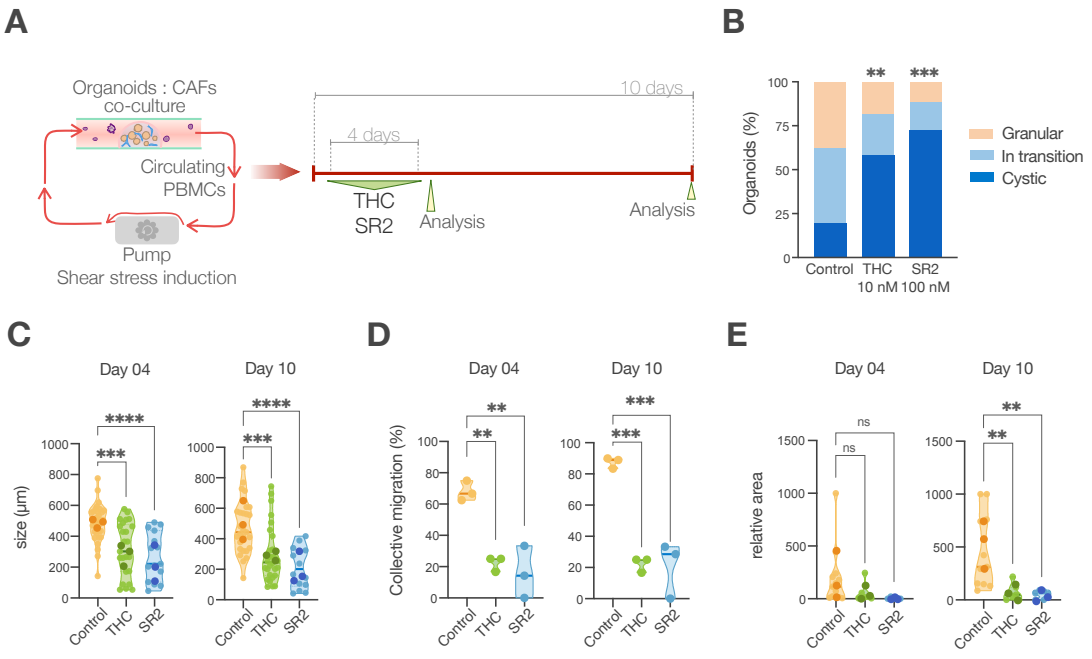

Figure R29. Both THC and SR2 promote stable differentiation, remodeling organoid architecture and migration in a 3D co-culture mimicking immune-stroma environment. A, Schematic of the experimental setup. Organoids embedded in BME were co-cultured with cancer-associated fibroblasts (CAFs) and exposed to circulating peripheral blood mononuclear cells (PBMCs), with continuous pumped flux inducing shear stress. Co-cultures were treated with vehicle, THC (10 nM), or SR2 (100 nM) for 4 days, followed by 10 days in drug-free media. Samples were analyzed at two time points as indicated. **B,** Quantification of organoid morphology (granular, in transition, cystic) at day 10 across conditions. n=3 independent experiments; **p<0.01 ***p<0.001 vs. control (granular) (Two-way ANOVA). **C,** Organoid size (µm) measured at day 4 and day 10. n=3 independent experiments; ***p<0.001; ****p<0.0001 vs. control (One-way ANOVA). **D,** Percentage of organoids exhibiting collective migration at day 4 and day 10 in each treatment condition. n=3 independent experiments; **p<0.01; ***p<0.001 vs. control (One-way ANOVA). **E,** Quantification of collective migratory projection area (μm^2) across conditions at day 4 and day 10. n=3 independent experiments; ns, not significant; **p<0.01 vs. control (One-way ANOVA).

to increase, reaching 90 % (**Figure R29D**). Furthermore, the area covered by migratory fronts was significantly reduced in treated conditions (**Figure R29E**), suggesting that CB_2R modulation limits both the initiation and expansion of invasive behavior, even after treatment cessation. This indicates a durable and robust reprogramming effect modulated by CB_2R targeting.

We also explored whether CB_2R-induced differentiation could influence immune signaling. CSCs are known to facilitate immune evasion by downregulating antigen presentation and recruiting pro-tumoral immunosuppressive populations such as tumor-associated macrophages (TAMs) and regulatory T cells, which release immunosuppressive cytokines and promote immune cell exhaustion [196]. Based on this knowledge, we investigated whether CB_2R-mediated differentiation could influence cytokine profiles and potentially counteract CSC-induced immune evasion.

To address this, we compared cytokine secretion profiles in the full co-culture bioreactor *versus* a simplified PBMC-only model. Notably, in the co-culture condition, we observed strong activation of macrophage and neutrophil colony-stimulating factors —M-CSF and G-CSF, respectively (**Figure R30A**), both of which are typically elevated in cancer contexts: M-CSF promotes the infiltration of TAMs, particularly in breast cancer, while G-CSF enhances the expansion of polymorphonuclear myeloid-derived suppressor cells (PMN-MDSCs), a cell population implicated in facilitating metastasis and invasion [197,198]. Interestingly, both cytokines were significantly reduced upon CB_2R modulation, with SR2 treatment producing a stronger effect, although not fully restored to baseline.

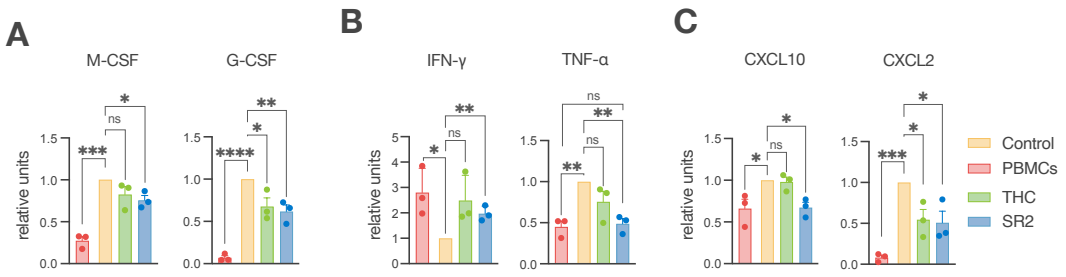

Figure R30. THC and SR2 impair cytokine and chemokine signaling in a 3D immune-stroma-tumor co-culture under shear stress. Streptavidin-HRP based analysis of cytokines and chemokines secreted into the culture medium at day 10 for each condition: PBMC alone (red) or organoids+PBMCs+CAFs treated with vehicle (yellow), THC (green) or SR2 (blue). n=3 independent experiments; ns, not significant; *p<0.05; **p<0.01 ; ***p<0.001; ****p<0.0001 vs. control (One-way ANOVA). Cytokines analyzed include: M-CSF, G-CSF (**A**), IFN-γ, TNF-α (**B**) and chemokines from the CXCL family CXCL10 and CXCL2 (**C**).

Moreover, we observed that interferon-γ (IFN-γ), a pleiotropic cytokine known to suppress stem cell plasticity in breast tumors [199,200], was significantly reduced in the co-culture condition but restored to PBMC-only levels upon THC/SR2 treatment (**Figure R30B**). In contrast, tumor necrosis factor-α (TNF-α) was markedly elevated —doubling the PBMCs control— in the co-culture condition but significantly reduced following SR2 treatment (**Figure R30B**). TNF-α is a pro-inflammatory cytokine with well-established roles in promoting tumor proliferation, invasion, and metastasis, and it also contributes to the recruitment of the PMN-MDSCs and TAMs [194]. Therefore, the reduction of TNF-α to baseline under SR2 reinforces the role of this treatment in tumor control.

Chemokine analysis revealed that CXCL10 and CXCL2 were significantly elevated in the co-culture but reduced after CB_2R modulation (**Figure R30C**). These chemokines are associated with TAMs and PMN-MDSCs recruitment, tumor progression and angiogenesis [196,201].

Collectively, the cytokine data suggest that CB_2R-mediated differentiation shifts the immune profile from a tumor-promoting to a more immune-activating state, potentially counteracting CSC-induced immune evasion.

To further validate this shift, we analyzed the long-term epigenetic effects of CB_2R modulation, focusing on previously detected bivalent chromatin-associated histone modifications. We observed a significant reduction in H3K4me3 nuclear intensity following treatment under these conditions (**Figure R31A**), consistent with the decrease previously observed in organoid-only

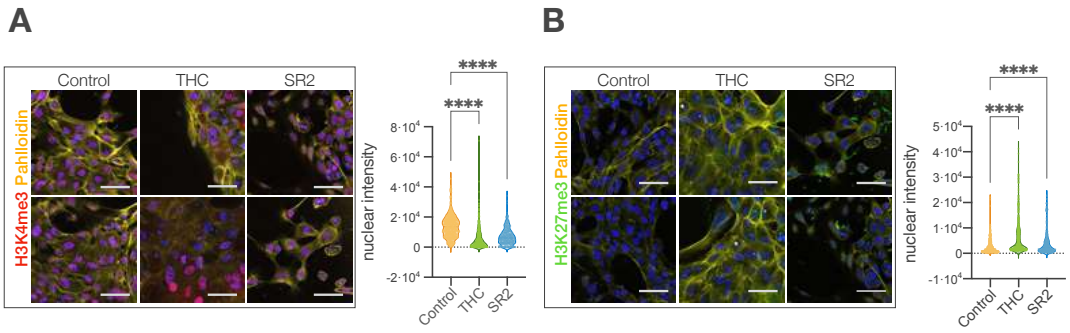

Figure R31. Cannabinoid-induced differentiation preserves epigenetic marks in a 3D immune-stroma-tumor co-culture under shear stress. Confocal images of organoids at day 10 stained for H3K4me3 (red) and phalloidin (yellow) (**A**) and for H3K27me3 (green) and phalloidin (yellow) (**B**), with DAPI (blue) marking nuclei. Violin plots show the quantification of total nuclear fluorescence intensity per nucleus (800-1500 nuclei were evaluated per condition) for every staining, as indicated. n=3 independent experiments. ****p<0.0001 vs. control (One-way ANOVA). Scale bar, 100 µm.

cultures (**Figure R25B and D**). Similarly, H3K27me3 levels increased in both THC- and SR2-treated conditions (**Figure R31B**), in line with earlier observations (**Figure R25B and D**). These results indicate that cannabinoid-treated organoids maintain sustained epigenetic remodeling, even within a highly aggressive and pro-tumorigenic microenvironment.

Collectively, these results demonstrate that CB_2R modulation via THC or SR2 triggers a durable, irreversible differentiation program that persists even under pro-aggressive cues. This reprogramming withstands continuous exposure to CAFs, PBMCs and shear stress, and is accompanied by sustained epigenetic changes that suppress stemness and invasion. These findings underscore the therapeutic potential of CB_2R targeting and THC in overcoming breast cancer cell plasticity and immune evasion.

CB_2R-driven differentiation sensitizes breast cancer cells to endocrine therapy.

Drug-resistant cancer cells often incur a fitness cost, manifested by reduced proliferation, higher metabolic demands, or lower competitiveness. Adaptive therapy seeks to exploit this trade-off by maintaining a population of drug-sensitive cells to suppress resistant clones, thereby delaying resistance emergence and improving long-term treatment efficacy [202]. Within this framework, differentiation therapies —including CB_2R-targeted approaches— may function as adaptive interventions by reducing tumor cell plasticity and stemness, ultimately reducing the capacity for therapeutic resistance.

To explore this potential therapeutic synergy, we assessed whether CB_2R-mediated differentiation could sensitize tumor cells to conventional endocrine therapy. Specifically, we tested the sequential treatment strategy involving CB_2R fine-tune modulation followed by tamoxifen, a selective estrogen receptor modulator commonly used in the treatment of estrogen receptor positive (ER+) breast cancer [203].

This combinatorial strategy was supported by prior transcriptomic profiling, which revealed that both THC and SR2 significantly upregulated the estrogen signaling pathway (**Figure R22**). Moreover, CB_2R modulation induced a clear basal-to-luminal phenotypic switch, evidenced by increased expression of luminal lineage markers (**Figure R4**). Given that tamoxifen exerts its therapeutic effects primarily in ER+/luminal contexts, these CB_2R-driven differentiation changes provided a strong rationale for evaluating tamoxifen sensitivity following pre-treatment.

PyMT-derived organoids were initially treated with CB_2R modulators for 4 days, followed by a 10-day drug withdrawal period—coinciding with the emergence of a stable differentiated phenotype. Organoids were then treated for 2 days with sub-micromolar concentrations of tamoxifen and maintained for 14 additional days. Following a six-day single-cell dissociation and recovery period, the total timeline for analysis spanned 34 days (**Figure R32**).

This sequential treatment led to a marked reduction in organoid viability, as measured by annexin V/PI staining. While control organoids showed minimal sensitivity to tamoxifen alone, those pre-treated with THC or SR2 exhibited a trend toward decreased viability and a corresponding increase in the apoptotic population, which was significant for SR2 treatment (**Figure R33A**). These results suggest that CB_2R-mediated pre-treatment primes tumor cells, rendering them more susceptible to apoptosis triggered by endocrine therapy.

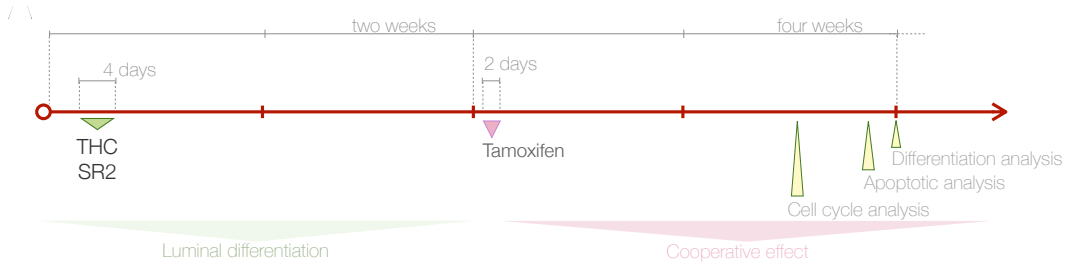

Figure R32. Experimental timeline for sequential cannabinoid and endocrine therapy in 3D organoid cultures. Schematic of the experimental design. MMTV-PyMT–derived organoids were pre-treated with vehicle, THC (10 nM), or SR2 (100 nM) for 4 days, followed by 10 days in drug-free media. Tamoxifen (0-5 μM) was then administered for 2 days, and cultures were analyzed immediately or up to 2 weeks later.

Consistently, CB_2R-mediated pretreated organoids displayed a trend toward G2-M cell cycle arrest following tamoxifen exposure (**Figure R33B**). This blockade, combined with the induction of apoptosis, underscores a potent therapeutic response to low-dose tamoxifen in differentiated organoids. In contrast, control organoids treated with tamoxifen showed an increased in the S phase population that was not observed in THC/SR2 pretreated organoids, suggestive of an adaptive proliferative response to therapy —a hallmark of resistance in non-differentiated cells (**Figure R33B**).

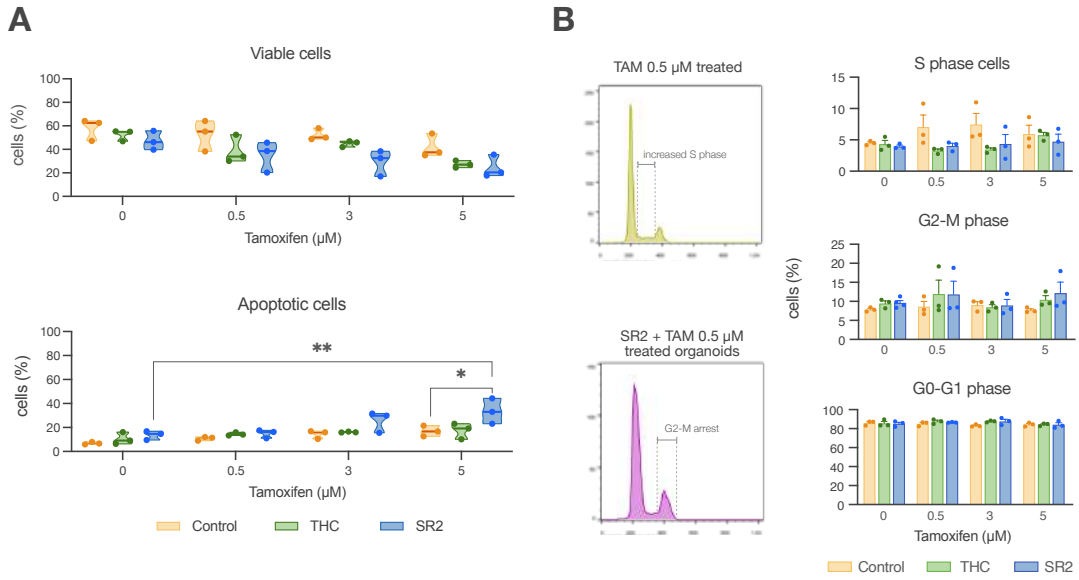

Figure R33. Pre-differentiation with THC and SR2 sensitizes 3D organoids to tamoxifen-induced apoptosis and cell cycle arrest. A, Flow cytometry analysis of apoptosis using PI and Annexin V. n=4 independent experiments; *p<0.05; **p<0.01 vs. control (Unpaired Student's t-test). **B,** Cell cycle profiles comparing tamoxifen alone to THC/SR2 + tamoxifen at increasing doses (0–5 μM). Left: representative flow cytometry plots. Right: quantification of cell cycle phases (G0/G1, S, G2/M). n=3 independent experiments.

By four weeks post-CB_2R modulation treatment and two weeks after tamoxifen exposure, the co-treatment strategy elicited a pronounced basal-to-luminal-like phenotypic transition (**Figure R34A**). In organoids pre-treated with THC or SR2, the proportion of cystic, non-granular organoids increased from 75 % to over 90 % after tamoxifen addition, whereas control organoids retained their original morphology, despite tamoxifen exposure. Moreover, differentiated organoids remained significantly smaller than controls even after endocrine therapy (**Figure R34B**), indicating that CB_2R-modulation driven differentiation imposes long-term constraints on organoid growth.

Importantly, strong effects were observed in terms of collective migration and self-renewal capacity. As expected, differentiation therapy alone significantly impaired the formation of collective migration fronts. This effect was further enhanced by subsequent tamoxifen treatment, as the proportion of collective invasion structures was markedly reduced when tamoxigen was applied following both THC and SR2 pretreatments, suggesting a synergistic effect (**Figure R34C**). Specifically, the proportion of organoids exhibiting collective invasion structures dropped from approximately 26-28 % in pretreated cultures to just 6-8 % following 5 µM tamoxifen addition.

The analysis of the self-renewal capacity, a measure of stemness potential, revealed that tamoxifen further impaired the ability of differentiated cells to form secondary organoids. Interestingly, tamoxifen appeared to increase the number of secondary organoids formed in a concentration-dependent manner, suggesting the emergence of therapy-resistant clones. Notably, CB_2R-targeted pre-treatment completely abolished the appearance of these tamoxifen-resistant clones (**Figure R34D**). These results demonstrate that cannabinoid-induced differentiation not only sensitized tumor cells to endocrine therapy but also effectively suppresses adaptive resistance.

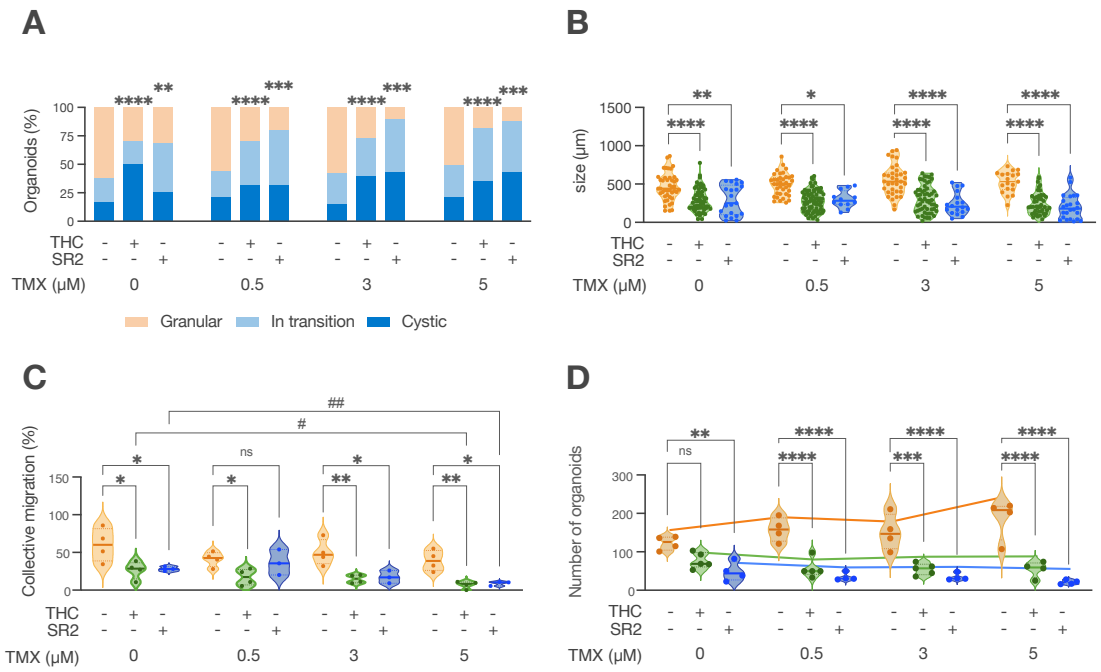

Figure R34. Differentiation by THC or SR2 promotes a luminal-like transition and reduces organoid fitness in response to tamoxifen. A, Quantification of organoid morphology at endpoint: granular (basal-like), in-transition, or cystic (luminal-like). n=4 independent experiments; **p<0.01; ***p<0.001 ****p<0.0001 vs. control (Two-way ANOVA). **B,** Organoid size (µm) at endpoint across treatment conditions. n=4; 80–100 organoids per condition; *p<0.05; **p<0.01; ****p<0.0001 vs. control (One-way ANOVA). **C,** Percentage of untreated (orange) and pre-treated (THC in green, SR2 in blue) organoids exhibiting collective migratory projections at endpoint. n=4; ns, not significant; *p<0.05; **p<0.01 vs. control; # p<0.05 vs. THC; ##p<0.01 vs. SR2 (One-way ANOVA). **D,** Self-renewal capacity assessed by quantification of secondary organoids formed after single-cell dissociation. n=4 independent experiments; ns, not significant; **p<0.01; ***p<0.001; ****p<0.0001 vs. control (One-way ANOVA).

To validate these findings in a clinically relevant context, we applied the combined treatment regimen to organoids derived from two breast tumor specimens obtained from a patient diagnosed with luminal A, grade II invasive ductal carcinoma, extracted at Hospital Universitario La Paz (Madrid, Spain). The efficacy of the SR2-tamoxifen regimen was assessed following the experimental timeline previously established: following a 4-day pulse of SR2 treatment and 10-day withdrawal, organoids were exposed to tamoxifen for 4 days. Self-renewal capacity was assessed 14 days post-tamoxifen exposure (**Figure R35**).

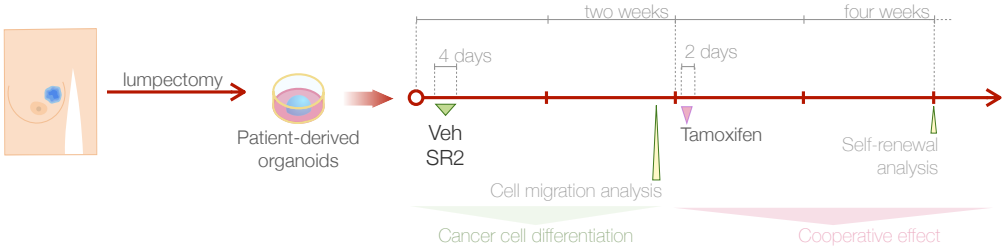

Figure R35. Experimental workflow for SR2 and tamoxifen co-treatment in patient-derived mammary tumor organoids. Surgical specimens were used to establish patient-derived organoid cultures. After expansion, organoids were treated with vehicle or SR2 (100 nM) for 4 days, followed by a 10-day drug-free period. Prior to tamoxifen treatment, cell dispersal from organoids was assessed using dynamic holographic imaging. Tamoxifen (5 µM) was then administered for 4 days. Organoids were analyzed two weeks later to evaluate cooperative effects on self-renewal. n=2 independent tumors, 3 technical replicates each.

Using phase holographic imaging, we monitored cancer cell motility and dispersal over a 40-h wound healing assay performed 10 days after SR2-induced differentiation. As shown in **Figure R36**, control organoids exhibited progressive surface expansion, while SR2-pretreated organoids failed to spread, showing poor adherence and limited surface coverage as early as 8 h into the assay. Quantitative analysis revealed that the uncovered surface area remained stable in SR2-treated organoids but significantly decreased in controls (**Figure R37A**).

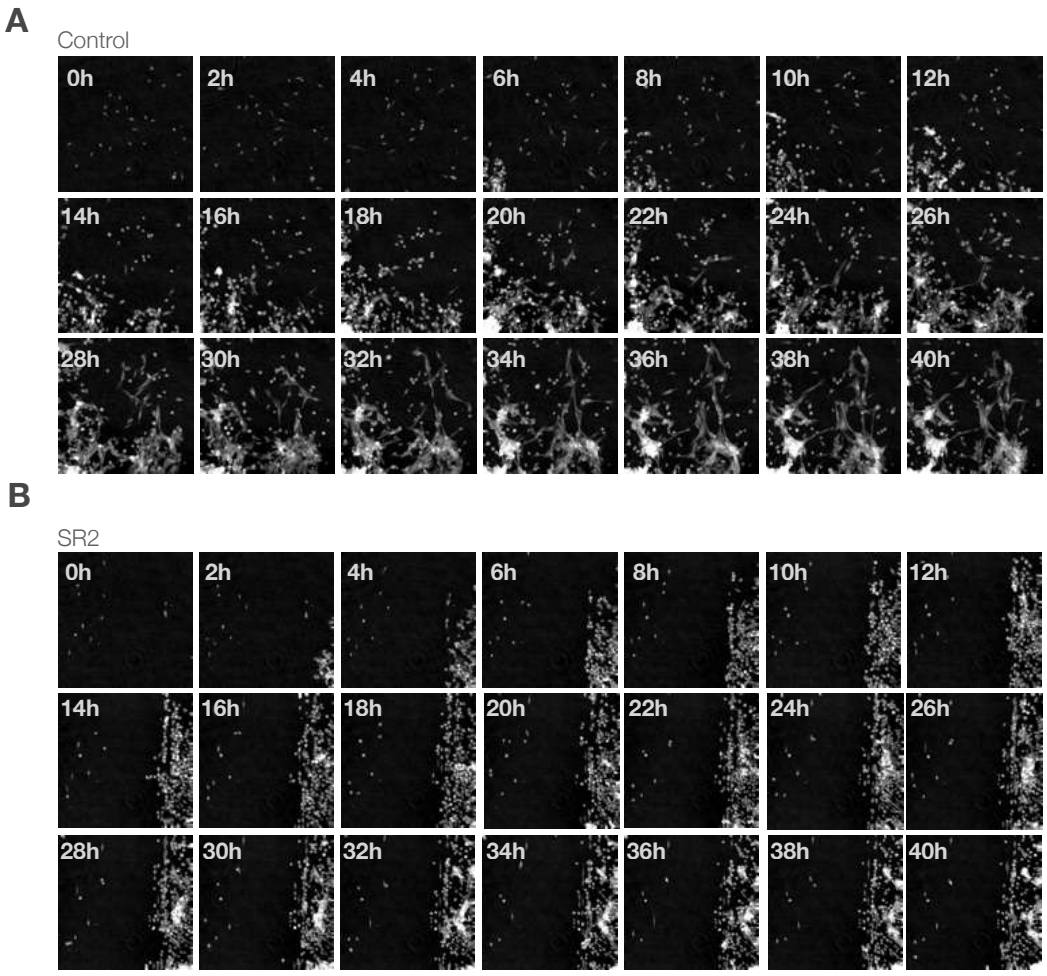

Figure R36. Holographic imaging reveals reduced adherent cell migration in SR2-treated patient-derived organoid culture. Phase holographic images showing representative 2D migration of patient-derived organoid cells treated with vehicle (**A**) or SR2 (100 nM) (**B**), assessed via wound healing assay at time points from 0 h to 40 h.

Moreover, untreated cells displayed greater shape irregularity compared to SR2-pretreated cells, reflecting enhanced morphological plasticity and migratory adaptation in the absence of differentiation (**Figure R37B**). Migratory parameters —including net migration distance, total motility and speed— were all significantly reduced in SR2-treated cells compared to controls (**Figure R37C-F**), confirming that CB_2R blockade-mediated differentiation severely restricts cell motility and invasive potential, even in patient-derived models.

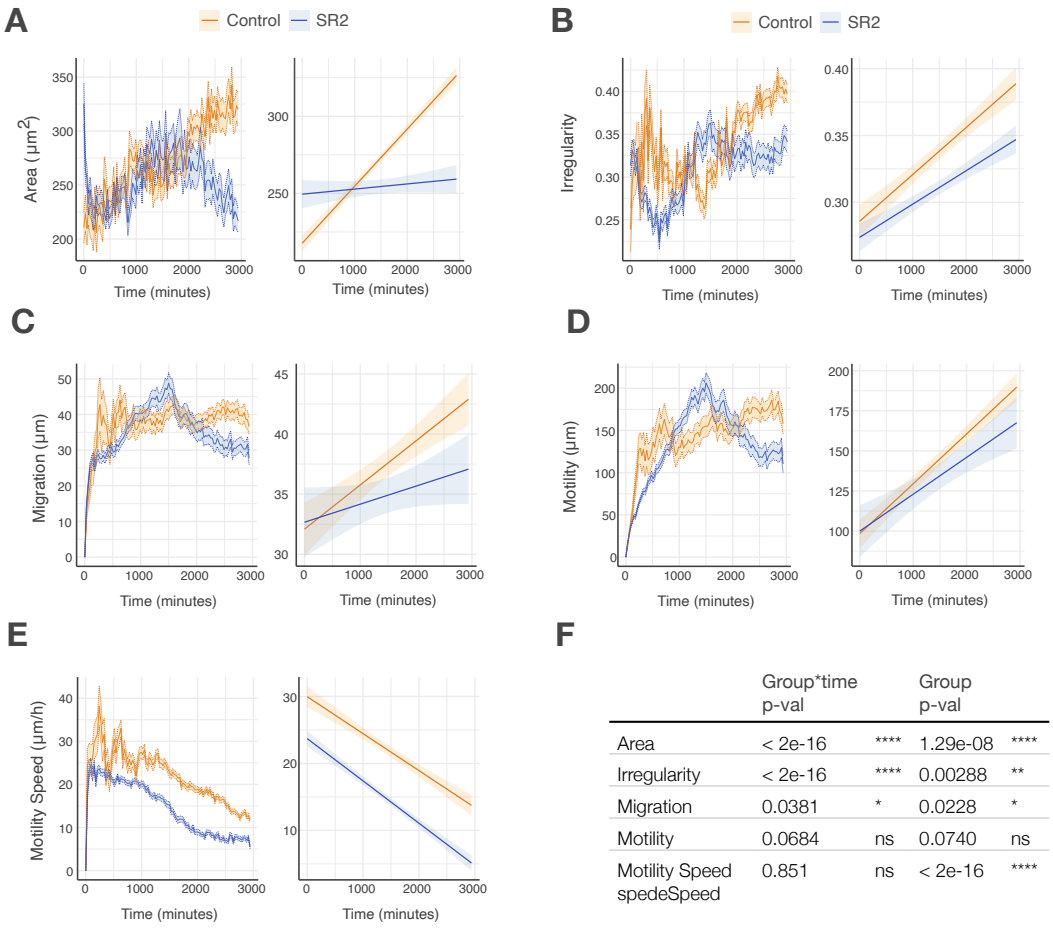

	Group*time p-val		Group p-val	
Area	< 2e-16	****	1.29e-08	****
Irregularity	< 2e-16	****	0.00288	**
Migration	0.0381	*	0.0228	*
Motility	0.0684	ns	0.0740	ns
Motility Speed spedeSpeed	0.851	ns	< 2e-16	****

Figure R37. Quantitative holographic imaging demonstrates impaired motility and migration dynamics in SR2-treated patient organoid-derived cells. A-E, Quantification of key wound healing parameters—cell area (µm^2) (**A**), shape irregularity (**B**), migration distance (µm) (**C**), motility (µm) (**D**) and migration speed (µm/h) (**E**) under treatment conditions. Data are presented as mean ± standard error of the mean (SEM) (left) and a fitted to a linear model to evaluate the effect of the treatment (right). **F,** Statistical analyses performed in R (version 4.5.0) of the indicated parameters. The Group × Time p-value column represents the ANOVA evaluation of treatment effects in a time-dependent manner (interaction term), whereas the Group p-value column represents the ANOVA evaluation of treatment effects alone (main effect). For all cases, model residuals were inspected to confirm assumptions of normality and homoscedasticity.

At the same time point, SR2-pretreated organoids also exhibited enhanced epithelial characteristics, including increased E-CAD and decreased SNAIL levels (**Figure R38A**). These molecular features were accompanied by a statistically significant reduction in organoid size, consistent with diminished proliferative capacity (**Figure R38B**) and a loss of collective migration structures (**Figure R38C**). Statistical analysis was not performed due to the reduced sample size.

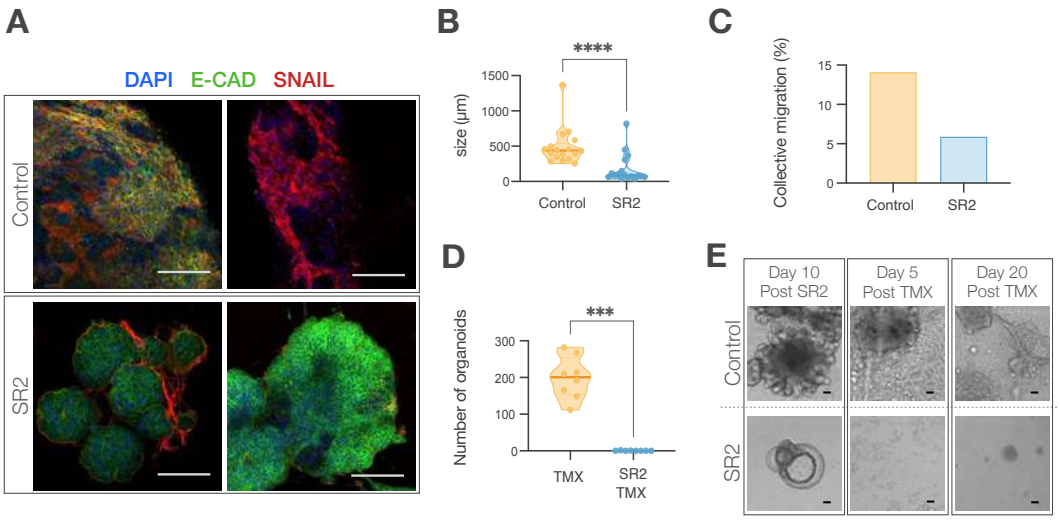

Figure R38. CB_2R pre-modulation enhances tamoxifen efficacy in patient-derived breast cancer organoids by reducing growth, migration and self-renewal. A, Confocal images of organoids stained for E-CAD (green) and SNAIL (red), analyzed 10 days post-differentiation. Nuclei were stained with DAPI (blue). Shown are representative 3D confocal stacks. Scale bar = 100 µm. **B,** Quantification of organoid size (µm) at day 10 post-differentiation. ****$p < 0.0001$ vs. control (one-way ANOVA). **C,** Percentage of organoids displaying collective migration at day 10 post-differentiation. **D,** Total number of secondary organoids formed after single-cell disaggregation, reflecting self-renewal capacity, measured two weeks after tamoxifen treatment. ***$p < 0.001$ vs. tamoxifen (TMX) (one-way ANOVA). **E,** Representative bright-field images of organoids at different time points: 10 days after differentiation, and 5 or 20 days after tamoxifen treatment, following the experimental timeline shown in Figure R35.

Functionally, these molecular and phenotypic shifts translated into a profound loss of self-renewal capacity following tamoxifen exposure. SR2-pretreated organoids generated only 0-2 secondary organoids, compared to approximately 200 in tamoxifen-only controls (**Figure R38D and E**). These data suggest that the SR2-induced differentiated state renders tumor cells highly susceptible to endocrine therapy, by eliminating plastic subpopulations capable of surviving the treatment.

Overall, tamoxifen monotherapy induced signs of adaptive resistance in tumor organoids, as evidenced by increased S phase entry, and a dose-dependent rise in self-renewal capacity. This outcome was anticipated, given that plasticity remains active in untreated cultures, allowing tumor cells to adapt and survive treatment by expanding resistant subpopulations. In contrast, CB_2R modulation-induced differentiation produced a durable shift characterized by reduced viability, impaired invasion, G2-M cell cycle arrest and apoptosis, effects that persisted for at least two weeks post-endocrine treatment.

Most critically, CB_2R-induced differentiation completely suppressed the emergence of resistant clones and blocked de-differentiation plasticity in both the PyMT model and patient-derived organoids. Notably, in patient samples, the SR2-tamoxifen sequential combination produced a striking collapse of the culture system, with virtually no surviving organoids.

These findings highlight the therapeutic potential of CB_2R modulation and THC as complementary approaches to standard-of-care treatments. By stabilizing tumor differentiation and preventing the reactivation of stem-like, resistant states, CB_2R modulation may offer a compelling strategy to enhance long-term treatment efficacy and avoid relapse in breast cancer.

miR-203 activation promotes lineage commitment in cancer stem cells

Brief exposure to miR-203 induces morphological and molecular changes suggestive of epithelial differentiation in mammary tumor-derived organoids.

MicroRNAs (miRNAs) are small non-coding RNAs that regulate gene expression post-transcriptionally, playing critical roles in cancer by acting as either oncogenes or tumor suppressors. Among them, microRNA 203 (miR-203) has been identified as a key regulator of stemness during epidermal development [145] and as a tumor suppressor in hematological malignancies, where it is frequently silenced by DNA hypermethylation [155]. Notably, miR-203 targets a variety of cancer-related genes involved in signaling, stemness, migration, and metastasis, underscoring its potential to shape tumor phenotype [149–154]. Previous work from our lab demonstrated that transient exposure to miR-203 can block cellular reprogramming and promote differentiation in stem cells through epigenetic remodeling [147]. Given the molecular parallels between pluripotency and tumorigenesis [82,173], we sought to determine whether miR-203 could promote cell differentiation in breast cancer cells.

To enable precise temporal control of miR-203 expression *in vitro* and *in vivo*, we generated a tetracycline-inducible knock in model, in which the miR-203 coding sequence was inserted downstream of the *Col1a1* locus, under the control of tetracycline-responsive element (TRE), activated by the tetracycline-responsive transactivator (rtTA) expressed from the *Rosa26* locus [144]. In this system, doxycycline (Dox) treatment induces robust and specific miR-203 expression in ($Col1a1^{miR\text{-}203/miR\text{-}203}$; $Rosa^{rtTA/rtTA}$) animals or derived cells. We crossed these mice with the PyMT model of mammary tumorigenesis to generate an inducible system where studying the effects of miR-203 in breast cancer, allowing us to finely modulate miR-203 expression in tumor cells via Dox administration.

To investigate the effects of miR-203 on mammary tumor cell populations, we exposed tumor-derived organoids from the $miR\text{-}203^{KI/KI}$-PyMT mouse model to Dox for 5 days to transiently induce miR-203 expression. Two weeks after induction, we analyzed the resulting organoid cultures to evaluate the long-term consequences of early miR-203 activation (**Figure R39A**).

When organoids were briefly exposed to miR-203, their morphology gradually changed, adopting hollow, cyst-like structures (**Figure R39B-C**). This suggests that miR-203 promotes the cyst-forming capacity of mammary epithelial tumor cells. Intriguingly, this phenotype closely resembled that of organoids derived from healthy mammary gland tissue, which also displayed cystic, organized, luminal-like morphology (**Figure R39D**). Of interest, this phenotype has

previously been associated with ALDH-positive progenitor cells [204]. Accordingly, we observed a notable reduction in ALDH1/2 expression following miR-203 exposure (**Figure R40**), suggesting that rather than promoting a shift toward luminal progenitor identity, miR-203 may drive terminal differentiation and loss of progenitor potential. Supporting this, miR-203-treated cystic organoids eventually collapsed in culture, whereas untreated control organoids were easily maintained and passaged for months, indicative of sustained stem/progenitor activity in the latter.

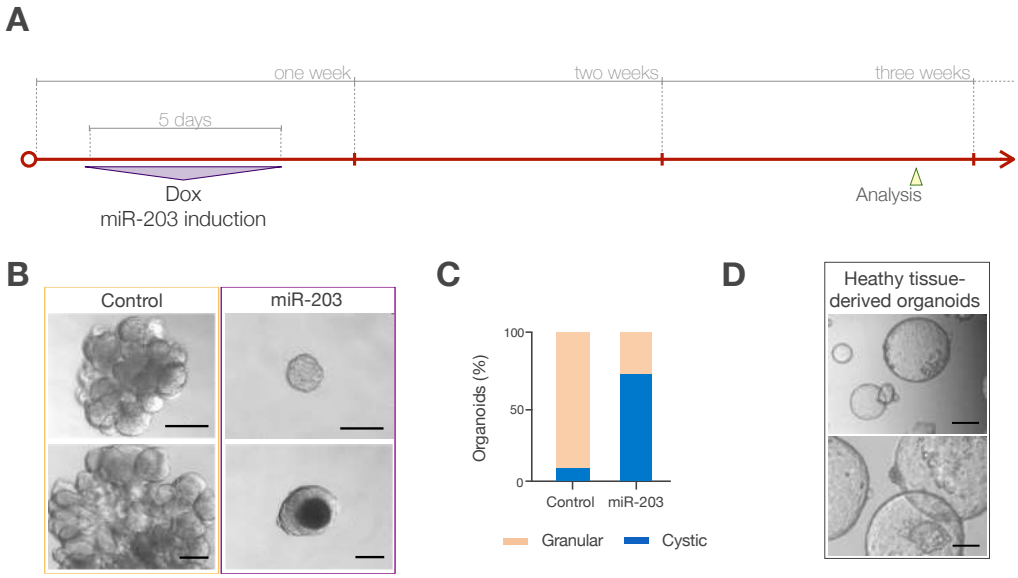

Figure R39. miR-203 transitory exposure regulates morphological features of PyMT-derived tumor organoids. A, Schematic of the experimental design. miR-203$^{KI/KI}$-PyMT-derived tumor organoids were exposed *in vitro* to control or miR-203 (Dox) during 5 days and followed by miR-203 withdrawal for 2 more weeks. **B,** Representative bright-field images of control or miR-203 Dox-treated organoids. Scale bar 100 µm. **C,** Quantification of the percentage of organoids exhibiting granular vs. cystic (luminal-like) morphology in every condition tested. **D,** Representative bright-field images of healthy mammary gland-derived organoids (from miR-203 wild-type; PyMT wild-type mice). Scale bar 100 µm.

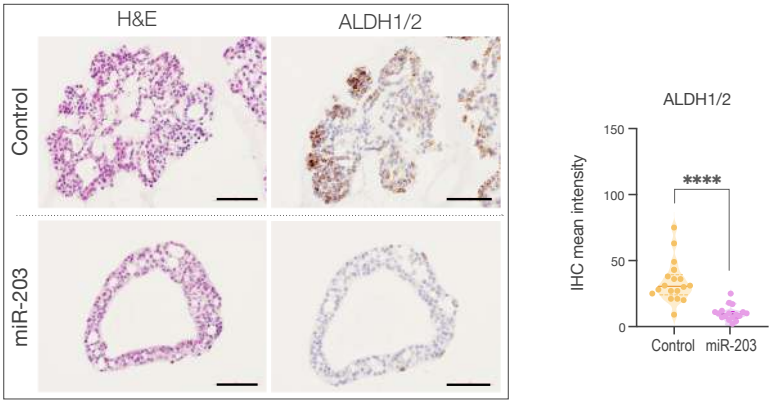

Figure R40. miR-203 transient exposure reduces progenitor identity in PyMT tumor-derived organoids. Left panel, representative images of H&E and ALDH1/2 IHC staining of control tumor-derived organoids, exposed to vehicle or miR-203 *in vitro* for 5 days and followed by miR-203 withdrawal. Scale bar: 100 µm. Right panel, violin plot showing the quantification of ALDH1/2 staining. Six different fields from three independent tumor samples were analyzed. ****$p < 0.0001$ vs. control (Student's t test).

To determine whether these morphological changes were also accompanied by molecular reprogramming, we analyzed the expression of cytokeratin markers by immunohistochemistry. Expression of basal markers CK5 and CK14 was markedly reduced, while luminal markers CK8 and CK18 were significantly upregulated in miR-203-treated organoids compared to controls (**Figure R41A-B**). Notably, the staining pattern in miR-203-exposed organoids closely resembled

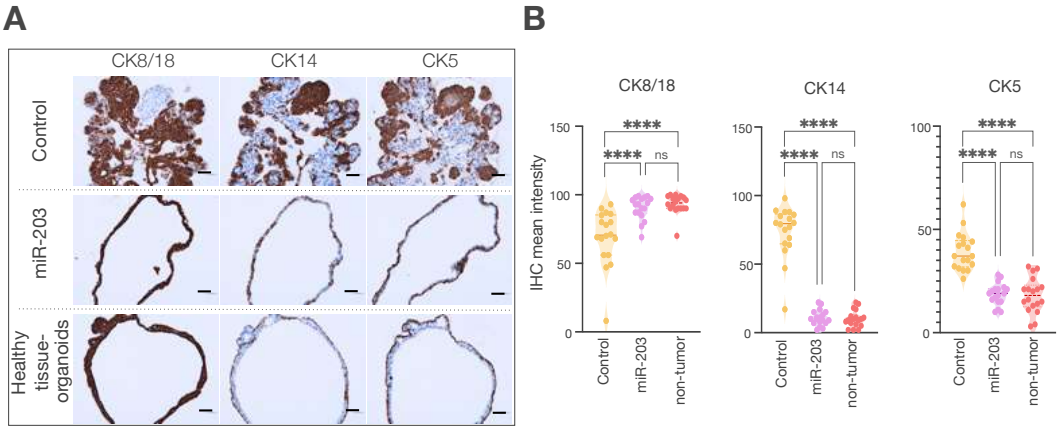

Figure R41. miR-203 transitory exposure induces a basal-to-luminal shift on PyMT mammary tumor-derived organoids. A, Illustrative IHC images of staining for CK8/18, CK14 and CK5 in control tumor-derived organoids, tumor-derived organoids treated with miR-203 during 5 days and healthy mammary gland-derived organoids. Scale bar: 500 µm. **B,** Violin plots showing the quantification of marker staining. Six different fields from three independent tumor samples were analyzed. ****$p < 0.0001$; n.s. not statistically different vs. control (One-way ANOVA).

that of healthy tissue-derived organoids, suggesting a shift away from a malignant phenotype and toward a differentiated state.

We further assessed expression of additional differentiation-associated markers, including prolactin, progesterone receptor (PR), estrogen receptor alpha (ERα), smooth muscle actin (SMA), and the epigenetic mark H3K27me3, known to be associated with lineage commitment (**Figure R42A**). Strikingly, miR-203-treated tumor organoids exhibited staining profiles nearly indistinguishable from those of healthy mammary-derived organoids across all tested markers except for SMA (**Figure R42B**), supporting that transient miR-203 activation drives epithelial differentiation of mammary tumor cells toward a mature, luminal-like fate.

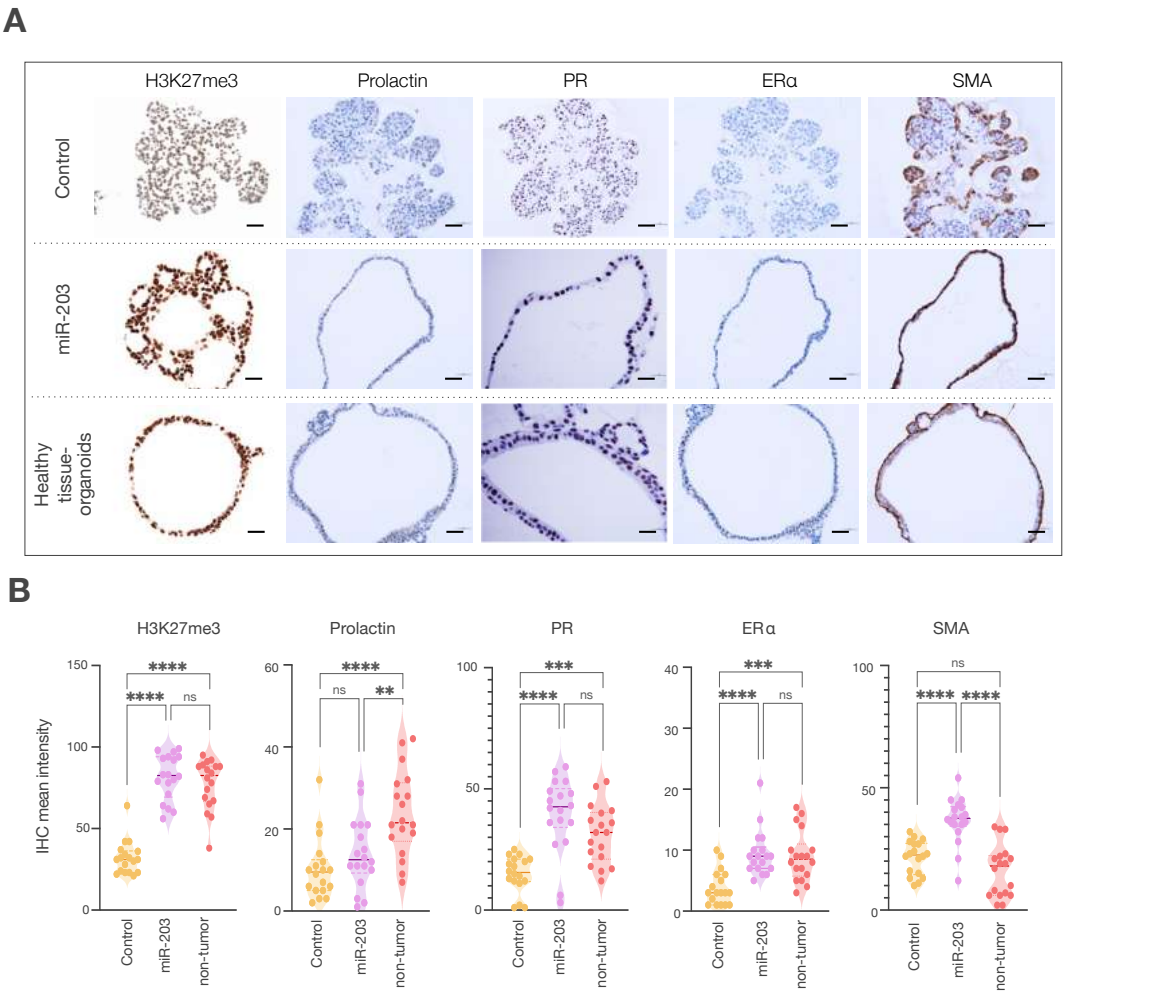

Figure R42. miR-203 induces epithelial maturation in tumor-derived organoids, recapitulating molecular features of healthy mammary organoids. A, Illustrative images of IHC staining for H3K27me3, Prolactin (PRL), progesterone receptor (PR), estrogen receptor alpha (ERα) and smooth muscle actin (SMA) in control tumor-derived organoids (upper panels), tumor-derived organoids treated with miR-203 during 5 days (middle panels) and healthy mammary gland-derived organoids (bottom panels). Scale bar: 500 μm. **B,** Violin plots showing the quantification of H3K27me3, PRL, PR, ERα and SMA staining in control tumor-derived organoids (control), tumor-derived organoids treated with miR-203 during 5 days (miR-203) and healthy mammary gland-derived organoids (non-tumor). Six different fields from three independent tumor samples were analyzed. **p < 0.01; ***p < 0.001; ****p < 0.0001; n.s. not statistically different vs. control (One-way ANOVA).

To explore the therapeutic potential of miR-203 in a clinically relevant context, we assessed its effects on patient-derived breast cancer organoids. Two primary tumor samples were obtained via core needle biopsy from patients diagnosed with Luminal B HER2+ breast cancer at Hospital 12 de Octubre (Madrid, Spain). Both patients initially received chemotherapy followed by surgery; however, upon relapse, their tumors progressed to an invasive phenotype and were subsequently enrolled in clinical trials.

After establishing 3D organoid cultures from these biopsies and expanding them over seven days, the organoids were transiently transfected either with synthetic miR-203 mimics or the corresponding empty vector as a control. Following miR-203 withdrawal, the cultures were maintained for an additional three more weeks prior to analysis (**Figure R43**).

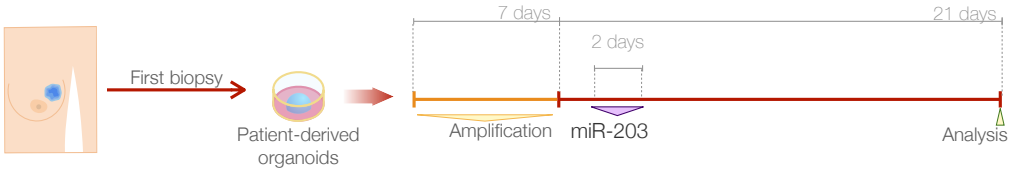

Figure R43. Experimental workflow for miR-203 transient transfection in patient-derived breast cancer organoids. Schematic showing the experimental procedures followed for patient-derived tumor processing, organoid culture establishment and miR-203 mimics transient transfection.

Throughout the experiment, bright-field microscopy was used to monitor morphological changes in the 3D cultures induced by transient miR-203 exposure. In untreated controls, we consistently observed the emergence of collective migration protrusions. Elongated cells emerged from the edges of organoids and eventually occupied the surrounding area, forming the collective invasion fronts (**Figure R44A**).

At the molecular level, CK14 and VIM were enriched in the invasive outer layers and at the base of the organoids in control cultures, while CK8/18, was expressed al lower levels. In contrast, miR-203 pretreated organoids showed a marked reduction in CK14 and VIM expression, accompanied by upregulation of CK8/18, consistent with a basal-to-luminal transition (**Figure R44B**).

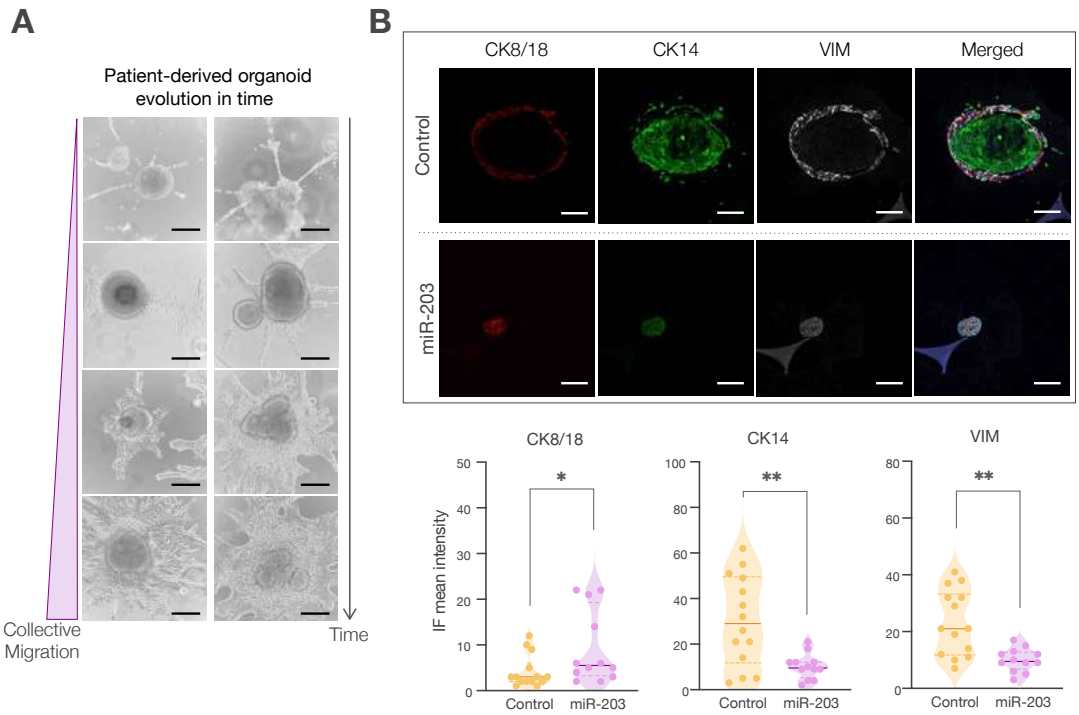

Figure R44. miR-203 modulates collective migration and epithelial-mesenchymal marker expression in patient-derived tumor organoids. A, Representative bright-field images showing the progressive collective cell migration projected from the 3D patient-derived organoids along time. Scale bar: 100 µm. **B,** Upper panel, detection of CK8/18 (red), CK14 (green) and VIM (white) by immunofluorescence in patient tumor-derived organoids, transiently exposed or not to miR-203 mimics *in vitro*. Scale bar: 100 µm. Lower panel, violin plots showing the quantification of marker staining. Six/seven different fields from two independent tumor samples were analyzed. *$p < 0.05$; **$p < 0.001$ vs. control (Student's t test).

Functionally, this molecular reprogramming was associated with impaired proliferation in miR-203-treated organoids, as reflected by both a decrease in total organoid number and a reduction in organoid size compared to controls (**Figure R45A-C**). Additionally, miR-203 exposure simplified the overall structure of the cultures, promoting the formation of uniform cystic organoids compared to the heterogeneous controls (**Figure R45D**), further supporting a cyst luminal-like differentiation outcome. Importantly, this brief and transient miR-203 exposure also blocked collective cell migration and inhibited the formation of invasive projections from the organoids (**Figure R45E**). These findings corroborate the differentiation potential of miR-203 in a patient-derived setting, demonstrating its ability to modulate epithelial identity and restrict tumor cell plasticity in breast cancer organoids.

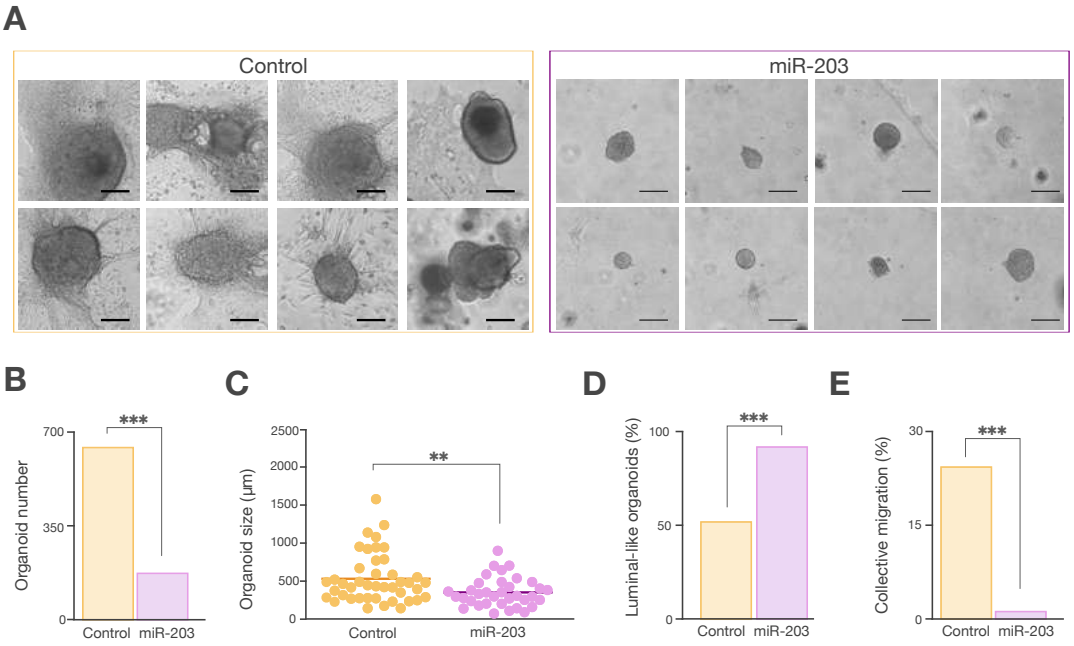

Figure R45. miR-203 transient exposure reduces growth, complexity, and collective migration in patient-derived breast cancer organoids. A, Representative bright-field images of patient-derived organoids, control vs. miR-203 briefly exposed, denoting the morphological differences in complexity, size and migration upon miR-203 treatment. Scale bar: 100 µm. **B-E,** Quantification of the total number of organoids (**B**), organoid size (C), percentage of organoids with luminal-like morphology (**D**), and percentage of organoids exhibiting collective migration (**E**), of control vs. miR-203 briefly exposed patient-derived organoids; n = 3 technical replicates from each 2 biological samples (2 independent biopsies). Receptor status of the two patient samples shown is the following: (1) 80 % ER; 60 % PR; 18 % KI67 index; and grade I HER2+. (2) 80 % ER; 80 % PR; 15 % KI67 index; and grade II HER2+. Both patients were enrolled in a clinical trial. ***$p < 0.001$; **$p < 0.01$ (Student's t test).

Altogether, these observations suggest that brief exposure to miR-203 promotes mammary epithelial differentiation in tumor organoids, inducing a basal-to-luminal transition evident both at the molecular level and through morphological changes toward cystic structures. This differentiation state is associated with a significant impairment in organoid propagation and expansion, consistent across both the PyMT mouse model and patient-derived samples. In summary, our results suggest that miR-203 activation promotes lineage commitment in cancer stem cells.

Transient exposure to miR-203 reveals an activation of epithelial commitment programs and a basal-to-luminal lineage switch in breast cancer organoids.

Since miR-203 induced morphological and molecular changes in the tumor-derived organoids suggestive of cell differentiation, we next examined whether these effects resembled those triggered by well-established differentiation stimuli. To this end, we tested a commercially available defined epithelial differentiation medium, optimized for the growth of mammary epithelial cells under serum-free conditions. This defined medium contains bovine pituitary extract (BPE), epidermal growth factor (EGF), insulin, and hydrocortisone, and was used here as a reference for inducing luminal differentiation.

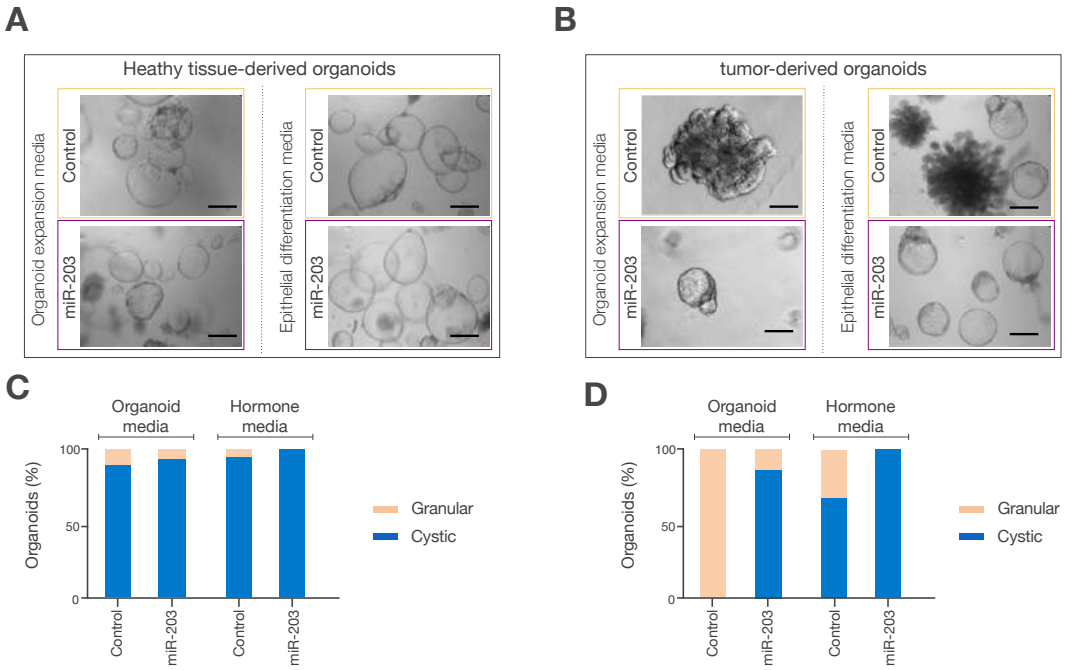

Figure R46. miR-203 promotes morphological changes on mammary tumor organoids comparable to those triggered by other well-known differentiation stimuli. A, Representative bright-filed images of healthy tissue-derived organoids exposed *in vitro* during 2 weeks to the indicated treatments: left panels, organoids cultured on basic expansion media, and treated with vehicle or miR-203 during the first 5 days; right panels, organoids cultured on epithelial differentiation media, and treated with vehicle or miR-203 during the first 5 days. Scale bar: 100 µm. **B,** Representative bright-filed images of tumor-derived organoids exposed *in vitro* during 2 weeks to the indicated treatments: left panels, organoids cultured on basic expansion media, and treated with vehicle or miR-203 during the first 5 days; right panels, organoids cultured on epithelial differentiation media, and treated with vehicle or miR-203 during the first 5 days. Scale bar: 100 µm. **C,** Percentage of organoids exhibiting cystic or granular shapes respect to the total number of organoids is shown for each condition tested of healthy tissue-derived organoids exposed to both differentiation media and/or miR-203. **D,** Percentage of organoids exhibiting cystic or granular shapes respect to the total number of organoids is shown for each condition tested of tumor-derived organoids.

As expected, healthy tissue-derived organoids predominantly displayed a cystic morphology across all tested conditions (**Figure R46A, C**). In contrast, tumor-derived organoids showed a higher sensitivity to treatment-induced changes: while they maintained a compact, bunch of grapes-like morphology under standard culture conditions, organoids transitioned to a predominantly cystic morphology when exposed to epithelial differentiation media, and even more prominently in response to miR-203 expression (**Figure R46B, D**). These morphological results suggest that both treatments enhance the cyst-forming capacity of mammary epithelial cells.

To gain deeper mechanistic insight into the differentiation-associated antitumor effects evoked by miR-203, we performed RNAseq on organoid samples derived from both healthy and tumor tissues, following *in vitro* exposure to either miR-203 or epithelial differentiation medium. Principal component analysis (PCA) revealed a prominent transcriptomic shift specifically in tumor-derived organoids treated with miR-203 (**Figure R47A**). Interestingly, this miR-203-induced

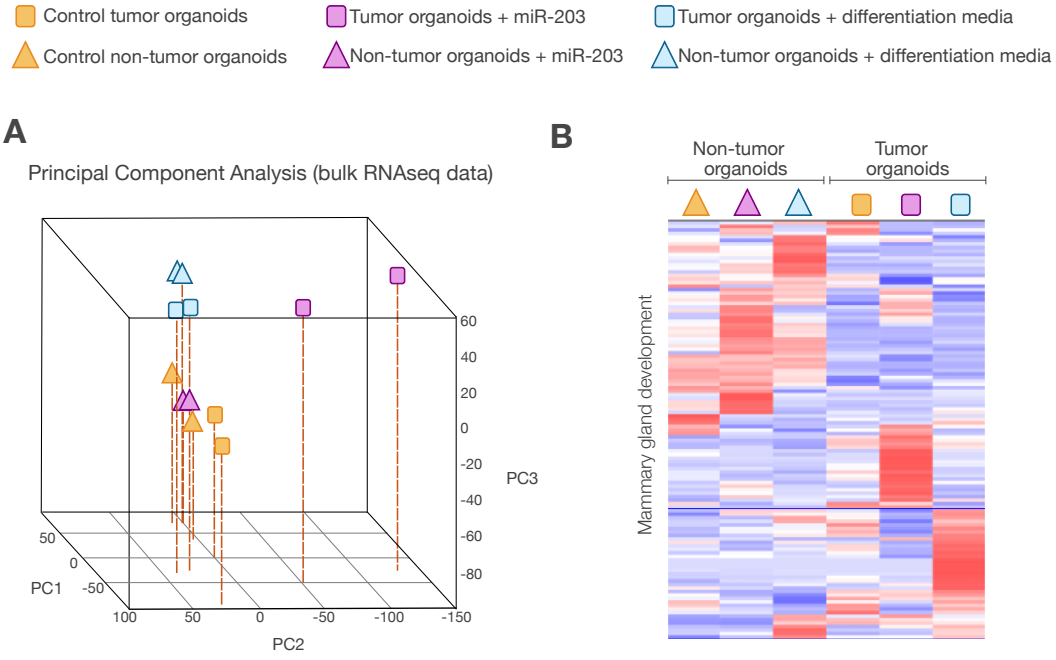

Figure R47. miR-203 drives transcriptional reprogramming towards mammary gland development. A, Principal Component Analysis (PC1, PC2, and PC3) of RNA sequencing performed on the samples indicated in the figure: non-tumor (triangles) or tumor (squares) mammary gland-derived organoids, exposed to either vehicle (in orange), miR-203 for 5 days *in vitro* (in purple) or differentiation media [consisting on prolactin, insulin, hEGF, hydrocortisone, BPE (bovine pituitary extract); in blue]. **B,** Heatmap showing the Gene Ontology signature for mammary gland development in all the samples tested by RNA sequencing, as indicated (color and shape code as in **A**). Red indicates higher relative expression, whereas blue denotes lower relative expression of the corresponding genes.

transcriptomic profile partially overlapped with that induced by the differentiation medium, suggesting some degree of similarity between both treatments. However, the differentiation medium notably altered the transcriptomic profile of healthy organoids, while miR-203 treatment had little to no effect on them (**Figure R47A**).

Focusing on the specific gene signature of *Mammary Gland Development*, we observed the expected divergence between healthy and tumor-derived organoids (**Figure R47B**). Notably, miR-203 treatment partially reverted these differences, but only in tumor-derived organoids. This reversion was particularly evident in genes associated with mammary gland development, especially within the sub-cluster associated with mammary gland epithelial differentiation, where miR-203 induced strong transcriptional changes in both healthy and tumor samples (**Figure R48A**).

Gene set enrichment analysis (GSEA) of *Mammary Gland Stem Cells* (MaSC) and *Mature Luminal Cells* signatures revealed that miR-203 exposure significantly enriched mature luminal gene expression, while showing no association with MaSC-related signatures (**Figure R48B**). Interestingly, analysis of the EMT signature showed that miR-203-treated samples displayed minimal correlation, in contrast to those treated with the differentiation medium.

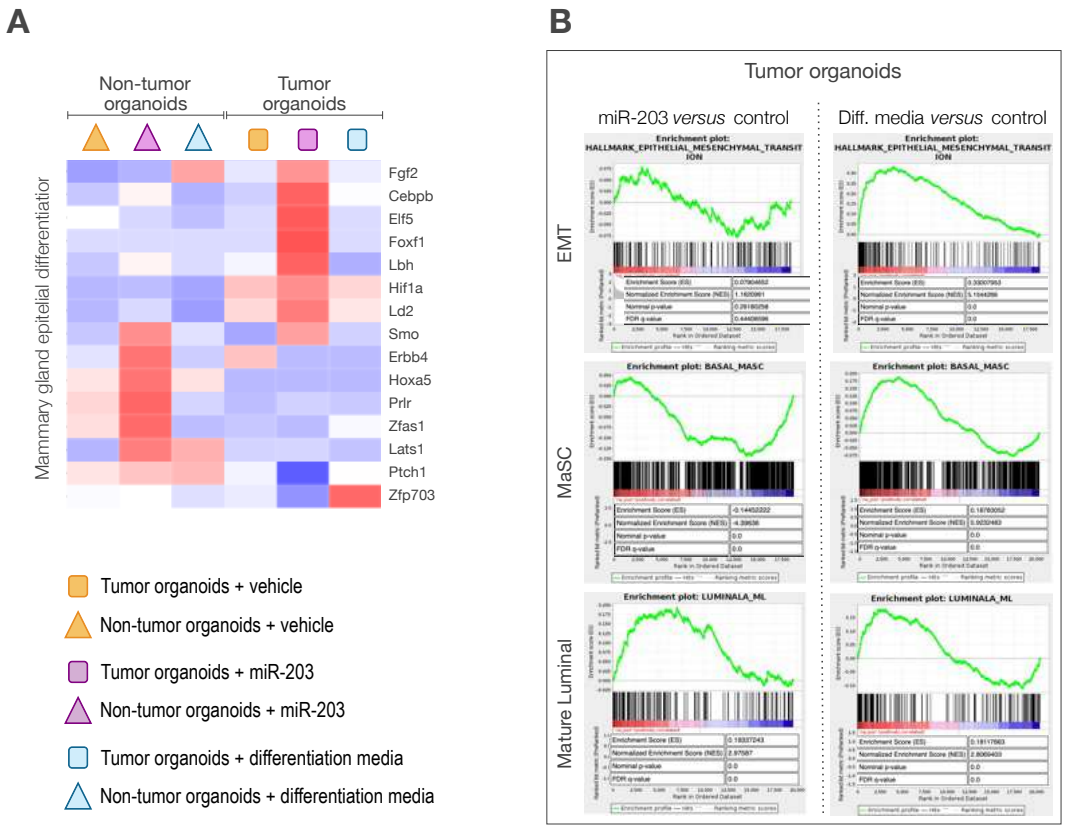

Figure R48. Gene expression signatures reveal miR-203 effects on mammary epithelial differentiation. **A,** Heatmap showing the Gene Ontology signature for mammary gland epithelial differentiation in all the samples tested by RNA sequencing, as indicated. **B,** Enrichment GSEA plots showing the induction of gene signatures characteristic of epithelial-to-mesenchymal transition (EMT), mammary stem cells (MaSC) and mature luminal cells in the comparisons indicated: miR-203-treated vs. control tumor organoids (left panels) and differentiation media-cultured vs. control tumor organoids (right panels). Insets in the GSEA plots include information about the enrichment score, normalized enrichment score, nominal p value and FDR q-value for each comparison.

ARCHS4 Tissues data base

term	p-value	q-value	overlap_genes
Basal cells	9.741974e-20	3.507111e-18	FOXE1, FAM57A, GALNT18, TNC, FOXI1, CALML3, TFCP2L1, PRSS22, ESPN, DMKN, AQP3, WFDC5, PTPRF, NKPD1, HK2, GJA1, CYP26B1, NIPAL1, TRIM29, SLC16A3, KRT6A, BOK, KRTDAP, CERS3, ELOVL4, IL18, KRT5, OVOL1, OSMR, HSPG2, SERPINB8, PGF, EPN3, PROCR, SLPI, ELF3, ADGRF4, MALL, DDIT4, LY6D, FSCN1, KCTD11, DSG3, IVL, HBEGF, SEMA3B, IL20RB, LYPD3, SBSN, KLK8, CST6, NDRG1, BARX2, KLK7, KLK6, MTHFD1L, SH3BP1, STC2, P2RY1, PLEK2, SFN, LY6G6C, TSPAN1, NGFR, WNT10A, JUP, CAVIN3, KLK13, G0S2, EPHX3, KLF4, KLK10, KLK11, VEGFA, GJB2, KRT17, NLRP10, P4HA2, REEP4, KRT14, BCAR1

PanglaoDB Augmented 2021

term	p-value	q-value	overlap_genes
Basal Cells	9.941465e-14	4.473659e-12	[BNIP3, KRT5, PRSS22, CST6, GJB2, SLPI, KRT17, TRIM29, ADGRF4, MALL, KRT14, LY6D, PLEK2, SFN, S100A14, SLC16A3, TSPAN1, KRT6A]

Figure R49. miR-203 exposure suppresses basal cell identity signatures in tumor organoids. Basal cell signatures differentially down-regulated in miR-203-exposed tumor organoids vs. their corresponding control counterparts, according to Enrichr (https://maayanlab.cloud/Enrichr/) in two different data bases: ARCHS4 and PanglaoDB.

Furthermore, *Basal Cell* identity gene signatures, as defined by two independent databases, were significantly downregulated upon miR-203 exposure (**Figure R49**), consistent with the previously observed changes in cytokeratin expression (**Figure R41**). Similarly, gene sets related to organ and cell development, cell migration and motility, cell metabolism, and cell cycle were all markedly suppressed in tumor organoids treated with miR-203 (**Figure R50**). These findings suggest that miR-203-induced differentiation not only promotes epithelial commitment but also reduces the proliferative and invasive traits typically associated with cancer cell plasticity.

This comparative analysis revealed key impact on mammary gland development and epithelial lineage commitment from miR-203 exposure. Comparing with differentiation media, while both treatments induced changes in the overall *Mammary Gland Development* signature, only miR-203 significantly altered genes specifically associated with epithelial differentiation. Moreover, enrichment plots showed that differentiation medium upregulated both EMT and MaSC-related gene signatures —an effect not observed with miR-203.

Term	GO	Count genes	%	P-value	Benjamini
Organ & Cell development					
Animal organ development	GO:0048513	71	30,5	2,8E-06	1,3E-03
Cell development	GO:0048468	37	15,9	5,7E-02	7,2E-01
Cell migration & Motility					
Cell Migration	GO:0016477	33	14,2	1,3E-04	2,3E-02
Regulation of cell migration	GO:0030334	24	10,3	2,8E-04	3,8E-02
Regulation of cell motility	GO:2000145	24	10,3	6,4E-04	5,7E-02
Positive regulation of cell migration	GO:0030335	15	6,4	3,6E-03	1,6E-01
Metabolism					
Protein metabolic process	GO:0019538	74	31,8	1,7E-03	1,1E-01
Negative regulation of protein metabolic process	GO:0051248	26	11,2	1,4E-03	9,8E-02
Regulation of protein metabolic process	GO:0051246	49	21,0	1,6E-03	1,0E-01
negative regulation of cellular metabolic process	GO:0031324	46	19,7	2,3E-03	1,2E-01
Cell cycle					
Cell Cycle	GO:0007049	13	5,6	6,7E-02	1,0E+00

Figure R50. miR-203 treatment downregulates gene programs associated with development, motility, metabolism, and proliferation in tumor-derived organoids. Gene Ontology (GO) signatures for organ and cell development, cell migration and motility, metabolism and cell cycle differentially down-regulated in miR-203-exposed tumor organoids vs. their corresponding control counterparts, as defined by "The Database for Annotation, Visualization and Integrated Discovery" DAVID (https://david.ncifcrf.gov/).

To further explore this distinction, we assessed the expression of the stemness marker Sox10 under both conditions. Organoids treated with differentiation medium showed increased Sox10 expression compared to controls, whereas this upregulation was absent in miR-203-treated cultures (**Figure R51**). These results suggest that although the differentiation medium induced a partial epithelial and luminal-like transition, it failed to promote full differentiation, instead enriching for a luminal progenitor-like state. In contrast, miR-203 expression appeared to drive a more advanced differentiation program, as indicated by the absence of Sox10, highlighting its potential role as a stronger inducer of epithelial and luminal differentiation compared with the differentiation medium alone.

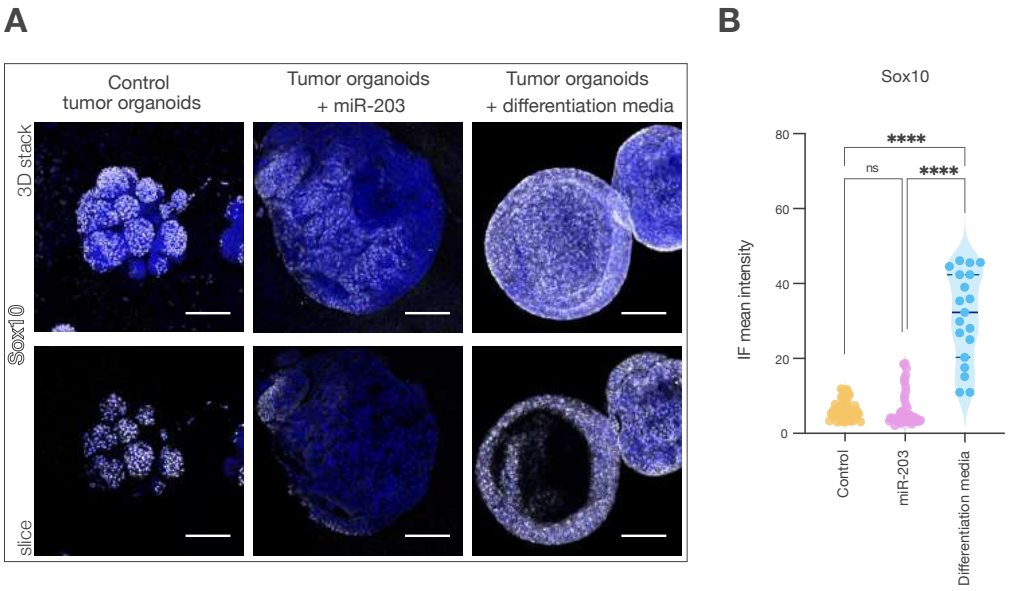

Figure R51. Transient exposure to miR-203, but not epithelial differentiation media, promotes mature differentiation in tumor-derived organoids. A, Detection of Sox10 (white) by immunofluorescence in tumor-derived organoids obtained from controls and treated with miR-203 or with epithelial differentiation media. Nuclei are stained with DAPI (in blue). Upper panels show Z stack projections of 3D; lower panels show representative single sections. Scale bar: 100 µm. **B,** Violin plots showing the quantification of marker staining. All stack fields from three independent tumor samples were analyzed. ****p < 0.0001; n.s. not statistically different (One-way ANOVA).

Altogether, these findings indicate that brief exposure to miR-203 promotes differentiation through luminal maturation. This maturation is associated with reduced cellular plasticity, loss of stemness features, diminished migratory capacity, and ultimately, collapse of the tumor organoid culture, highlighting the potent differentiation-inducing capacity of miR-203 in breast cancer cells.

Different schedules of miR-203 treatment prevent tumor initiation, growth and metastasis in the PyMT breast cancer mouse model.

Having demonstrated that short-term exposure to miR-203 induces epithelial differentiation in both mouse- and patient-derived breast cancer organoids, we next sought to evaluate its therapeutic potential *in vivo*. Using the PyMT-miR-203 knock-in mouse model, we designed a series of Dox treatment schedules to assess whether miR-203 could prevent tumor initiation and progression.

To this end, we implemented three induction protocols: (1) early and transient induction: miR-203 expression was initiated at tumor onset and sustained for two weeks, after which Dox was withdrawn for the remainder of the experiment; (2) continuous induction: Dox was administered at tumor onset and sustained throughout the entire experiment; or (3) intermittent induction: Dox was administered every two weeks, starting once tumors were already established and undergoing exponential growth. Tumor progression was monitored via micro-computed tomography (micro-CT), and tumor volume was measured throughout the experiment.

In the first schedule, miR-203 was induced during a two-week window starting at the histologically defined tumor onset —between weeks 10 and 12, prior to micro-CT detectability. After Dox withdrawal, tumor development was monitored to evaluate whether this transient induction of miR-203 could exert lasting antitumor effects (**Figure R52A**).

Mice receiving miR-203 treatment displayed a significantly lower incidence of tumors per animal compared to controls (**Figure R52B-C**). miR-203 effect was also observed in tumor volume, which was markedly reduced following the induction at tumor onset (**Figure R52D**). Immunohistochemical analysis of tumor samples at endpoint revealed a downregulation of the proliferation marker Ki67 in tumors briefly exposed to miR-203, suggesting a less aggressive phenotype (**Figure R52E-F**).

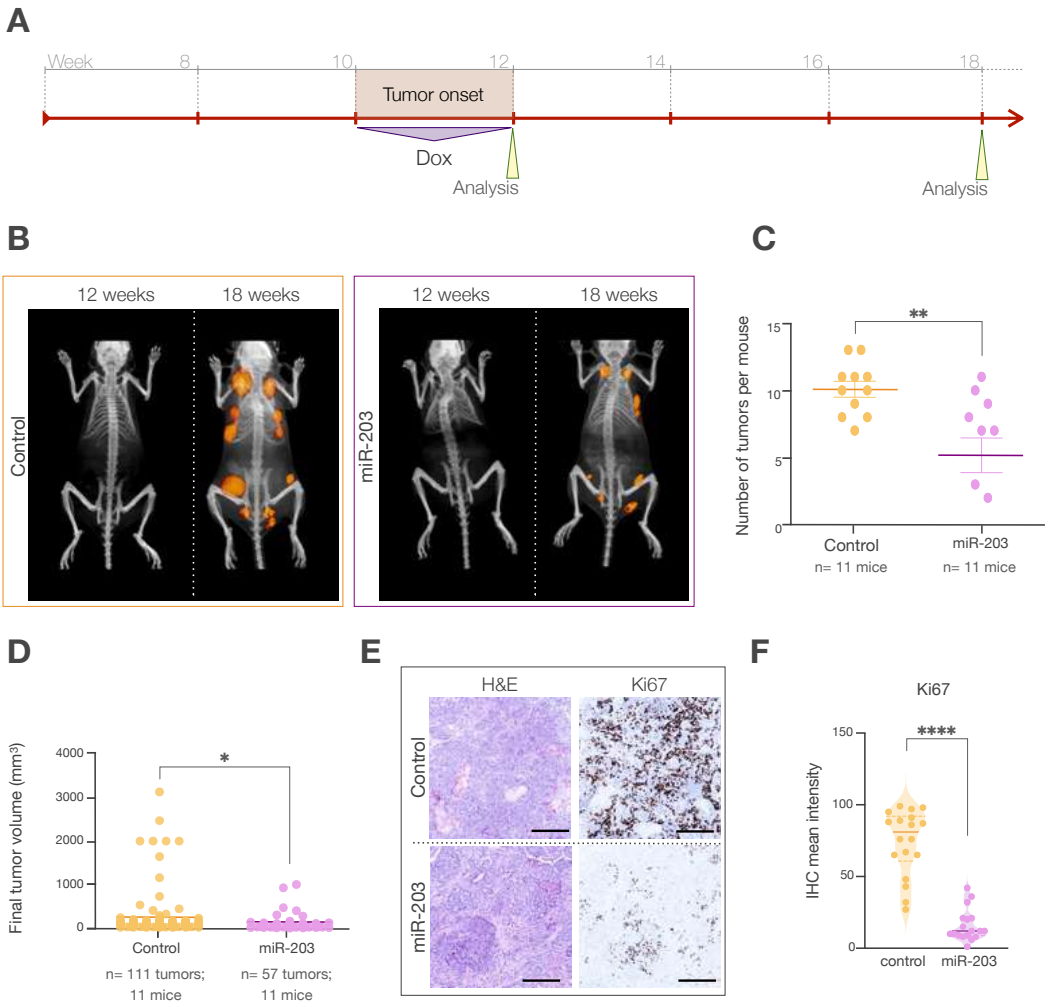

Figure R52. ***In vivo*** **effects of miR-203 treatment on PyMT mice, started at tumor onset and sustained for two weeks. A,** Schematic of the doxycycline treatment (Dox, in purple) schedule, on miR-203 wild-type or miR-203$^{KI/KI}$PyMT mice, during two weeks from tumor onset (before the tumors are detected by micro-CT). **B,** Representative micro-CT images of mice subjected to Dox treatment (in the figures, "control" indicates miR-203 wild-type; "miR-203" indicates knock-in mice), after Dox treatment (12 weeks of age) and at the endpoint (18 weeks of age). **C,** Number of tumors per mouse at the endpoint, in control and miR-203-treated mice; ** $p < 0.01$ vs. control (Student's test). **D,** Final tumor volume of control and miR-203-treated mice; *$p < 0.05$ vs. control (Student's t test). **E,** Illustrative hematoxylin and eosin (H&E) and Ki67 immunohistochemistry (IHC) staining of control and miR-203-treated tumors at the endpoint. Scale bar: 500 μm. **F,** Violin plot showing the quantification of Ki67 staining. Six different fields from three independent tumor samples were analyzed; ****$p < 0.0001$ vs. control (Student's t test).

To further examine the effect of miR-203 on tumor initiation capacity over the course of tumor development, we next sustained Dox treatment from tumor onset until endpoint (defined by humane criteria in control animals; **Figure R53A**). In these settings, miR-203 antitumor effects were even more pronounced: tumor formation was almost completely blocked in treated mice

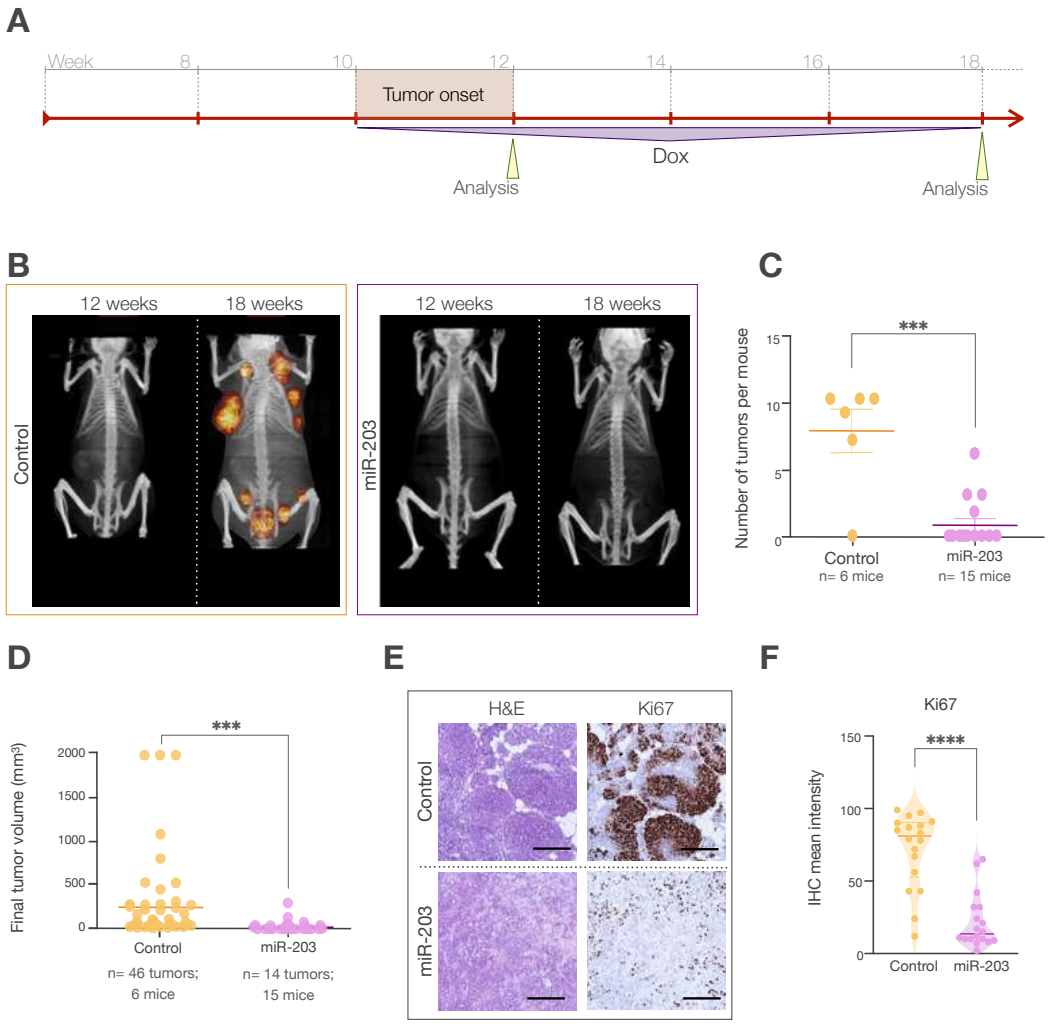

Figure R53. ***In vivo*** **effects of miR-203 treatment on PyMT mice, started at tumor onset and sustained to the humane endpoint. A,** Schematic of the Dox treatment (in purple) schedule, on miR-203 wild-type or miR-203$^{KI/KI}$PyMT mice, from week 10 to the experimental endpoint. **B,** Representative micro-CT images of mice subjected to the Dox treatment (in the figures, "control" indicates miR-203 wild-type; "miR-203" indicates knock-in mice), at 12 weeks of age and at the endpoint (18 weeks of age). **C,** Number of tumors per mouse at the endpoint, in control and miR-203-treated mice; ***p< 0.001 vs. control (Student's test). **D,** Final tumor volume of control and miR-203-treated mice; ***p< 0.001 vs. control (Student's t test). **E,** Illustrative hematoxylin and eosin (H&E) and Ki67 immunohistochemistry (IHC) staining of control and miR-203-treated tumors at the endpoint. Scale bar: 500 μm. **F,** Violin plot showing the quantification of Ki67 staining. Six different fields from three independent tumor samples were analyzed; ****p < 0.0001 vs. control (Student's t test).

(**Figure R53B**). Indeed, only a few tumors developed in the miR-203-treated group and they were significantly smaller than their control counterparts (**Figure R53C-D**). Once again, Ki67 staining revealed that the rare tumors that did emerge under miR-203 treatment had markedly reduced proliferation capacity (**Figure R53E-F**).

To model a more clinically relevant scenario, we tested a third *in vivo* schedule in which miR-203 treatment began only after tumors became detectable by micro-CT (around week 14) and was then administered intermittently every two weeks until the experimental endpoint (**Figure R54A**).

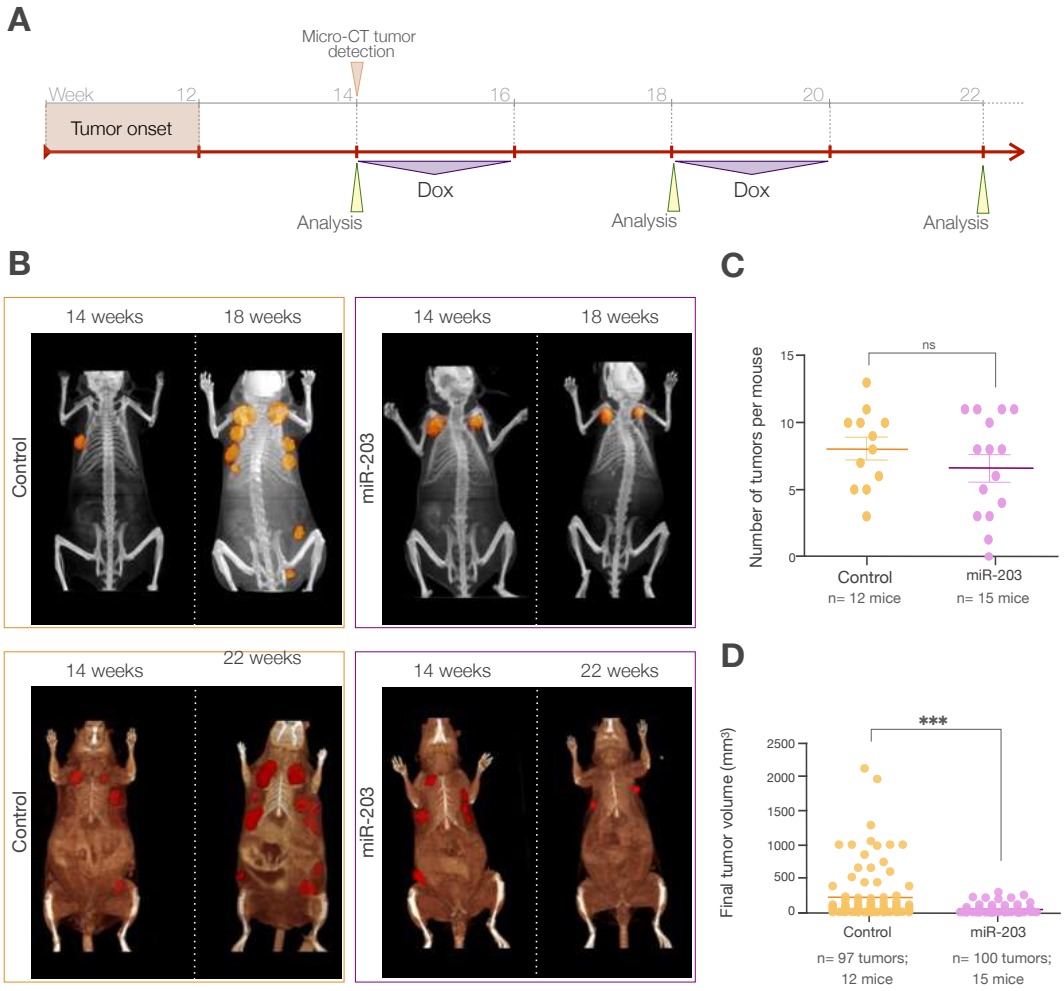

Figure R54. *In vivo* effects of miR-203 treatment on PyMT mice, started at tumor micro-CT detection and administered every two weeks. A, Schematic of the Dox treatment (in purple) schedule, on miR-203 wild-type or miR-203$^{KI/KI}$PyMT mice, starting when tumors are found by micro-CT imaging (around week 14) to the endpoint, every two weeks. **B,** Representative micro-CT images of mice subjected to the Dox treatment (in the figures, "control" indicates miR-203 wild-type; "miR-203" indicates knock-in mice) at tumor detection by micro-CT (14 weeks), four weeks later (18 weeks) and at the endpoint (22 weeks). **C,** Number of tumors per mouse at the endpoint, in control and miR-203-treated mice; n.s. not statistically different (Student's t test). **D,** Final tumor volume of control and miR-203-treated mice; ***$p < 0.001$ (Student's t test).

Of interest, this schedule effectively reduced the tumor volume, but did not prevent the generation of new tumor masses (**Figure R54B-D**). These findings suggest that, while intermittent miR-203 exposure can suppress tumor growth, it may not be sufficient to block tumor initiation once tumors are already established.

Given that tumor-initiating capacity is closely associated with undifferentiated cancer cells, we examined the expression of well-established dedifferentiation markers [205] in tumors exposed to miR-203. Notably, CD44 and NeuN expression levels were significantly decreased in miR-203-treated tumors, as was the proliferation marker Ki67 (**Figure R55A**), indicating a shift toward a less proliferative and more differentiated state.

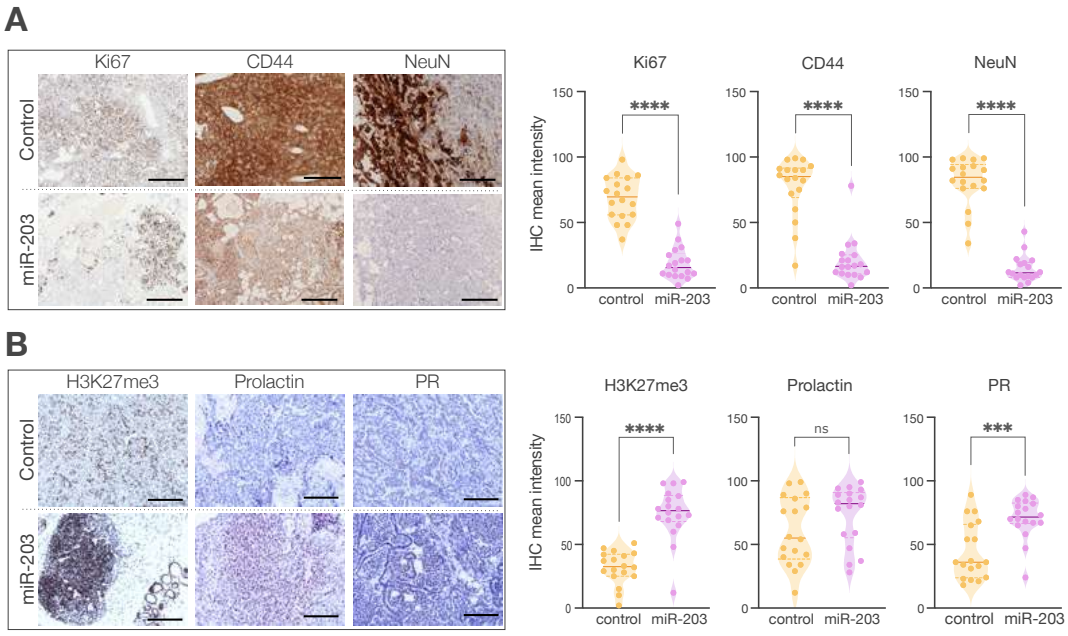

Figure R55. *In vivo* miR-203 induction reduces proliferation and stemness while promoting differentiation markers in mammary tumors. A, Left panel, Representative images of IHC staining for Ki67 (to test proliferation), CD44 and NeuN (as stem-like cell markers) in control and miR-203-treated tumors, at the experimental endpoint and after exposure to Dox on every two weeks from tumor detection by micro-CT. Scale bar: 500 μm. Right panel, violin plots showing the quantification of marker staining. Six different fields from three independent tumor samples were analyzed; ****$p < 0.0001$ (Student's t test). **B,** Left panel, representative images of IHC staining for H3K27me3, prolactin (PRL) and progesterone receptor (PGR), to test evidences of differentiation on control and miR-203-treated tumors. Scale bar: 500 μm. Right panel, violin plots showing the quantification of marker staining. Six different fields from three independent tumor samples were analyzed; ****$p < 0.0001$; ***$p < 0.001$; n.s. not statistically different (Student's t test).

Consistent with our organoid model findings, markers of epithelial differentiation and maturation — including H3K27me3, and PR— were upregulated in miR-203-treated tumors compared to controls (**Figure R55B**).

In all *in vivo* experiments, we systematically evaluated the metastatic potential of miR-203-treated tumors. Remarkably, none of the miR-203-treated mice (n=41) developed lung metastases under any of the miR-203 treatment regimens, whereas 31 % of control animals (n=29) did (**Figure R56**). These findings highlight miR-203 ability not only to suppress tumor proliferation and growth but also to significantly inhibit metastasis.

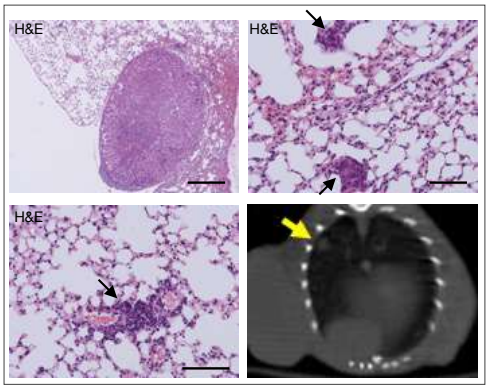

Lung metastasis incidence	
Control	9 out of 29
miR-203	0 out of 41

***

Figure R56. *In vivo* miR-203 induction fully prevents lung metastases. Illustrative H&E staining of lung macro- and micro-metastasis, found in several control mice at the experimental human endpoint. Representative examples are shown, from the 9 metastasis cases identified throughout the three *in vivo* experiments. As shown in the table, the overall incidence of metastasis was 31.03 % in control mice vs. 0 % in miR-203-treated mice. The bottom right panel shows a representative micro-CT image, pointing to one evident macro-metastasis (yellow arrow) found in a control mouse. Scale bar, 500 μm.

To further explore the effects of miR-203 on cancer cell plasticity and self-renewal, we established organoid cultures from tumors obtained under the last *in vivo* treatment scheme —intermittent miR-203 induction initiated after micro-CT tumor detection (**Figure R57A**). Morphological evaluation revealed striking differences between organoids derived from control *versus* miR-203-treated tumors (**Figure R57B**). Organoids from miR-203-treated mice were predominantly cystic, structured, and exhibited a luminal-like phenotype, similar to that observed upon transient *in vitro* miR-203 exposure. Of note, immunohistochemical analysis further confirmed a reduced proliferative index in organoids derived from miR-203-treated tumors (**Figure R57B**).

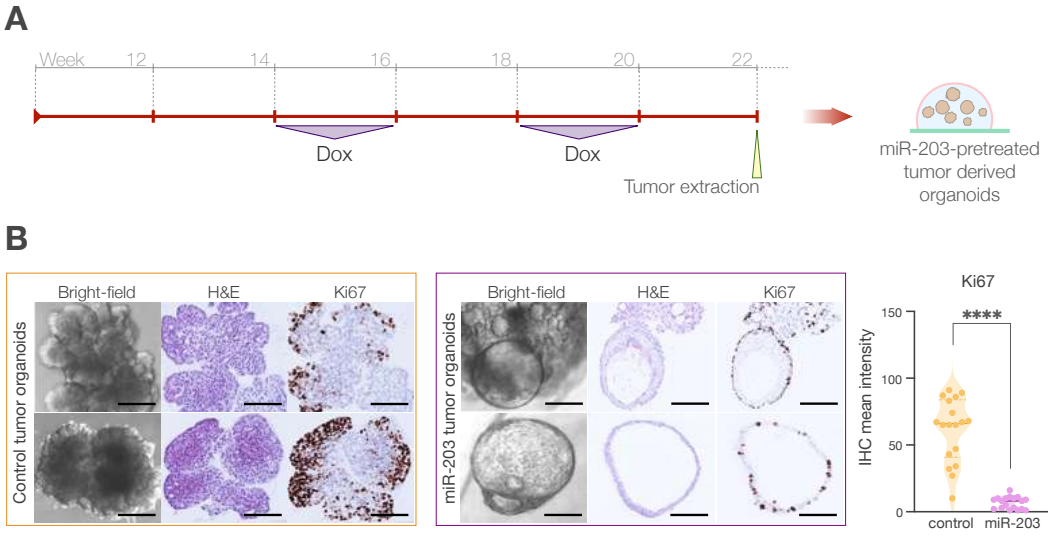

Figure R57. *In vivo* miR-203 induction promotes a morphological switch and reduces proliferation in tumor-derived organoids. A, Schematic of the Dox treatment (in purple) schedule *in vivo*, on miR-203 wild-type or miR-203$^{KI/KI}$PyMT mice, starting when tumors are found by micro-CT imaging to the endpoint, on every two weeks. Organoids were generated from miR-203 and control-pretreated tumors. **B**, Left panel, Representative bright-field images and the corresponding H&E and Ki67 IHC staining of tumor-derived organoids (tumors from miR-203 wild-type or miR-203$^{KI/KI}$PyMT mice treated *in vivo* with Dox. Scale bar: 100 µm. Right panel, violin plot showing the quantification of Ki67 staining. Six different fields from three independent tumor samples were analyzed. ****$p < 0.0001$ (Student's t test).

To validate these findings at the molecular level, we performed immunofluorescence on tumor-derived organoids (**Figure R58**). Control-derived organoids (upper panels) expressed high levels of CK14 and low levels of CK8/18, whereas miR-203-treated tumor-derived organoids (middle panels) shifted the cytokeratin expression profile: CK8/18 became predominant, while CK14 was drastically reduced or absent. Notably, healthy tissue-derived organoids (bottom panels) showed a similar profile to the miR-203-treated tumor-derived organoids, supporting the idea that miR-203 drives a stable basal-to-luminal epithelial differentiation program in tumor cells, both *in vitro* and *in vivo*.

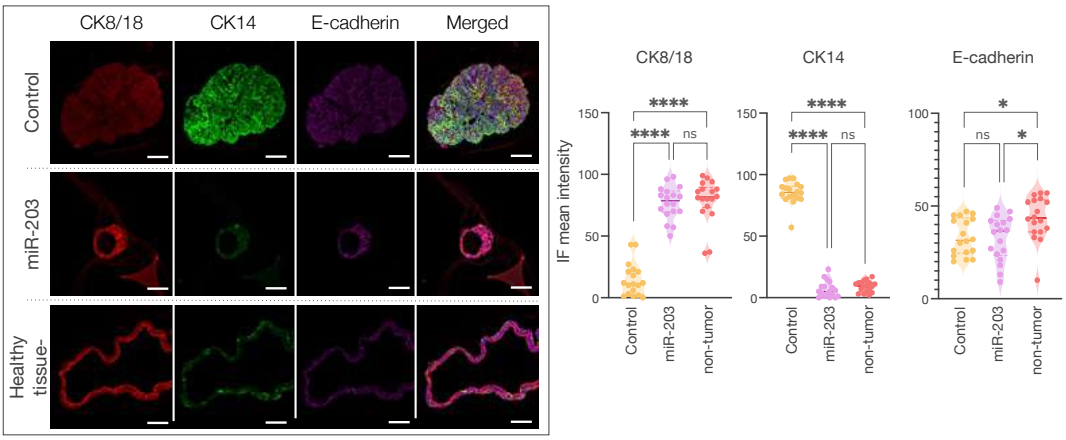

Figure R58. ***In vivo*** **miR-203 induction promotes luminal cytokeratin expression and epithelial features in tumor-derived organoids.** Left panel, detection of CK8/18 (red), CK14 (green) and E-cadherin (purple) by immunofluorescence in tumor-derived organoids, extracted from control tumors, miR-203-treated tumors or healthy mammary gland tissue samples. Scale bar: 100 µm. Right panel, violin plots showing the quantification of marker staining. Six different fields from three independent tumor samples were analyzed. ****p < 0.0001; *p < 0.05; n.s. not statistically different vs. control (One-way ANOVA).

Altogether, these *in vivo* experiments demonstrate that miR-203 has a potent antitumor effect across diverse therapeutic contexts. When induced transiently at tumor onset, miR-203 delayed tumor initiation and reduced both tumor incidence and growth. Sustained induction from tumor onset nearly abolished tumor formation and significantly lowered proliferation in those few tumors that did arise. Importantly, even when administered after tumors had already formed, intermittent miR-203 treatment was able to restrain tumor growth and reduce dedifferentiation markers. Furthermore, across all treatment regimens, miR-203 consistently prevented lung metastases, highlighting its strong potential to inhibit tumor cell dissemination. Organoid cultures derived from these *in vivo*-treated tumors further validated the differentiation-inducing effects of miR-203, closely resembling organoids from healthy mammary tissue or from *in vitro* transiently treated tumor cells. These findings reinforce the concept that miR-203 promotes a stable and functionally differentiated state that exhausts tumor plasticity and invasive potential.

Discussion

Ultimately, cancer is described as a reflected mirror of normal tissue development, where cellular programs that usually guide plasticity, self-renewal, and differentiation become deregulated. Under physiological conditions, these processes are tightly coordinated to ensure tissue homeostasis and regeneration. In tumors, however, such mechanisms are unbalanced, driving cells into immature or dedifferentiated states. This reprogramming toward progenitor-like fates is now recognized as a central step in tumor initiation and progression, and it drives many of the traits associated with relapse and metastasis [5,206].

One of the most fundamental hallmarks of this transformation is the loss of lineage-specific differentiation and the acquisition of enhanced plasticity and self-renewal. These features provide tumors with evolutionary advantages, enabling them to bypass natural selection barriers [9]. The standard anticancer therapies —chemotherapy, radiotherapy, and cytotoxic drugs—, mainly targeting proliferating cells, induce cell damage and death of cancer cells. However, such approaches often generate selective pressure that fosters the emergence of resistant and more aggressive clones, or simply enable the activation and growth of dormant cells that were inhibited by their surrounding proliferative cancer sister cells.

In this context, there has been growing interest in strategies that do not rely solely on killing cancer cells but instead reactivate their latent differentiation programs. Differentiation therapy seeks to inhibit aberrant self-renewal and redirect malignant cells toward maturation, thereby diminishing their tumorigenic potential. This concept, proposed decades ago, remains particularly attractive because it builds on principles of developmental biology to counteract tumor plasticity instead of inducing cell death, guiding tumor to terminal differentiation. Its clinical relevance is best exemplified by the treatment of APL, where retinoic acid induces terminal differentiation of leukemic cells, and in combination with conventional therapy achieves high remission rates, suggesting that combination therapies generate better results [82].

In contrast, the application of differentiation therapies in solid tumors remains at an early stage [83]. Nonetheless, the recognition that tumor cells exploit blocked differentiation pathways to sustain growth and plasticity has opened opportunities for novel therapeutic approaches in this direction. Differentiation therapy, particularly when combined with other strategies, holds promise as an alternative or complementary modality to conventional advanced treatment in cancer. In breast cancer, this concept is especially relevant, as tumor cells often hijack developmental programs of the active mammary stem cells and progenitors, using them to sustain dedifferentiation, plasticity and metastatic spread.

CB_2R modulation as differentiation therapy

For decades, the scientific community has been interested in the endocannbinoid system, as it regulates multiple physiological processes, including pain perception and the control of nausea and vomiting, symptoms that are among the most frequent side effect of chemotherapy [207]. In this context, cannabinoids have been used as efficient treatments of chemotherapy-induced nausea and vomiting, as well as to alleviate loss of appetite related to chemotherapy [208].

In addition, since the early 2000s, cannabinoids have been investigated for their potential antitumor properties [209–211], with numerous studies demonstrating their ability to inhibit tumor cell proliferation, migration, and angiogenesis in preclinical models of various types of cancer [212]. These preclinical observations led to the first clinical trial assessing the effect of cannabinoids in an antitumor context. This phase Ib randomized, placebo-controlled trial evaluated the cannabis-based formulation Sativex — containing an approximate 1:1 concentration of THC and CBD— in patients with recurrent glioblastoma [213]. The trial established the safety and tolerability of Sativex, showed no interference with standard temozolomide therapy, and most importantly, reported a notable improvement in one-year survival outcomes, that lead to a follow-up phase II clinical trial to evaluate the overall survival of treatment [214]. Today, the interest in the therapeutic potential of the ECS in cancer has expanded, a trend that is closely related to the increasing legalization of cannabis worldwide.

While cannabinoids have been implicated in nearly all cancer hallmarks [212], their role in regulating cellular differentiation has received less attention. Only two studies have directly addressed differentiation as a primary endpoint showing cannabinoid effects in glioma stem cells. Notably, synthetic activation of CB_1R/CB_2R have shown to promote glial differentiation and reduces tumorigenicity in glioma stem cells [135]. In the same direction, CBD has been demonstrated to induce glial differentiation via TRPV2 while enhancing chemosensitivity [215]. Beyond these strategies, some studies have hinted at differentiation-related effects, particularly in the context of combined therapies. For instance, in leukemia, THC has been shown to sensitize cancer cells to chemotherapeutic agents, showing a synergistic effect that enhance overall therapeutic efficacy [216]. Similarly, in glioblastoma, a 1:1 combination of THC and CBD enhances the activity of temozolomide by reducing the stem cell population [217]. CBD co-administered with chemotherapy also increases cytotoxicity in squamous cell carcinoma [218]. In addition, the FDA-approved dronabinol has been reported to overcome differentiation blockade in acute leukemia cells [219], while in myeloma, THC has been found to promote the differentiation of myeloid-derived suppressor cells through epigenetic mechanisms [220]. Here, we identify the role for CB_2R in

promoting stable cancer cell differentiation in breast cancer. We show that a brief, low-dose exposure to cannabinoids reshapes mammary tumor organoids, triggering a basal-to-luminal switch, reducing stemness, and impairing migration, self-renewal, and metastatic potential — effects that persist both *in vitro* and *in vivo*.

Most studies showing antitumor effect of cannabinoids in cell culture models have employed concentrations in the micromolar range (1-25 μM), with effects typically assessed after prolonged exposure and immediately evaluated after the cannabinoid treatment. In contrast, we report for the first time in the context of breast cancer, a pro-differentiation effect at nanomolar concentrations, within the same range of concentrations previously shown to promote glioma stem cell differentiation [135,215]. Furthermore, we evaluate the long-term consequences of a brief cannabinoid pulse (4 days), followed by drug withdrawal for at least two weeks, underscoring a durable response. This novel approach highlights the capacity of cannabinoids to induce terminal differentiation, ultimately impairing cellular plasticity, suggesting a potential strategy to limit tumor aggressiveness and stemness. These findings expand the current understanding of cannabinoid biology in cancer, showing that transient treatments can have sustained phenotypic consequences.

Furthermore, the differentiation effect of cannabinoids presented here was obtained using three-dimensional organoid structures, which not only allow the assessment of stem cell-related properties but also faithfully recapitulate the inherent plasticity and heterogeneity of tumors [221]. This represents a clear advantage over the previous cannabinoid studies related to stemness, which have primarily focused on spheroid assays to evaluate self-renewal capacity alone, or the use of stemness markers using established cell lines or two-dimensional primary cultures [135,215]. As demonstrated in previous stem cell identification studies and in this Thesis —through the characterization of breast stem cells using CD49f/EpCAM populations— such markers do not accurately reflect the true plasticity of the tumor or capture the full spectrum and functional capacity of stem cell populations. By contrast, the use of organoids provides a more comprehensive and physiologically relevant platform to evaluate how treatment influences differentiation, plasticity, and tumor heterogeneity, allowing the study of sustained phenotypic changes induced by cannabinoids.

Building on this, in this Thesis we not only aimed to induce a differentiation process —which in many contexts may be reversible and potentially lost after treatment withdrawal— but also sought to uncover the plastic capacity of CSCs. To this end, we extended our analysis beyond long-term

evaluation by incorporating key components of the breast cancer microenvironment that critically modulate tumor behavior.

Specifically, we developed a microfluidic device enabling a multicellular co-culture system that includes CAFs and PBMCs, under circulating conditions that support long-term immune cell survival and activation through shear stress–dependent mechanisms. While most current co-culture systems in cancer research focus on interactions between two cell types —CAFs-organoids co-cultures to evaluate invasion, singular members of immune system such as T cells or macrophages with organoids co-culture to evaluate immune activation [222–225]—, our approach integrates three key players simultaneously within a dynamic system. Moreover, by applying physiologically relevant levels of shear stress, we not only enhance cellular activation but also recapitulate features of the vascular environment, further increasing the translational value of the model.

Using this system, we demonstrated that cannabinoid treatment can drive terminal differentiation of tumor cells even within complex microenvironment cues. Despite the additional stimuli provided, cannabinoids impaired the plastic distribution of tumor cell states and disrupted the invasive capacity of the culture, not only during treatment but also after treatment withdrawal. Remarkably, the microenvironment failed to reprogram the cells or restore their plasticity, indicating that proliferation, invasion, and differentiation remain durably and irreversibly impaired.

It is important to note that, in our co-culture system, cannabinoid treatment with either THC or SR2 did not appear to induce a negative alteration to the tumor microenvironment itself. Fibroblasts, which under inflammatory conditions and during wound repair display a CB_2R-dependent regulation of contractile functions, induce proliferative features, and extracellular matrix remodeling to facilitate migration [226], did not exhibit adverse responses in our settings, maybe due to the relatively low concentrations used. Similarly, immune cells are strongly regulated by CB_2R signaling. Such modulation has sometimes been associated with reduced immune competence, raising the possibility that cannabinoids could impair antitumor immunity [227,228]. However, our results do not support this scenario. We observed increased markers for recruitment of macrophages and neutrophils into the system, which may suggest that a global immunosuppressive effect is unlikely to be occurring. Yet, it remains important to further investigate these interactions in greater depth, as subtle effects on CAFs or immune cells cannot be fully excluded. Based on our findings, any such effects appear minor compared to the robust and sustained differentiation response induced in cancer cells. This may reflect how cannabinoids

reshape tumor cell plasticity and communication, promoting a coordinated response in which stromal and immune components act in concert with —rather than independently of— the tumor compartment.

The demonstrated terminal differentiation induced by brief exposure to CB_2R ligands and maintained across multiple passages and generations of cancer cells, suggest the involvement of an epigenetic mechanism that reorganizes intercellular relationships. Indeed, RNAseq analysis revealed early remodeling of the epigenetic landscape, which further promoted this sustained differentiated state. Among the top genes regulated by THC and SR2, UTF1 likely plays a central role. Extensive research supports UTF1 as a key mediator of epigenetic stability, governing lineage specification during early embryogenesis [229] and, in cancer, altering chromatin availability through histone-regulated dynamics to maintain nuclear structure during cell fate transitions [181,230,231]. Mechanistically, UTF1 localized to promoters of developmental genes —particularly those that are silenced or bivalently marked, related to the Polycomb Repressive Complex 2 (PRC2)— fine-tuning the balance between self-renewal and differentiation [182]. In fact, its expression diminishes as cells undergo differentiation. Moreover, CB_2R modulation is accompanied by concurrent upregulation of FOXA1, a transcription factor strongly associated with luminal progenitor states during mammary gland development [41,44]. This demonstrates that CB_2R modulation primes cells toward luminal lineage commitment, establishing a differentiation trajectory that is maintained long after treatment withdrawal. Collectively, this positions UTF1 as a key mediator linking transient CB_2R signaling to long-term epigenetic remodeling and stable cancer cell differentiation.

Differentiation-based approaches have long been studied as co-treatment strategies, aiming to reduce tumor plasticity and enhance the response to conventional therapies [83]. By forcing cancer stem cells into a terminal state, differentiation therapy increases tumor sensitivity to chemotherapy and limits relapse. In line with this, we demonstrate that after cannabinoid-induced differentiation, tumors can be subjected to chemotherapy at reduced doses while still achieving enhanced therapeutic efficacy. While these effects were evident in the mouse model, they were even more pronounced in patient-derived samples, underscoring the translational relevance of cannabinoid-based co-treatment strategies and reinforcing their potential as clinically therapeutic options. Findings herein presented highlight the potential application of adaptive therapy, in which modulation of tumor plasticity complements cytotoxic treatment, thereby impairing relapse and resistance.

Furthermore, given the disparity between the nanomolar doses used in this Thesis to induce differentiation and the substantially higher, micromolar concentrations typically related to trigger cell death, these findings highlight distinct layers of ECS-mediated regulation in breast cancer. In this sense, these dual mechanisms —differentiation at low doses versus cytotoxicity at high dose — can be rationalized as complementary therapeutic strategies: one selectively constraining tumor plasticity, and the other targeting bulk tumor cell viability.

Importantly, when assessing higher cannabinoid doses in our organoid model, we observed an increased in the stemness marker SOX10 and the emergence of invasive features, rather than a complete collapse of the culture. Upon pharmacological withdrawal, these viable, highly plastic cells appeared to withstand the cytotoxic pressure, suggesting that high-dose cannabinoid exposure may paradoxically enrich for a resilient, stem-like subpopulation. A similar pattern was observed when tamoxifen was administered without prior CB_2R-mediated differentiation, further supporting the notion that plastic, undifferentiated cells can counteract cytotoxic stress.

These observations lead us to propose that adressing this resistance may requiere a sequential therapeutic strategy that exploits both cannabinoid-mediated effects, similar to the approach used in tamoxifen co-treatment. In this strategy, a low-dose differentiation-inducing phase would applied first, followed by high-dose cytotoxic exposure and, potentially, concomitant treatments such as tamoxifen or other chemotherapy. Nevertheless, this plausible combination requires careful evaluation, as it remains unknown whether CB_2R-mediated differentiation alters the subsequent cytotoxic response —a particularly relevant consideration given that the cytotoxic effects of cannabinoids in breast cancer have been strongly linked to CB_2R activity [121-125, 131, 132].

Mechanistic insights into CB_2R-mediated tumor cell differentiation

Our findings demonstrate that a brief, nanomolar-dose of CB_2R modulation can induce a durable differentiation program in breast tumor organoids, challenging the conventional paradigm that state cannabinoid-driven antitumor effects require prolonged, micromolar-dose cytotoxic exposure. Notably, we also found that THC, SR2, and genetic ablation of CB_2R (CB_2KO) elicited similar differentiation outcomes. Although this may seem counterintuitive, given that THC functions as a partial CB_1R/CB_2R agonist [109] and SR2 as a CB_2R inverse agonist [108], both compounds led to comparable phenotypic outcomes in our system. This apparent paradox prompts us to deeper evaluate the critical role of ligand dose and receptor engagement context.

Micromolar concentrations frequently produce cytotoxic, that are more likely to be non-specific or membrane-perturbing effects, while nanomolar concentrations are more likely to elicit

physiologic, receptor-mediated signaling and modulation of transcription or epigenetics. Thus, whereas previous studies in tumor models typically relied on high-dose cannabinoids to induce acute cell death or growth inhibition, our approach underscores a different mechanism: the perturbation of a CB_2R-dependent stemness axis leading to phenotypic commitment rather than immediate cytotoxicity. Consistent with this Soethoudt et al. emphasize that the same CB_2R ligand can exhibit very different signaling fingerprints depending on the concentrations used, assay readouts and system context [229]. These context- and dose-dependent differences indicate that the mode of CB_2R engagement drives distinct downstream outcomes.

This interpretation aligns mechanistically with the concept of biased signaling at GPCRs, whereby different ligand concentrations and cellular contexts stabilize distinct receptor conformations that drive divergent signaling pathways. For instance, it has been shown that CB_1R and CB_2R can adopt different conformations depending on the ligand that binds to them [233]. Each conformation selectively activates particular downstream pathways, such as $G\alpha_i$, β-arrestin or ERK signaling. Thus, cannabinoids stabilize distinct receptor conformations and thereby yield divergent signaling outputs rather than a single "on/off" switch. More specifically, the detailed ligand profiling by Soethoudt et al. has demonstrated that certain CB_2R ligands, including THC, are biased towards pERK rather than β-arrestin or GIRK pathways, and that inverse agonism or competition at CB_2R can perturb basal receptor activity [232]. If the axis that maintains stemness requires basal G-protein (Gi) or β-arrestin signaling, a ligand that reduces that pathway (either via inverse agonism or by displacing endogenous agonists while not activating that pathway) would push cells to differentiate. In our system, the observation that both THC (a partial agonist) and SR2 (an inverse agonist) yield similar differentiation phenotypes, and that CB_2R knock-out mirrors this effect, suggests that loss or re-wiring of a tonic CB_2R-mediated signal rather than classical agonist activation may underlie stemness exit.

Looking ahead, dissecting the mechanistic sequence from CB_2R perturbation to epigenetic differentiation commitment will be essential.

First, acute signaling fingerprinting in our organoid model (e.g., measurement of cAMP, pERK, β-arrestin recruitment at the nanomolar pulse) will clarify which downstream pathways are modulated by THC and SR2. Finding that both compounds reduce Gi-mediated signaling or β-arrestin engagement would strongly favor a tonic-signal-disruption model. If instead, THC selectively activates ERK while SR2 suppresses Gi, a biased signaling interpretation would be more likely.

Next, given our sustained phenotype and the early up-regulation of UTF1 and FOXA1, we propose an epigenetic transition model in which transient CB_2R perturbation triggers chromatin remodeling (e.g., PRC2/H3K27me3 dynamics) and establishes a new differentiated state. Although UTF1 has been well-characterized in embryonic and cancer stem cells as a regulator of chromatin bivalency and lineage commitment [186,234], its upstream regulation by cannabinoid receptor signaling has not previously been reported. Time-series RNA-seq coupled with ATAC-seq or ChIP for UTF1 and H3K27me3 marks would help to test causality: if early UTF1 induction precedes chromatin closure at stemness loci and persists after ligand withdrawal, this would support the epigenetic-lock model.

Finally, in neuronal differentiation contexts, it has been reported that CB_2R downregulation can be accompanied by a compensatory upregulation of CB_1R (CB_2R-CB_1R switch) [235–237]. This phenomenon may be particularly relevant in scenarios where brief perturbations of CB_2R lead to its downregulation, thereby enhancing CB_1R-mediated signaling pathways. Such shift could promote or sustain luminal differentiation, potentially explaining the persistence of this differentiated state even after the initial perturbation is withdrawn. To empirically test this hypothesis, we propose a more systematic and deeper investigation into the kinetics of CB_2R and CB_1R expression during the differentiation process. This could involve measuring receptor expression levels at various time points, assessing the impact of CB_1R antagonism during the post-pulse phase. Such deeper approach would help determine whether the CB_2R-to-CB_1R receptor switch underpins the maintenance of the differentiated state.

In sum, by integrating acute signaling, pharmacological bias, transcriptional and chromatin dynamics, we could establish a mechanistic model in which transient CB_2R perturbation serves as a gate to tumor cell differentiation commitment. While these studies extend beyond the immediate scope of this Thesis, they build directly on its foundational insights, and represent a critical next step toward fully understanding how transient CB_2R modulation can durably reprogram tumor cell fate. Extending this work would have relevant implications, not only for deciphering the mechanisms of tumor plasticity but also for guiding the rational development of cannabinoid-based differentiation therapies grounded in the principles established here.

Building on this mechanistic framework, the results presented in this Thesis further reinforce the potential of synthetic CB_2R ligands as therapeutic agents, extending their promise beyond the effects of phytocannabinoids in cancer. Although clinical testing of CB_2R-targeted compounds is still limited [238], these data demonstrate that inverse agonism robustly induces differentiation in cancer organoids, even more effectively than THC. Importantly, SR2 has the potential advantage

of not eliciting psychoactive effects, as it functions as a CB_2R target and does not subject CB_1R, the primary mediator of cannabinoid-induced psychoactivity. Combined with the recent advances in CB_2R pharmacology, these findings position synthetic CB_2R ligands as powerful, safe, and clinically relevant tools for innovative cancer therapies, offering a strategy to target cancer stemness, limit tumor plasticity, working as reprogramming inducers, and reducing the risk of relapse.

miR-203 remodels breast cancer stemness

MicroRNAs have been widely described as critical regulators of epigenetic modulation in both developmental processes and cancer outcomes. Among them, miR-203 has emerged as a key factor in lineage commitment and tumor suppression. Originally linked to skin lineage specification [142], miR-203 expression has also been associated with better prognosis across several cancer types [146-152]. Over the past years, it has therefore been studied as a tumor suppressor candidate in different carcinomas. In squamous cell carcinoma, low levels of miR-203 correlate with a dedifferentiated phenotype, while its overexpression suppresses tumor growth by inhibiting proliferation, motility, and angiogenesis through c-MYC interaction [239]. In the same context, miR-203 has been reported to strongly reduce metastatic potential at the primary tumor site [240]. Similar effects have been observed in lung and ovarian cancers, where miR-203 interferes with EMT and migration [241–243], and in colon cancer, where its upregulation decreases proliferation and migration [244].

Although these preclinical studies largely focused on its tumor suppressor function rather than its differentiation potential, they consistently point to miR-203 as a central regulator of proliferation, invasion, and migration —processes fundamentally tied to CSC plasticity and non-CSC transitions. Supporting this, our group has shown that miR-203 fine-tunes the balance between reprogramming, stemness and differentiation programs, acting as a barrier to somatic-to-pluripotency reprogramming while promoting the differentiation of stem cells into mature lineages [147]. Based on these properties, we proposed that miR-203 may act as a driver of cancer cell differentiation, establishing it as a promising candidate for differentiation-based antitumor therapy.

In this doctoral Thesis, we demonstrate that transient exposure to miR-203 in both mouse and human breast cancer-derived organoids induces a striking morphological transition. Organoids exposed to miR-203 consistently shifted toward a predominantly cystic architecture, resembling the ductal organization of the mammary gland, with hollow lumens surrounded by spatially and temporally organized epithelial cells. This effect was reproducibly observed both after *in vitro*

treatment and in organoids derived from miR-203-treated tumors *in vivo*. This treatment reduced the expression of proliferation, basal and stemness-associated markers, while upregulating luminal differentiation markers, indicating a shift from a basal, dedifferentiated phenotype toward a more differentiated luminal-like state.

Importantly, organoids undergoing this cystic transition exhibited a markedly shortened lifespan in culture. Unlike untreated controls, which could be propagated long-term as previously described [163,245], miR-203-exposed organoids collapse after a few passages. This collapse points to exhaustion of self-renewal capacity, likely coupled to increased cell death, and strongly supports that miR-203 drives terminal differentiation within the breast cancer cell population.

Although we demonstrate that miR-203 exposure promoted a luminal differentiation phenotype in breast cancer organoids, other studies show that it can also shift toward alternative developmental patterns, such as branching morphogenesis and MET [246,247]. These observations suggest that, under differentiation-inducing conditions, miR-203 functions as a differentiation enhancer rather than as a reprogramming inducer, reinforcing existing lineage trajectories instead of irreversibly fixing cell fate. This interpretation points to an epigenetic mode of action, whereby miR-203 interacts with the regulatory landscape to guide cell fate decisions, consistent with previous reports [147,157,248]. To directly test whether miR-203 could alter CSC to non-CSC plasticity, we incorporated the *in vivo* tumor environment.

Using different treatment schedules, we found that continuous administration of miR-203 from tumor onset to the end of the experiment completely prevented tumor initiation and growth. By contrast, intermittent exposure, although significantly delaying tumor initiation and controlling tumor growth, did not fully prevent tumor formation. This pattern is consistent with the notion that CSCs and non-CSCs plasticity is capable of dynamic phenotypic transitions in response to appropriate stimuli [35,249]. Intermittent withdrawal of miR-203 likely allowed undifferentiated populations to be restored, thereby sustaining tumor initiation. Thus, miR-203 does not irreversibly reprogram the tumor population; instead, it transiently enhances differentiation, a state that can be, at least partially, reversed through tumor-environment interactions.

Importantly, *in vivo* experiments revealed that miR-203 consistently suppressed metastasis across all treatment schedules tested. None of the miR-203 treated mice developed metastases, while controls showed a 31 % incidence. Supporting this, both mouse- and patient-derived *in vitro* cultures with polarized and migratory phenotypes lost their invasive capacity after miR-203 treatment. These results align with previous studies that report metastasis impairment when

miR-203 is activated [224,240–242,244], strengthening the evidence that miR-203–induced differentiation is intrinsically linked to reduced invasion and metastatic potential.

miR-203 functions as a differentiation enhancer

Data from miR-203-treated organoids reveal a clear luminal phenotype switch derived from the induced differentiation process. Previous studies have shown that miR-203 is activated during luminal epithelial differentiation observed within the mammary hierarchy and is largely restricted to the luminal lineage in both mouse and human tissues [148,250]. Although further analysis is required to determine the specific cellular switches underlying this effect, we can speculate that miR-203 over-expression in breast cancer cells amplifies an intrinsic differentiation program already present in luminal mammary epithelial cells.

To better characterized the differentiation process, we evaluated miR-203 induced differentiation in our organoid platform along with a well-established differentiation condition of mammary gland: a commercial culture medium previously described to promote mammary epithelial cell maturation. Under both conditions, a hollow cystic morphology was generated, suggesting that both treatments enhance the cyst-forming potential of the mammary cells. However, transcriptomic profiling by RNAseq revealed a striking distinction: while the differentiation medium promoted a luminal progenitor-like state, miR-203 treatment uniquely drove a robust epithelial differentiation signature, even within the pro-stemness context of the organoid media.

Notably, this differentiation effect was highly pronounced in tumor-derived organoids, whereas it was absent in healthy mammary tissue, where organoids showed minimal changes upon miR-203 exposure. This differential response highlights the context-dependent action of miR-203, suggesting that its impact is specifically amplified in tumor settings.

Several targets have been identified for miR-203 in cancer, where it has been described predominantly as a tumor suppressor [251], but in some contexts also as a tumor promoter [251,252]. This apparent discrepancy likely reflects the strong influence of the cellular context on microRNA targets and functional outcomes, further supporting the notion that miR-203 acts as a differentiation enhancer rather than a strict reprogramming inducer. In this role, miR-203 appears to reinforce pre-existing developmental trajectories, toward luminal epithelial identity. Here, we demonstrate that by strengthening luminal committed programs, miR-203 reduces stemness and self-renewal potential, while restricting invasive and proliferative capacities, thereby shifting tumor cells into a more differentiated and less aggressive state. Our findings

confirm the antitumoral role of miR-203 and extend its influence on breast cancer differentiation, opening new perspectives for the therapeutic application of miR-203 in cancer.

Shaping tumor plasticity

The data shown in this Thesis demonstrate that differentiation therapies can reshape tumor plasticity by redirecting malignant cells into more stable and less aggressive states. Cannabinoids, acting through CB_2R, drive breast cancer cells into terminal luminal differentiation, exhausting their self-renewal potential and irreversibly limiting the plastic transitions that sustain tumor growth and relapse. miR-203 operates as a differentiation enhancer, strengthening luminal lineage commitment and reducing proliferation, motility, and metastasis. Both treatments converge on a shared outcome: the induction of a luminal-like epithelial phenotype, associated with diminished invasiveness and reduced tumorigenic potential.

The way we have traditionally understood biology —both in organism's development and in disease conditions— has been largely gene-centered, interpreting biological organization as a mechanistic system [253]. Within this framework, deciphering the function of each gene and its contribution to specific pathways was thought to provide the necessary knowledge to block or enhance gene expression, thereby controlling the pathological disruptions associated with disease. This view is based on the idea that the structure of an organism resembles that of a machine, in which development proceeds as a pre-structured, hierarchical process encoded within the genome [254]. Extending this same reductionist perspective to the cellular level, cell functions have been explained as outcomes of pathways governed by networks of proteins, which in turn are regulated by differentially expressed genes [253,255]. While this framework has led to major discoveries identifying pathways, defining critical gene functions, ultimately advancing biological knowledge over the years, it cannot provide a complete picture of how organisms and biological systems actually emerge and organize [256,257].

With the discoveries of epigenetic regulators —such as chromatin remodelers, histone modifiers, non-coding RNAs fine tune elements, or DNA modifiers — science has gradually shifted away from a strictly reductionist view of molecular pathways and their disruption in disease. Thus, the model fails to capture the inherent flexibility and adaptability of biological systems, as well as their intrinsic connection to evolution and emergent properties [258]. This is dramatically evident in cancer research, where the concepts of emergent systems and adaptability are fully exemplified [5]. By exploiting the molecular tools of their tissue of origin, cancer cells operate as highly adaptive evolutionary systems, capable of efficiently responding to a wide variety of stimuli.

In cancer, this emergent behavior manifests as a defining trait of cellular plasticity and adaptability to the environment [259]. Social interactions within species and between species —such as mutualism or parasitism— mirror the interactions of cells within organs and between organs in an organism, which in turn resemble the collective distribution and cooperation of prokaryotic populations [260]. This reflects a conserved adaptability trait in nature, maintained at the level of organ development and carried through the evolutionary transition of cancer cells and the tumor itself —including both cancer cells and the non-tumoral supportive cells. Just as social cues guide the migratory distribution of birds toward areas of optimal food availability, or human movement patterns decides urban future plannings, tumors exhibit a remarkable capacity to sense, adapt, and reorganize in response to microenvironmental and external cues, enabling them to overcome directed therapeutic interventions [261–265].

The recently recognized cancer characteristics of plasticity and self-organization better account for this adaptability, reflecting an intrinsic capacity derived from the developmental biology of their tissue of origin [9]. This perspective views cancer as a system capable of sensing external cues, coordinating internally, and ultimately self-directing its future behavior [266]. In breast cancer, this capacity is highly represented, as tumors display remarkable heterogeneity in cellular composition and behavior, enabling adaptation to therapy, metastasis, and microenvironmental changes.

Notably, based on their plasticity, breast cancer subtypes can shift following neoadjuvant treatment. Studies assessing biomarker changes show that 70 % of tumors undergo changes to a different type after therapy, reflecting their capacity to reprogram in response to therapeutic pressures [267]. A clear illustration of this plastic potential is provided by organoid models, used alongside this Thesis, where tumor cells demonstrate their ability to self-renew and reconstitute the heterogeneity of the original carcinoma.

Organoids faithfully capture both the heterogeneity and the plasticity of tumors. Generating organoids from breast cancer samples allows us to interrogate their capacity for self-organization, self-renewal, and adaptation. Interestingly, organoid-forming efficiency varies considerably among patient-derived samples, independently of canonical tumor subtype or histological grade (**Figure D1**), which enforces that plastic potential is not strictly tied to conventional classifications, but rather reflects an intrinsic or patient-specific adaptability trait, further supporting the flexible transition between breast cancer subtypes observed after treatment [267].

A

Clinico pathological data								Age	Neoadjuvant treatment	Type of surgery	Tumor focality	Tumor organoids (days in culture)
Molecular subtype	Histologic type	Grade	ER	PR	HER2	Ki67	Nodes					
Luminal A	ILC	II	100 %	90 %	-	22 %	Pos	47	Upfront surgery	Mastectomy	Multicentric	6
HER2+	IDC	I	Neg	Neg	+	52 %	Neg	75	Neoadjuvant chemo + HER2 therapy	Tumorectomy	Unifocal	23
TNBC	ACC	III	Neg	Neg	-	14 %	Neg	65	Upfront surgery	Tumorectomy	Unifocal	34
TNBC	IDC	III	Neg	Neg	-	75 %	Neg	33	Neoadjuvant chemotherapy	Mastectomy	Multicentric	8
TNBC	IDC	III	Neg	Neg	-	75 %	Pos ext.	88	Upfront surgery	Tumorectomy	Unifocal	24
Luminal A	IDC	II	100 %	90 %	-	12 %	Neg	49	Upfront surgery	Tumorectomy	Multicentric	4
Luminal B	IDC	II	100 %	100 %	-	25 %	Pos	49	Upfront surgery	Tumorectomy	Multicentric	6
Luminal A[1]	ILC	II	100 %	100 %	-	10 %	Neg	53	Upfront surgery	Tumorectomy	Multicentric	3
Luminal A[1]	DCIS	II	100 %	100 %	-	10 %	Neg	53	Upfront surgery	Mastectomy	Unifocal	40
Luminal B[2]	IDC	II	100 %	90 %	-	25 %	Neg	44	Upfront surgery	Mastectomy	Unifocal	53
Luminal A[2]	ILC	II	100 %	100 %	-	15 %	Neg	44	Upfront surgery	Mastectomy	Multicentric	6
TNBC	IDC	III	Neg	Neg	-	70 %	Neg	53	Neoadjuvant chemotherapy	Tumorectomy	Unifocal	23

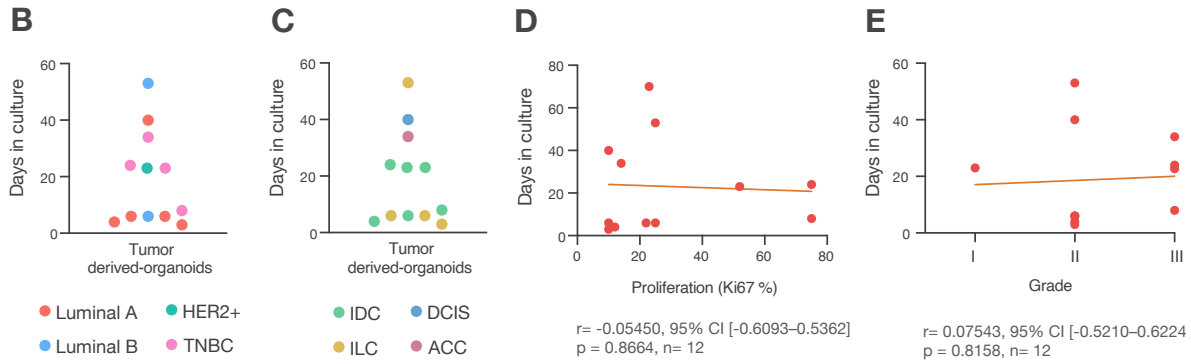

Figure D1. Long-term viability of patient-derived tumor organoids is independent of tumor type, histological classification, grade, and proliferation rate. A, Clinicopathological characteristics of patient-derived organoid samples, including molecular subtype (luminal A, luminal B, HER2+, or TNBC), histological type [invasive ductal carcinoma (IDC), invasive lobular carcinoma (ILC), ductal carcinoma *in situ* (DCIS), or adenoid cystic carcinoma (ACC)], tumor grade, receptor expression, proliferation rate (Ki67 staining), axillary node status, age, neoadjyuvant treatment, type of surgery, tumor focality, and organoid viability (days in culture). (1,2) Two samples were obtained from the same patient, who presented with a unifocal tumor in one breast and a multicentric tumor in the contralateral breast. **B–E,** Duration of organoid viability for each patient-derived sample, illustrating no correlation with molecular subtype (**B**), histological type (**C**), proliferation rate (**D**), or tumor grade (**E**).

Even more revealing is that organoids derived from histologically confirmed clean-margin, non-tumoral tissue —originating from regions that initially showed low adaptability— were able to generate tumor-like organoids that, interestingly, persisted long term in culture (**Figure D2**). Such evidence highlights the necessity of understanding tumors not as static entities fixed at diagnosis,

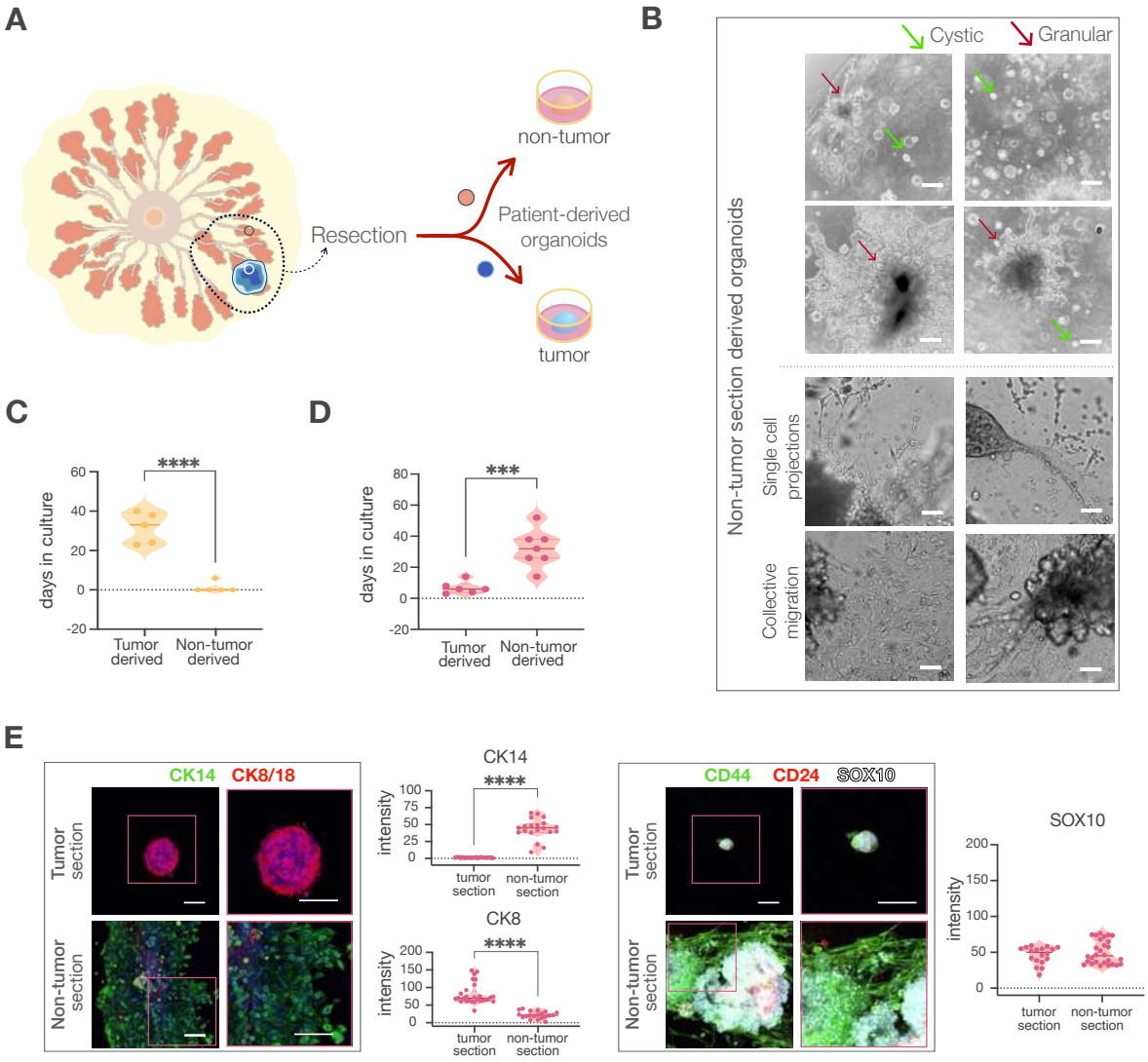

Figure D2. Patient-derived organoids from non-tumor breast tissue generate invasive granular structures in a subset of samples. A, Schematic representation of mammary gland resections used to obtain organoids from tumor and adjacent non-tumor breast tissue. **B,** Representative bright-field images of patient-derived non-tumor organoids after 20 days in culture. Green arrows indicate cystic non-aggressive organoids, while red arrows mark granular invasive organoids. Scale bar: 100 µm. **C,** Violin plot showing the duration of organoid viability in culture, for tumor and non-tumor samples obtained from multicentric cases. *** $p < 0.001$ vs. control (Student's test). **D,** Violin plot showing the duration of organoid viability in culture, for tumor and non-tumor samples obtained from unifocal cases. **** $p < 0.0001$ vs. control (Student's test). **E,** Representative immunofluorescence images of organoids derived from multifocal cases. Left, detection of CK8/18 (red), CK14 (green). Right, detection of CD24 (green), CD44 (red) and SOX10 (white). Scale bar: 100 µm. Violin plots showing mean intensity.

but as emergent, adaptive systems capable of reshaping themselves, and even migrate, in response to environmental or therapeutic cues. Consequently, therapeutic strategies that rely solely on the molecular profiling of the initial biopsy risk overlooking this adaptability and may fail to anticipate relapse driven by hidden plasticity.

Clinically, such adaptive capacity is mirrored in the pathological presentation of breast tumors, which can appear as unifocal or multicentric lesions (**Figure D2D-E**). Although evidence indicates that poorer survival and greater metastatic potential are associated with multicentric tumors [265,266], this distinction is most often used as a descriptive pathological feature rather than a decisive criteria for systemic treatment selection. Importantly, this phenotype appears to reflect an intrinsic capacity of plasticity and adaptation, enabling the dissemination within the mammary niche, contributing to local relapse and systemic spread. While traditional views might attribute this migratory behavior to fixed, patient-specific characteristics, such plasticity seems to be an emergent property of the tumor itself, revealed through its capacity to adapt and reorganize under selective pressures (**Figure D3**).

This drastically highlights breast cancer plasticity as a driver of adaptability which in long term induces relapse and metastasis, and it provides a conceptual bridge to differentiation-based therapies, making them one of the most compelling directions for cancer treatment. Targeting differentiation alters the rules of the system itself, redirecting its trajectory toward stability and exhaustion rather than growth and dissemination. Unlike canonical treatments that primarily target tumor survival, differentiation therapies act as regulators of plasticity. Their strength lies not in eliminating cells but in fine-tuning the transitions that connect development with malignancy, thereby disrupting the homeostatic balance that sustains cancer. In doing so, they compel tumor cells to establish a new equilibrium —in which self-directed adaptation is restricted.

Plasticity, often regarded as a driver of resistance and heterogeneity, is manifested here as a target that can be redirected. CB_2R modulation and miR-203 activation treatments exemplify how forced terminal differentiation can effectively abolish plasticity and exhaust tumor-propagating cells. In this context, it is also worth considering whether combining both CB_2R modulation and miR-203 activation could yield an additive effect on differentiation, with CB_2R signaling acting as a promoter of the differentiation trajectory and miR-203 serving to stabilize the terminal fate commitment. Such a dual strategy may better constrain cellular plasticity and more effectively reduce the dynamics of tumor-propagating cells.

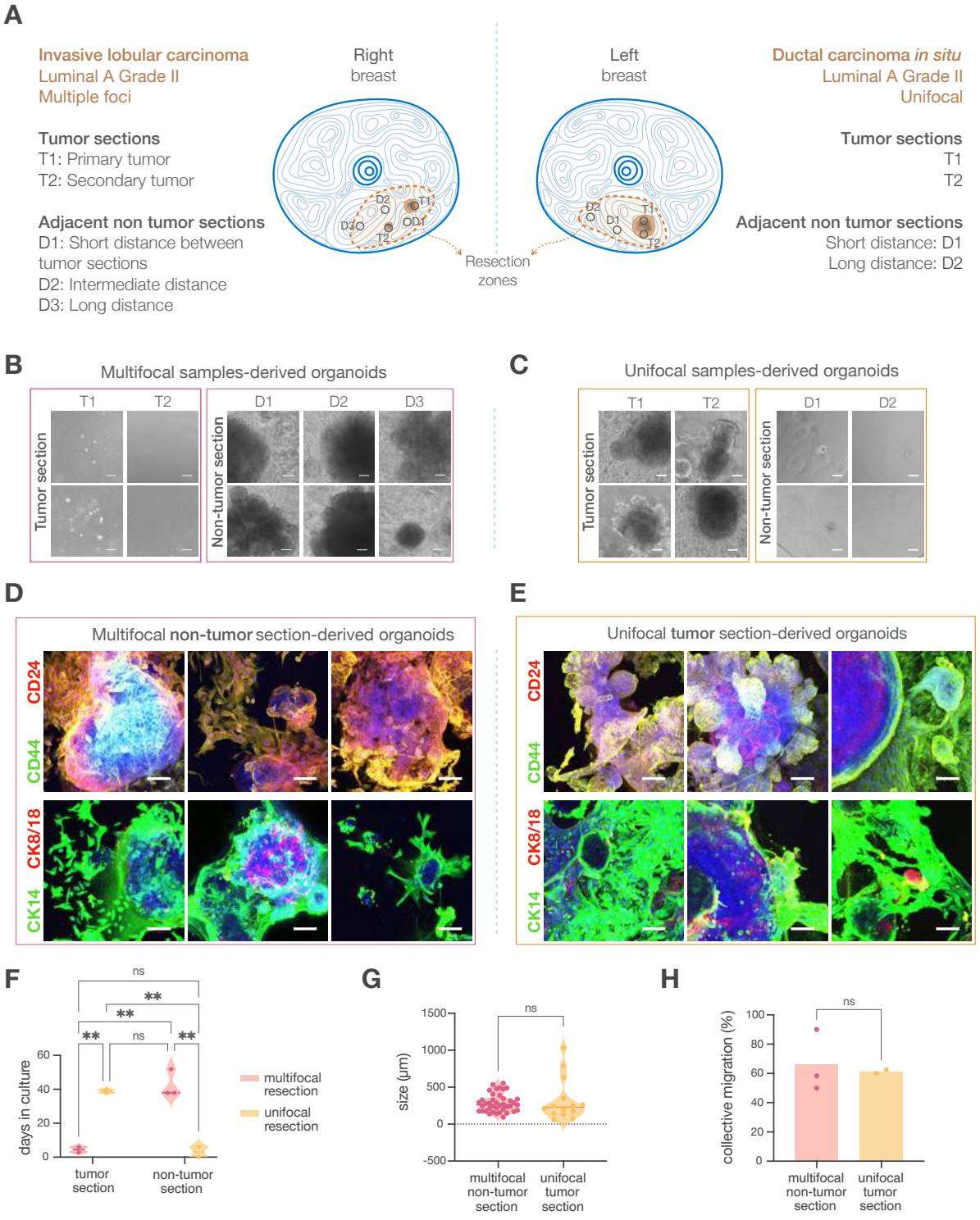

Figure D3. Tumor cell plasticity and local dissemination reflects intrinsic properties rather than patient-specific background effects. **A,** Schematic of mammary gland samples from a patient, with a unifocal tumor in the left breast and multiple tumor foci in the contralateral breast. **B,** Representative bright-field images of organoids from tumor (T1, T2) and adjacent non-tumor regions (D1–D3) of the right (multifocal) breast after 5 days in culture. Scale bar: 100 µm. **C,** Representative bright-field images of organoids from tumor (T1, T2) and adjacent non-tumor regions (D1, D2) of the left (unifocal) breast after 5 days in culture. Scale bar: 100 µm.

D-E, Representative immunofluorescence images of non-tumor organoids (multifocal, right breast, **D**) and tumor organoids (unifocal, left breast, **E**). Upper panels: CD24 CD44 (green), CD244 (red). Bottom panels: CK14 (green), CK8/18 (red). DAPI stains nuclei. Scale bar: 100 µm. **F**, Violin plot showing organoid viability duration for cultures derived from tumor and non-tumor regions of both mammary glands (**p < 0.01, Student's t-test). **G**, Organoid size (µm) measured at day 20 for cultures derived from unifocal tumor and multifocal non-tumor sections. No significant differences detected (Student's t-test). **H**, Percentage of organoids exhibiting collective migration at day 20 in cultures derived from unifocal tumor and multifocal non-tumor sections. No significant differences detected (Student's t-test).

In this Thesis, differentiation-based strategies are not conceived merely as a tool to suppress tumor proliferation, but as approaches that redefine tumor cell fate, shifting the balance away from stemness and toward functional commitment. Tumors behave as emergent systems, capable of shifting between cellular states as a result of their intrinsic adaptability. This dynamic behavior becomes evident in multicellular organoid models, where morphological transitions observed during differentiation —from granular to cystic structures— closely resemble the canonical ductal expansion that occurs during pubertal development of the mammary gland. In this process, an invasive front formed by cap cells advances, while apoptotic events among body cells beneath enable lumen formation, recapitulating features of terminal end buds [41].

Furthermore, another key factor contributing to the success of these two differentiation processes is that neither miR-203 nor cannabinoid-based interventions exert their effects through known canonical pathways. Instead, both appear to function as subtle modulators of cellular homeostasis, fine-tuning the balance of cell states rather than directly targeting known cancer drivers. This mode of action is particularly powerful, as it does not impose a strong selective pressure on tumor cells, which could otherwise promote adaptive resistance and relapse. Rather, it reshapes the equilibrium of plasticity itself, thereby limiting tumor adaptability, and ultimately reducing cellular heterogeneity.

Altogether, we demonstrate that modulation of CB_2R and activation of miR-203 constitute promising differentiation-based strategies, that could represent a future avenue for breast cancer treatment. These approaches reinforce the concept that differentiation therapies can effectively reshape tumor behavior, reveal hidden vulnerabilities, and complement conventional treatment strategies, understanding the tumor as a whole complex system.

Conclusions

Based on the data presented in this doctoral Thesis, the following conclusions can be drawn (**see Figure C1**):

- **CB_2R modulation induces differentiation of breast cancer cells.** Targeting CB_2R through low-dose, short-term treatment with THC or SR2 drives terminal differentiation of breast cancer stem cells into a luminal-like phenotype.
- **Fine-tuning CB_2R signaling irreversible reprograms cancer cell plasticity.** CB_2R-targeting strategies effectively prevent the reversible transition between CSCs and non-CSCs, thereby blocking a key mechanism of tumor plasticity and adaptability.
- **Cannabinoids function as reprogramming agents.** The results identify cannabinoids as powerful agents capable of inducing tumor cell reprogramming, overcoming mechanisms of adaptive resistance without relying on cytotoxicity, and sensitizing treatments for co-therapies with chemotherapy.
- **miR-203 enhances differentiation toward a luminal-like phenotype.** Transient expression of miR-203 reinforces luminal lineage commitment in breast cancer cells, promoting differentiation and reducing tumor aggressiveness.
- **miR-203 suppresses stemness and invasiveness.** By amplifying intrinsic differentiation programs, miR-203 limits stem-like features and invasiveness, steering tumor cells away from a plastic and aggressive state.
- **CB_2R and miR-203 share a common therapeutic outcome.** Despite their distinct molecular targets, both CB_2R modulation and miR-203 expression converge on a shared mechanism: the enforcement of luminal differentiation to reduce breast cancer cell plasticity.
- **CB_2R- and miR-203-mediated differentiation strategies stabilize tumor identity.** Rather than inducing tumor cell death, both strategies stabilize tumor cell identity, limiting the phenotypic shifts that contribute to heterogeneity and relapse.

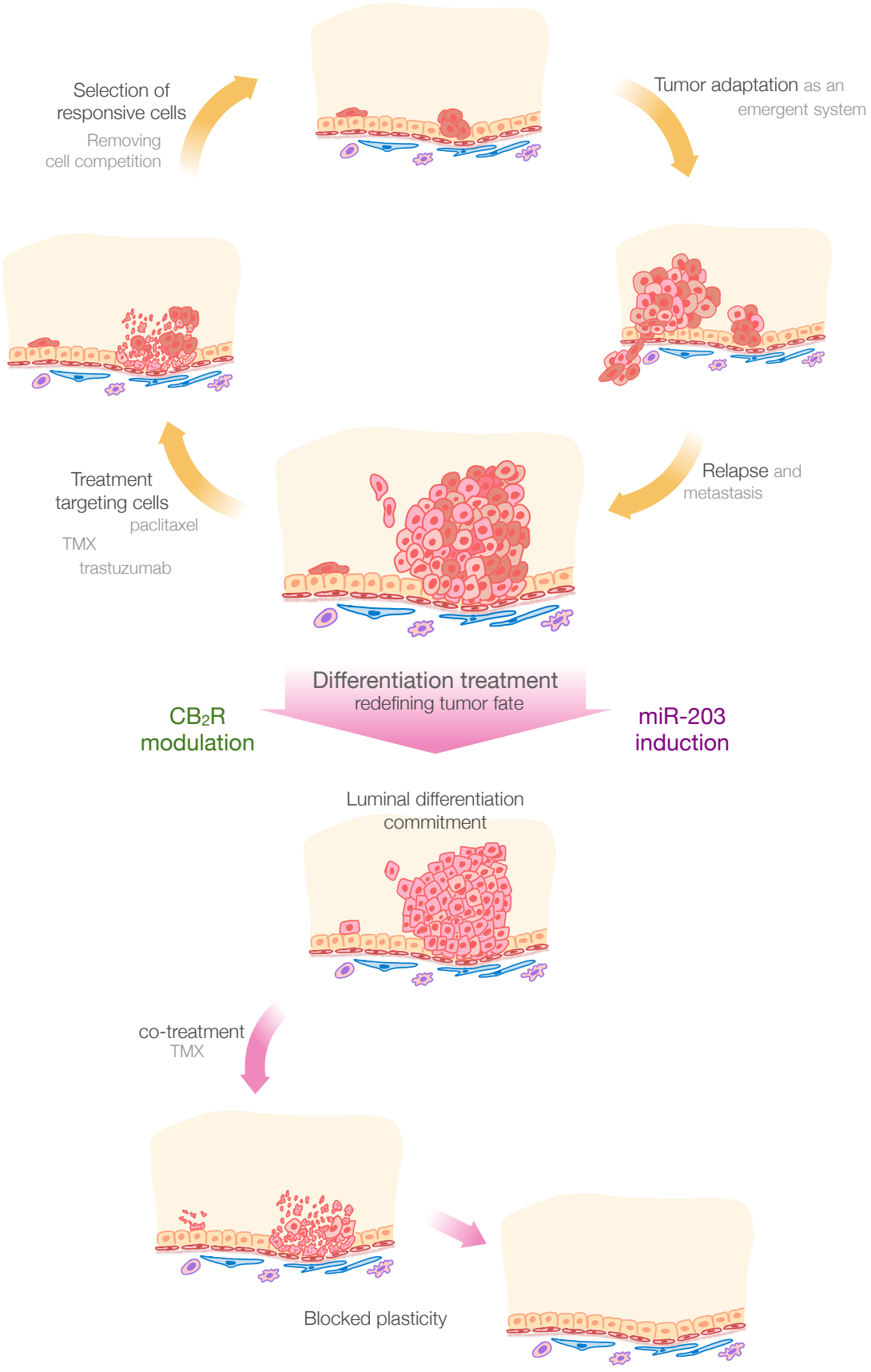
Selection of
responsive cells
Removing
cell competition
Tumor adaptation as an
emergent system
Treatment
targeting cells
paclitaxel
TMX
trastuzumab
Relapse and
metastasis
Differentiation treatment
redefining tumor fate
CB2R
modulation
miR-203
induction
Luminal differentiation
commitment
co-treatment
TMX
Blocked plasticity

Figure C1. Graphical representation of miR-203 and CB_2R modulation in the induction of tumor differentiation. Schematic overview of tumor evolution under different therapeutic pressures. Conventional targeted therapies —such as endocrine targeted tamoxifen (TMX), chemotherapy as paclitaxel or anti-HER2 as trastuzumab—, while effective at initial tumor reduction, often promote the selection of resistant clones, ultimately enabling tumor adaptation and relapse. In contrast, differentiation-based approaches, through modulation of CB_2R (via THC or SR2), or re-expression of miR-203, redirect tumor cells toward a stable luminal phenotype. This reprogramming reduces plasticity and stemness, and may act synergistically with existing therapies to enhance long-term tumor control and reduce recurrence.

Beyond the experimental conclusions, the results of this Thesis support a wider perspective on therapeutic strategies, leading to the following **concluding remarks**:

- **Targeting plasticity may prevent therapeutic resistance.** By constraining the adaptive transitions that drive resistance, CB_2R modulation and miR-203 represent promising tools to limit tumor evolution and improve treatment durability.

- **Reprogramming tumor cell states offers clinical potential.** These findings support a therapeutic paradigm shift: moving from direct cytotoxic agents to differentiation-inducing strategies that reprogram tumors with presumably fewer side effects and longer-lasting responses.

- **Differentiation-based therapies could mitigate intratumoral heterogeneity.** Enforcing a uniform, less aggressive phenotype through CB_2R or miR-203 may help overcome one of the major barriers to effective cancer therapy: the dynamic heterogeneity that fuels adaptation and relapse.

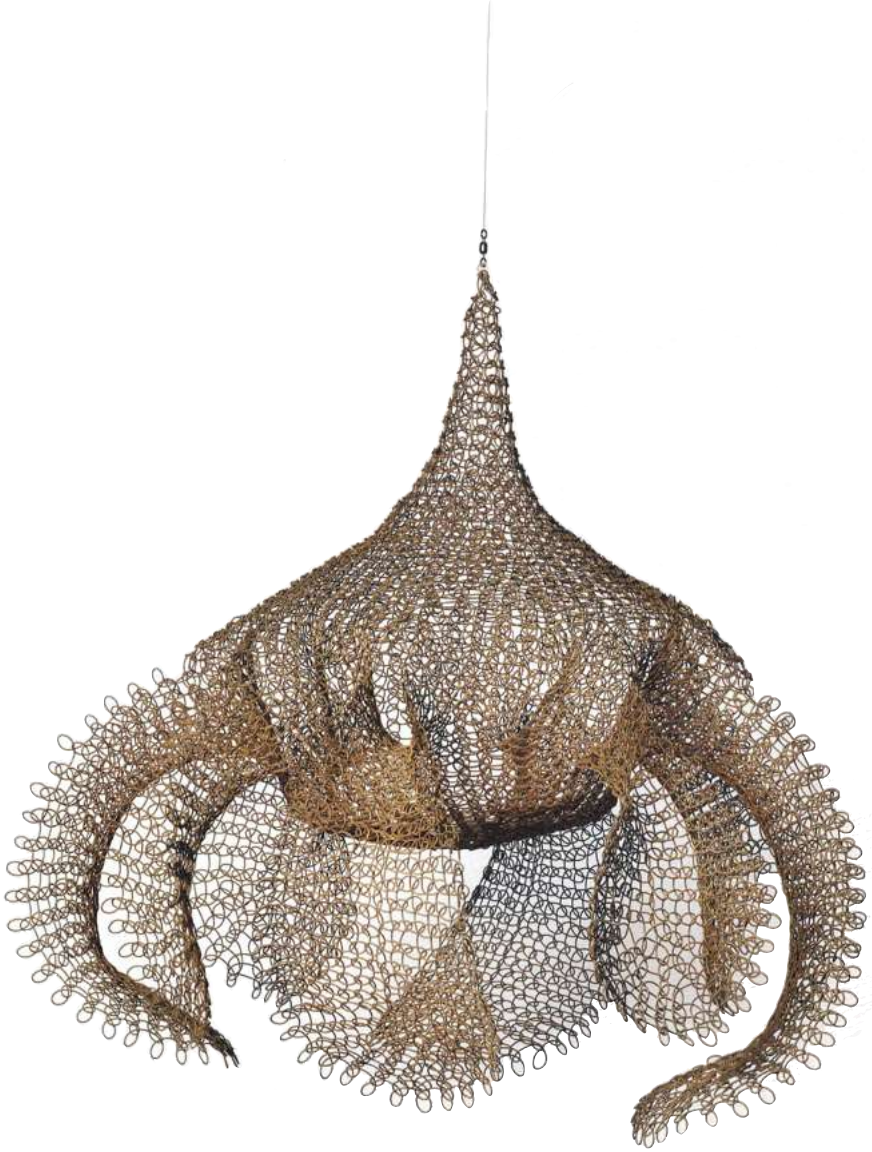

Bibliography

1. Nwosu, N. Cancer: A Disease of Modern Times? *Cureus* (2024) doi:10.7759/cureus.74666.
2. Siegel, R. L., Kratzer, T. B., Giaquinto, A. N., Sung, H. & Jemal, A. Cancer statistics, 2025. *CA Cancer J Clin* **75**, 10–45 (2025).
3. Duesberg, P. H. & Vogt, P. K. Differences between the Ribonucleic Acids of Transforming and Nontransforming Avian Tumor Viruses. *Proceedings of the National Academy of Sciences* **67**, 1673–1680 (1970).
4. Friend, S. H. *et al.* A human DNA segment with properties of the gene that predisposes to retinoblastoma and osteosarcoma. *Nature* **323**, 643–646 (1986).
5. Hanahan, D. & Weinberg, R. A. The Hallmarks of Cancer Review Evolve Progressively from Normalcy via a Series of Pre. Cell vol. 100 (2000).
6. Schmidt, A. & Weber, O. F. In Memoriam of Rudolf Virchow: A Historical Retrospective Including Aspects of Inflammation, Infection and Neoplasia. in *Infection and Inflammation: Impacts on Oncogenesis* 1–15 (KARGER, Basel, 2006). doi:10.1159/000092961.
7. Kalluri, R. & Zeisberg, M. Fibroblasts in cancer. *Nat Rev Cancer* **6**, 392–401 (2006).
8. Ribatti, D. Judah Folkman, a pioneer in the study of angiogenesis. *Angiogenesis* **11**, 3–10 (2008).
9. Hanahan, D. Hallmarks of Cancer: New Dimensions. *Cancer Discovery* vol. 12 31–46 Preprint at https://doi.org/10.1158/2159-8290.CD-21-1059 (2022).
10. Hanahan, D. & Weinberg, R. A. Hallmarks of cancer: The next generation. *Cell* vol. 144 646–674 Preprint at https://doi.org/10.1016/j.cell.2011.02.013 (2011).
11. Pérez-González, A., Bévant, K. & Blanpain, C. Cancer cell plasticity during tumor progression, metastasis and response to therapy. *Nature Cancer* vol. 4 1063–1082 Preprint at https://doi.org/10.1038/s43018-023-00595-y (2023).
12. Ordóñez-Morán, P., Dafflon, C., Imajo, M., Nishida, E. & Huelsken, J. HOXA5 Counteracts Stem Cell Traits by Inhibiting Wnt Signaling in Colorectal Cancer. *Cancer Cell* **28**, 815–829 (2015).
13. Perekatt, A. O. *et al.* SMAD4 suppresses WNt-driven dedifferentiation and oncogenesis in the differentiated gut epithelium. *Cancer Res* **78**, 4878–4890 (2018).
14. Shah, M. *et al.* A role for ATF2 in regulating MITF and melanoma development. *PLoS Genet* **6**, 1–21 (2010).
15. Saha, S. K. *et al.* Mutant IDH inhibits HNF-4α to block hepatocyte differentiation and promote biliary cancer. *Nature* **513**, 110–114 (2014).

16. Morris, J. P. *et al.* α-Ketoglutarate links p53 to cell fate during tumour suppression. *Nature* **573**, 595–599 (2019).

17. Kaufman, C. K. *et al.* A zebrafish melanoma model reveals emergence of neural crest identity during melanoma initiation. *Science (1979)* **351**, (2016).

18. Phan, T. G. & Croucher, P. I. The dormant cancer cell life cycle. *Nature Reviews Cancer* vol. 20 398–411 Preprint at https://doi.org/10.1038/s41568-020-0263-0 (2020).

19. Krah, N. M. *et al.* Prevention and Reversion of Pancreatic Tumorigenesis through a Differentiation-Based Mechanism. *Dev Cell* **50**, 744-754.e4 (2019).

20. Kopp, J. L. *et al.* Identification of Sox9-Dependent Acinar-to-Ductal Reprogramming as the Principal Mechanism for Initiation of Pancreatic Ductal Adenocarcinoma. *Cancer Cell* **22**, 737–750 (2012).

21. Mu, P. *et al.* SOX2 promotes lineage plasticity and antiandrogen resistance in TP53- and RB1-deficient prostate cancer. *Science (1979)* **355**, 84–88 (2017).

22. Von Hoff, D. D. *et al.* Inhibition of the Hedgehog Pathway in Advanced Basal-Cell Carcinoma. *New England Journal of Medicine* **361**, 1164–1172 (2009).

23. Chu, X. *et al.* Cancer stem cells: advances in knowledge and implications for cancer therapy. *Signal Transduct Target Ther* **9**, 170 (2024).

24. Bonnet, D. & Dick, E. Human Acute Myeloid Leukemia Is Organized as a Hierarchy That Originates from a Primitive Hematopoietic Cell. http://www.nature.com/naturemedicine (1997).

25. Al-Hajj, M., Wicha, M. S., Benito-Hernandez, A., Morrison, S. J. & Clarke, M. F. Prospective identification of tumorigenic breast cancer cells. *Proceedings of the National Academy of Sciences* **100**, 3983–3988 (2003).

26. Singh, S. K. *et al.* Identification of human brain tumour initiating cells. *Nature* **432**, 396–401 (2004).

27. O'Brien, C. A., Pollett, A., Gallinger, S. & Dick, J. E. A human colon cancer cell capable of initiating tumour growth in immunodeficient mice. *Nature* **445**, 106–110 (2007).

28. Li, C. *et al.* Identification of Pancreatic Cancer Stem Cells. *Cancer Res* **67**, 1030–1037 (2007).

29. Collins, A. T., Berry, P. A., Hyde, C., Stower, M. J. & Maitland, N. J. Prospective Identification of Tumorigenic Prostate Cancer Stem Cells. *Cancer Res* **65**, 10946–10951 (2005).

30. Taussig, D. C. *et al.* Anti-CD38 antibody-mediated clearance of human repopulating cells masks the heterogeneity of leukemia-initiating cells. (2008) doi:10.1182/blood-2008-10-118331.

31. Ginestier, C. *et al.* ALDH1 Is a Marker of Normal and Malignant Human Mammary Stem Cells and a Predictor of Poor Clinical Outcome. *Cell Stem Cell* **1**, 555–567 (2007).

32. Kreso, A. & Dick, J. E. Evolution of the cancer stem cell model. *Cell Stem Cell* vol. 14 275–291 Preprint at https://doi.org/10.1016/j.stem.2014.02.006 (2014).

33. Schepers, A. G. *et al.* Lineage tracing reveals Lgr5+ stem cell activity in mouse intestinal adenomas. *Science (1979)* **337**, 730–735 (2012).

34. Zomer, A. *et al.* Intravital Imaging of Cancer Stem Cell Plasticity in Mammary Tumors. *Stem Cells* **31**, 602–606 (2013).

35. Batlle, E. & Clevers, H. Cancer stem cells revisited. *Nature Medicine* vol. 23 1124–1134 Preprint at https://doi.org/10.1038/nm.4409 (2017).

36. Pellacani, D., Tan, S., Lefort, S. & Eaves, C. J. Transcriptional regulation of normal human mammary cell heterogeneity and its perturbation in breast cancer. *EMBO J* **38**, (2019).

37. Visvader, J. E. & Stingl, J. Mammary stem cells and the differentiation hierarchy: Current status and perspectives. *Genes and Development* vol. 28 1143–1158 Preprint at https://doi.org/10.1101/gad.242511.114 (2014).

38. Brownfield, D. G. *et al.* Patterned collagen fibers orient branching mammary epithelium through distinct signaling modules. *Current Biology* **23**, 703–709 (2013).

39. Avagliano, A. *et al.* Influence of fibroblasts on mammary gland development, breast cancer microenvironment remodeling, and cancer cell dissemination. *Cancers* vol. 12 1–35 Preprint at https://doi.org/10.3390/cancers12061697 (2020).

40. Howard, B. A. & Lu, P. Stromal regulation of embryonic and postnatal mammary epithelial development and differentiation. *Seminars in Cell and Developmental Biology* vols 25–26 43–51 Preprint at https://doi.org/10.1016/j.semcdb.2014.01.004 (2014).

41. Fu, N. Y., Nolan, E., Lindeman, G. J. & Visvader, J. E. Stem cells and the differentiation hierarchy in mammary gland development. *Physiol Rev* **100**, 489–523 (2020).

42. Inman, J. L., Robertson, C., Mott, J. D. & Bissell, M. J. Mammary gland development: Cell fate specification, stem cells and the microenvironment. *Development (Cambridge)* vol. 142 1028–1042 Preprint at https://doi.org/10.1242/dev.087643 (2015).

43. Spina, E. & Cowin, P. Embryonic mammary gland development. *Seminars in Cell and Developmental Biology* vol. 114 83–92 Preprint at https://doi.org/10.1016/j.semcdb.2020.12.012 (2021).

44. Watson, C. J. & Khaled, W. T. Mammary development in the embryo and adult: A journey of morphogenesis and commitment. *Development* vol. 135 995–1003 Preprint at https://doi.org/10.1242/dev.005439 (2008).

45. Anderson, S. M., Rudolph, M. C., McManaman, J. L. & Neville, M. C. Key stages in mammary gland development. Secretory activation in the mammary gland: It's not just about milk protein synthesis! *Breast Cancer Research* vol. 9 Preprint at https://doi.org/10.1186/bcr1653 (2007).

46. De Ome, K. B., Faulkin, L. J., Bern, H. A. & Blair, P. B. Development of mammary tumors from hyperplastic alveolar nodules transplanted into gland-free mammary fat pads of female C3H mice. *Cancer Res* **19**, 515–20 (1959).

47. Smith, G. H. & Medina, D. A Morphologically Distinct Candidate for an Epithelial Stem Cell in Mouse Mammary Gland. (1988).

48. Young, L. J. T., Medina, D., DeOme, K. B. & Daniel, C. W. The influence of host and tissue age on life span and growth rate of serially transplanted mouse mammary gland. *Exp Gerontol* **6**, 49–56 (1971).

49. Dos Santos, C. O. *et al.* Molecular hierarchy of mammary differentiation yields refined markers of mammary stem cells. *Proc Natl Acad Sci U S A* **110**, 7123–7130 (2013).

50. Raouf, A. *et al.* Transcriptome analysis of the normal human mammary cell commitment and differentiation process. *Cell Stem Cell* **3**, 109–118 (2008).

51. van Amerongen, R., Bowman, A. N. & Nusse, R. Developmental Stage and Time Dictate the Fate of Wnt/β-Catenin-Responsive Stem Cells in the Mammary Gland. *Cell Stem Cell* **11**, 387–400 (2012).

52. Stingl, J. *et al.* Purification and unique properties of mammary epithelial stem cells. *Nature* **439**, 993–997 (2006).

53. Plaks, V. *et al.* Lgr5-expressing cells are sufficient and necessary for postnatal mammary gland organogenesis. *Cell Rep* **3**, 70–8 (2013).

54. Anstine, L. J. & Keri, R. A new view of the mammary epithelial hierarchy and its implications for breast cancer initiation and metastasis. *Journal of Cancer Metastasis and Treatment* vol. 5 Preprint at https://doi.org/10.20517/2394-4722.2019.24 (2019).

55. Kim, J. *et al.* Global patterns and trends in breast cancer incidence and mortality across 185 countries. *Nat Med* **31**, 1154–1162 (2025).

56. Yousefnia, S. Breast Cancer, Subtypes, Risk Factors, and Treatment. in *The Palgrave Encyclopedia of Disability* 1–14 (Springer Nature Switzerland, 2024). doi:10.1007/978-3-031-40858-8_324-1.

57. Nascimento, R. G. do & Otoni, K. M. Histological and molecular classification of breast cancer: what do we know? *Mastology* **30**, (2020).

58. Avera, E., Valentic, L. & Bui, L. Current understanding and distinct features of multifocal and multicentric breast cancers. *Cancer Reports* vol. 6 Preprint at https://doi.org/10.1002/cnr2.1851 (2023).

59. Neri, A. *et al.* Clinical significance of multifocal and multicentric breast cancers and choice of surgical treatment: A retrospective study on a series of 1158 cases. *BMC Surg* **15**, (2015).

60. Gentilini, O. *et al.* Conservative surgery in patients with multifocal/multicentric breast cancer. *Breast Cancer Res Treat* **113**, 577–583 (2009).

61. Kaplan, J. *et al.* Breast conservation in patients with multiple ipsilateral synchronous cancers. *J Am Coll Surg* **197**, 726–729 (2003).

62. Tan, M. P., Sitoh, N. Y. & Sitoh, Y. Y. Optimising Breast Conservation Treatment for Multifocal and Multicentric Breast Cancer: A Worthwhile Endeavour? *World J Surg* **40**, 315–322 (2016).

63. Harbeck, N. *et al.* Breast cancer. *Nat Rev Dis Primers* **5**, (2019).

64. Perou, C. M. *et al.* Molecular portraits of human breast tumours. *Nature* **406**, 747–752 (2000).

65. Sørlie, T. *et al.* Gene expression patterns of breast carcinomas distinguish tumor subclasses with clinical implications. *Proceedings of the National Academy of Sciences* **98**, 10869–10874 (2001).

66. Jardé, T. *et al.* Wnt and Neuregulin1/ErbB signalling extends 3D culture of hormone responsive mammary organoids. *Nat Commun* **7**, (2016).

67. Jamieson, P. R. *et al.* Derivation of a robust mouse mammary organoid system for studying tissue dynamics. *Development (Cambridge)* **144**, 1065–1071 (2017).

68. Jozwik, K. M., Chernukhin, I., Serandour, A. A., Nagarajan, S. & Carroll, J. S. FOXA1 Directs H3K4 Monomethylation at Enhancers via Recruitment of the Methyltransferase MLL3. *Cell Rep* **17**, 2715–2723 (2016).

69. Michalak, E. M. & Visvader, J. E. Dysregulation of histone methyltransferases in breast cancer – Opportunities for new targeted therapies? *Molecular Oncology* vol. 10 1497 Preprint at https://doi.org/10.1016/j.molonc.2016.09.003 (2016).

70. Zhang, Z. *et al.* Mammary-Stem-Cell-Based Somatic Mouse Models Reveal Breast Cancer Drivers Causing Cell Fate Dysregulation. *Cell Rep* **16**, 3146–3156 (2016).

71. Kamalakaran, S. *et al.* DNA methylation patterns in luminal breast cancers differ from non-luminal subtypes and can identify relapse risk independent of other clinical variables. *Mol Oncol* **5**, 77–92 (2011).

72. Wang, X. *et al.* Overcoming cancer treatment resistance: Unraveling the role of cancer-associated fibroblasts. *Journal of the National Cancer Center* Preprint at https://doi.org/10.1016/j.jncc.2025.03.002 (2025).

73. Peng, D. *et al.* Myeloid-derived suppressor cells endow stem-like qualities to breast cancer cells through IL6/STAT3 and NO/NOTCH cross-talk signaling. *Cancer Res* **76**, 3156–3165 (2016).

74. Jin, H., Meng, X. & Feng, J. Mechanisms of tumor-associated macrophages in breast cancer and treatment strategy. *Front Immunol* **16**, (2025).

75. Taurin, S. & Alkhalifa, H. Breast cancers, mammary stem cells, and cancer stem cells, characteristics, and hypotheses. *Neoplasia (United States)* vol. 22 663–678 Preprint at https://doi.org/10.1016/j.neo.2020.09.009 (2020).

76. Song, K. & Farzaneh, M. Signaling pathways governing breast cancer stem cells behavior. *Stem Cell Research and Therapy* vol. 12 Preprint at https://doi.org/10.1186/s13287-021-02321-w (2021).

77. Ordaz-Ramos, A., Tellez-Jimenez, O. & Vazquez-Santillan, K. Signaling pathways governing the maintenance of breast cancer stem cells and their therapeutic implications. *Frontiers in Cell and Developmental Biology* vol. 11 Preprint at https://doi.org/10.3389/fcell.2023.1221175 (2023).

78. Regua, A. T., Arrigo, A., Doheny, D., Wong, G. L. & Lo, H. W. Transgenic mouse models of breast cancer. *Cancer Lett* **516**, 73–83 (2021).

79. Murayama, T. & Gotoh, N. Patient-Derived Xenograft Models of Breast Cancer and Their Application. *Cells* **8**, 621 (2019).

80. Ciringione, A. & Rizzi, F. Facing the Challenge to Mimic Breast Cancer Heterogeneity: Established and Emerging Experimental Preclinical Models Integrated with Omics Technologies. *Int J Mol Sci* **26**, 4572 (2025).

81. Nilsson, B. Probable in vivo induction of differentiation by retinoic acid of promyelocytes in acute promyelocytic leukaemia. *Br J Haematol* **57**, 365–371 (1984).

82. De Thé, H. Differentiation therapy revisited. *Nature Reviews Cancer* vol. 18 117–127 Preprint at https://doi.org/10.1038/nrc.2017.103 (2018).

83. Zhu, K. *et al.* Characterization and therapeutic perspectives of differentiation-inducing therapy in malignant tumors. *Frontiers in Genetics* vol. 14 Preprint at https://doi.org/10.3389/fgene.2023.1271381 (2023).

84. Abemayor, E., Changb, B., Sidellb, N. & Sidell, N. Effects of Retinoic Acid on the in Vivo Growth of Human Neuroblastoma Cells. Cancer Letters vol. 55 (1990).

85. Wang, C. *et al.* Alternative approaches to target Myc for cancer treatment. *Signal Transduct Target Ther* **6**, 117 (2021).

86. Ji, H. *et al.* HDAC3 Deficiency Promotes Liver Cancer through a Defect in H3K9ac/H3K9me3 Transition. *Cancer Res* **79**, 3676–3688 (2019).

87. Salmon, J. M. *et al.* Epigenetic Activation of Plasmacytoid DCs Drives IFNAR-Dependent Therapeutic Differentiation of AML. *Cancer Discov* **12**, 1560–1579 (2022).

88. Mody, D., Bouckaert, J., Savvides, S. N. & Gupta, V. Rational Design and Development of HDAC Inhibitors for Breast Cancer Treatment. *Curr Pharm Des* **27**, 4610–4629 (2021).

89. Rettig, I. *et al.* Selective inhibition of HDAC8 decreases neuroblastoma growth in vitro and in vivo and enhances retinoic acid-mediated differentiation. *Cell Death Dis* **6**, e1657–e1657 (2015).

90. Naveen, C. R., Gaikwad, S. & Agrawal-Rajput, R. Berberine induces neuronal differentiation through inhibition of cancer stemness and epithelial-mesenchymal transition in neuroblastoma cells. *Phytomedicine* **23**, 736–744 (2016).

91. Matsuda, L. A., Lolait, S. J., Brownstein, M. J., Young, A. C. & Bonner, T. I. Structure of a cannabinoid receptor and functional expression of the cloned cDNA. *Nature* **346**, 561–564 (1990).

92. Wood, T. B., Spivey, W. T. N. & Easterfield, T. H. III.—Cannabinol. Part I. *J. Chem. Soc., Trans.* **75**, 20–36 (1899).

93. Gaoni, Y. & Mechoulam, R. Isolation, Structure, and Partial Synthesis of an Active Constituent of Hashish. *J Am Chem Soc* **86**, 1646–1647 (1964).

94. Munro, S., Thomas, K. L. & Abu-Shaar, M. Molecular characterization of a peripheral receptor for cannabinoids. *Nature* **365**, 61–65 (1993).

95. Devane, W. A. *et al.* Isolation and Structure of a Brain Constituent That Binds to the Cannabinoid Receptor. *Science (1979)* **258**, 1946–1949 (1992).

96. Mechoulam, R. *et al.* Identification of an endogenous 2-monoglyceride, present in canine gut, that binds to cannabinoid receptors. *Biochem Pharmacol* **50**, 83–90 (1995).

97. Pacher, P., Bátkai, S. & Kunos, G. The endocannabinoid system as an emerging target of pharmacotherapy. *Pharmacological Reviews* vol. 58 389–462 Preprint at https://doi.org/10.1124/pr.58.3.2 (2006).

98. Pacher, P., Kogan, N. M. & Mechoulam, R. Beyond THC and Endocannabinoids. *Annu Rev Pharmacol Toxicol* **60**, 637–659 (2020).

99. Solymosi, K. & Kofalvi, A. Cannabis: A Treasure Trove or Pandora's Box? *Mini-Reviews in Medicinal Chemistry* **17**, (2016).

100. Lu, H. C. & MacKie, K. An introduction to the endogenous cannabinoid system. *Biological Psychiatry* vol. 79 516–525 Preprint at https://doi.org/10.1016/j.biopsych.2015.07.028 (2016).

101. Pacher, P. & Mechoulam, R. Is lipid signaling through cannabinoid 2 receptors part of a protective system? *Progress in Lipid Research* vol. 50 193–211 Preprint at https://doi.org/10.1016/j.plipres.2011.01.001 (2011).

102. Lu, H.-C. & Mackie, K. Review of the Endocannabinoid System. *Biol Psychiatry Cogn Neurosci Neuroimaging* **6**, 607–615 (2021).

103. Mechoulam, R., Hanuš, L. O., Pertwee, R. & Howlett, A. C. Early phytocannabinoid chemistry to endocannabinoids and beyond. *Nature Reviews Neuroscience* vol. 15 757–764 Preprint at https://doi.org/10.1038/nrn3811 (2014).

104. Blebea, N. M., Pricopie, A. I., Vlad, R. A. & Hancu, G. Phytocannabinoids: Exploring Pharmacological Profiles and Their Impact on Therapeutical Use. *International Journal of Molecular Sciences* vol. 25 Preprint at https://doi.org/10.3390/ijms25084204 (2024).

105. Di Marzo, V. & Piscitelli, F. The Endocannabinoid System and its Modulation by Phytocannabinoids. *Neurotherapeutics* vol. 12 692–698 Preprint at https://doi.org/10.1007/s13311-015-0374-6 (2015).

106. Ben-Shabat, S. et al. An Entourage Effect: Inactive Endogenous Fatty Acid Glycerol Esters Enhance 2-Arachidonoyl-Glycerol Cannabinoid Activity. European Journal of Pharmacology vol. 353 (1998).

107. Blasco-Benito, S. *et al.* Appraising the "entourage effect": Antitumor action of a pure cannabinoid versus a botanical drug preparation in preclinical models of breast cancer. *Biochem Pharmacol* **157**, 285–293 (2018).

108. Whiting, Z. M., Yin, J., de la Harpe, S. M., Vernall, A. J. & Grimsey, N. L. Developing the Cannabinoid Receptor 2 (CB2) pharmacopoeia: past, present, and future. *Trends in*

Pharmacological Sciences vol. 43 754–771 Preprint at https://doi.org/10.1016/j.tips.2022.06.010 (2022).

109. Shahbazi, F., Grandi, V., Banerjee, A. & Trant, J. F. iScience Cannabinoids and Cannabinoid Receptors: The Story so Far. *iScience* **23**, 101301 (2020).
110. Randall, M. D. Endocannabinoids and the haematological system. *British Journal of Pharmacology* vol. 152 671–675 Preprint at https://doi.org/10.1038/sj.bjp.0707420 (2007).
111. Jiang, S. *et al.* Cannabinoid receptor 2 and its agonists mediate hematopoiesis and hematopoietic stem and progenitor cell mobilization. (2011) doi:10.1182/blood-2010-01.
112. Zimmermann, T. *et al.* Neural stem cell lineage-specific cannabinoid type-1 receptor regulates neurogenesis and plasticity in the adult mouse hippocampus. *Cerebral Cortex* **28**, 4454–4471 (2018).
113. Compagnucci, C. *et al.* Type-1 (CB1) Cannabinoid Receptor Promotes Neuronal Differentiation and Maturation of Neural Stem Cells. *PLoS One* **8**, (2013).
114. Molina-Holgado, F. *et al.* CB2 cannabinoid receptors promote mouse neural stem cell proliferation. *European Journal of Neuroscience* **25**, 629–634 (2007).
115. Palazuelos, J., Ortega, Z., Díaz-Alonso, J., Guzmán, M. & Galve-Roperh, I. CB 2 cannabinoid receptors promote neural progenitor cell proliferation via mTORC1 signaling. *Journal of Biological Chemistry* **287**, 1198–1209 (2012).
116. Aguado, T. *et al.* The endocannabinoid system drives neural progenitor proliferation. *The FASEB Journal* **19**, 1704–1706 (2005).
117. Galve-Roperh, I. *et al.* Cannabinoid receptor signaling in progenitor/stem cell proliferation and differentiation. *Progress in Lipid Research* vol. 52 633–650 Preprint at https://doi.org/10.1016/j.plipres.2013.05.004 (2013).
118. Tundidor, I. *et al.* Fatty acid amide hydrolase drives adult mammary gland development by promoting luminal cell differentiation. *Cell Death Discov* **10**, 12 (2024).
119. Kovalchuk, O. & Kovalchuk, I. Cannabinoids as anticancer therapeutic agents. *Cell Cycle* vol. 19 961–989 Preprint at https://doi.org/10.1080/15384101.2020.1742952 (2020).
120. Caffarel, M. M., Sarrió, D., Palacios, J., Guzmán, M. & Sánchez, C. Δ9-tetrahydrocannabinol inhibits cell cycle progression in human breast cancer cells through Cdc2 regulation. *Cancer Res* **66**, 6615–6621 (2006).
121. Pérez-Gómez, E. *et al.* Role of cannabinoid receptor CB2 in HER2 pro-oncogenic signaling in breast cancer. *J Natl Cancer Inst* **107**, (2015).

122. Caffarel, M. M. *et al.* Cannabinoids reduce ErbB2-driven breast cancer progression through Akt inhibition. *Mol Cancer* **9**, 196 (2010).

123. Blasco-Benito, S. *et al.* Therapeutic targeting of HER2–CB2R heteromers in HER2-positive breast cancer. *Proceedings of the National Academy of Sciences* **116**, 3863–3872 (2019).

124. De Petrocellis, L. *et al.* The endogenous cannabinoid anandamide inhibits human breast cancer cell proliferation. *Proceedings of the National Academy of Sciences* **95**, 8375–8380 (1998).

125. Qamri, Z. *et al.* Synthetic cannabinoid receptor agonists inhibit tumor growth and metastasis of breast cancer. *Mol Cancer Ther* **8**, 3117–3129 (2009).

126. Laezza, C., Simona Pisanti, Crescenzi, E. & Bifulco, M. Anandamide inhibits Cdk2 and activates Chk1 leading to cell cycle arrest in human breast cancer cells. *FEBS Lett* **580**, 6076–6082 (2006).

127. Hanlon, K. *et al.* Modulation of breast cancer cell viability by a cannabinoid receptor 2 agonist, JWH-015, is calcium dependent. *Breast Cancer: Targets and Therapy* 59 (2016) doi:10.2147/BCTT.S100393.

128. Laezza, C. *et al.* Anandamide inhibits the Wnt/β-catenin signalling pathway in human breast cancer MDA MB 231 cells. *Eur J Cancer* **48**, 3112–3122 (2012).

129. Nasser, M. W. *et al.* Crosstalk between Chemokine Receptor CXCR4 and Cannabinoid Receptor CB2 in Modulating Breast Cancer Growth and Invasion. *PLoS One* **6**, e23901 (2011).

130. Grimaldi, C. *et al.* Anandamide inhibits adhesion and migration of breast cancer cells. *Exp Cell Res* **312**, 363–373 (2006).

131. Coke, C. J. *et al.* Simultaneous Activation of Induced Heterodimerization between CXCR4 Chemokine Receptor and Cannabinoid Receptor 2 (CB2) Reveals a Mechanism for Regulation of Tumor Progression. *Journal of Biological Chemistry* **291**, 9991–10005 (2016).

132. Elbaz, M., Ahirwar, D., Ravi, J., Nasser, M. W. & Ganju, R. K. Novel role of cannabinoid receptor 2 in inhibiting EGF/EGFR and IGF-I/IGF-IR pathways in breast cancer. *Oncotarget* **8**, 29668–29678 (2017).

133. Picardi, P., Ciaglia, E., Proto, M. & Pisanti, S. Anandamide inhibits breast tumor-induced angiogenesis. *Transl Med UniSa* **10**, 8–12 (2014).

134. Singer, E. *et al.* Reactive oxygen species-mediated therapeutic response and resistance in glioblastoma. *Cell Death Dis* **6**, (2015).

135. Aguado, T. *et al.* Cannabinoids induce glioma stem-like cell differentiation and inhibit gliomagenesis. *Journal of Biological Chemistry* **282**, 6854–6862 (2007).

136. Bhaskaran, M. & Mohan, M. MicroRNAs: History, Biogenesis, and Their Evolving Role in Animal Development and Disease. *Vet Pathol* **51**, 759–774 (2014).

137. Saliminejad, K., Khorram Khorshid, H. R., Soleymani Fard, S. & Ghaffari, S. H. An overview of microRNAs: Biology, functions, therapeutics, and analysis methods. *Journal of Cellular Physiology* vol. 234 5451–5465 Preprint at https://doi.org/10.1002/jcp.27486 (2019).

138. Lee, R. C., Feinbaum, R. L. & Ambrost, V. The C. Elegans Heterochronic Gene Lin-4 Encodes Small RNAs with Antisense Complementarity to &II-14. Cell vol. 75 (1993).

139. Pasquinelli, A. E. *et al.* Conservation of the sequence and temporal expression of let-7 heterochronic regulatory RNA. *Nature* **408**, 86–89 (2000).

140. Vidigal, J. A. & Ventura, A. The biological functions of miRNAs: Lessons from in vivo studies. *Trends in Cell Biology* vol. 25 137–147 Preprint at https://doi.org/10.1016/j.tcb.2014.11.004 (2015).

141. Wu, D., Thompson, L. U. & Comelli, E. M. MicroRNAs: A Link between Mammary Gland Development and Breast Cancer. *International Journal of Molecular Sciences* vol. 23 Preprint at https://doi.org/10.3390/ijms232415978 (2022).

142. Muñoz, J. P., Pérez-Moreno, P., Pérez, Y. & Calaf, G. M. The Role of MicroRNAs in Breast Cancer and the Challenges of Their Clinical Application. *Diagnostics* vol. 13 Preprint at https://doi.org/10.3390/diagnostics13193072 (2023).

143. Park, J., Kim, M. E. & Lee, J. S. MicroRNAs: Novel clinical biomarkers for cancer radiotherapy (Review). *Molecular Medicine Reports* vol. 32 Preprint at https://doi.org/10.3892/mmr.2025.13619 (2025).

144. Peng, Y. & Croce, C. M. The role of microRNAs in human cancer. *Signal Transduction and Targeted Therapy* vol. 1 Preprint at https://doi.org/10.1038/sigtrans.2015.4 (2016).

145. Yi, R., Poy, M. N., Stoffel, M. & Fuchs, E. A skin microRNA promotes differentiation by repressing 'stemness'. *Nature* **452**, 225–229 (2008).

146. Tavazoie, S. F. *et al.* Endogenous human microRNAs that suppress breast cancer metastasis. *Nature* **451**, 147–152 (2008).

147. Salazar-Roa, M. *et al.* Transient exposure to miR-203 enhances the differentiation capacity of established pluripotent stem cells. *EMBO J* **39**, (2020).

148. DeCastro, A. J. *et al.* MiR203 mediates subversion of stem cell properties during mammary epithelial differentiation via repression of ΔnP63α and promotes mesenchymal-to-epithelial transition. *Cell Death Dis* **4**, (2013).

149. Zhang, W., Liu, J., Wu, Q., Liu, Y. & Ma, C. HOTAIR Contributes to Stemness Acquisition of Cervical Cancer through Regulating miR-203 Interaction with ZEB1 on Epithelial-Mesenchymal Transition. *J Oncol* **2021**, (2021).

150. Lai, H. T., Tseng, W. K., Huang, S. W., Chao, T. C. & Su, Y. MicroRNA-203 diminishes the stemness of human colon cancer cells by suppressing GATA6 expression. *J Cell Physiol* **235**, 2866–2880 (2020).

151. Ju, S. Y., Chiou, S. H. & Su, Y. Maintenance of the stemness in CD44+ HCT-15 and HCT-116 human colon cancer cells requires miR-203 suppression. *Stem Cell Res* **12**, 86–100 (2014).

152. Dasgupta, P. *et al.* MicroRNA-203 inhibits long noncoding RNA hotair and regulates tumorigenesis through epithelial-to-mesenchymal transition pathway in renal cell carcinoma. *Mol Cancer Ther* **17**, 1061–1069 (2018).

153. Jiang, Q. *et al.* A directly negative interaction of miR-203 and ZEB2 modulates tumor stemness and chemotherapy resistance in nasopharyngeal carcinoma. *Oncotarget* **7**, 67288–67301 (2016).

154. Tian, X., Tao, F., Zhang, B., Dong, J. T. & Zhang, Z. The miR-203/SNAI2 axis regulates prostate tumor growth, migration, angiogenesis and stemness potentially by modulating GSK-3β/β-CATENIN signal pathway. *IUBMB Life* **70**, 224–236 (2018).

155. Bueno, M. J. *et al.* Genetic and Epigenetic Silencing of MicroRNA-203 Enhances ABL1 and BCR-ABL1 Oncogene Expression. *Cancer Cell* **13**, 496–506 (2008).

156. Zhao, S. *et al.* MicroRNA-203 regulates growth and metastasis of breast cancer. *Cellular Physiology and Biochemistry* **37**, 35–42 (2015).

157. Taube, J. H. *et al.* Epigenetic silencing of microRNA-203 is required for EMT and cancer stem cell properties. *Sci Rep* **3**, (2013).

158. Song, S. *et al.* Nanoliposomal delivery of microrna-203 suppresses migration of triple-negative breast cancer through distinct target suppression. *Noncoding RNA* **7**, (2021).

159. Salem, S. & Mosaad, R. Crosstalk between miR-203 and PKCθ regulates breast cancer stem cell markers. *Ann Hum Genet* **85**, 105–114 (2021).

160. Maglione, J. E. *et al.* Transgenic Polyoma middle-T mice model premalignant mammary disease. *Cancer Res* **61**, 8298–305 (2001).

161. Lin, E. Y. *et al.* Progression to Malignancy in the Polyoma Middle T Oncoprotein Mouse Breast Cancer Model Provides a Reliable Model for Human Diseases. *American Journal of Pathology* **163**, 2113–2126 (2003).

162. Guy, C. T. et al. Expression of the Neu Protooncogene in the Mammary Epithelium of Transgenic Mice Induces Metastatic Disease. Genetics vol. 89 https://www.pnas.org (1992).

163. Sachs, N. *et al.* A Living Biobank of Breast Cancer Organoids Captures Disease Heterogeneity. *Cell* **172**, 373-386.e10 (2018).

164. Clevers, H. Modeling Development and Disease with Organoids. *Cell* vol. 165 1586–1597 Preprint at https://doi.org/10.1016/j.cell.2016.05.082 (2016).

165. Fowler, E. E., Sellers, T. A., Lu, B. & Heine, J. J. Breast Imaging Reporting and Data System (BI-RADS) breast composition descriptors: Automated measurement development for full field digital mammography. *Med Phys* **40**, (2013).

166. Primac, I. *et al.* Stromal integrin α11 regulates PDGFRβ signaling and promotes breast cancer progression. *Journal of Clinical Investigation* **129**, 4609–4628 (2019).

167. Sharon, Y., Alon, L., Glanz, S., Servais, C. & Erez, N. Isolation of normal and cancer-associated fibroblasts from fresh tissues by fluorescence activated cell sorting (FACS). *Journal of Visualized Experiments* (2013) doi:10.3791/4425.

168. Salazar-Martín, A. G. *et al.* Single-Cell RNA Sequencing Reveals That Adaptation of Human Aortic Endothelial Cells to Antiproliferative Therapies Is Modulated by Flow-Induced Shear Stress. *Arterioscler Thromb Vasc Biol* **43**, 2265–2281 (2023).

169. Hinz, B. & Ramer, R. Cannabinoids as anticancer drugs: current status of preclinical research. *British Journal of Cancer* vol. 127 1–13 Preprint at https://doi.org/10.1038/s41416-022-01727-4 (2022).

170. Willyard, C. Cancer therapy: an evolved approach. *Nature* 166–168 (2016).

171. Rosenbluth, J. M. *et al.* Organoid cultures from normal and cancer-prone human breast tissues preserve complex epithelial lineages. *Nat Commun* **11**, (2020).

172. Cheung, K. J. *et al.* Polyclonal breast cancer metastases arise from collective dissemination of keratin 14-expressing tumor cell clusters. *Proc Natl Acad Sci U S A* **113**, E854–E863 (2016).

173. Fares, J., Fares, M. Y., Khachfe, H. H., Salhab, H. A. & Fares, Y. Molecular principles of metastasis: a hallmark of cancer revisited. *Signal Transduction and Targeted Therapy* vol. 5 Preprint at https://doi.org/10.1038/s41392-020-0134-x (2020).

174. Raz, N. *et al.* Selected cannabis terpenes synergize with THC to produce increased CB1 receptor activation. *Biochem Pharmacol* **212**, (2023).

175. LaVigne, J. E., Hecksel, R., Keresztes, A. & Streicher, J. M. Cannabis sativa terpenes are cannabimimetic and selectively enhance cannabinoid activity. *Sci Rep* **11**, (2021).

176. Nishimoto, M., Fukushima, A., Okuda, A. & Muramatsu, M. The Gene for the Embryonic Stem Cell Coactivator UTF1 Carries a Regulatory Element Which Selectively Interacts with a Complex Composed of Oct-3/4 and Sox-2. MOLECULAR AND CELLULAR BIOLOGY vol. 19 (1999).

177. Sugimoto, K. *et al.* The Tight-Junction Protein Claudin-6 Induces Epithelial Differentiation from Mouse F9 and Embryonic Stem Cells. *PLoS One* **8**, (2013).

178. Ghosh, A. *et al.* The GATA transcriptional program dictates cell fate equilibrium to establish the maternal-fetal exchange interface and fetal development. *Proc Natl Acad Sci U S A* **121**, (2024).

179. Habashy, H. O. *et al.* Forkhead-box A1 (FOXA1) expression in breast cancer and its prognostic significance. *Eur J Cancer* **44**, 1541–1551 (2008).

180. Lewis, M. T. *Homeobox Genes in Mammary Gland Development and Neoplasia*. http://breast-cancer-research.com/content/2/3/158http://breast-cancer-research.com/content/2/3/158 (2000).

181. Raina, K., Dey, C., Thool, M., Sudhagar, S. & Thummer, R. P. An Insight into the Role of UTF1 in Development, Stem Cells, and Cancer. (2015) doi:10.1007/s12015-021-10127-9/ Published.

182. Jia, J. *et al.* Regulation of pluripotency and self- renewal of ESCs through epigenetic-threshold modulation and mRNA pruning. *Cell* **151**, 576–589 (2012).

183. Comet, I., Riising, E. M., Leblanc, B. & Helin, K. Maintaining cell identity: PRC2-mediated regulation of transcription and cancer. *Nature Reviews Cancer* vol. 16 803–810 Preprint at https://doi.org/10.1038/nrc.2016.83 (2016).

184. Kumar, B. *et al.* Polycomb repressive complex 2 shields naïve human pluripotent cells from trophectoderm differentiation. *Nat Cell Biol* **24**, 845–857 (2022).

185. Shan, Y. *et al.* PRC2 specifies ectoderm lineages and maintains pluripotency in primed but not naïve ESCs. *Nat Commun* **8**, (2017).

186. Bao, Q. *et al.* Utf1 contributes to intergenerational epigenetic inheritance of pluripotency. *Sci Rep* **7**, (2017).

187. Bannister, A. J. & Kouzarides, T. Regulation of chromatin by histone modifications. *Cell Research* vol. 21 381–395 Preprint at https://doi.org/10.1038/cr.2011.22 (2011).

188. Levinsky, A. J., McEdwards, G., Sethna, N. & Currie, M. A. Targets of histone H3 lysine 9 methyltransferases. *Frontiers in Cell and Developmental Biology* vol. 10 Preprint at https://doi.org/10.3389/fcell.2022.1026406 (2022).

189. Padeken, J., Methot, S. P. & Gasser, S. M. Establishment of H3K9-methylated heterochromatin and its functions in tissue differentiation and maintenance. *Nature Reviews Molecular Cell Biology* vol. 23 623–640 Preprint at https://doi.org/10.1038/s41580-022-00483-w (2022).

190. Jiang, G. *et al.* Single-cell transcriptomics reveal the heterogeneity and dynamic of cancer stem-like cells during breast tumor progression. *Cell Death Dis* **12**, (2021).

191. Rahmati, N. & Maftoon, N. Computational analysis of cancer cell adhesion in curved vessels affected by wall shear stress for prediction of metastatic spreading. *Front Bioeng Biotechnol* **12**, (2024).

192. Xin, Y., Li, K., Yang, M. & Tan, Y. Fluid shear stress induces emt of circulating tumor cells via jnk signaling in favor of their survival during hematogenous dissemination. *Int J Mol Sci* **21**, 1–16 (2020).

193. Xu, Z. *et al.* Fluid shear stress regulates the survival of circulating tumor cells via nuclear expansion. *J Cell Sci* **135**, (2022).

194. Miranda, A. *et al.* Cancer stemness, intratumoral heterogeneity, and immune response across cancers. *Proc Natl Acad Sci U S A* **116**, 9020–9029 (2019).

195. Han, H., He, T., Wu, Y., He, T. & Zhou, W. Multidimensional analysis of tumor stem cells: from biological properties, metabolic adaptations to immune escape mechanisms. *Frontiers in Cell and Developmental Biology* vol. 12 Preprint at https://doi.org/10.3389/fcell.2024.1441081 (2024).

196. Lei, M. M. L. & Lee, T. K. W. Cancer Stem Cells: Emerging Key Players in Immune Evasion of Cancers. *Frontiers in Cell and Developmental Biology* vol. 9 Preprint at https://doi.org/10.3389/fcell.2021.692940 (2021).

197. Rodríguez-Bejarano, O. H., Parra-López, C. & Patarroyo, M. A. A review concerning the breast cancer-related tumour microenvironment. *Critical Reviews in Oncology/Hematology* vol. 199 Preprint at https://doi.org/10.1016/j.critrevonc.2024.104389 (2024).

198. Mouchemore, K. A., Anderson, R. L. & Hamilton, J. A. Neutrophils, G-CSF and their contribution to breast cancer metastasis. *FEBS Journal* vol. 285 665–679 Preprint at https://doi.org/10.1111/febs.14206 (2018).

199. Zhuang, X. *et al.* Interferon-gamma inhibits aldehyde dehydrogenasebright cancer stem cells in the 4T1 mouse model of breast cancer. *Chin Med J (Engl)* **135**, 194–204 (2022).

200. Castro, F., Cardoso, A. P., Gonçalves, R. M., Serre, K. & Oliveira, M. J. Interferon-gamma at the crossroads of tumor immune surveillance or evasion. *Frontiers in Immunology* vol. 9 Preprint at https://doi.org/10.3389/fimmu.2018.00847 (2018).

201. Kim, M., Choi, H. Y., Woo, J. W., Chung, Y. R. & Park, S. Y. Role of CXCL10 in the progression of in situ to invasive carcinoma of the breast. *Sci Rep* **11**, (2021).

202. Gatenby, R. A., Silva, A. S., Gillies, R. J. & Frieden, B. R. Adaptive therapy. *Cancer Res* **69**, 4894–4903 (2009).

203. Breast Cancer Trialists, E. & Group, C. Relevance of breast cancer hormone receptors and other factors to the effi cacy of adjuvant tamoxifen: patient-level meta-analysis of randomised trials. (2011) doi:10.1016/S0140.

204. Zhang, X. *et al.* FGF ligands of the postnatal mammary stroma regulate distinct aspects of epithelial morphogenesis. *Development (Cambridge)* **141**, 3352–3362 (2014).

205. Lloyd-Lewis, B., Harris, O. B., Watson, C. J. & Davis, F. M. Mammary Stem Cells: Premise, Properties, and Perspectives. *Trends in Cell Biology* vol. 27 556–567 Preprint at https://doi.org/10.1016/j.tcb.2017.04.001 (2017).

206. Greaves, M. & Maley, C. C. Clonal evolution in cancer. *Nature* vol. 481 306–313 Preprint at https://doi.org/10.1038/nature10762 (2012).

207. Pagano, C. *et al.* Cannabinoids: Therapeutic Use in Clinical Practice. *International Journal of Molecular Sciences* vol. 23 Preprint at https://doi.org/10.3390/ijms23063344 (2022).

208. Castle, R. D., Marzolf, J., Morris, M. & Bushell, W. C. Meta-analysis of medical cannabis outcomes and associations with cancer. *Frontiers in Oncology* vol. 15 Preprint at https://doi.org/10.3389/fonc.2025.1490621 (2025).

209. Sánchez, C., Galve-Roperh, I., Canova, C., Brachet, P. & Guzmán, M. Δ9-Tetrahydrocannabinol induces apoptosis in C6 glioma cells. *FEBS Lett* **436**, 6–10 (1998).

210. Sánchez, C. et al. Inhibition of Glioma Growth in Vivo by Selective Activation of the CB 2 Cannabinoid Receptor 1. CANCER RESEARCH vol. 61 http://aacrjournals.org/cancerres/article-pdf/61/15/5784/2485361/5784.pdf (2001).

211. Galve-Roperh, I. *et al.* Anti-tumoral action of cannabinoids: Involvement of sustained ceramide accumulation and extracellular signal-regulated kinase activation. *Nat Med* **6**, 313–319 (2000).

212. Velasco, G., Sánchez, C. & Guzmán, M. Towards the use of cannabinoids as antitumour agents. *Nature Reviews Cancer* vol. 12 436–444 Preprint at https://doi.org/10.1038/nrc3247 (2012).

213. Twelves, C. *et al.* A phase 1b randomised, placebo-controlled trial of nabiximols cannabinoid oromucosal spray with temozolomide in patients with recurrent glioblastoma. *Br J Cancer* **124**, 1379–1387 (2021).

214. Bhaskaran, D. *et al.* A randomised phase II trial of temozolomide with or without cannabinoids in patients with recurrent glioblastoma (ARISTOCRAT): protocol for a multi-centre, double-blind, placebo-controlled trial. *BMC Cancer* **24**, (2024).

215. Nabissi, M. *et al.* Cannabidiol stimulates A ml-1a-dependent glial differentiation and inhibits glioma stem-like cells proliferation by inducing autophagy in a TRPV 2-dependent manner. *Int J Cancer* **137**, 1855–1869 (2015).

216. Liu, W. M., Scott, K. A., Shamash, J., Joel, S. & Powles, T. B. Enhancing the in vitro cytotoxic of Δ9-tetrahydrocannabinol in leukemic cells through a combinatorial approach. *Leuk Lymphoma* **49**, 1800–1809 (2008).

217. López-Valero, I. *et al.* Targeting Glioma Initiating Cells with A combined therapy of cannabinoids and temozolomide. *Biochem Pharmacol* **157**, 266–274 (2018).

218. Go, Y. Y., Kim, S. R., Kim, D. Y., Chae, S. W. & Song, J. J. Cannabidiol enhances cytotoxicity of anti-cancer drugs in human head and neck squamous cell carcinoma. *Sci Rep* **10**, (2020).

219. Kampa-Schittenhelm, K. M. *et al.* Epigenetic activation of O-linked β-N-acetylglucosamine transferase overrides the differentiation blockage in acute leukemia. *EBioMedicine* **54**, (2020).

220. Sido, J. M., Yang, X., Nagarkatti, P. S. & Nagarkatti, M. Δ9-Tetrahydrocannabinol-mediated epigenetic modifications elicit myeloid-derived suppressor cell activation via STAT3/S100A8. *J Leukoc Biol* **97**, 677–688 (2015).

221. Christin, J. R. & Shen, M. M. Modeling tumor plasticity in organoid models of human cancer. *Trends Cancer* **8**, 161–163 (2022).

222. Yakavets, I. *et al.* Advanced co-culture 3D breast cancer model for investigation of fibrosis induced by external stimuli: optimization study. *Sci Rep* **10**, (2020).

223. Strating, E. *et al.* Co-cultures of colon cancer cells and cancer-associated fibroblasts recapitulate the aggressive features of mesenchymal-like colon cancer. *Front Immunol* **14**, (2023).

224. Ma, Y., Xue, F., Pei, Z. & Zhao, Y. Constructing a co-culture model of cancer-associated fibroblasts and ovarian cancer organoids and studying mechanisms of drug resistance. *Exp Cell Res* **450**, (2025).

225. Wang, J. *et al.* Tumor organoid-immune co-culture models: exploring a new perspective of tumor immunity. *Cell Death Discovery* vol. 11 Preprint at https://doi.org/10.1038/s41420-025-02407-x (2025).

226. Correia-Sá, I. *et al.* Targeting cannabinoid receptor 2 (CB2) limits collagen production—An in vitro study in a primary culture of human fibroblasts. *Fundam Clin Pharmacol* **36**, 89–99 (2022).

227. Xiong, X. *et al.* Cannabis suppresses antitumor immunity by inhibiting JAK/STAT signaling in T cells through CNR2. *Signal Transduct Target Ther* **7**, (2022).

228. Rieder, S. A., Chauhan, A., Singh, U., Nagarkatti, M. & Nagarkatti, P. Cannabinoid-induced apoptosis in immune cells as a pathway to immunosuppression. *Immunobiology* vol. 215 598–605 Preprint at https://doi.org/10.1016/j.imbio.2009.04.001 (2010).

229. Okuda, A. et al. UTF1, a Novel Transcriptional Coactivator Expressed in Pluripotent Embryonic Stem Cells and Extra-Embryonic Cells. The EMBO Journal vol. 17 https://www.embopress.org (1998).

230. Wu, X. L. & Zheng, P. S. Undifferentiated embryonic cell transcription factor-1 (UTF1) inhibits the growth of cervical cancer cells by transactivating p27kip1. Carcinogenesis 34, 1660–1668 (2013).

231. Lou, Y., Jin, S., Hong, X., Hong, Z. & Xu, C. Expression and clinical significance of undifferentiated embryonic cell transcription factor 1 in breast cancer. Transl Cancer Res 12, 150–162 (2023).

232. Soethoudt, M. et al. Cannabinoid CB2 receptor ligand profiling reveals biased signalling and off-target activity. Nat Commun 8, 13958 (2017).

233. Ibsen, M. S., Connor, M. & Glass, M. Cannabinoid CB1 and CB2 Receptor Signaling and Bias. Cannabis Cannabinoid Res 2, 48–60 (2017).

234. Raina, K., Dey, C., Thool, M., Sudhagar, S. & Thummer, R. P. An Insight into the Role of UTF1 in Development, Stem Cells, and Cancer. Stem Cell Rev Rep 17, 1280–1293 (2021).

235. Begbie, J., Doherty, P. & Graham, A. Cannabinoid Receptor, CB1, Expression Follows Neuronal Differentiation in the Early Chick Embryo. J. Anat (2004).

236. Mulder, J. et al. Endocannabinoid Signaling Controls Pyramidal Cell Specification and Long-Range Axon Patterning. www.pnas.org/cgi/content/full/ (2008).

237. Wang, X., Dow-Edwards, D., Keller, E. & Hurd, Y. L. Preferential limbic expression of the cannabinoid receptor mRNA in the human fetal brain. *Neuroscience* **118**, 681–694 (2003).

238. Smoum, R. *et al.* Editorial: Therapeutic potential of the cannabinoid CB2 receptor. *Frontiers in Pharmacology* vol. 13 Preprint at https://doi.org/10.3389/fphar.2022.1039564 (2022).

239. Lohcharoenkal, W. *et al.* MicroRNA-203 Inversely Correlates with Differentiation Grade, Targets c-MYC, and Functions as a Tumor Suppressor in cSCC. *Journal of Investigative Dermatology* **136**, 2485–2494 (2016).

240. Benaich, N. *et al.* Rewiring of an epithelial differentiation factor, miR-203, to inhibit human squamous cell carcinoma metastasis. *Cell Rep* **9**, 104–117 (2014).

241. Wang, N. *et al.* miR-203 suppresses the proliferation and migration and promotes the apoptosis of lung cancer cells by targeting SRC. *PLoS One* **9**, (2014).

242. Huang, W., Wu, Y., Cheng, D. & He, Z. Mechanism of epithelial-mesenchymal transition inhibited by miR-203 in non-small cell lung cancer. *Oncol Rep* **43**, 437–446 (2020).

243. Lawrence M, J. Y. miR-203 Functions as a Tumor Suppressor by Inhibiting Epithelial to Mesenchymal Transition in Ovarian Cancer. *J Cancer Sci Ther* **07**, (2015).

244. Deng, B. *et al.* MiRNA-203 suppresses cell proliferation, migration and invasion in colorectal cancer via targeting of EIF5A2. *Sci Rep* **6**, (2016).

245. Sato, T. *et al.* Single Lgr5 stem cells build crypt-villus structures in vitro without a mesenchymal niche. *Nature* **459**, 262–265 (2009).

246. Briem, E. *et al.* MiR-203a is differentially expressed during branching morphogenesis and EMT in breast progenitor cells and is a repressor of peroxidasin. *Mech Dev* **155**, 34–47 (2019).

247. Martínez-Illescas, N. G. *et al.* miR-203 drives breast cancer cell differentiation. *Breast Cancer Research* **25**, (2023).

248. Sańchez-Vaśquez, E., Bronner, M. E. & Strobl-Mazzulla, P. H. Epigenetic inactivation of mir-203 as a key step in neural crest epithelial-to-mesenchymal transition. *Development (Cambridge)* **146**, (2019).

249. Gupta, P. B. *et al.* Stochastic state transitions give rise to phenotypic equilibrium in populations of cancer cells. *Cell* **146**, 633–644 (2011).

250. Pal, B. *et al.* Integration of microRNA signatures of distinct mammary epithelial cell types with their gene expression and epigenetic portraits. *Breast Cancer Research* **17**, (2015).

251. Michel, C. & Malumbres, M. microRNA-203: Tumor Suppression and Beyond. *MicroRNA* **2**, 118–126 (2013).

252. He, S., Zhang, G., Dong, H., Ma, M. & Sun, Q. miR-203 facilitates tumor growth and metastasis by targeting fibroblast growth factor 2 in breast cancer. *Onco Targets Ther* **9**, 6203–6210 (2016).

253. Jacques Monod. Chance and Necessity: An Essay on the Natural Philosophy of Modern Biology. (1972).

254. Derényi, I. & Szöllsi, G. J. Hierarchical tissue organization as a general mechanism to limit the accumulation of somatic mutations. *Nat Commun* **8**, (2017).

255. Alberts, B. The Cell as a Collection of Protein Machines: Preparing the Next Generation of Molecular Biologists. *Cell* **92**, 291–294 (1998).

256. Nicholson, D. J. Organisms≠Machines. Studies in History and Philosophy of Science Part C :Studies in History and Philosophy of Biological and Biomedical Sciences **44**, 669–678 (2013).

257. Nicholson, D. J. The machine conception of the organism in development andevolution: A critical analysis. Studies in History and Philosophy of Science Part C :Studies in History and Philosophy of Biological and Biomedical Sciences **48**, 162–174 (2014).

258. Shyer, A. E. & Rodrigues, A. R. Transcending the hegemony of the molecular machine through an organic renewal of biology and biomedicine. *Cells and Development* (2025) doi:10.1016/j.cdev.2025.204018.

259. Bar-Hai, N. & Ishay-Ronen, D. Engaging plasticity: Differentiation therapy in solid tumors. *Frontiers in Pharmacology* vol. 13 Preprint at https://doi.org/10.3389/fphar.2022.944773 (2022).

260. Wagensberg, J. La Rebelión de Las Formas: O Cómo Perservar Cuando La Incertidumbre Aprieta. (2004).

261. Rosenbaum, S. R., Fields, K. M. & Ford, H. L. Masters of adaptation: How cancer and immune cell plasticity mediates tumor progression. *PLoS Biol* **23**, (2025).

262. de Visser, K. E. & Joyce, J. A. The evolving tumor microenvironment: From cancer initiation to metastatic outgrowth. *Cancer Cell* vol. 41 374–403 Preprint at https://doi.org/10.1016/j.ccell.2023.02.016 (2023).

263. Nakahara, R., Maeda, K., Aki, S. & Osawa, T. Metabolic adaptations of cancer in extreme tumor microenvironments. *Cancer Science* vol. 114 1200–1207 Preprint at https://doi.org/10.1111/cas.15722 (2023).

264. Shi, Z. D. *et al.* Tumor cell plasticity in targeted therapy-induced resistance: mechanisms and new strategies. *Signal Transduction and Targeted Therapy* vol. 8 Preprint at https://doi.org/10.1038/s41392-023-01383-x (2023).

265. Wu, P. *et al.* Adaptive Mechanisms of Tumor Therapy Resistance Driven by Tumor Microenvironment. *Frontiers in Cell and Developmental Biology* vol. 9 Preprint at https://doi.org/10.3389/fcell.2021.641469 (2021).

266. Nicholson, D. J. & Dupré, J. Reconceptualizing the Organism: From Complex Machine to Flowing Stream. in *Everything flows: Towards a Processual Philosophy of Biology* 139–168 (2018).

267. Hariri, N., Roma, A. A., Hasteh, F., Walavalkar, V. & Fadare, O. Phenotypic alterations in breast cancer associated with neoadjuvant chemotherapy: A comparison with baseline rates of change. *Ann Diagn Pathol* **31**, 14–19 (2017).

268. Boros, M. et al. Clinical Implications of Multifocality as a Prognostic Factor in Breast Carcinoma-a Multivariate Analysis Study Comprising 460 Cases. Int J Clin Exp Med vol. 8 www.ijcem.com/ (2015).

269. Weissenbacher, T. M. *et al.* Multicentric and multifocal versus unifocal breast cancer: Is the tumor-node-metastasis classification justified? *Breast Cancer Research and Treatment* vol. 122 27–34 Preprint at https://doi.org/10.1007/s10549-010-0917-9 (2010).